

Queensland University of Technology

School of Natural Resource Sciences

Patterns of Coal Sedimentation in the
Ipswich Basin
Southeast Queensland

By

Peter Kyaw Zaw Naing Chern

Bachelor of Science (Rangoon University)
Bachelor of Applied Science (Distinction) (QUT)
Bachelor of Applied Science (Honours) (QUT)

Supervisor
Dr Lloyd Hamilton
Queensland University of Technology

Co-Supervisor
Dr Joan Esterle
Commonwealth Scientific and Industrial Research Organisation

A thesis submitted in partial fulfillment of the requirements for the Master
of Applied Science Degree in Geology

Key words

Ipswich Coal Measures, Triassic coal basins, Intermontane Ipswich Basin, Blackstone Formation, Tivoli Formation, Brassall Subgroup, Kholo Subgroup, West Ipswich Fault, peat-mire aggradation, peat-mire progradation, terrestrialisation, paludification, depocentres, sedimentary splitting, tectonic splitting, brightness profiles, Dicroidium, structured macerals, vitrinite, liptinite, inertinite, clay and other mineral matter

ABSTRACT

The intermontane Ipswich Basin, which is situated 30km south-west of Brisbane, contains coal measures formed in the Late Triassic Epoch following a barren non-depositional period. Coal, tuff, and basalt were deposited along with fluvial dominated sediments. The Ipswich Coal Measures mark the resumption of deposition in eastern Australia after the coal hiatus associated with a series of intense tectonic activity in Gondwanaland during the Permo-Triassic interval. A transtensional tectonic movement at the end of the Middle Triassic deformed the Toogalawah Group before extension led to the formation of the Carnian Ipswich Coal Measures in the east.

The Ipswich Coal Measures comprise the Brassall and Kholo Subgroups. The Blackstone Formation, which forms the upper unit of the Brassall Subgroup, contains seven major coal seams. The lower unit of the Brassall Subgroup, the Tivoli Formation, consists of sixteen stratigraphically significant coal seams. The typical thickness of the Blackstone Formation is 240m and the Tivoli Formation is about 500m.

The coal seams of the Ipswich Basin differ considerably from those of other continental Triassic basins. However, the coal geology has previously attracted little academic attention and the remaining exposures of the Ipswich coalfield are rapidly disappearing now that mining has ceased. The primary aim of this project was to study the patterns of coal sedimentation and the response of coal seam characteristics to changing depositional environments.

The coal accumulated as a peat-mire in an alluvial plain with meandering channel systems. Two types of peat-mire expansion occurred in the basin. Peat-mire aggradation, which is a replacement of water body by the peat-mire, was initiated by tectonic subsidence. This type of peat-mire expansion is known as terrestrialisation. It formed thick but laterally limited coal seams in the basin. Whereas, peat-mire progradation was related to paludification and produced widespread coal accumulation in the basin.

The coal seams were separated into three main groups based on the mean seam thickness and aerial distribution of one-meter and four-meter thickness contour intervals. Group 1 seams within the one-meter thickness interval are up to 15,000m² in area, and seams within the four-meter interval have an aerial extent of up to 10,000m². Group 1A contains the oldest seam with numerous intraseam clastic bands and shows a very high thickness to area ratio, which indicates high subsidence rates. Group 1B seams have moderately high thickness to area ratios. The lower clastic influx and slower subsidence rates favoured peat-mire aggradation. The Group 1A seam is relatively more widespread in aerial extent than seams from Group 1B. Group 1C seams have low mean thicknesses and small areas, suggesting short-lived peat-mires as a result of high clastic influx. Group 2 seams are

between 15,000 and 35,000m² in area within the one-meter interval, and between 5,000 and 10,000m² within the four-meter interval. They have moderately high area to thickness ratios, indicating that peat-mire expansion occurred due to progressively shallower accommodation and a rising groundwater table. Group 3 seams, which have aerial extents from 35,000 to 45,000m² within the one-meter thickness contour interval and from 10,000 to 25,000m² within the four-meter interval, show high aerial extent to thickness ratios. They were deposited in quiet depositional environments that favoured prolonged existence of peat-mires. Group 3 seams are all relatively young whereas most Group 1 seams are relatively old seams.

All the major fault systems, F1, F2 and F3, trend northwest-southeast. Apart from the West Ipswich Fault (F3), the F1 and F2 systems are broad Palaeozoic basement structures and thus they may not have had a direct influence on the formation of the much younger coal measures. However, the sedimentation patterns appear to relate to these major fault systems. Depocentres of earlier seams in the Tivoli Formation were restricted to the northern part of the basin, marked by the F1 system. A major depocentre shift occurred before the end of the deposition of the Tivoli Formation as a result of subsidence in the south that conformed to the F2 system configuration. The Blackstone Formation depocentres shifted to the east (Depocentre 1) and west (Depocentre 2) simultaneously. This depocentre shift was associated with the flexural subsidence produced by the rejuvenation of the West Ipswich Fault. Coal accumulation mainly occurred in Depocentre 1.

Two types of seam splitting occurred in the Ipswich Basin. Sedimentary splitting or autosedimentation was produced by frequent influx of clastic sediments. The fluvial dominant depositional environments created the random distribution of small seam splits. However, the coincidence of seam splits and depocentres found in some of the seams suggests tectonic splitting. Furthermore, the progressive splitting pattern, which displays seam splits overlapping, was associated with continued basin subsidence. The tectonic splitting pattern is more dominant in the Ipswich Basin.

Alternating bright bands shown in the brightness profiles are a result of oscillating water cover in the peat-mire. Moderate groundwater level, which was maintained during the development of the peat, reduced the possibility of salinisation and drowning of the peat swamp. On the other hand, a slow continuous rise of the groundwater table, that kept pace with the vertical growth of peat, prevented excessive oxidation of peat.

Ipswich coal is bright due to its high vitrinite content. The cutinite content is also high because the dominant flora was pteridosperms of *Dicroidium* assemblage containing waxy and thick cuticles. Petrographic study revealed that the depositional environment was telmatic with bog forest formed under ombrotrophic to mesotrophic hydrological conditions. The high preservation of woody or structured macerals such as telovitrinite and semifusinite

indicates that coal is autochthonous. The high mineral matter content in coal is possibly due to the frequent influx of clastic and volcanic sediments.

The Ipswich Basin is part of a much larger Triassic basin extending to Nymboida in New South Wales. Little is known of the coal as it lacks exposures. It is apparently thin to absent except in places like Ipswich and Nymboida. This study suggests that the dominant control on depocentres of thick coal at Ipswich has been the tectonism. Fluvial incursions and volcanism were superimposed on this.

TABLE OF CONTENTS

Title Page	I
Paragraph of Key Words	II
Abstract	III
<u>Table of Contents</u>	VI
List of Figures	X
List of Tables	XIII
Statement of Original Work	XV
Acknowledgments	XVI
<u>INTRODUCTION</u>	1
Aim	3
Objectives	3
Significance of Research	4
Exploration and Mining History	4
Previous Studies	5
Methods	5
Brightness Profiling and Sampling	5
Petrographic Study and Point Counting	6
Borehole Correlation and Contouring	6
Geophysical Map Interpretation	6
Digital Maps and Drawings	6

<u>BACKGROUND AND GEOLOGICAL SETTINGS</u>	7
Ipswich Basin	7
Stratigraphy of Ipswich Basin	7
The Kholo Subgroup	9
The Brassall Subgroup	9
Structural Elements	17
Triassic Coal Basins	19
Global Tectonic Events in the Permo-Triassic Interval	19
Formation of Continental Triassic Coal Basins in Eastern Australia	21
<u>COAL SEAMS</u>	22
Tivoli Formation	22
Blackstone Formation	23
Coal Seam Characteristics and Lithotypes	32
Brightness Profiles	32
Highwall Brightness Profiles	35
Drill-core Sample Brightness Profiles	48
<u>COAL PETROLOGY</u>	50
Ipswich Flora and Fauna	50
Climatic Effect on Flora	50
Triassic Megafloora	50
Miospores	53
Relation to Coal Petrography	53
Peat-mire Types and Vegetation	54

Petrographic Study of Ipswich Coal	55
Results	56
Vitrinite Group	56
Liptinite Group	58
Inertinite Group	59
Clay and other Mineral Matter	59
Maceral Data Analysis	60
Coal Lithotypes vs. Maceral Groups	74
<u>PATTERNS OF COAL SEAM ACCUMULATION</u>	81
Results	81
Seam Contour Maps and Seam Split Maps	83
Tivoli Formation	83
Waterworks Seam	83
Benley Seam	83
Eclipse Seam	83
Poverty Seam	84
Tivoli Seam	84
Waterstown Seam	84
Fiery Seam	84
Tantivy Seam	84
Westfalen Top Seam	84
Garden Seam	84
Swanbank Area Seams	85
Cochrane Seam	85

Blackstone Formation	86
Rob Roy Seam	86
Striped Bacon-Rob Roy Interval	86
Striped Bacon Seam	86
Bergin Seam	86
Fourfoot Seam	86
Bluff Seam	86
Aberdare Seam	87
Thomas Seam	87
Total Thickness Contour Maps	146
Area vs. Thickness	150
Mean Thickness vs. Depth	150
Geophysical Map Interpretation	154
Basement Structural Cross-sections	162
DISCUSSION	167
Evolution of Coal Sedimentation Patterns	167
Tivoli Formation	167
Blackstone Formation	169
Effects of Faulting	172
Compaction	175
Depositional Environments and Associated Sedimentary Patterns	176
Coal Petrology	177
Clay Mineralogy	180
Seam Splits	181

CONCLUSIONS	183
REFERENCES	185

APPENDICES

Appendix I: Drillhole Brightness Profiles (Appendix I - Figures 1 to 28)	
Appendix II: Tables (Tables 11 to 14 and 18, 19 and 23)	
Appendix III: Coal Atlas Photographs 1 to 88	
Appendix IV: Borehole Correlation Sections 1 to 50 (Cross-sections and Borehole Sections)	
Appendix V: Ipswich Basin Borehole Location Plan and Large Cross-sections	

LIST OF FIGURES

Figure 1: Locality Map	1
Figure 2: Locality Map Showing Cultural Features	2
Figure 3: Coal Seams Correlated by the Department of Mines and Energy	10
Figure 4: Borehole Location Map	11
Figure 5: Some of the Major Mines in the Ipswich Basin	12
Figure 6: New Hope Mines in the Swanbank Lagoon Area	13
Figure 7: Sample Location Map, Swanbank Area (New Hope)	14
Figure 8: Sample Location Map, Bogsid Mine (New Hope)	15
Figure 9: Landset Image of the Study Area	16
Figure 10: Southeast Queensland Structural and Tectonic Elements	17
Figure 11: Triassic Mesozoic Basins in Eastern Australia	18
Figure 12: Australian Triassic Coal Basins with Triassic Poles	20

Figure 13: New Hill Mine Area General Stratigraphic Column	26
Figure 14: Seam Splitting Diagram (Blackstone Formation)	27
Figure 15: Blackstone Formation (Bundamba Area) Stratigraphic Column	28
Figure 16: Blackstone Formation (Swanbank Area) Stratigraphic Column	29
Figure 17: Seam Splitting Diagram (Tivoli Formation)	30
Figure 18: Box Flat and Westfalen Mines Stratigraphic Columns	31
Figure 19: Location Map of Brightness Profiles	34
Figure 20 to 31: Highwall Sample Brightness Profiles	36 to 47
Figure 32: Sample Location Map	57
Figure 33: TPI – GI Crossplot	61
Figure 34: Modified Hacquebard’s Double Triangle	65
Figure 35: DTF Facies Diagram	66
Figure 36: RWD Facies Diagram	67
Figure 37: ABC Facies Diagram	68
Figure 38: Maceral Compositions of Ipswich Coal (Modified Smyth’s Diagram)	69
Figure 39: Maceral and Mineral Compositions of Grainmount Samples	70
Figure 40: Maceral and Mineral Compositions of Polished Block Samples	71
Figure 41: GWI – VI Crossplot	73
Figures 42A and 42B: Lithotypes vs. Vitrinite and Lithotype vs. Liptinite	77
Figures 43A and 43B: Lithotypes vs. Inertinite and Lithotype vs. Mineral Matter	78
Figure 44: Percentages of Telovitrinite and Detrovitrinite vs. Lithotypes	79

Figure 45: Ipswich Basin Surface Contour Map	82
Figures 46 to 102: Seam Contour Maps and Seam Split Maps	89 to 145
Figure 103: Tivoli Formation Total Coal Thickness Contour Map	147
Figure 104: Blackstone Formation Total Thickness Contour Map	148
Figure 105: Blackstone Formation Total Coal Thickness Contour Map	149
Figure 106: Mean Thickness vs. Aerial Extent (1m Thickness Interval)	151
Figure 107: Mean Thickness vs. Aerial Extent (4m Thickness Interval)	152
Figure 108: Mean Thickness vs. Average Depth	153
Figure 109: Gravity Map	156
Figures 110 and 111: Northern and Southern Gravity Profiles	157 and 158
Figure 112: Magnetic Map	159
Figure 113: Major Fault Systems	160
Figure 114: Depocentres for Blackstone and Tivoli Formations	161
Figure 115: Cross-section Location Map	163
Figures 116 to 118: Basement Structural Cross-sections	164 to 166
Figure 119: Cartoon Illustrating the Flexural Subsidence Initiated by F3 System	171
Figure 120: Thermal Maturity Pattern (Tivoli Formation)	173
Figure 121: Thermal Maturity Pattern at the top of the Ipswich Basin	174

LIST OF TABLES

Table 1: The Ipswich Basin Stratigraphic Succession	8
Table 2: Major Coal Seams in the Tivoli Formation	23
Table 3: Major Coal Seams in the Blackstone Formation	24
Table 4: Total Interburden Thickness and Total Coal Thickness	24
Table 5: Highwall Brightness Profiles Summary Statistics	35
Table 6: Drillhole Brightness Profiles Summary Statistics	48
Table 7: Four Oppel-zones	51
Table 8: Mesozoic Floral Associations	52
Table 9: Peat-mire, Vegetation and Peat Type	54
Table 10: Different Conditions of Peat Forming Environments	55
Table 11 (Appendix II): Sample List (Grainmount Samples)	
Table 12 (Appendix II): Sample List (Polished Block Samples)	
Table 13 (Appendix II): Maceral Point Count Results (Grainmount Samples)	
Table 14 (Appendix II): Maceral Point Count Results (Polished Block Samples)	
Tables 15A and 15B: Grainmount and Polished Blocks Samples Statistics	58
Table 16: Various Indices of Maceral Associations used in Ternary Diagrams	64
Table 17: Brightness Profile Ranking	74
Table 18 (Appendix II): Samples used in Lithotypes vs. Maceral Types Plots	
Table 19 (Appendix II): Samples used in Telovitrinite/Detrovitrinite vs. Lithotypes Plot	
Table 20: Tivoli Formation Seam Thickness and Structural Description	85

Table 21: Blackstone Formation Seam Thickness and Structural Description	87
Table 22: Aerial Extent for 1m and 4m Seam Thickness Intervals	150
Table 23 (Appendix II): Average Depth vs. Average Thickness	
Table 24: Highwall and Core Sample Brightness Profile Patterns	179

Statement of Original Work

This thesis only contains original research work carried out by the author, except where it is appropriately acknowledged. To the best of my knowledge and belief, the work contained in this thesis has not been previously submitted to any other higher educational institution for a degree or diploma.

Peter Chern

Signed:.....

Date:.....

ACKNOWLEDGEMENTS

Firstly, I would like to thank my supervisor Associate Professor Lloyd Hamilton (QUT) for his guidance and excellent supervision. Without his tireless help and encouragement I would not be able to complete my thesis. I also thank my co-supervisor Dr Joan Esterle (CSIRO) for her useful advice and commentary.

Thanks are due to many people from the department of Mines and Energy including Len Cranfield for allowing me to use the Southeast Queensland digital map, David Coffee for giving me a permission to look at archived files, Richie Huber for gravity and magnetic maps, and a special thank to Ray Smith, whose help with petrographic samples is greatly appreciated.

I thank Barry Saunders (Queensland Geological Services Pty Ltd) for lending me his personal collection of company reports, and Blair Richardson from New Hope Mines Limited, who provided me with the geological data of the Swanbank area. Landset images were provided by Brad Pinder from Arrow Energy N.L., whose help is gratefully acknowledged. I would also like to thank Dr Gary Huftile (QUT) for his help with the structural interpretation.

Finally, I would like to thank my wife, Nilar, for her support and assistance. I am grateful for her patience and understanding during my long study.

INTRODUCTION

The Ipswich Basin is situated in southeast Queensland, approximately 30km southwest of Brisbane and about 13km east of the city of Ipswich (Falkner, 1986) (Figure 1). The coalfield occupies 250km² to the northeast and southeast of Ipswich (Staines, 1995).

The access to the basin is from either Cunningham Highway or Warrego Highway. The main railway line linking Brisbane and Toowoomba passes through the Ipswich city. The Brisbane River and Bremer River traverse across the Ipswich Basin (Figure 2).

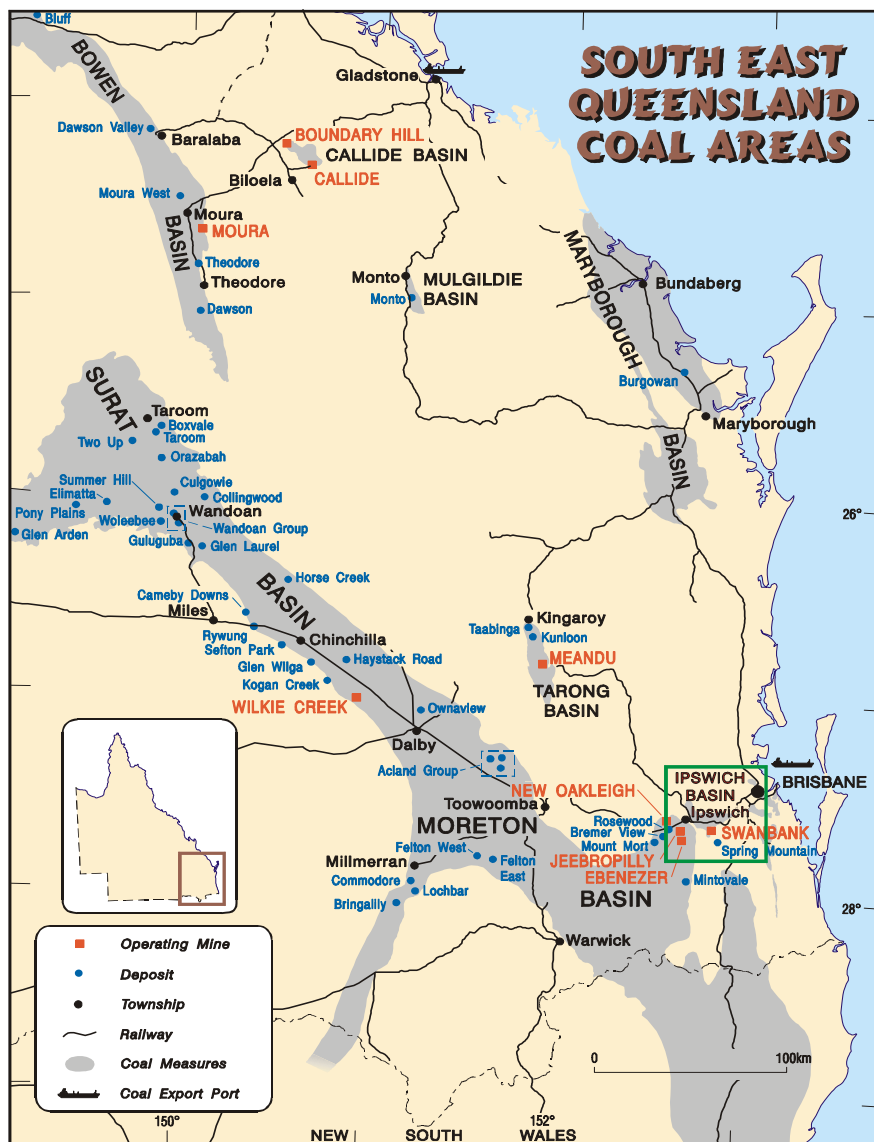


Figure 1: Locality map (After Queensland Department of Mines and Energy, 2000)

This image is not available online. Please consult the hardcopy thesis available from the QUT library

Figure 2: Locality map showing cultural features (eg. roads, tracks, railway lines, rivers and creeks) (Source: Geoscape, 1997)

The Ipswich Basin is an aeri ally restricted and relatively shallow intermontane basin, formed within the New England Foldbelt near the eastern margin of the cratonised orogenic zone (Gould and Shibaoka, 1980). The basin formation was associated with tensional movements in the Late Triassic Epoch (Ties et al., 1985). The basin developed during the post-orogenic phase of the Tasman Orogenic Zone (Galligan, 1979). According to Cook (1975), the basin extent, including the coalfield and Triassic sedimentary rock units, is about 700km², but the full extent of the basin cannot be clearly defined because younger Tertiary and Cainozoic rocks of the Clarence-Moreton Basin superimpose part of the older Triassic rocks of the Ipswich Basin. Furthermore, McElroy (1962 and 1969b) described similar Triassic coal deposits in the south extending into New South Wales to Evans Head and Nymboida. This gives the extended Triassic basin an area of about 18, 000km². Coal accumulation occurred in the Ipswich Basin during the Late Triassic Epoch. Locally thick, but aeri ally limited and laterally impersistent coal seams were produced by several interrelated events of differential subsidence, fluvial incursion and interrupted by volcanism. The complex coal seam architecture shown in the Ipswich coals is related to tectonic-controlled subsidence as well as folding, faulting, and

periodic volcanism. Correlation of coal seams across the basin was hindered by seam discontinuities and post-depositional deformation. Coal seams coalesce and split in different combinations, suggesting the high fluvial and tectonic activity in the basin. However, the variation in petrographic composition of the Ipswich coal is comparatively less than that of other Australian Triassic coals such as Callide and Tarong coals. The high cutinite content, bright and friable nature, and the uniformity and coherence as a group make Ipswich coals unique among Triassic coals.

Two main coal-producing areas were defined within the Ipswich Basin. The North Ipswich coalfield is located north of Bremer River, and the Bundamba coalfield lies on and adjacent to the Bundamba Anticline and extends southward for about 12km (Cranfield, 1981). Small-scale low-wall mining still occurs in the Swanbank area, which lies in the Bundamba coalfield. Coal is currently extracted from seams in the Blackstone Formation but it is likely that most coal mining activity will cease before 2005.

AIM

The primary aim of this project was to study the sedimentation patterns of various coal seams and their maceral distributions in relation to depositional environments, and to explain the unusual nature of the coal relative to other Australian coals.

This study focuses on the main mechanisms and processes which control the formation of terrestrial and limnotelmatic basins that produce bright coals.

OBJECTIVES

The main objectives were:

- To characterize the unusual nature of the coal, eg. coal seam architecture and coal petrology.
- To clarify different maceral associations and relate their distribution patterns to palaeodepositional environments.
- To compile a systematic coal atlas for the Ipswich coals.
- To study and record the coal seam architecture and brightness profiles, eg. vertical and horizontal variations of bright and dull bands, as well as claystone bands.
- To correlate coal seams across the basin and define seam split patterns.

- To define depocenters for the Blackstone and Tivoli Formations and study the movements of depocentres in relation to time and coal deposition.
- To apply *some of the basic concepts* of sequence stratigraphy, geostatistics and geophysical methods to identify the controlling factors on patterns and distribution of coal sedimentation.

Significance of Research

The coal seam characteristics of the Ipswich Basin differ considerably from those of other Triassic coal basins in Australia. However, the coal geology has previously attracted little academic attention. Remaining exposures of Ipswich coalfield are rapidly disappearing now that mining has ceased. Furthermore, formation and movement of depocentres were unknown. Coal seams show complex architecture and maceral composition is unusual for a Triassic continental basin. There is an urgent need for further research of Ipswich coal that epitomizes the characteristics of a unique Triassic coal basin.

Exploration and Mining History

Mining in the Ipswich area has been continuously operating since 1843. The Ipswich Coalfield was a principal coal producer in Queensland until the 1960's when development of the Bowen Basin coal was initiated. The railway system was the principal user until the introduction of diesel trains in the early 1950's. The electricity generation remains the largest user (Staines,1995).

According to Denmead (1955) and Mengel (1976) coal in Ipswich was first noticed by Captain Logan in 1827. However, Whitmore (1981 in Cranfield 1989) argued that coal outcrops were first discovered by Oxley in 1824 and Lockyer in 1825.

Little systematic exploration was carried out in the Ipswich Basin prior to 1949. As a result of recommendation made by Powell Duffryn Technical Services Limited (Tucker, 1949) an extensive diamond drilling program was undertaken by the Department of Mines and the Queensland Coal Board. A total of 587 cored boreholes was drilled and underground coal reserves were proved (Mengel, 1975). Mengel and Carr (1976) reported in situ measured and indicated resources as 575Mt, of which 474Mt would be mined by underground methods. Queensland Coals (2001) reported the total resources as 463Mt (excluding the Spring Mountain area). However, most of the economically minable coal has been extracted and recovery of remaining coal resources are affected by faulting, surface constraints, difficulty of

access in previously worked areas and mining conditions at depth. The total production of coal from the Ipswich mining area is less than 100Mt and probably about 80Mt (L. Hamilton, QUT, personal communication).

Since the major flooding of the North Ipswich Coalfield in 1974 and the subsequent abandonment of all underground operations, the supply is exclusively from the Blackstone Formation. After the establishment of the Tarong power station and downgrading of the Swanbank power station, coal production has gradually declined. In 1996, the New Hill underground mine was closed down after a section of the roof collapsed and killed one miner and injured another person.

Previous Studies

Denmead (1955) produced the first comprehensive study of the Ipswich coalfield, but his report is only relevant to this study in certain areas as most of the old mines have been closed down and the coal seam nomenclature and correlation have been changed and revised several times. Cook and Taylor (1963) studied coal petrology of the Blackstone Formation and Smyth (1988) compared petrographic compositions of Triassic coals in Australia. Cranfield, Schwarzbock and Day (1976) studied and published the regional and structural geology of the Ipswich Basin. Most of the palynological studies were conducted by de Jersey during the 1960's and the 1970's. Various authors, including Carr, Mengel, Staines, and Cranfield, have written numerous papers which are mainly concerned with coal mining operations and drilling activities. After A. Falkner's research in 1986, most of the research studies in the area have ceased.

METHODS

This study is mainly based on drill hole information, using **587** NS-series boreholes from the Department of Mines and Energy, and **644** boreholes from the New Hope Mines. Several open-cut mines, including Box Flat open-cut, New Hope No. 7, Bogside, Wattle Glen (New Brick), and Aberdare No. 2 (Barcley Street Tip), were visited for highwall mapping, brightness profiling and petrographic sampling purposes.

Brightness Profiling and Sampling

Twenty-one highwall brightness profiles and twenty-eight borehole brightness profiles were drawn to clarify the internal coal seam architecture and patterns of lithotype distribution. Coal samples were taken from common and relatively thicker bright and dull bands of each profile. Maceral type versus lithotype graphs were drawn to establish the relationship between the maceral contents of coal and brightness characters

of coal lithotypes. High-wall block samples for maceral analysis were selected with regard to the lithotype brightness character of the seam.

Petrographic Study and Point Counting

Thirty-seven highwall samples and forty-one borehole samples were selected for petrographic analysis. Borehole samples were made as grain mounts due to their powdery nature, whereas, highwall samples were made as polished blocks. Each sample was point-counted to 300 points in reflected light using a *40 oil immersion objective and a *10 ocular lens which gives a combined magnification of *400. All photographs were taken with oil immersion lenses except for thin sections which were taken in transmitted light.

Fluorescence microscopy was used to observe certain components in coal, particularly the liptinite macerals, which show auto-fluorescence when irradiated with blue light. The samples selected for fluorescence microscopy were excited with blue light and the fluorescence intensity was measured at a specific wavelength of about 546nm. The fluorescence colours of liptinite macerals show strong to weak, yellow, orange and brown variations (see Appendix III).

Borehole Correlation and Contouring

Fifty cross-sections and borehole sections were drawn for borehole correlation and structural interpretation (Appendix IV). Three major cross sections were also drawn for basin basement structural delineation (see Page 155 - Basement Structural Cross-sections). Furthermore, I generated thickness isopach maps, seam roof structure contour maps, and seam split maps from borehole data using Surfer™ and CorelDraw™ software packages.

Geophysical Map Interpretation

Gravity (bouguer anomaly) and magnetic maps were studied in conjunction with geological maps to define major structural elements and basin configuration. I have generated these geophysical maps through MapInfo™ application system (see Pages 149, 152 and 153 for geophysical maps).

Digital Maps and Drawings

I created, modified and edited most of the maps, diagrams, and drawings in this study, using various software packages including CorelDraw™, MapInfo™ with GeoBase Map™, Discover™ and GeoImage™ add-on applications, and AutoCAD™, except where appropriately acknowledged. Ternary facies diagrams were created in Igp32® software package. ECSI-

Minex™ mining software system was used to create a borehole location plan and large cross-sections (see Appendix V).

Background and Geological Settings

Ipswich Basin

The Ipswich Basin is a partially fault-bounded, asymmetric interior cratonic intermontane basin, dominated by fluvial settings (Falkner, 1986; Cranfiled, 1981; Cook, 1975). Day and others (1975) defined the depositional environments as continental, fluvial, and paludal (or lacustrine). The Ipswich Basin contains Triassic clastic sedimentary rocks, basic and acid volcanic rocks, and coals (Table 1). The Ipswich coal is high-volatile bituminous coal in rank with moderate to high ash (10% to 30%) and low sulphur (~0.3%) contents. The average vitrinite reflectance in the Blackstone formation is about 0.92% (in oil) and 0.99% (in oil) in the Tivoli Formation. The average specific energy in the Blackstone Formation is 25.12MJ/kg (air-dried) and the Tivoil Formation contains 26.26MJ/kg (air-dried). The Ipswich coal type is classified as thermal coal and thus, Geiseler Plasticity test was not performed as it is mainly related to coking coal properties. All seams usually contain high ash content but beneficiation by washing produces less than 23% ash content. The coal is mainly used for steam raising for power generation. (Wilson, 1975).


According to Chern (1997) clay mineralogy is uniform throughout the Ipswich Coal Measures. The clay samples mainly contain kaolinite. Illite is the second dominant clay type and it is commonly associated with illite-smectite mixed layers (see ‘**Clay Mineralogy**’ in ‘**Discussion**’ section for details).

The Stratigraphy of the Ipswich Basin

The earliest deposits in the Ipswich Basin have been identified as basaltic volcanic rocks of Early Triassic Epoch in the Mt Crosby and Mogill areas (Houston, 1965; Webb and McNaughton, 1978). The lower part of the sequence contains rhyolitic pyroclastic rocks of Chillingham Volcanics (Toogoolawah Group) and Brisbane Tuff. They are unconformably overlain and partly faulted against by the Upper Triassic Kholo Subgroup, which formed the basal unit of the Ipswich Coal Measures. The Brassall Subgroup, containing the coal-bearing Blackstone and Tivoli Formations, conformably overlies the Kholo Subgroup. The Ipswich Coal Measures comprise approximately 1000m of sedimentary, volcanic and pyroclastic rocks and coal seams (Bower, 1987). Table 1 shows the stratigraphic succession of the Ipswich Basin and detailed sequence of the Ipswich Coal Measures. The Ipswich Coal Measures are divided into two subgroups.

Table 1: The Ipswich Basin stratigraphic succession (Compiled after Mengel and Carr, 1976; Day et al., 1979; Cranfield, 1981; Cranfield, Hutton and Green, 1989; Falkner, 1986; Bowern, 1987; Staines, 1995)

Age	Group	Subgroup	Formation	Thickness (m)	Lithology	Depositional Environment
Tertiary	Booval		Silkstone Formation	300	Claystone, siltstone, sandstone	Terrestrial (mainly)
	Group		Redbank Plains Formation		Claystone, sandstone	Terrestrial (mainly)
Jurassic	Walloon Coal Measures (Moreton Basin)			250	Mudstone, siltstone, clayey lithic sandstone, coal	Fluvial to lacustrine
	Jurassic to Late Triassic	Bundamba Group		Marburg Formation	800	Lithic to feldspathic labile to sublabile sandstone, siltstone, shale and coal
			Helidon Sandstone (Esk Trough)	250	Feldspathic sublabile and quartzose sandstone, siltstone, minor shale and conglomerate	Fluvial, braided streams
Woogaroo Subgroup			Ripley Road Sandstone	365	Sublabile to quartzose sandstone	High energy fluvial, braided
			Raceview Formation	120	Sublabile to quartzose sandstone, siltstone, shale and coal	Lacustrine to fluvial
			Aberdare Conglomerate	30	Polymictic, pebble to cobble conglomerate, sandstone, and shale	High energy fluvial-point bar deposit
Unconformity						
Late Triassic	Ipswich Coal Measures (typical 750m) (Total ~1000m)	Brassall Subgroup	Blackstone Formation	240	Shale, siltstone, sandstone lenses, coal	Floodplain adjacent to high energy river channel
			Tivoli Formation	480-500	Sandstone, conglomerate, siltstone, shale, coal	Meandering systems in alluvial plain setting
		Kholo Subgroup	Cribb Conglomerate	20	Pebble conglomerate, feldspathic sandstone	Fluvial, high energy
			Hector Tuff	12-37	Acid tuff	Air fall tuff
			Colleges Conglomerate	160-240	Pebble to cobble conglomerate, sandstone, shale	Fanglomerate
			Mt. Crosby Formation	20-35	Conglomerate, sandstone, siltstone, shale, rhyolitic tuff	Fanglomerate, Alluvial fan with local lacustrine deposits
			Sugars Basalt	37-95	Basaltic flows and pyroclastics	Volcanic
			Weir Basalt	10	Basalt	Volcanic
		Blackwall Breccia	9	Sedimentary breccia	debris flow, scree deposit	
		Early to Mid Triassic	<i>(Lower part of Ipswich Basin sequence but not part of Ipswich Coal Measures)</i>		Brisbane Tuff	<250
	Chillingham Volcanics			100	Rhyolitic tuff, conglomerate	Volcanic
Early to Mid Triassic	Toogoolawah Group (Esk Trough)			~7300	Polymictic, pebble to cobble conglomerate, siltstone, shale, sandstone, minor crystal tuff and coal	Continental, fluvial
Unconformity						
Palaeozoic	Neranleigh-Fernvale Beds (South D'Aguillar Block)				Shale and mudstone (argillite), arenite, jasper, chert, spilitic metavolcanics	

 Indicates not part of the Ipswich Basin sequence but included in the Southeast Queensland stratigraphic succession.

The Kholo Subgroup

This Mesozoic non-coal bearing unit unconformably overlies the Palaeozoic Nerenleigh-Fernvale Beds of Devonian to Carboniferous age. It consists of approximately 360m of polymictic pebble and cobble conglomerate with minor breccia, tuff, basalt and agglomerate.

The accumulation of basin fills started with an eruption of basaltic lavas and deposition of thick layers of gravel in alluvial fans. Finer sediments and air-fall tuff accumulated in more tranquil inter-fan areas (Staines, 1995). According to Cranfield (1981) two episodes of volcanism occurred during the formation of the Kholo Subgroup, an earlier basal basaltic episode which formed the Sugar and Weir Basalts, and a later episode of volcanism that produced the Hector Tuff.

The Brassall Subgroup

This coal-bearing unit of the Late Triassic Epoch conformably overlies the Kholo Subgroup, and is in turn overlain by the Jurassic Woogaroo Subgroup. This unit contains approximately 720m of sandstone, siltstone and claystone (Falkner, 1986).

Two coal-bearing formations are present in the Brassall Subgroup. The lower unit, Tivoli Formation, contains sixteen stratigraphically important coal seams and the upper Blackstone Formation comprises seven major coal seams of economic significance. Detailed account of each coal seam is given in the “**Coal Seams**” section.

Figure 3 shows coals seams found in the Bundamba and North Ipswich mining areas. Figure 4 indicates boreholes used in this study. They include the NS-series Queensland Government diamond drillholes and the New Hope Mines boreholes. Figures 5 and 6 are location maps of old mines and recently closed down New Hope mines in the Ipswich coalfield. Figures 7 and 8 show detailed mine plans of Swanbank mines. Figure 9 is the satellite image of the part of southeast Queensland showing the study area.

This image is not available online. Please consult the hardcopy thesis available from the QUT library

Figure 3: Coal seams correlated by the Queensland Department of Mines and Energy in the North Ipswich and Bundamba Coalfields using previous mine records and the Mines Department drillhole data (Digital basemap courtesy of the Queensland Department of Mines and Energy, 1999)

This image is not available online. Please consult the hardcopy thesis available from the QUT library

Figure 4: Map showing drillholes used in this study (Source: Queensland Department of Mines and Energy, Resource Development Division, 1999) (See Appendix V, Ipswich Basin Borehole Location Plan for details)

This image is not available online. Please consult the hardcopy thesis available from the QUT library

Figure 5: Map showing town plan and some of the major mines in the Ipswich Basin (Source: Queensland Department of Mines and Energy, 1999, and New Hope Mines Ltd., 2000)

This image is not available online. Please consult the
hardcopy thesis available from the QUT library

Figure 6: Mines operated by New Hope Ltd in the Swanbank Lagoon area, Blackstone Formation (Source: New Hope Mines Ltd., 2000)

This image is not available online.
Please consult the hardcopy thesis
available from the QUT library

Figure 8: Bogside lowwall mine plan, Swanbank area, (grey shaded area represents completed mining) (use grids for scale) (Source: New Hope Mine Ltd., 2000)

This image is not
available online.
Please consult
the hardcopy
thesis available
from QUT library

Landsat image of the Ipswich Basin showing low relief
region surrounded by high relief terrain with densed
vegetation

Structural Elements

The northern and eastern edges of the basin are marked by the D'Aguiar Block and the Beenleigh Block (Day et al., 1975) (see Figure 10). The Triassic sedimentary rocks of the Ipswich Basin lie unconformably over the Palaeozoic metamorphic and volcanic rocks of the D'Aguiar and Beenleigh Blocks (Bowern, 1987). The overlying sedimentary rocks of the Nambour Basin cover the northeast limit of the Ipswich Basin. The West Ipswich Fault is the prominent structure in the western edge, while the southern edge is obscured by the overlying Moreton Basin sedimentary rocks. Cook (1975) stated that the Ipswich Basin is approximately 700Km² but Falkner (1986) and Day, Cranfield and Schwarzbock (1974) argued that the basin probably extends as far as Nymboida in the New South Wales (Figure 11).

The Ipswich Basin displays broad folding with northwest to north trends. Dips are generally shallow, but local steep dips occur adjacent to faults (Day et al., 1975).

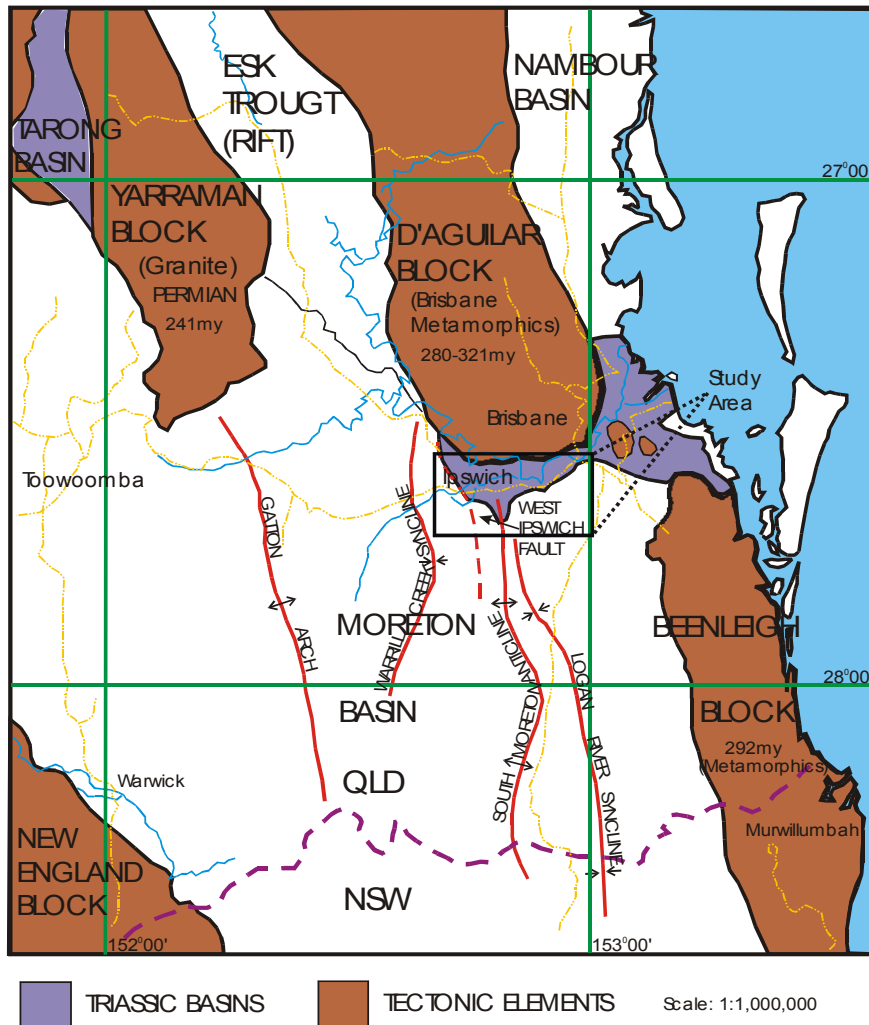


Figure 10: SOUTHEAST QUEENSLAND STRUCTURAL AND TECTONIC ELEMENTS
(After Saunders, 1983; Esso, 1974)

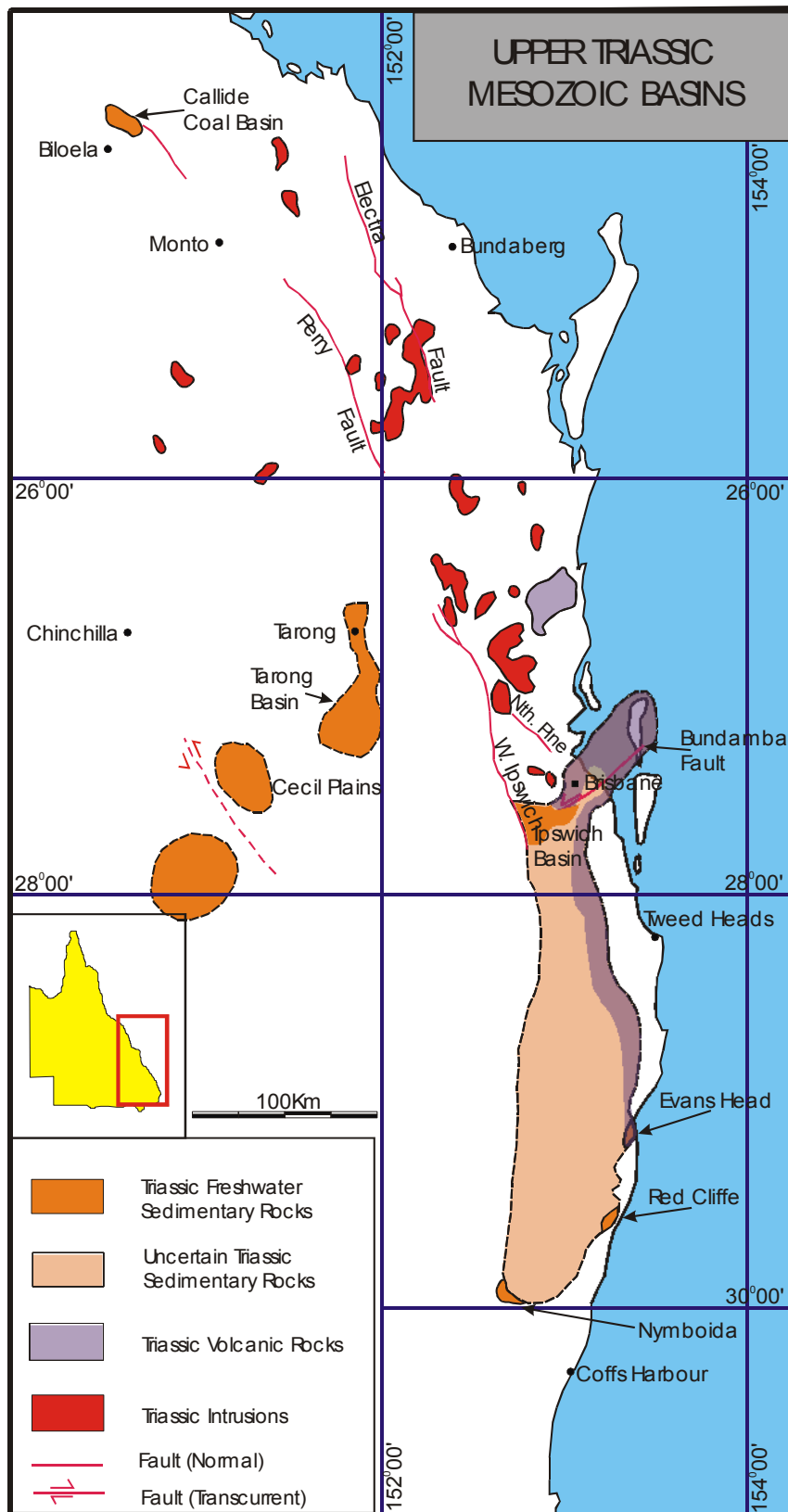


Figure 11: Triassic Mesozoic basins (Modified from Day, Cranfield and Schwarzbock, 1974)

Triassic Coal Basins

Global Tectonic Events in the Permo-Triassic Interval

The Permo-Triassic boundary initiated a palaeoclimatic regime of warm and humid climate even at high latitudes in Gondwanaland. These climatic conditions are different from the relatively cooler climatic conditions indicated by Permian coal seams similar to those coal seams formed in boreal aapamires and palsamires (Retallack, 1996). An event at the Permo-Triassic boundary also extinguished most peat-forming plant communities. At this time, Gondwana and Laurasia were subjected to accretion tectonism, which created uplifts, land deformations, and climatic changes (Faure et al., 1994). In addition, the greenhouse effect generated by the effusion of Siberian Traps (Veevers et al., 1994) and subsequent rising of extreme CO₂ level in the atmosphere which caused global warming (Hallam, 1985), may have prohibited the growth of certain plant communities. Under some conditions an increase in CO₂ can promote plant growth but the opposite effect may occur if the atmosphere contains excessive CO₂. The rise in CO₂ level also resulted from massive oxidation of organic carbon as indicated by the dramatic depletion in $\delta^{13}\text{C}$ isotope in organic matter (Retallack, 1997). The mass extinction associated with major climatic changes at the end of Permian Period largely affected the major peat accumulation and preservation of organic matter throughout the world. Thus, the Early Triassic Epoch was peculiar in lacking coal.

The cessation of coal accumulation was accompanied by a progressive decrease in the topographic relief of source areas in relation to basin morphology, change in climatic conditions and vegetation, rates of denudation, rates of response to tectonic subsidence and limitations of sediment dispersal (Jensen, 1975; Blair and Bilodeau, 1988). A combination of climatic changes and tectonic events has been cited as a cause of the absence of Early Triassic coal in the Sydney Basin (McElroy, 1969a).

The Permo-Triassic Interval tectonic events were followed by the Triassic tectonic regime which reshaped major continents and established new sedimentation patterns.

In the early Mesozoic Era, breakup of the supercontinent Pangea occurred with initial rifting between Laurasia and Gondwana. This event was followed by the two stages of separation of the Gondwana continent in the Late Triassic Epoch (Miller, 1999). Firstly, Australia, Antarctica and India separated from Africa and South America. Then, India separated from Australia and Antarctica. The subsidence occurred after the breakup of Pangea and created the Gondwana basins of India (Kailasham, 1976). Similarly, Late Triassic basins developed after the breakup of Gondwana land (Ziegler, 1977, 1978, 1982, 1987 and 1988).

The Late Triassic Ipswich Coal Measures mark the resumption of deposition in east Australia after folding of the early Ladinia Moolayember (Mid Triassic Epoch) and older strata to the west (Veevers et al., 1994). This coal formation coincided with other coal accumulations in Australia, including Tarong and Callide Basins in Queensland, Leigh Creek in South Australia, and in Tasmania (Figures 11 and 12), and also in the world such as Karoo Basin (South Africa), Central Transantarctic (Retallack, 1977a), and in peninsular India. Veevers et al. (1994) characterized this event as the Carnian singularity in Pangea history. It was a change from the greatest aggregation after the collision of Cimmeria with Asia (Indosinian Orogeny), to incipient dispersal with the onset of rifting that prefigured the Atlantic and Indian Oceans. Busby and Ingersoll (1995) identified sedimentary sequences of intercratonic basins in North America, Africa, Europe, and South America. These sequences show similar age for interregional unconformities that separate intercratonic sedimentary sequences, and similar trends in thicknesses and volumes. This similarity of formation from both North America (earliest Palaeozoic) and Eurasia (early Mesozoic) intercratonic basins implies large-scale tectonic processes that caused both rifting and thermal subsidence.

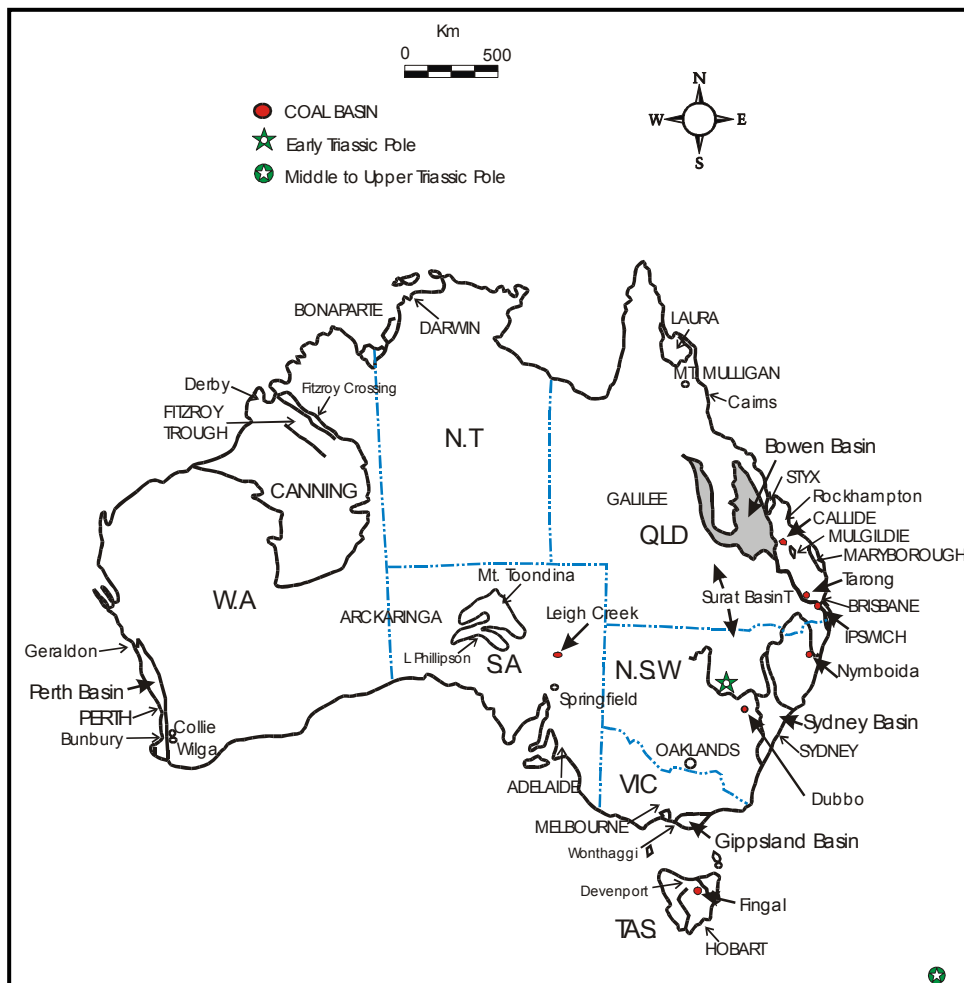


Figure 12: Australian Triassic coal basins with Triassic poles (After Cook, 1975, Smyth, 1980)

Formation of Continental Triassic Coal Basins in Eastern Australia

The Mesozoic intermontane basins of eastern Australia, including the Tarong, Callide and Ipswich Basins, developed during the post-orogenic phase of the Tasman Orogenic Zone (Galligan, 1979) (Figures 11 and 12). Following a brief compressional phase in the Mid Triassic Epoch, the tensional period began in the Late Triassic Epoch with the development of a number of small infra-basins (Ties et al., 1985). The Ipswich and Tarong Basins formed after the rifting of Nerenleigh-Fernvale Beds by right lateral transtension (Veevers et al., 1994). A transpressive movement at the end of Mid Triassic Epoch deformed the Toogoolawah Group before extension led to the deposition of the Carnian Ipswich Coal Measures.

A new pattern of sedimentation was established in eastern Australia during the Late Triassic Epoch. Felsic tuff, basaltic lavas and dykes, and coal were deposited with fluvial sediments. Aerially restricted coal measures accumulated in the Ipswich, Tarong, Callide, and an unnamed shallow basin near Cecil Plains about 100km southwest of Tarong (Day et al., 1975). The Nymboida Coal Measures (~1050m thick), Red Cliff Coal Measures (~600m thick), and Evans Head Coal Measures (45m+ thick) in northern New South Wales also show similar age and lithology to the Ipswich Coal Measures. They were correlated with the Ipswich Coal Measures by McElroy (1962 and 1969) and Scott (1982) based on lithological and palynological evidence. The Evans Head Coal Measures contain thin (<1m) but high vitrinite (>70%) coal seams, namely, the Upper Iron Gates, Middle Iron Gates and Lower Iron Gates seams. They were formed in the fluvial environment with meandering channel systems. The dominant floras were *Dicroidium* species which define the Yabeilla Opper-zone (Scott, 1982). The Tarong Basin contains a much thinner sedimentary succession than the Ipswich Basin. The Tarong coal has been palynologically dated by de Jersey (1970) as equivalent to the Tivoli Formation. However, there is no evidence of contemporaneous volcanism as in Ipswich, Callide and Evans Head Coal Measures. Coal deposition in the Ipswich Basin was accompanied by frequent volcanism. Therefore, the Ipswich Coal Measures contain numerous intraseam tuffaceous claystone (tonstein) bands. However, no significant separate interseam tuff unit has been recorded in the coal-bearing Brassall Subgroup. Tuff bands are mainly contained in coal seams intraseam claystone bands. The Chillingham Volcanics (Early-Mid Triassic), which formed the lower part of the Ipswich Basin sequence, was produced by widespread volcanism. This was followed by the formation of Brisbane Tuff before the deposition of Late Triassic Kholo Subgroup. The lower part of Kholo Subgroup also contains the volcanic units such as Weir Basalt and Sugar Basalt. The Hector Tuff (air fall tuff) was deposited before the formation of Cribb Conglomerate. The Brassall Subgroup overlies the Kholo Subgroup (see Table 1). Forsyth (1989) stated that, like in Ipswich, peat-mires proximity to fluvial systems in the Tasmanian basin were also affected by fluvial incursion and channel migration.

Furthermore, Ward (1984) noted that Mesozoic coal-bearing sequences of the Southern Hemisphere (eg. eastern Australian coal basins) are mainly of fluvial and deltaic origin, and thus, do not contain the same abundance of marine beds as those of the Northern Hemisphere Carboniferous successions. In contrast to the Permian coals in Australia, the Triassic coal basins formed in high latitudes, such as the Ipswich Basin (70⁰S), do not show any marine connection.

Coal Seams

Coal seams in the Ipswich Coal Measures commonly split and coalesce in different combinations and contain numerous intraseam clastic bands. The most common lithotype is banded bright coal but it is varied. Brightness profile patterns are usually oscillating and kaolinite-rich tonstein bands dominate the intraseam lutites (Chern, 1997).

Characteristics of major coal seams in the Tivoli and Blackstone Formations were studied in order to identify the patterns of coal sedimentation and to have an understanding of the major controlling factors on coal accumulation within the basin.

Tivoli Formation

There are at least twenty-one seams, which have been recorded in the Tivoli Formation, but only sixteen widespread and/or stratigraphically significant seams were included in this study for seam thickness and structural contouring. All the seams in descending stratigraphic order are shown in Table 2 with the Waterworks seam at the base and the Cochrane seam at the top. Depths are from drillholes at a variety of places, and thus, these depths are not related to stratigraphic positions.

Table 2: Major coal seams in the Tivoli Formation (Cochrane – Youngest seam, Waterworks – Oldest seam)

Seam Name	Depth (m)			Thickness (m)			Number of Drillholes	Other Name(s)
	Average	Maximum	Minimum	Average	Maximum	Minimum		
Cochrane	120.84	690.47	2.00	3.73	27.99	<0.1	359	Lindsay's Hard
Unnamed	105.77	438.68	13.87	4.63	15.90	0.61	28	
CL	31.31	64.00	5.49	3.27	1.44	4.57	9	
Ritchie#	102.12	340.66	Surface	2.13	4.03	0.40	139	
Taylor#	84.22	248.43	13.73	1.56	2.75	0.30	59	
Livermore#	85.51	230.30	16.49	2.38	4.10	0.95	55	
Matthews#	142.06	204.10	67.00	1.12	3.70	0.40	7	
Hillier#	275.00	N/A	N/A	1.35	N/A	N/A	1	
Garden	81.34	171.75	5.18	4.45	19.53	<0.1	47	
Westfalen Top	59.73	117.83	16.28	8.38	29.39	<0.1	44	Garden-Tantivy
Tantivy	122.06	282.83	4.57	3.42	10.06	<0.1	57	
Fiery	145.28	300.76	18.69	4.49	25.60	<0.1	82	Chuwar
Waterstown	122.28	277.44	19.61	3.95	15.47	<0.1	83	
Unnamed 2	158.00	327.89	58.45	4.58	38.07	<0.1	53	
Tivoli	209.31	343.43	23.77	3.67	12.85	0.38	47	
Poverty*	273.35	355.60	147.27	2.65	9.63	0.30	13	
Eclipse	241.77	378.89	48.26	3.74	14.17	<0.1	52	
Francis*	353.79	435.15	270.84	0.98	1.80	<0.1	3	
Benley	304.78	479.27	41.05	7.01	18.21	<0.1	30	
Morris*	365.56	489.51	10.87	3.16	6.88	0.33	5	
Waterworks**	78.44	525.20	14.43	22.70	30.58	16.15	10	

(#Only found in Swanbank mining area)

(*Relatively small, **very banded and inferior coal)

Blackstone Formation

Seven main coal seams have been identified in the Blackstone Formation (eg. Denmead, 1955, Mengel and Carr, 1969). These seams in descending order are shown in Table 3. It should be noted that seam depths are recorded from depth at which a borehole intersected a seam. Therefore, the average seam depths for some of the seams in the higher stratigraphic order are deeper than the average depths for seams in the lower stratigraphic order. For example, the average depth for the Thomas seam is deeper than the Aberdare seam. This is due to the absence of the Thomas seam in an area where the Aberdare seam was intersected at shallow depth. The Thomas seam may have been eroded and replaced by Tertiary sediments. The average seam depth is therefore, entirely dependant on the location of boreholes and not related to stratigraphic order.

Table 3: Major coal seams in the Blackstone Formation (Thomas – Youngest seam, Rob Roy – Oldest seam)

Seam Name	Depth (m)			Thickness (m)			Number of Drillholes	Other Name(s)
	Average	Maximum	Minimum	Average	Maximum	Minimum		
Thomas	362.43	624.74	35.89	8.17	20.73	0.86	53	
Aberdare	249.52	670.81	3.85	5.18	11.28	0.15	108	
Bluff	218.98	704.62	2.70	7.68	22.83	<0.1	270	
Fourfoot	241.37	719.81	2.00	4.29	14.76	<0.1	284	Fourfeet/ Wright/ New Chum
Bergin	234.26	765.30	Surface	4.20	15.21	<0.1	297	Lagoon
Striped Bacon*	199.57	813.18	0.75	2.52	11.89	<0.1	172	
Rob Roy*	152.60	663.07	Surface	4.30	21.89	<0.1	292	

(*The Striped Bacon and Rob Roy commonly combine and form a single seam containing numerous tuffaceous claystone bands. The Rob Roy is the oldest and The Thomas is the youngest in the stratigraphic order)

Table 4 summarises the total interburden and coal thicknesses in three major mining areas within the Ipswich Basin.

Table 4: Total interburden thicknesses and total coal thicknesses

Area	Bundamba Mining Area	North Ipswich Mining Area	Swanbank Mining Area
Interval	Top of Rob Roy to base of Thomas	Top of Waterworks to base of Cochrane	Top of Hillier to bottom of City Lower
Total Interburden Thickness	144m	452m	236m
Interval	Rob Roy to Thomas	Waterworks to Cochrane	Hillier to City Lower
Total Coal Thickness	36m	82m	12m
Average Seam Thickness	5m	5m (including Waterworks seam) 4m (excluding Waterworks seam)	2m

(Note: All these figures are approximate)

Average seam depths were used when interburden depths were not available.

Average bottom depth of City Lower seam = 35m

Average top depth of Ritchie seam = 102m

Thus, average interburden thickness between two seams = 68m

Average bottom depth of Matthews seam = 143m

*Average top depth of Hillier seam = 275m

Thus, average interburden thickness between two seams = 132m

(*Hillier seam depth is recorded in only one drillhole)

Average bottom depth of Westfalen Top seam = 68m

Average top depth of Tantivy seam = 122m

Thus, average interburden thickness between two seams = 54m

The Waterworks seam is the thickest seam in the Tivoli Formation, but it is very banded and contains poor quality coal. Therefore, the seam is not economically minable. However, inclusion of the Waterworks can significantly change the average seam thickness of the Tivoli Formation.

The Swanbank area seams have been separated from the Tivoli Formation (North Ipswich Area) because they are very localised and found only in New Hope mines (Bundamba Area). They are not generally recognized across the basin.

Figure 13 shows the stratigraphic column of seams in the Tivoli Formation in the New Hill mine area. Figure 14 shows the schematic seam splitting of the Tivoli Formation including seam thicknesses and interburden thicknesses.

Figures 15 and 16 are stratigraphic columns of main seams in the Blackstone Formation in the Bundamba and Swanbank areas. Figure 17 shows splitting and jointing of seams in various combinations in the Blackstone Formation. Figure 18 shows comparison of seams in the Tivoli and Blackstone Formations in the Box Flat and Westfalen mines.

This image is not available online. Please consult the hardcopy thesis available from the QUT library

Figure 13: New Hill Mine general stratigraphic column (Source: New Hope Mines Ltd)

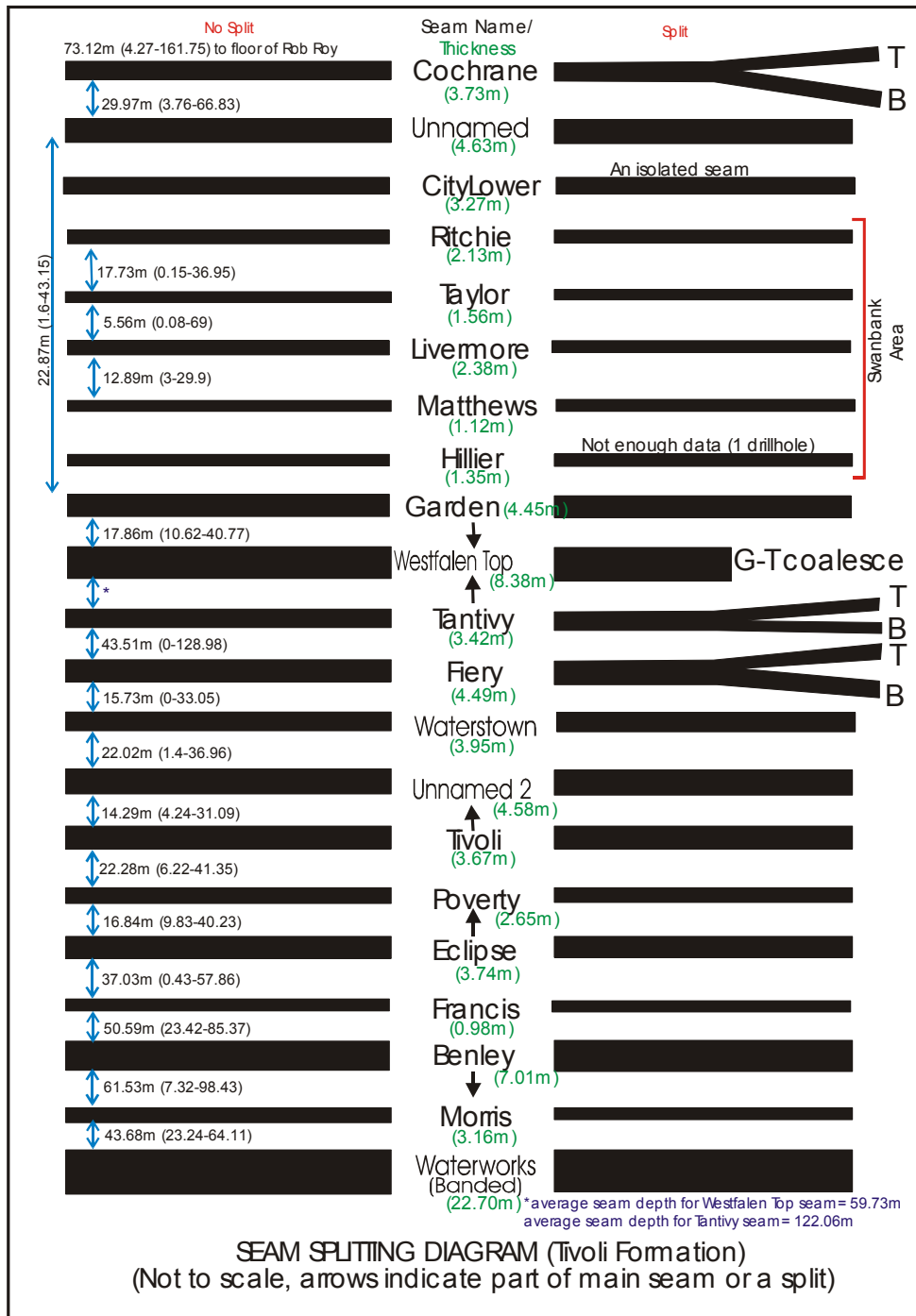


Figure 14: Schematic seam splitting-Tivoli Formation (not to scale)
(Note: most of the seams have no splits or they are named as individual seams such as Unnamed and Westfalen Top, see ‘Discussion’ section for detailed explanation of seam splitting)

This image is not available online. Please consult the hardcopy thesis available from the QUT library

Figure 15: General stratigraphic column of the Blackstone Formation in the Ipswich coalfield (Bundamba area) (not to scale) (Source: Queensland Geological Services Pty Ltd)

This image is not available online. Please consult the hardcopy thesis available from the QUT library

Figure 16: Blackstone Formation (Swanbank area) general stratigraphic column (note the coarsening upward sequence) (Source: New Hope Mines Ltd)

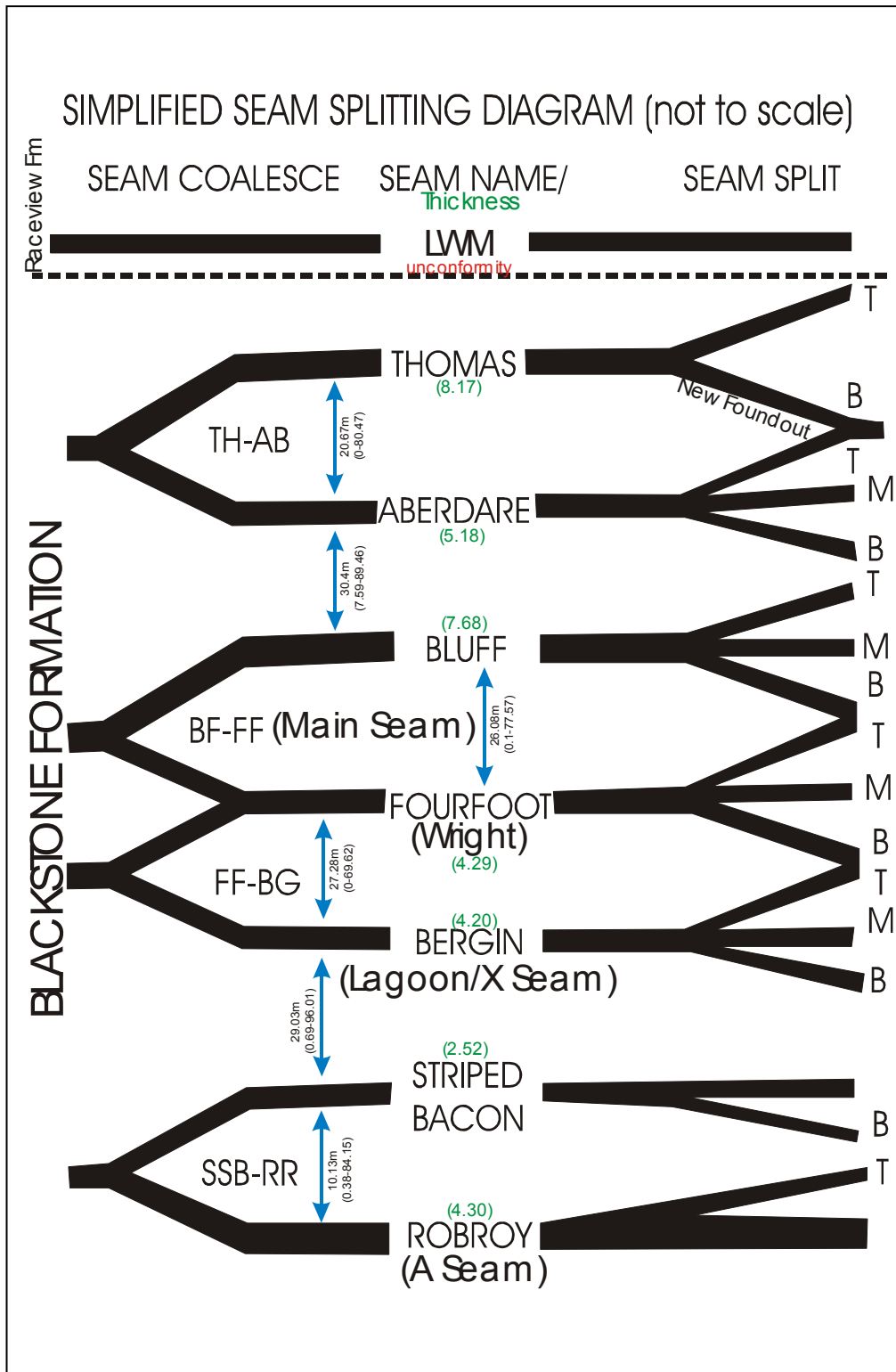


Figure 17: Schematic seam splitting-Blackstone Formation, showing average, minimum and maximum interburden thicknesses for main seams. Seam splits are highly variable and discontinuous and therefore, interburden thicknesses for splits are not described here (not to scale) (T=top, M=middle, B=bottom) (After Falkner, 1986)

This image is not available online. Please consult the hardcopy thesis available from the QUT library

Figure 18: Box Flat Mine area and Westfalen Mine Area stratigraphic columns (for comparison only, not to scale) (Source: Queensland Geological Services Pty Ltd)

Coal Seam Characteristics and Lithotypes

Lithotypes in coal generally represent a broad spectrum of depositional environments from arboreal forest swamps to dry, herbaceous and shrubby marshes (Lamberson et al., 1991). The bright and banded bright coals generally represent wet forest swamps, whereas dull and banded dull coals reflect various types of environment, such as drier phase of deep water swamps, dry forest swamps, open marshes and clastic marshes. For example, the *Taxodium* peat of Okefenokee Swamp (Georgia, U.S.A) formed from *Taxodium* plant species, has a high proportion of twig and leaf litter and commonly contains abundant charcoal (Cohen, 1973). This type of plant community tends to produce banded dull coal (eg. duroclarain). Compositional differences between lithotypes are mainly caused by the vegetational characteristics, as well as differences in the rate of accumulation and decomposition of plant material. The lateral and vertical variations in lithotypes are controlled by hydrological factors such as groundwater level and proximity to an active fluvial system. However, abrupt facies changes are more likely to be due to abrupt events such as channel avulsions and fires (Falcon and Snyman, 1986). The patterns and distribution of coal facies provide an indication of ancient wetland environments.

Brightness Profiles

Total of twenty-one highwall brightness profiles from the Bluff, Fourfoot, Bergin, Striped Bacon and Rob Roy seams were drawn to study the nature of seam lithotype and internal seam architecture (see Figure 19 for location and Figures 20 to 31 for brightness profiles). Lithotypes mainly contain banded bright coal with claystone, siltstone, carbonaceous shale, mudstone and in some places dull bands. However, the brightness profiles are highly variable and they do not display any consistently identifiable patterns such as brightening upward and/or dulling upward successions. They generally show oscillating bright and dull bands, with the bright being the dominant lithotype. The oscillating patterns suggest oscillating water cover in the wet forest swamp environment. Striped Bacon-Rob Roy brightness profiles contain abundant tuffaceous claystone bands which is indicative of the frequent volcanism.

In addition, twenty-eight brightness profiles were generated from New Hope Mines borehole logs to compare with highwall brightness profiles (see Appendix I). They include the Bluff, Fourfoot, Bergin, Striped Bacon, Rob Roy, Cochrane, Ritchie, Taylor, Livermore, Matthews, and Hillier seams. Table 5 shows statistical analysis of each borehole brightness profile. In contrast to the highwall brightness profiles, the borehole brightness profiles show more dull components with general dulling upward successions. This may be partly due to the high content of detrovitrinite in the groundmass. The heterogeneous type groundmass usually produces dull appearance with very thin bright bands even though the total vitrinite content is high. It is important to note that I have

mapped all highwall brightness profiles, whereas borehole brightness profiles were logged by geologists from the New Hope Mines. This may create variations in highwall and borehole brightness profiles. The Bluff seam profiles are mainly dull, for example, in borehole number C5003 it contains 69.58% dull bands and in C5206, dull component is 68.78%. The Fourfoot seam brightness values vary and lithotypes show oscillating patterns. The seam contains 73.33% dull component in borehole C5003, but in C5650 it shows 60.10%, 60.74% and 65.19% bright components in top middle and bottom parts of the seam, respectively. In general, the Cochrane seam shows slightly more dull bands, but the Ritchie seam contains abundant bright bands. Other localised seams such as the Taylor, Livermore, Matthews, and Hillier seams appear to have dull bands only.

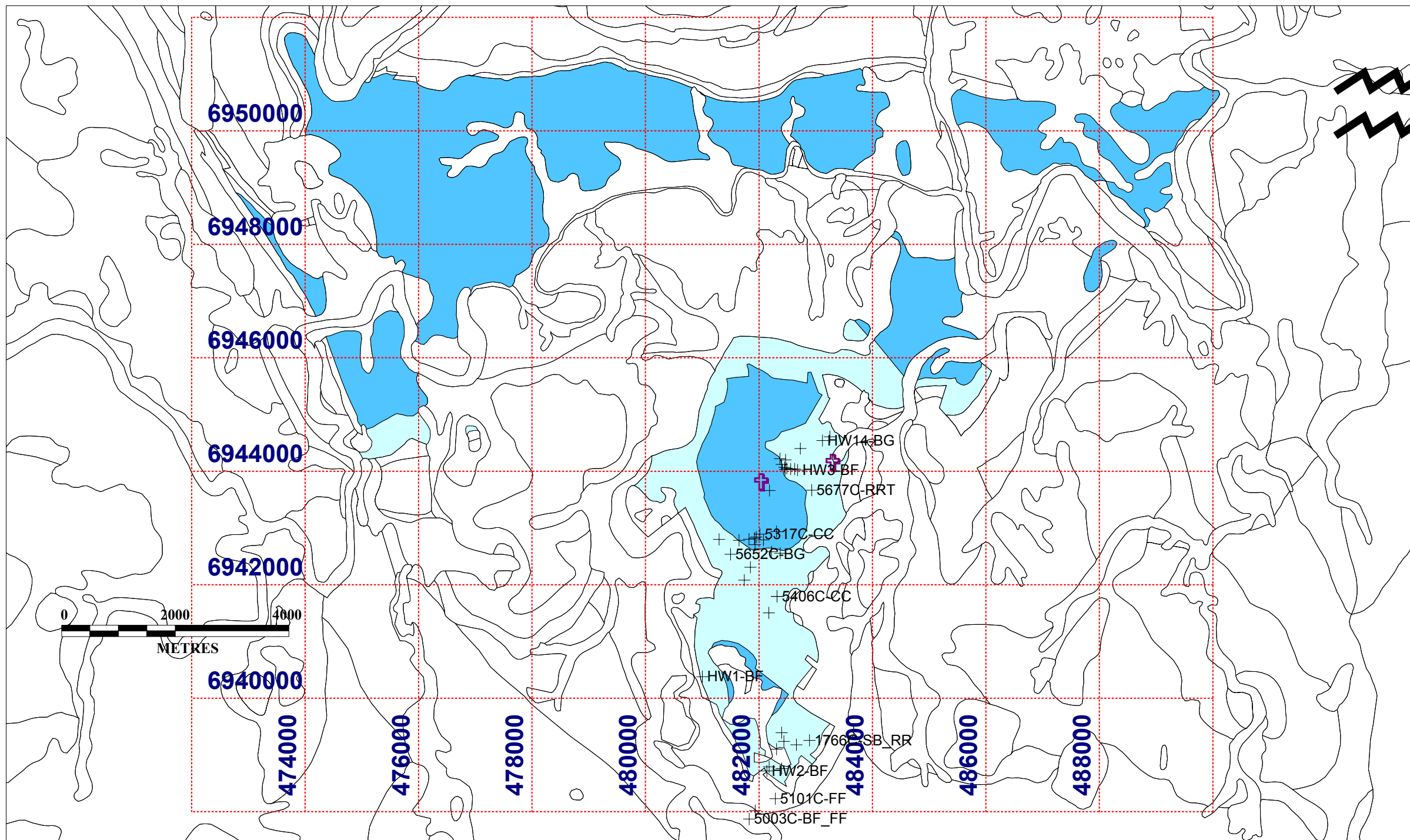


Figure 19: Brightness profile locations (HW = highwall brightness profile, 5003C = drillhole number, BF = Bluff, FF = Four Foot, BG = Bergin, SB = Striped Bacon, RR = Rob Roy, RRT = Rob Roy Top, CC = Cochrane, RIT = Ritchie, TAY = Taylor, LIV = Livermore, MAT = Matthews, HIL = Hillier, eg. HW1-BF = Highwall Brightness Profile 1-Bluff Seam, 5003C-BF_FF = Hole 5003C-Bluff and Four Foot Seams) (Also see Appendix I)

Highwall Brightness Profiles

Table 5 summarises the statistical data of highwall brightness profile lithotypes. The table shows the bright and dull components of each brightness profile with and without intraseam clastic bands (Stone). The bright components largely dominate the lithotypes as illustrated in Figures 20 to 31.

Table 5: Highwall brightness profiles summary statistics

	Stone	Dull (0-40%)	Bright (40-100%)
Highwall Profile 1	18.54%	3.01%	78.45%
Normalised to 100% without Stone	0	3.70	96.30
Highwall Profile 2	22.25%	11.25%	66.50%
Normalised to 100% without Stone	0	14.47	85.53
Highwall Profile 3	10.53%	0.00%	89.47%
Normalised to 100% without Stone	0	0	100
Highwall Profile 4	20.40%	0.00%	79.60%
Normalised to 100% without Stone	0	0	100
Highwall Profile 5	13.25%	5.30%	81.46%
Normalised to 100% without Stone	0	6.11	93.90
Highwall Profile 6	7.83%	0.00%	92.17%
Normalised to 100% without Stone	0	0	100
Highwall Profile 7	10.38%	0.00%	89.62%
Normalised to 100% without Stone	0	0	100
Highwall Profile 8	24.21%	0.00%	75.79%
Normalised to 100% without Stone	0	0	100
Highwall Profile 9	14.45%	0.00%	85.55%
Normalised to 100% without Stone	0	0	100
Highwall Profile 10	5.85%	0.00%	94.15%
Normalised to 100% without Stone	0	0	100
Highwall Profile 11	3.57%	0.00%	96.43%
Normalised to 100% without Stone	0	0	100
Highwall Profile 12	35.53%	24.67%	39.80%
Normalised to 100% without Stone	0	38.27	61.73
Highwall Profile 13	15.35%	0.00%	84.65%
Normalised to 100% without Stone	0	0	100
Highwall Profile 14	30.30%	0.00%	69.70%
Normalised to 100% without Stone	0	0	100
Highwall Profile 15	4.79%	0.00%	95.21%
Normalised to 100% without Stone	0	0	100
Highwall Profile 16	0.00%	0.00%	100.00%
Normalised to 100% without Stone	0	0	100
Highwall Profile 17	1.35%	0.00%	98.65%
Normalised to 100% without Stone	0	0	100
Highwall Profile 18A	0.00%	16.75%	83.25%
Normalised to 100% without Stone	0	16.75	83.25
Highwall Profile 18B	99.09%	0.00%	0.91%
Normalised to 100% without Stone	0	0	100
Highwall Profile 19	24.80%	16.00%	59.20%
Normalised to 100% without Stone	0	21.28	78.72
Highwall Profile 20	28.94%	5.53%	65.53%
Normalised to 100% without Stone	0	7.78	92.22
Highwall Profile 21	79.68%	1.40%	18.91%
Normalised to 100% without Stone	0	6.89	93.06

0 – 40% = coal contains zero to forty percent bright bands
 40 – 100% = coal contains forty to hundred bright bands

LEGEND	
D	<1% bright
Dm	<10% bright
DB	10 – 40% bright
IB	40 – 60% bright
BB	60 – 90% bright
BR	>90% bright

These brightness profiles are diagrammatic only and not to scale. Please use top and bottom depths shown on the right hand side of profiles (eg. 0.00cm to 103.00cm) to estimate the thickness of profiles and lithotype layers.

Datcol software application was used to produce these highwall brightness profiles. Arrows with numbers (eg. 2A) indicate petrographic samples. See Figure 19 for location.

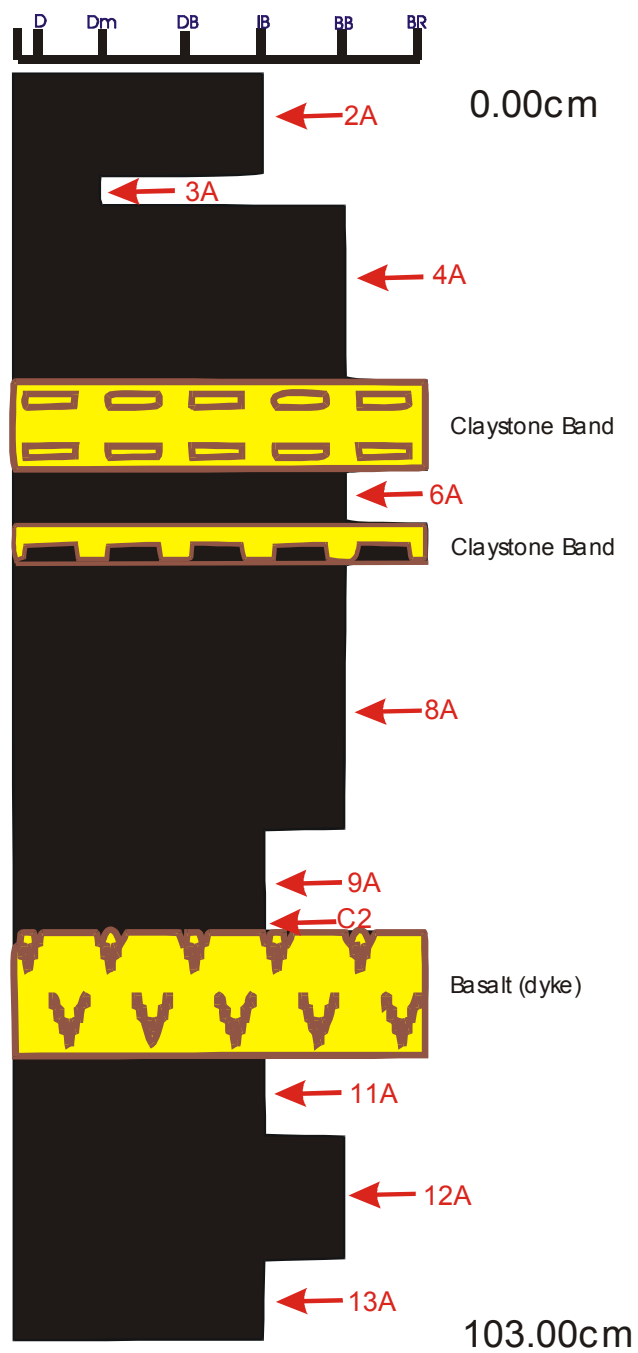


Figure 20: Bluff seam brightness profile (Boxflat Open-cut)

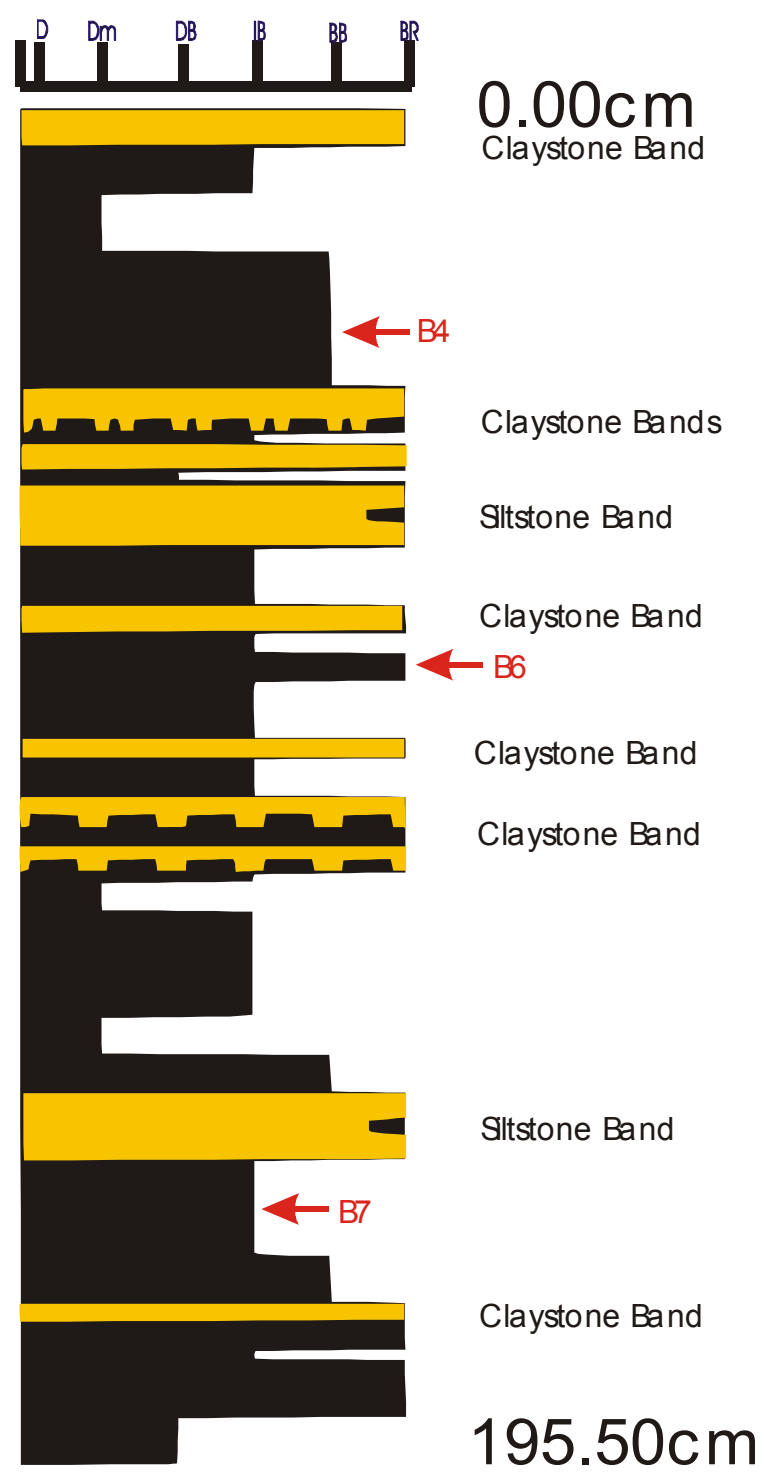


Figure 21: Bluff seam – Western Leases (New Hope Mines)

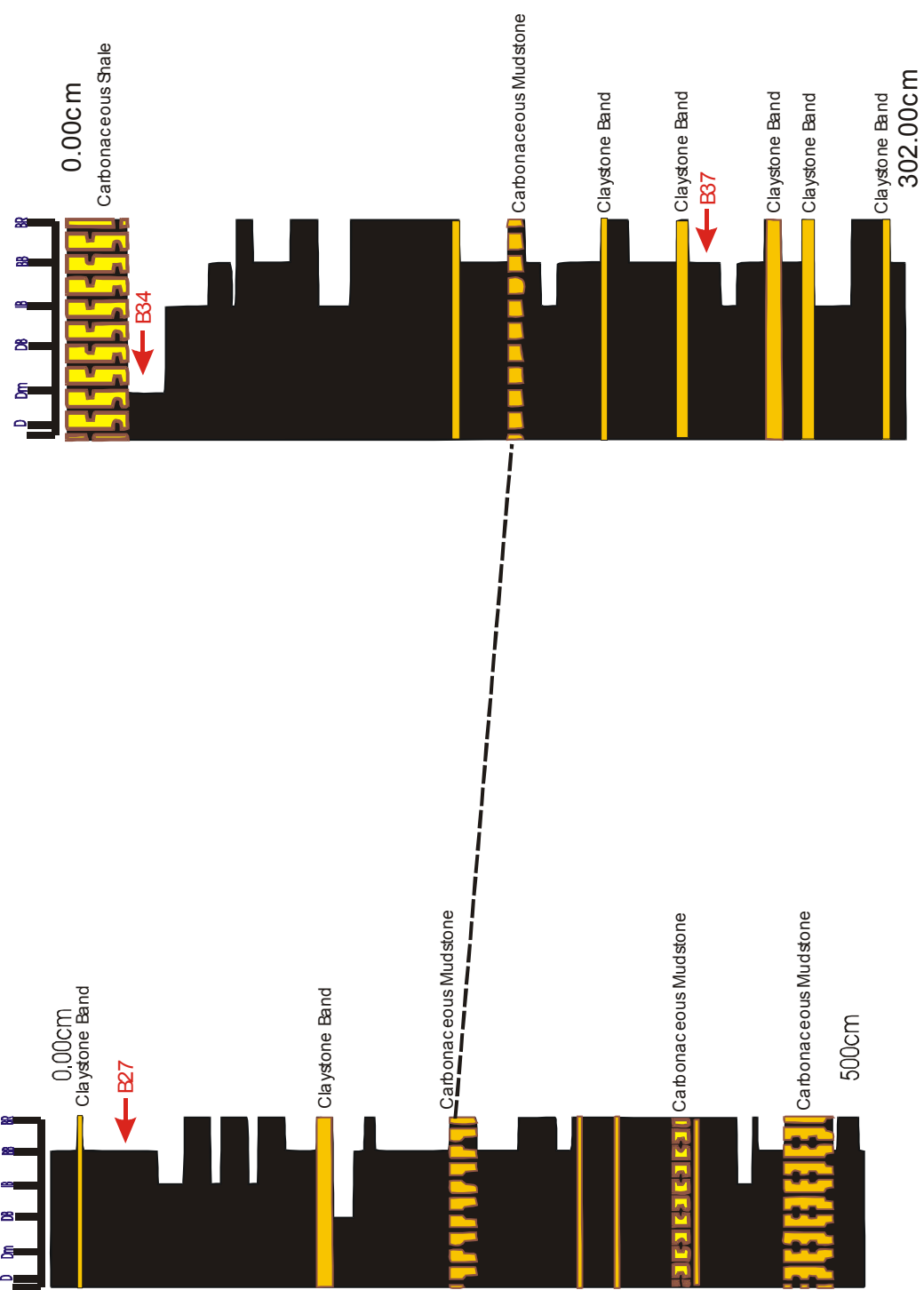
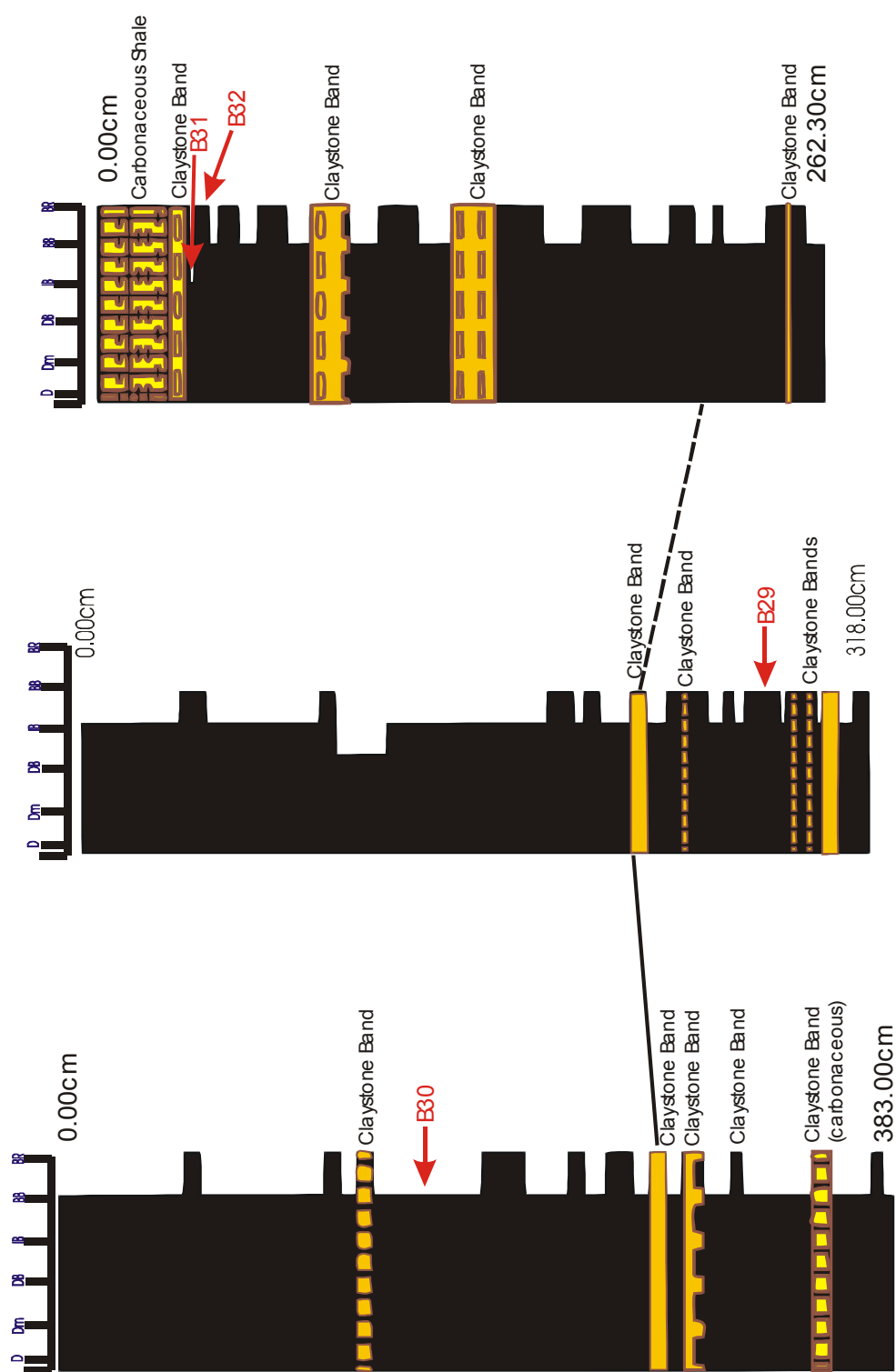
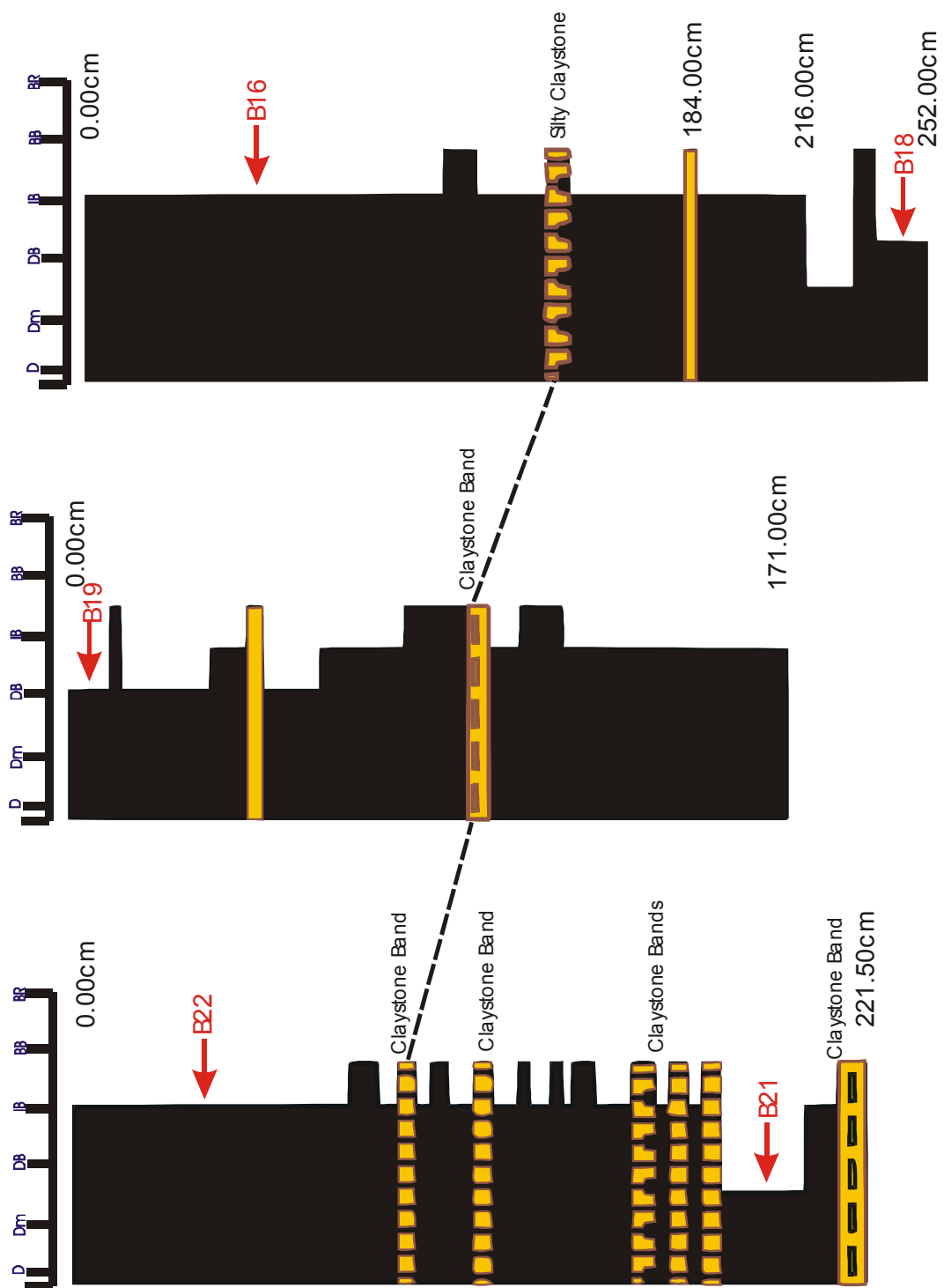


Figure 22: Bluff seam, Outcrop 'A' and outcrop 'AA'
Wattle Glen North (New Brick)



**Figure 23: Bluff seam, Outcrops 'D', 'C' and 'B'
Wattle Glen (New Brick)**



**Figure 24: Bluff seam, Outcrops 'G1', 'G' and 'E'
Wattle Glen North (New Brick)**



Figure 25: Bluff Bottom seam, Wattle Glen North (New Brick)

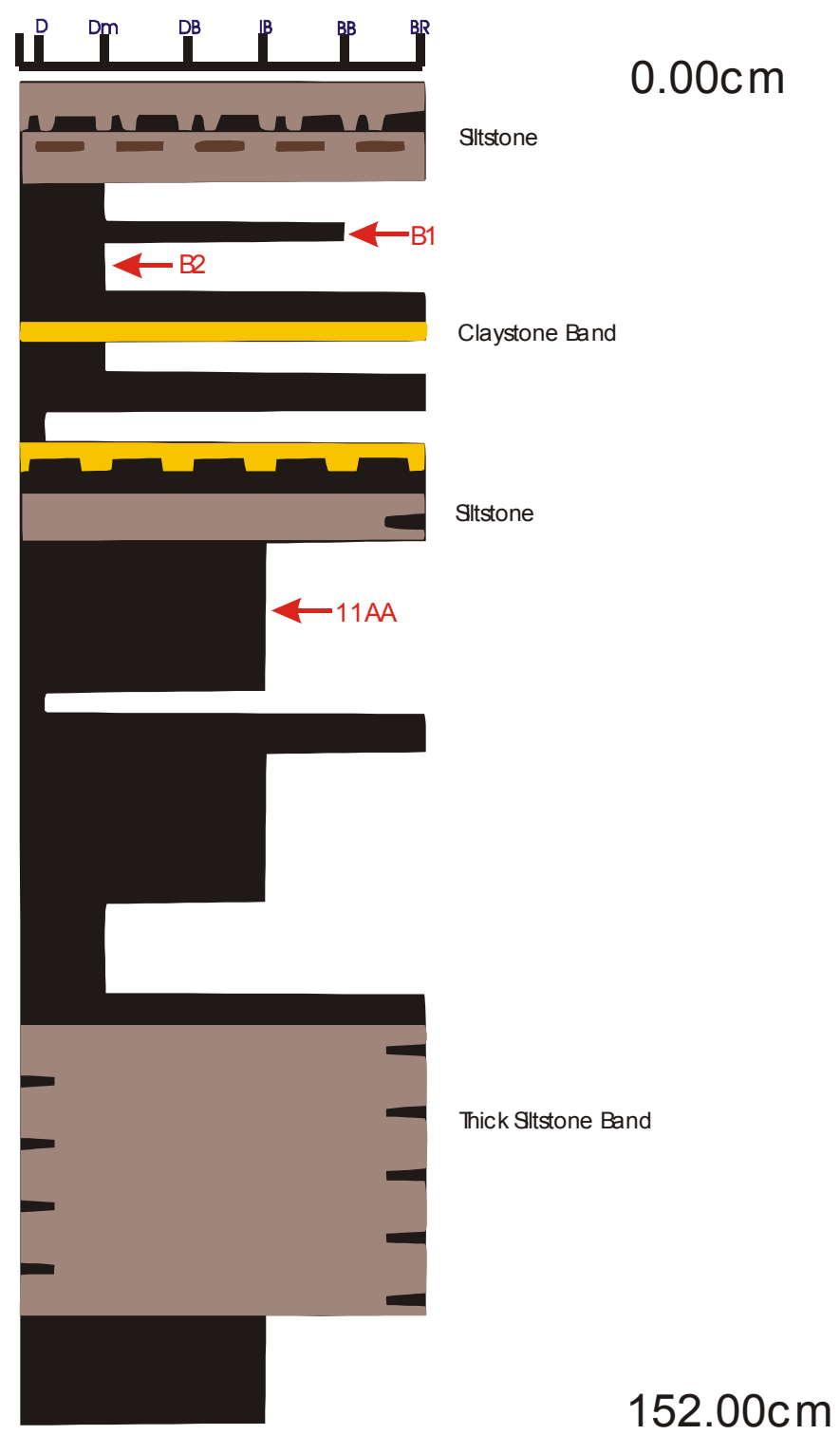


Figure 26: Fourfoot seam (Wright seam), Western Leases (New Hope Mines)

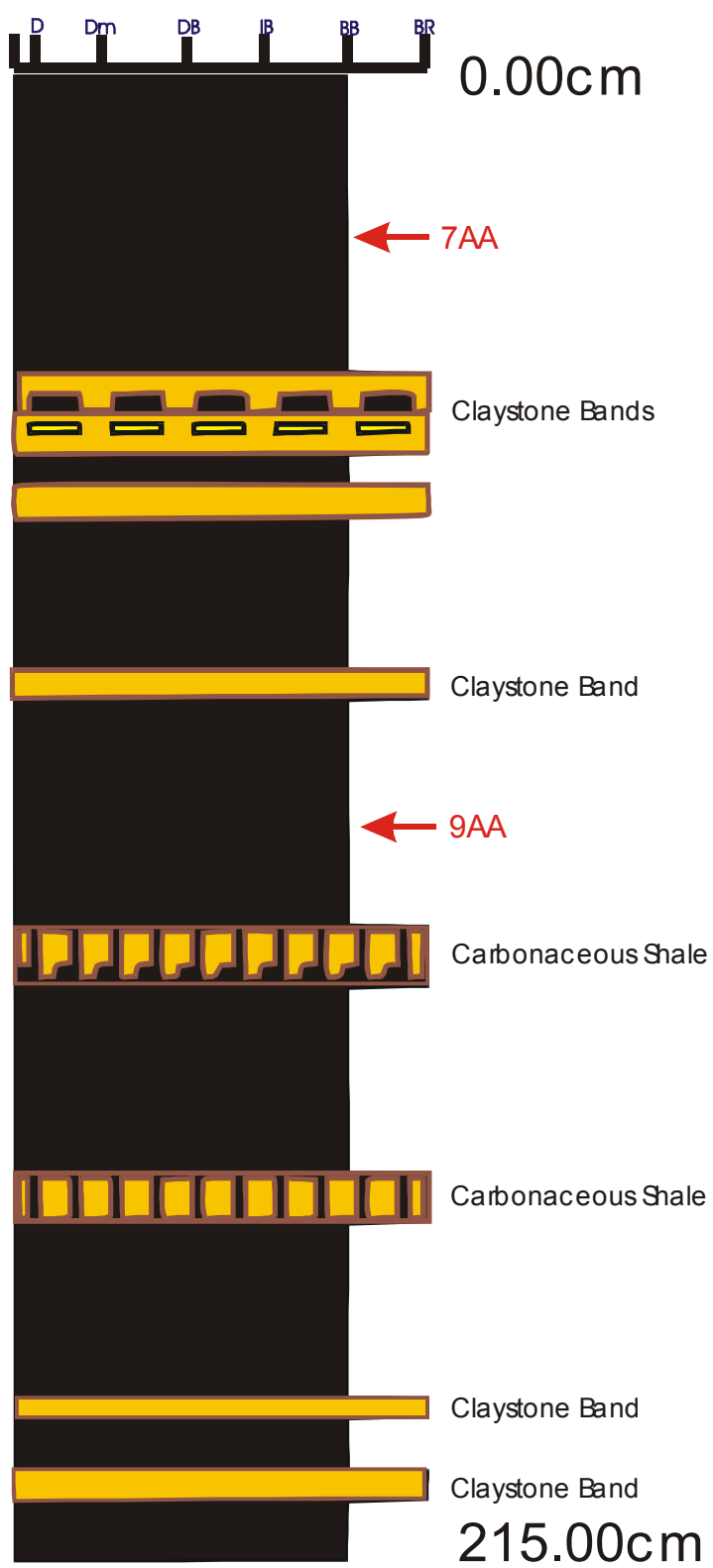


Figure 27: Bergin (Lagoon) seam, Western Leases (New Hope Mines)

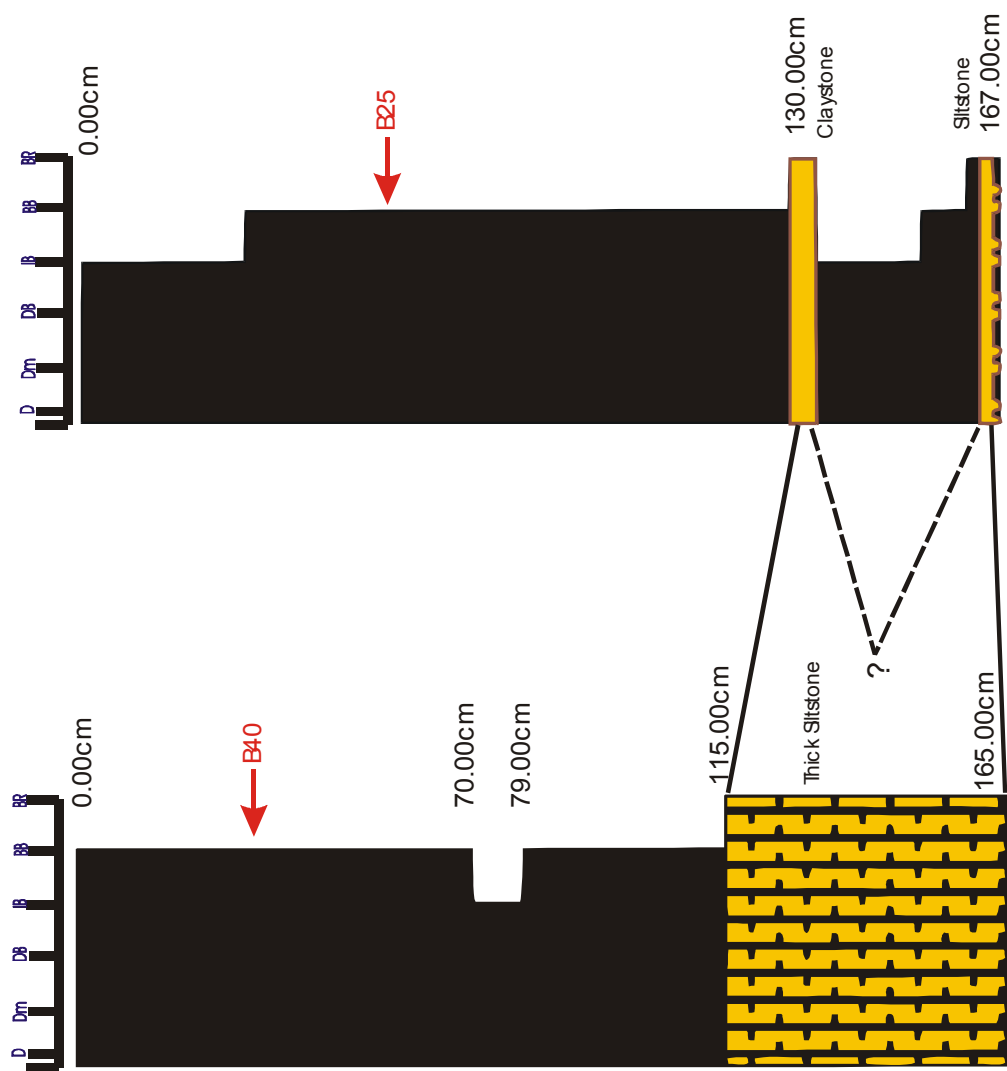


Figure 28: Bergin seam, Wattle Glen North (New Brick)
A small outcrop near Rhondda Road

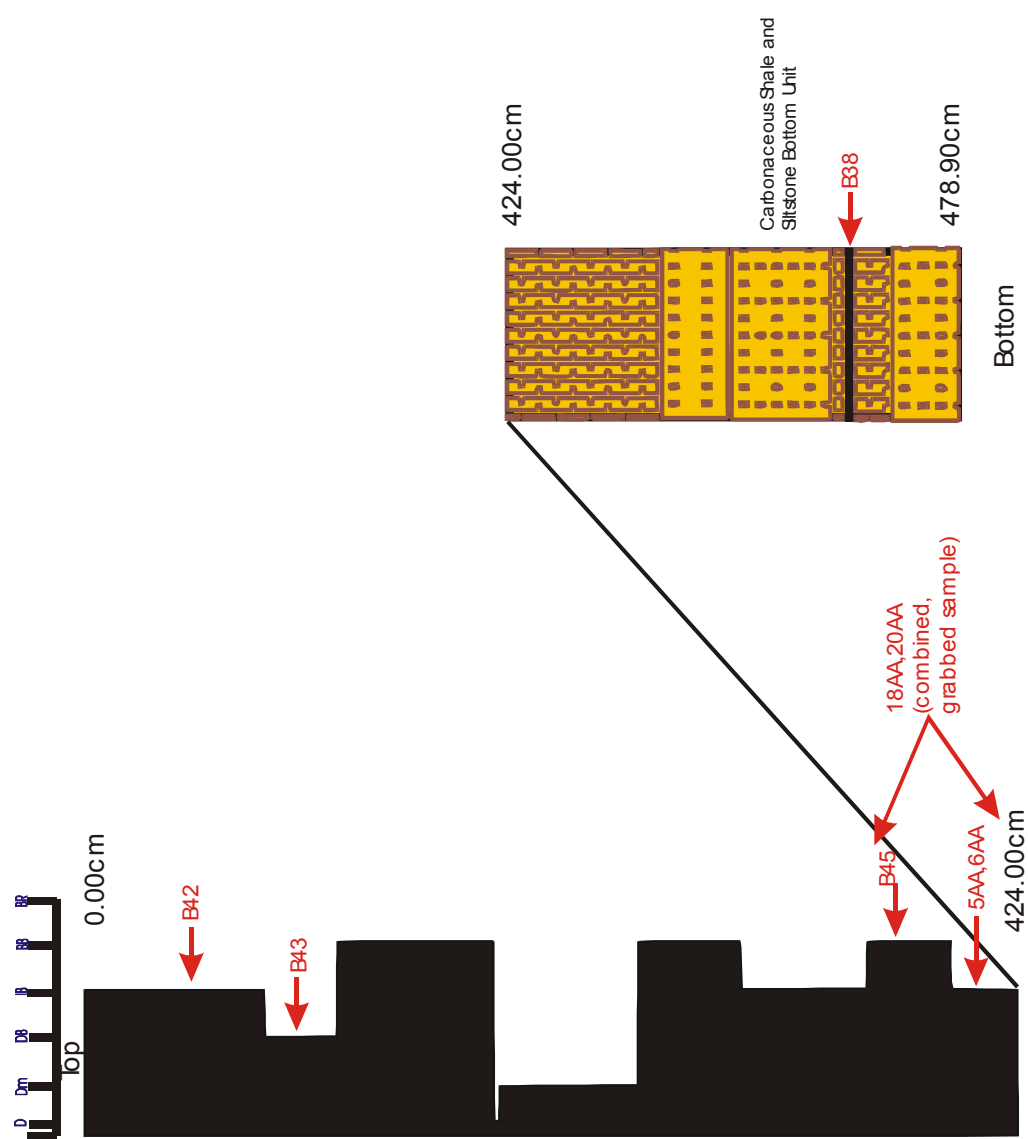
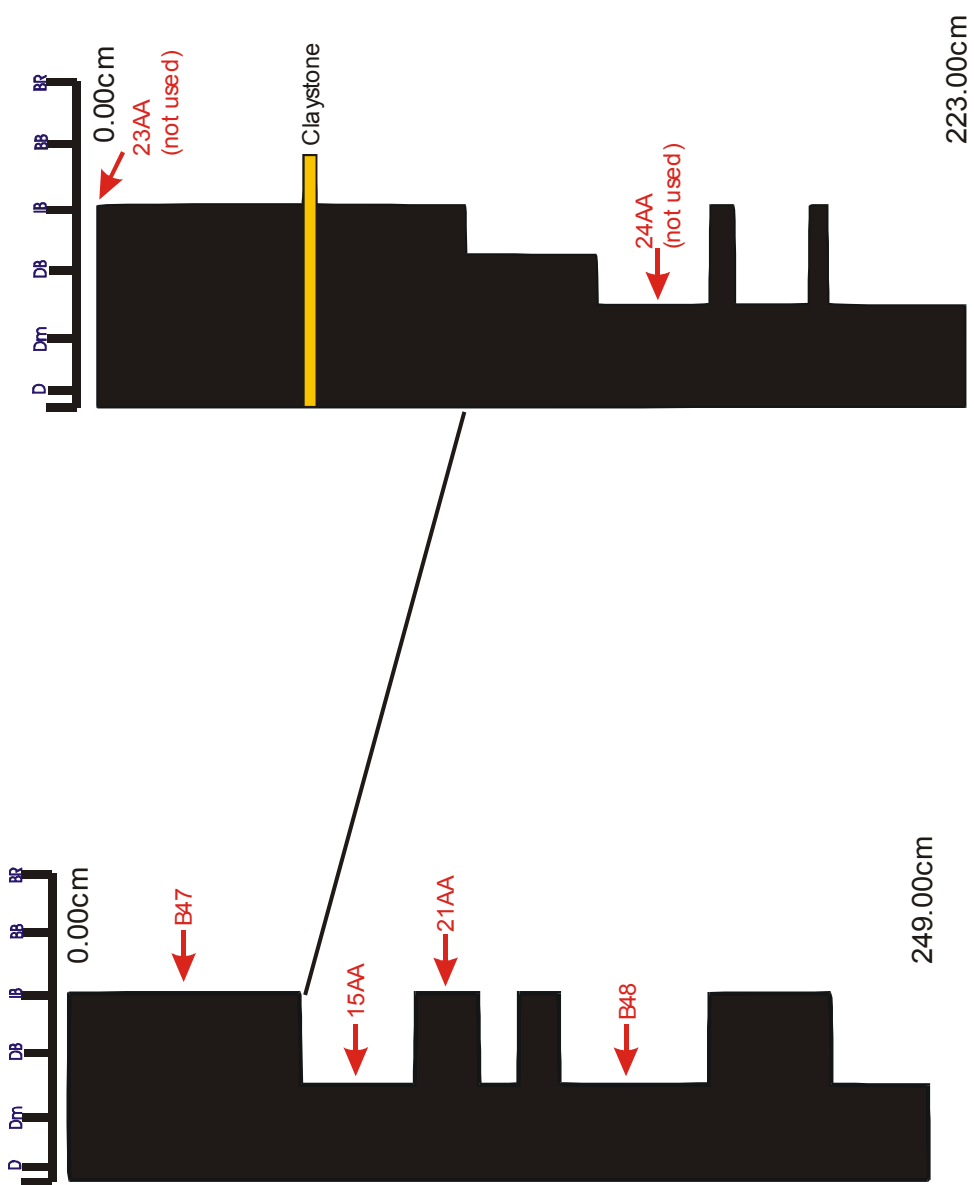
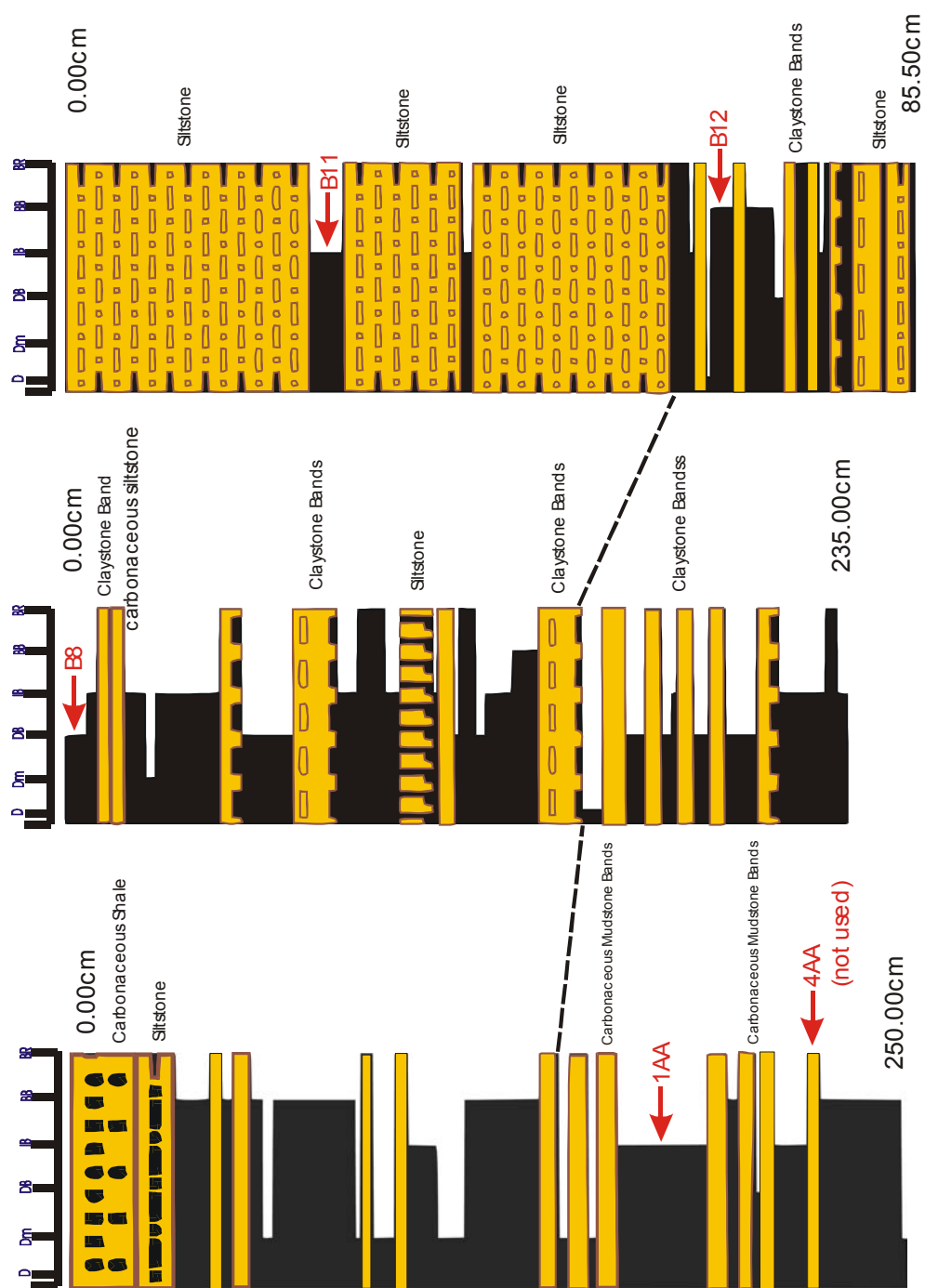


Figure 29: Bergin seam, Aberdare No. 2 (Barcle Street Tip)



**Figure 30: Bergin seam, Wattle Glen Extended Open-cut
Highly weathered outcrop**



**Figure 31: Striped Bacon seam, New Hope No. 7
Outcrops '1', '2' and '3'**

Drill-core Samples Brightness Profiles

A total of twenty-eight brightness profiles and statistical analysis for each profile have been produced to compare and contrast the different coal seams and seam profiles of the same seam from different locations (see Table 6 and Appendix I). Statistical data are used to determine the variations between the seams (eg. brightness and thickness variations). Depth scales of brightness profiles have been varied to suit the different seam thicknesses. The brightness profile data were extracted from the New Hope Mines database which was compiled from lithological logs of geologists from the New Hope Mines. Several brightness profiles were generated for some of the seams which may not have the complete seam sections. It should be noted that these brightness profiles may not represent the typical profiles of coal seams as they were randomly selected from the database. However, they give an indication of the brightness characters of coal seams.

Some of the coal seams, such as Taylor, Livermore, Matthews and Hillier, contain only dull components. This may be partly due to larger scale logging (eg. >1cm) of brightness profiles which excluded thin bright bands (eg. <1mm) in the logs.

Appendix I contains brightness profiles of various coal seams in the Ipswich Coal Measures from drillhole logs and Table 5 shows brief statistical analyses of these brightness profiles.

Table 6: Drillhole brightness profile summary statistics

Hole No	Seam	Percentages	Stone	Dull (0-40%)	Bright (40-100%)
C5003	Bluff	Total Percentages	28.79%	69.58%	1.62%
C5003	Bluff	Normalised to 100% without Stone	0	97.72	2.28
C5206	Bluff	Total Percentages	31.58%	47.06%	21.35%
C5206	Bluff	Normalised to 100% without Stone	0	68.78	31.2
C5003	Fourfoot	Total Percentages	26.67%	73.33%	0.00%
C5003	Fourfoot	Normalised to 100% without Stone	0	100	0
C5101	Fourfoot	Total Percentages	39.62%	52.51%	7.88%
C5101	Fourfoot	Normalised to 100% without Stone	0	86.97	13.05
C5650	Fourfoot Top	Total Percentages	33.02%	6.89%	60.10%
C5650	Fourfoot Top	Normalised to 100% without Stone	0	10.29	89.73
C5650	Fourfoot Middle	Total Percentages	12.59%	26.67%	60.74%
C5650	Fourfoot Middle	Normalised to 100% without Stone	0	30.51	69.49
C5650	Fourfoot Bottom	Total Percentages	31.96%	2.85%	65.19%
C5650	Fourfoot Bottom	Normalised to 100% without Stone	0	4.19	95.81
C5652	Bergin	Total Percentages	36.54%	28.85%	34.62%
C5652	Bergin	Normalised to 100% without Stone	0	45.46	54.55
C5657	Bergin	Total Percentages	42.34%	5.84%	51.82%
C5657	Bergin	Normalised to 100% without Stone	0	10.13	89.87
C1766	Striped Bacon	Total Percentages	73.00%	2.11%	24.89%
C1766	Striped Bacon	Normalised to 100% without Stone	0	7.81	92.19

C1766	Rob Roy	Total Percentages	31.36%	12.22%	56.42%
C1766	Rob Roy	Normalised to 100% without Stone	0	17.8	82.2
C5677	Rob Roy Top	Total Percentages	60.39%	0.00%	39.61%
C5677	Rob Roy Top	Normalised to 100% without Stone	0	0	100
C5317	Cochrane	Total Percentages	27.72%	31.23%	41.05%
C5317	Cochrane	Normalised to 100% without Stone	0	43.21	56.79
C5318	Cochrane	Total Percentages	39.10%	60.90%	0.00%
C5318	Cochrane	Normalised to 100% without Stone	0	100	0
C5320	Cochrane	Total Percentages	31.31%	30.35%	38.34%
C5320	Cochrane	Normalised to 100% without Stone	0	44.18	55.82
C5362	Cochrane	Total Percentages	55.40%	30.66%	13.94%
C5362	Cochrane	Normalised to 100% without Stone	0	68.74	31.26
C5368	Cochrane	Total Percentages	34.44%	42.38%	23.18%
C5368	Cochrane	Normalised to 100% without Stone	0	64.64	35.36
C5406	Cochrane	Total Percentages	38.27%	22.45%	39.29%
C5406	Cochrane	Normalised to 100% without Stone	0	36.37	63.65
C5452	Cochrane	Total Percentages	23.12%	42.71%	34.17%
C5452	Cochrane	Normalised to 100% without Stone	0	55.55	44.45
C5521	Cochrane	Total Percentages	20.42%	39.64%	39.94%
C5521	Cochrane	Normalised to 100% without Stone	0	49.81	50.19
C5536	Cochrane	Total Percentages	24.47%	57.96%	17.57%
C5536	Cochrane	Normalised to 100% without Stone	0	76.74	23.26
C5179	Cochrane	Total Percentages	32.73%	38.83%	28.44%
C5179	Cochrane	Normalised to 100% without Stone	0	57.72	42.28
C5406	Ritchie	Total Percentages	18.13%	18.96%	62.91%
C5406	Ritchie	Normalised to 100% without Stone	0	23.16	76.84
C5464	Ritchie	Total Percentages	14.13%	0.00%	85.87%
C5464	Ritchie	Normalised to 100% without Stone	0	0	100
CS33	Taylor	Total Percentages	43.84%	56.16%	0.00%
CS33	Taylor	Normalised to 100% without Stone	0	100	0
CS3	Livermore	Total Percentages	50.00%	50.00%	0.00%
CS3	Livermore	Normalised to 100% without Stone	0	100	0
5407	Matthews	Total Percentages	14.86%	85.14%	0.00%
5407	Matthews	Normalised to 100% without Stone	0	100	0
5575	Hillier	Total Percentages	37.04%	62.96%	0.00%
5575	Hillier	Normalised to 100% without Stone	0	100	0

See Appendix I for core samples brightness profiles

Coal Petrology

Ipswich Flora and Fauna

Climatic Effect on Flora

Ziegler (1993) suggested that the direct evidence of palaeoclimates is through the plants and animals that actually had to endure them, as well as through the sedimentological products of their environments.

The sedimentary records of lakes and associated fluvial deposits in conjunction with palaeolatitude data have been used by Yemane (1993) to define realistic boundary conditions for palaeoclimate simulations. She has studied the integrated climatic records of the biotic and sedimentary data from the Upper Permian and Lower Mesozoic deposits formed at high latitudes (55° - 60°) in South Africa, and concluded that the climatic conditions in these areas were cool to temperate, humid, and seasonal during the Triassic Period.

The Triassic configuration of the Pangea supercontinent caused relatively humid conditions over the southeastern margin of Gondwana, including Eastern Australia (Robinson, 1973; Parrish et al., 1982). Regional climate in eastern Australia during the Early Triassic Epoch was sub-humid, cool to temperate, with periodic drier conditions (Retallack, 1977a). The increased diversity of the Triassic peat in central Transantarctic, as compared with the Permian peat, may represent a relatively warmer and more equitable climate during the Triassic Period (Taylor et al., 1989). This is consistent with the humid belt formed in high latitudes in the Late Triassic Epoch postulated by Ziegler (1987). According to White (1990), there was only one large ocean, Panthalassa, that existed during the Triassic Period. It extended over approximately 70% of the earth at the equator. As a result, warmer equatorial currents were free to flow and travel polewards along the shores. On the other hand, there were no circum-polar currents and thus no polar isolation and cooling. Consequently, there was little gradation in temperature from equator to poles.

Triassic Megafloora

Triassic floras of Gondwanaland are uniform, consisting largely of endemic species (Staines et al., 1995). *Dicroidium*, the most abundant flora in the Australian Triassic coals, shows bipinnate fronds in the Early Triassic Epoch to small unipinnate leaves in the Late Triassic Epoch. This demonstrates a change from the relatively wet to drier conditions. The climate became increasingly hot and dry as the Triassic Period proceeded. Consequently, many plants of the Late Triassic Epoch, e.g. *Xylopteris*, show drought resistant adaptations (White, 1994). According to Retallack (1980) the successive appearance of the various species of *Xylopteris* in

the Ipswich Coal Measures is possibly due to changing environmental conditions.

The Late Triassic Epoch coal swamp vegetation consisted of herbaceous and shrubby *Dicroidium* and *Dejerseya*. Coal seams formed from the accumulation of leaves, stems, roots and pollens of these plants such as ferns, together with conifer and other gymnosperms (Retallack, 1977a; Webb, 1980; Falkner, 1986). The adjacent floodplains carried a more diverse flora of cycadophyte, ginkgoalean, and voltziacean conifer trees with an understorey of ferns, equisetaleans, *Dicroidium*, and other pteridosperms. Meandering and branching channels were inhabited by tall coniferous forests, while *Dicroidium-voltziopsis* grew mainly in swampy woodlands (Retallack, 1977a). The Carnian Period displays the greatest radiation of *Dicroidium*. The absence of *Dicroidium* plant association in the Early Triassic Epoch may partly account for the lack of coal accumulation at that time (Gould and Shibaoka, 1980).

Dicroidium assemblages are used to define four Opperl-zones for the pteridosperm dominated Triassic floras of Gondwanaland. These fossil plant associations succeeded *Glossopteris* dominated floras during Late Permian Epoch and were followed by *Otozamites* dominated floras in the Early Jurassic Epoch. Retallack (1977b) classified Opperl-zones based evolution of a prominent group of plants in conjunction with the ranges of other plant megafossil associations. These Opperl-zones include *Thinnfeldia callipteroides* (Chidruan to Smithian, 250-230*10⁶ years), *Dicroidium zuberi* (Smithian to Middle Anisian, 230-220*10⁶ years), *Dicroidium odontopteroides* (Late Anisian to Ladinian, 220-210*10⁶ years), and *Yabeiella* (Carnian to Rhaetian, 210-200*10⁶), which characterizes the Ipswich Coal Measures (Table 7). In addition, there are twelve Mesozoic floral associations in eastern Australia, based on ecological and environmental factors (Table 8). It includes plant associations and depositional environments that existed in the Triassic Ipswich Basin.

Table 7: Four Opperl-zones (After Retallack, 1977b)

Opperl-zone	First Opperl-zone	Second Opperl-zone	Third Opperl-zone	Fourth Opperl-zone*
Dominant flora	<i>Thinnfeldia callipteroides</i>	<i>Dicroidium zuberi</i> and its reproductive structures: <i>Pterorrachis barrealeensis</i> , and large cupulate organ similar to <i>Umkomasia</i>	<i>Dicroidium odontopteroides</i> , and its reproductive structures: <i>Pteruchus johnstonii</i> , <i>Pilophorosperma</i> spp.	<i>Yabeiella</i> leaves, <i>Fraxinopsis</i> , <i>Dicroidium</i>
Common flora	<i>Voltziopsis</i> spp., <i>Danaeopsis hughesii</i> , <i>Dicroidium brownii</i>	<i>D. zuberi</i> 's polymorphic, large, coriaceous <i>Dicroidium</i> leaves and its low species diversity	<i>Dicroidium eskense</i>	<i>Pterophyllum multilineatum</i>
Geological Setting	Sandy/silty river deposits overlying either crystalline basement or <i>Glossopteris</i> -bearing coal measures	Silty/sandy and conglomeratic river deposits, occasionally with conspicuous redbed interpolations	River sediments with calcareous matrix and interbedded extrusive volcanic rocks	Finer grained, less conglomeratic, and lack calcareous matrix of older alluvial sequences

* Ipswich Coal Measures are characterized by the Fourth Opperl-zone.

Table 8: Mesozoic floral associations in relation to depositional environments (After Retallack, 1977b)

Plant association	Dominant flora	Common flora	Depositional environment
'Thinnfeldietum' callipteroidium (levee bank scrub) (Derived from Callipteris and conifer dominated associations)	'Thinnfeldia' callipteroides	- Schizoneura gondwanensis - Isoetes-like leaflet groups - Sterile cladophlebid fern fronds, and conifer shoots including Voltziopsis africana, and undescribed remains similar to Podozamites	Bushy scrub vegetation, colonizing scroll bars, levees of meandering streams
Voltziopsetum (coniferous forest) (Derived from Callipteris and conifer dominated associations)	Voltziopsis and fragmentary conifer twigs and log accumulations (Voltziopsetum was similar to ever green forests now growing in the cool-temperate zones of the northern hemisphere)	- Protophloxypinus reticulatus - P. samoilovichii - Lunatisporites pellucidus	Mineralogically immature soil (eg. volcanic soils)
Dicroidietum zuberi (broadleaf forest and heath)	Dicroidium (D. zuberi is similar to D.odontopteroidium)	- equisetaleans (Neocalamites) - filicaleans (Cladophlebis) - pteridosperms (Lepidopteris and Pachydermophyllum) - cycadophytes (Taeniopteris) - large corystosperm reproductive structures	Delta top heath and a lagoon-margin swamp woodland forested the less disturbed floodplain
Pleuromeietum (marine and lagoonal bay meadows)	Monospecific lycopod association	Pleuromeia longicaulis, its supposed cones (Cylostrobus sydneyensis) and leaves – Sigillariophyllum	Formed dense meadows around coastal lakes, lagoons and protected seashores
Taeniopteretum lentriculiformis (coastal scrub)	Characterized by abundant leaves of Taeniopteris lentriculiformis	Also contains rare elements of D. zuberi	Diffuse shrub growing on slightly higher, better drained and more exposed areas
Dicroidium zuberi xylopterisum (xerophytic woodland)	Characterized by Xylopteris and narrow-leaved species		Drier palaeoenvironments (<i>eg. Ipswich Basin - later stage of deposition</i>)
Dicroidietum odontopteroidium (broadleaf forest)	D. odontopteroides (unequivocally forked)	- equisetaleans (Neocalamites, Phyllothea) - filicaleans (Asterothea, Cladophlebis, 'Coniopteris', Dictyophyllum) - Pteridosperm leaves (Lepidopteris, Pachydermophyllum, Dicroidium, Johnstonia, Tetraptilon) - Smaller corystosperm reproductive structures (Pteruchus and Pilophorosperma) - Ginkgoales (Sphenobaiera, Ginkgoites, Phoenicopsis) - Conifers (Rissikia) - Cycadophytes (Taeniopteris, Pterophyllum, Pseudoctenis)	Meandering and braided streams, shaly overbank deposits, river deposits, interbedded extrusive volcanics (<i>eg. Ipswich Basin - earlier stage of deposition</i>)
Phoenicopsetum (levee bank scrub)	Phoenicopsis leaves	Very few remains of plant also found in the D. dontopteroidium	Levee and point bar scrub or woodland whose leaf litter was scoured out during floods
Johnstonietum (mallee-like woodland)	Johnstonia coriacea	Also includes species found in D. odontopteroidium, but pteridophytic remains are not usually present	Inland of a coastal dividing range, well-spaced woody association of moderate height with a sparse, loose leaf litter
Dicroidietum odontopteroidium xylopterisum (xerophytic woodland)	Ecologically analogue to the Dicroidietum zuberi xylopterisum	It contains at least one and commonly several species of Xylopteris and Dicroidium odontopteroides, together with various species common in Dicroidium odontopteroidium	Communities of more complex structures
Pachydermophylletum (mangrove scrub)	Monospecific association of Pachydermophylletum leaves		Coastal, tidal flat deposits
Linguifolietum (coastal swamp woodland)	Linguifolium	- Cladophlebis 'Chiropteris' - Phoenicopsis	Coal measures associated with shallow marine rocks

This table shows Dicroidium plant associations radiated in the Triassic Ipswich Coal Basin.

Falkner (1986) stated that the Ipswich Coal Measures have an abundant pteridosperm (seed-ferns) dominated macroflora, indicating that the basin lay in a relatively humid belt during the Triassic Period.

In the Triassic Period, the Southern Hemisphere hosted unique and uniform floral assemblages which differ from flora found in other ages (eg. glossopteris plants found in the Permian coal measures), and from flora in different parts of the world (eg. northern hemisphere flora). This reflects the peculiar nature of the Triassic coals in eastern Australia (eg. high cutinite contents, see '**Maceral Data Analysis**' section for details).

Miospores

Miospore assemblages define three biostratigraphic units in the Triassic Ipswich Basin. They include *Duplexisporites problematicus*, *Craterisporites rotundus*, and *Polycingulatisporites crenulatus* zones (de Jersey, 1970). Some of the variations in the proportion of microflora appear to be related to environmental facies (de Jersey, 1964). For example, *Stereisporites antiquasporites* and *Circulisporites parvus* are relatively abundant in thicker seams, suggesting that they favour quiet and stable depositional environments. However, variation in miospore distribution alone is not an indicative of depositional environment change as some species may produce more spores and pollens than other species.

The Ipswich Coal Measures are defined by the *Craterisporites rotundus* zone. The miospore assemblages are used to identify age and correlate coal measures.

Relation to Petrography

Coal facies, in general, is determined by organic plant material from which it is derived, and by the decomposition and preservation of these plant remains. For example, spore-bearing leafy plants would produce sporinite and cutinite-rich coal, whereas woody plants with large stems form vitrinite-rich coal. Inertinite macerals are derived from the similar basic organic matter as vitrinite, but oxidation of plant materials occurs at an early stage of peat formation.

The predominance of cutinite and sporinite in dull coals as at Callide and Tarong is a characteristic of dull coals since the liptinite macerals, cutinite and sporinite, are more resistant to biodegradation and chemical weathering. Furthermore, the main floral types in the Ipswich and Callide coals are similar and this suggests that floral type is not the cause of different coal characteristics between the two deposits (Read, 1997, Rigby, QUT research fellow, personal communication). The brighter nature of Ipswich coal is mainly due to its predominant leaf source and leaf-shedding nature of the *Dicroidium* swamp flora (Falkner, 1986).

Peat-Mire Types and Vegetation

Osvald (1937) defined three main zones within the peat-mire environments related to water level.

1. Terrestrial zone: above high water level
2. Telmatic zone: between high and low water level, and
3. Limnic zone: subaquatic conditions

Karmasin (1952), on the other hand, proposed four major types of vegetation which are commonly associated with peat-mires.

1. Forest-moor
2. Forest-terrestrial-moor
3. Reed-moor, and
4. Open-moor

Furthermore, Teichmüller (1989) has shown the relationship between the mire type, vegetation, and peat type, based on palynological data.

Table 9: Peat-mire, Vegetation, and Peat Type (After Teichmüller, 1989)

PEAT-MIRE	VEGETATION	PEAT TYPE
Forest swamps	Various plant associations	Forest peat
Marshes	Herbaceous vegetation (sedges, grasses)	Reed peat
Open swamps	Submerged and floating plants	Subaquatic peat or organic mud
Raised bogs	Mosses or shrubs or trees	Peats of raised bogs

These peat-mire types can be further divided into sub-environments according to the type of vegetation, groundwater level, and floodwater incursion in fluvial dominated settings.

Based on coal facies analysis, Falkner (1986) produced five sub-environments of the Blackstone Formation. They include pond, fen (marsh), wet carr (swamp), dry carr (swamp), and floodplain margin.

Diessel (1982) produced facies maps based on petrographic analysis of coal. They are used in conjunction with sedimentological data to provide an indication of coal producing palaeodepositional environments.

In addition, Diessel (1982) described conditions for peat formation and its results in terms of peat and lithotypes of black coal (as illustrated in Table 10).

Table 10: Different conditions of peat forming environments (Compiled after Diessel, 1982; Mackowski, 1953; Teichmüller, 1962; Plumstead, 1966; and Hacquebard and Donaldson, 1967)

Zone	Zone 1	Zone 2*	Zone 3	Zone 4
Water Cover	None	Oscillating	Almost Complete	Complete
Acidity	High	Medium	Low	Very Low
Atmospheric O₂	Present	Partly Present	Largely Absent	Absent
Chem. Reaction	Oxidation	Oxidation and Reduction	Mainly Reduction	Reduction
Organic Activity	Fungi, Insects, Aerobic Bacteria	Actinomyces, Aerobic and Anaerobic Bacteria	Mainly Anaerobic Bacteria	Anaerobic Bacteria
Mode of Plant Decomposition	Rotting (O ₂ decay)	Main Zone of Peatification		Putrefaction
Peat Type	Woody with Resin Bodies	Woody with increasing Humid Collids →	Fibrous to Earthy	Organic Mud
Lithotype	Fusain and Durain	Vitrain, Clarain, and Duro-clarain	Claro-durain and some Durain	Durain, Canel and Boghead Coal, Torbanite, Oil Shale
Environment	Dry Forest Swamp	Wet Forest Swamp	(Fen) Reed Moor	Moor Lake
Location	Continental	Telmatic	Limnotelmatic	Limnic

*The Ipswich Basin probably represents Zone 2.

Petrographic Study of Ipswich Coal

The Ipswich coal is unique owing to its complex and variable coal seam architecture, distinctive association with clay, common seam splitting, and different brightness and maceral associations from other Australian Triassic and non-Triassic coals such as Tasmanian Triassic coal (dull) and Cooper Basin Permian coal (very low liptinite) (Ward, 1980; Smyth, 1980).

According to Cook and Taylor (1963) the variation in petrographic composition of the Ipswich coal is relatively less than that of other Australian coals. The Ipswich coal is rich in vitrinite. Cutinite is the most common liptinite maceral. Coal seams were formed from autochthonous origin and deposited under fairly rapid subsidence conditions. The Ipswich Coal Measures sequence is thicker and contains more coal seams than other Australian Triassic coal formations. This indicates that coal-forming conditions in the Ipswich Basin were better and peat formation may have continued much longer. The mineral matter content of the Ipswich coal is relatively high with clay, mainly kaolinite, being most abundant.

Results

In order to petrographically study the peculiar nature of Ipswich coal, forty-one drillhole samples (grainmounts) and thirty-eight highwall samples (polished blocks) were chosen for maceral analyses. In addition, two thin sections were included in the maceral analysis. Grainmount samples were collected from different seam intervals of diamond cored samples (see Appendix II, Table 11) and block samples were collected from various intervals of highwall brightness profiles (see Appendix II, Table 12, and Figures 20 to 31, highwall brightness profiles).

The point counting of maceral types was performed separately for grainmount and polished block samples (see Appendix II, Tables 13 and 14). Figure 32 shows sample locations of polished blocks, grainmounts, and thin sections. However, there were not enough samples to effectively differentiate the petrographic characters between the Blackstone and Tivoli Formations as all polished blocks and majority of grainmount samples were taken from the Blackstone Formation (see Appendix II, Tables 11 and 12).

Vitrinite Group

Vitrinite is the most abundant maceral group in the Ipswich coal reflecting the brighter nature of lithotypes (Tables 15A and 15B). Three types of vitrinite have been identified, namely, telovitrinite, detrovitrinite and gelovitrinite. Telovitrinite is slightly more abundant than detrovitrinite, while gelovitrinite occurs in minor amounts. Telovitrinite occurs as thin homogeneous bands or thick layers showing weak cell structures. Oxidised and broken telovitrinite (probably heat affected or weathered) is commonly associated with clay and secondary calcite veins. Detrovitrinite is commonly associated with cutinite and sporinite. It mainly occurs as ground mass to liptinite and inertinite. Gelovitrinite only occurs in minor quantity infilling gaps and cell walls of liptinite and inertinite macerals. It is also found as massive oblong or oval shaped bodies showing low to medium reflectance (Appendix III - Coal Atlas).

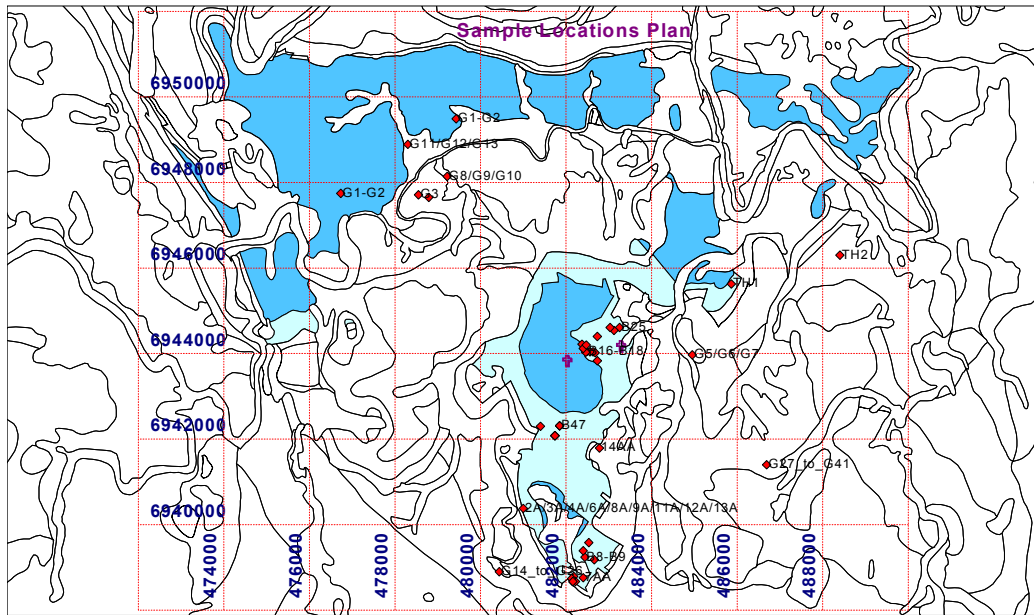


Figure 32: Sample location map (G = grainmount samples, TH = thin sections, A/AA/B = polished block samples) (B, G and TH are prefixes, A and AA are surfixes, eg. B6, G1, TH9, 4A and 9AA, see Appendix I for details)

**Dark blue = Tivoli Formation, Light blue = Blackstone Formation
 Scale: One grid distance = 2000m
 See grids for eastings and northings**

Block samples were used in some cases where grainmounts were not available and when plots of lithotypes versus maceral groups were made. The grainmounts give reliable statistics and it can be seen in petrographic study that the block sample values are more variable, as expected, but still useful for basic data. Thin sections were also used to study maceral types and mineral matter in coal (see Appendix I for drillhole brightness profiles, Appendix II, Tables 11 and 12 for sample lists, and Figures 20 to 31 for highwall brightness profile petrographic sample intervals).

Table 15A and 15B: Statistical analysis of grainmount and polished block samples (37 blocks and 41 grainmounts were used and each sample was point-counted to 300 points)

Table 15A: Block Samples		Table 15B: Grainmount Samples	
<i>Total %Vitrinite</i>		<i>Total %Vitrinite</i>	
Mean	65.89	Mean	64.54
Median	71.60	Median	64.30
Standard Deviation	21.83	Standard Deviation	8.28
Range	91.60	Range	35.20
Minimum	1.60	Minimum	45.00
Maximum	93.20	Maximum	80.20
Total	37.00	Total	41.00
<i>Total %Liptinite</i>		<i>Total %Liptinite</i>	
Mean	8.39	Mean	6.37
Median	3.90	Median	5.30
Standard Deviation	11.06	Standard Deviation	3.93
Range	47.30	Range	16.30
Minimum	0.00	Minimum	0.30
Maximum	47.30	Maximum	16.60
Total	37.00	Total	41.00
<i>Total %Inertinite</i>		<i>Total %Inertinite</i>	
Mean	14.85	Mean	8.35
Median	11.20	Median	7.60
Standard Deviation	11.06	Standard Deviation	3.36
Range	46.50	Range	15.30
Minimum	0.00	Minimum	3.90
Maximum	46.50	Maximum	19.20
Total	37.00	Total	41.00
<i>Clay+other Min. Matter%</i>		<i>Clay+other Min. Matter%</i>	
Mean	10.59	Mean	20.42
Median	2.00	Median	18.70
Standard Deviation	23.51	Standard Deviation	9.26
Range	98.30	Range	44.30
Minimum	0.00	Minimum	0.00
Maximum	98.30	Maximum	44.30
Total	37.00	Total	41.00

Liptinite Group

In comparison with other Australian Triassic coals, the Ipswich coal contains high liptinite content (mainly cutinite) (eg. Smyth, 1991), averaging 8.39% in block samples and 6.37% in grainmount samples. However, liptinite content can be highly variable, ranging from 0 to 47% in blocks and 0.3 to 16.6% in grainmounts (as shown in Tables 15A and 15B).

The liptinite group consists of cutinite, sporinite, resinite and suberinite. Cutinite is the most dominant maceral of the group. It occurs as thin but high relief cell walls in phyllovitrinite or is found in a detrovitrinite matrix. Sporinite occurs as thin elongated bodies around telovitrinite or in detrovitrinite matrix mixed with cutinite. Resinite is less common and found only as small dark low relief elongated bodies in telovitrinite

showing high fluorescent intensity. Suberinite occurs as weak cell walls of telovitrinite (Appendix III – Coal Atlas).

Inertinite Group

Inertinite content in the coal is also high but variable, ranging from 0 to 46% in blocks and 4% to 19% in grainmounts. Average content is 15% in blocks while only 8% in grainmounts (see Tables 15A and 15B).

Fusinite, semifusinite, and macrinite are commonly found in the coal. Some inertinite macerals appear to have been derived from oxidation of vitrinite macerals. Pseudocoprosclerotinite or sclerotodetrinite (Beeston, 1987) occurs in detrovitrinite matrix. Lyons (2000) introduced two new terms, funginite and secretinite, to replace sclerotinite. However, Scott (2002) argued that there was no attempt by Lyons to discuss what type of fungus was being described or any attempt to isolate the fungus and describe it morphologically. Furthermore, assumption of botanical (or even animal) identification based on polished blocks alone would be unsubstantiated. Therefore, the term sclerotinite is retained in this thesis. Other inertinite macerals, inertodetrinite and micrinite are commonly found in detrovitrinite and clay groundmass (Appendix III – Coal Atlas).

Clay and other Mineral Matter

Clay, essentially kaolinite, is commonly found as multicoloured or pale brown material in thin section. It is the dominant form of mineral matter. Calcite, pyrite and siderite are commonly found in Ipswich coal. These carbonate and sulphide minerals are generally diagenetic occurring as veins, lumen fillings or as micro-nodules. Quartz is rare and mostly occurs as rounded detrital grains. However, quartz can be anhedral to euhedral. They are probably volcanic quartz formed from felsic tuff. Most quartz crystals are monocrystalline and transparent (Appendix III – Coal Atlas).

Relatively high mineral matter content was recorded in Ipswich coal, averaging 10% to 20%, as a result of periodic fluvial incursion in the peat-mire. This is consistent with fluvial dominated peat-mire environments suggested by Falkner (1986).

Maceral Data Analysis

Numerous studies have been conducted to establish the relationship between coal petrology and depositional environment (eg. Diessel, 1982; Hunt et al., 1986; Teichmüller, 1989). Kent (1995), in his study of the Walloon Coal Measures, divided four categories for the palaeodepositional environment interpretation which was based on maceral analysis. For Ipswich, five categories were chosen to suit the unusual nature of coal. These are:

1. The indices of the tissue preservation and the gelification (TPI-GI crossplot of Diessel, 1986).
2. Petrographic indices and vegetation types (RWD facies diagram, Diessel 1982).
3. Maceral associations and petrographic indices (DTF ternary diagram, Diessel 1982).
4. The maceral associations and mineral matter contents in relation to groundwater table (ABC ternary diagram, Kalkreuth et al. 1991).
5. The indices of the groundwater influence and the vegetation (Calder et al., 1991).

Diessel (1986 and 1992) used two indices to define the palaeodepositional environment of the peat-mire. The Tissue Preservation Index (TPI) is a ratio of tissue derived structured macerals of the vitrinite and inertinite groups to their tissue derived unstructured macerals. The TPI can be used to measure the degree of humification as well as the proportions of wood which have been preserved in the peat-mire. The Gelification Index (GI) is a ratio between gelified macerals (eg. vitrinite and macrinite) to fusinitised macerals (eg. fusinite and semifusinite).

The TPI-GI crossplot with logarithmic scale for GI values was created to study the depositional environments and maceral types (see Figure 33).

$$\text{TPI} = \frac{\text{Telovitrinite} + \text{Semifusinite} + \text{Fusinite} + \text{Sclerotinite}}{\text{Detrovitrinite} + \text{Gelovitrinite} + \text{Inertodetrinite} + \text{Macrinite} + \text{Micrinite}}$$

$$\text{GI} = \frac{\text{Vitrinite} + \text{Macrinite}}{\text{Other Inertinite}}$$

Results obtained from point counting of maceral types are given in Tables 13 and 14 in Appendix II. These data have been used to produce cross-plots and various ternary facies diagrams to interpret the coal forming depositional environments.

Figure 33 shows that both TPI and GI are generally moderately high, but polished block sample values are more variable as expected. The greater variability in the results with the block samples than those with the grain

mounts could be expected because the grain mounts are more statistically representative. Relatively high ratio values of most samples indicate the low percentage in variations of maceral groups and uniformity of the coal. This is consistent with Diessel (1992) and Lamberson et al. (1991) who stated that high TPI and GI represents bright to banded bright coal formed in wet forest swamp environment. It also shows higher vitrinite to inertinite ratio and structured or woody vitrinite being more abundant than degradovitrinite.

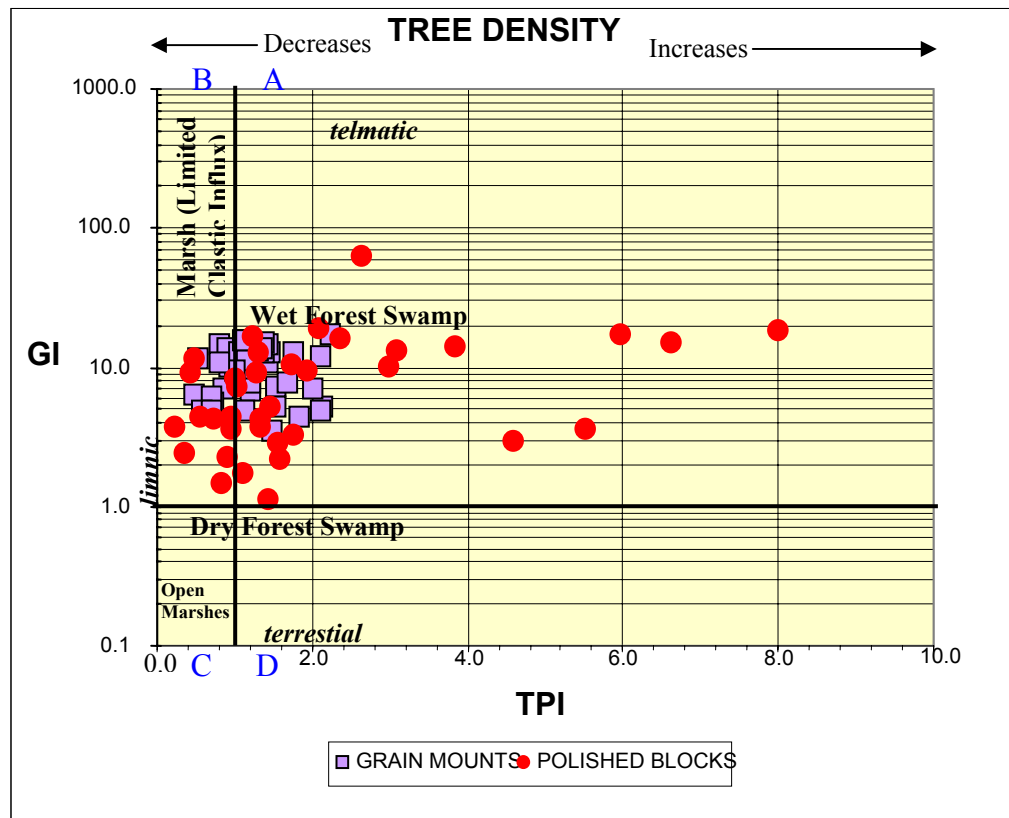


Figure 33: Tissue Preservation Index – Gelification Index Crossplot (logarithmic scale) (After Diessel, 1992; Kalkreuth et al., 1991; Lamberson et al., 1991)

- Quadrant A = Vitrinite>Inertinite, Structured Vitrinite>Degrato-vitrinite
- Quadrant B = Vitrinite>Inertinite, Degrato-vitrinite>Structured Vitrinite
- Quadrant C = Inertinite>Vitrinite, Inertodetrinite>Fusinite + Semifusinite
- Quadrant D = Inertinite>Vitrinite, Fusinite + Semifusinite>Inertodetrinite

Hacquebard et al. (1964 and 1967) developed a four component facies diagram (double triangle) based on four peat facies and mire zones. Figure 34 (modified Hacquebard's Double Triangle) shows maceral associations in relation to depositional environments. This diagram is based on maceral associations (Table 16) and it is used to compare with Hacquebard's original facies diagram which is related to microlithotype associations. Both diagrams, Hacquebard's original diagram and the modified diagram used in this study, which show similar trends. If the coal contains less than 20% of D components, the upper triangle is used for maceral analysis and A and D apexes are combined. If the coal contains greater than 20% of D components, B and C apexes are combined and the lower triangle is used (see Table 16 for explanation of components A, B, C and D). Following is the classification system used by Kent (1995) and in this study to develop the modified Hacquebard's diagram.

Hacquebard's original diagram

(Based on microlithotypes)

A-components (sporoclarite and duroclarite)

B-components (fusitoclaurite-fusinite in clarite matrix)

C-components (vitrinite-rich clarite and cuticlocclarite-cutinite based clarite)

D-components (clarodurite, durite, carbargillite and other dispersed matter)

Modified Hacquebard's diagram

(Based on maceral associations)

Sporonite+Detrovitrinite+Inertodetrinite

Sclerotinite+Fusinite+Semifusinite

Cutinite+Resinite+Suberinite

+Telovitrinite+Gelovitrinite

Macrinite+Inertodetrinite+Mineral Matter

In Figure 34 (upper triangle), most samples lie in the telmatic forest zone, but several points also lie in the telmatic reed zone. In the lower triangle, most samples are plotted in the limnotelmatic zone, and few samples lie in the limnic zone. This suggests some variations in depositional environment during the coal accumulation, but mainly between telmatic and limnotelmatic environments depending on local climatic changes and seasonal variations.

Diessel (1982) developed a DTF facies diagram to define coal facies zones. D component comprises detrital material such as sporinite and inertodetrinite. T represents telovitrinite maceral, while F is composed of fusinitised macerals such as fusinite and semifusinite. Figure 35 shows most samples lying in the telmatic zone (wet forest swamp) with a few samples plotted in the limno-telmatic zone.

Diessel (1982) also defined a RWD ternary facies diagram. D components represent detrital material such as sporinite and inertodetrinite, while W components contain woody macerals including fusinite, semifusinite and telovitrinite. R is the remaining macerals. He used RWD and DTF facies diagrams to form a basis for the construction of coal facies maps (eg. Maules Creek area, Gunnedah Basin). Figure 36 shows the high content of wood ratio, probably representing the telmatic forest growth. The high preservation of structured macerals also suggests that coal is mainly of autochthonous origin formed in cool temperate climatic conditions.

Kalkreuth et al. (1991) defined a ternary plot based on maceral associations and mineral matter contents to give an indication of groundwater influence on coal lithotypes. Figure 37 - ABC Plot suggests that groundwater decreases with increasing brightness of coal. Most samples fall in the telmatic zone with moderate groundwater level (see Table 16 for explanation of A, B and C components).

Smyth (1984) produced a facies diagram based on microlithotype analyses. In Figure 38, microlithotypes were replaced by main maceral groups in three apices to compare with Smyth's (1984) interpretation on depositional environment of Cooper Basin coals related to microlithotypes. Therefore, Smyth's (1984) diagram is only used for comparison purposes and not as a guide for depositional interpretation. The bright nature of Ipswich coal is apparent in Figure 38, showing a high concentration of sample points that fall within the greater than 50% vitrinite zone (Smyth's diagram), indicating the fluvial dominated depositional environment. This is consistent with Falkner's (1986) interpretation which stated that the Ipswich Coal Measures were deposited in the fluvial environments. This also reflects the uniformly high vitrinite content of Ipswich coal. According to Gould and Shibaoka (1980) coals formed in areas of rapid subsidence usually contain high vitrinite content. Following is the comparison between Smyth's (1984) diagram and Figure 38.

Smyth's (1984) diagram
(Based on microlithotypes)
 Vitrite-Clarite
 Intermediates
 Durite-Inertite

Figure 38
(Based on maceral groups)
 Vitrinite Group
 Liptinite Group
 Inertinite Group

Figures 39 and 40 show the maceral and mineral compositions of grainmount and polished block samples. They are roughly placed in stratigraphic order, from the youngest seam (left) to the oldest seam (right). The results are highly variable and show no significant progressive patterns in relation to age or any particular seam. It indicates the dynamic depositional system in the Ipswich Basin during the coal formation. Vitrinite content, however, is high in most samples.

Table 16: Various indices of maceral associations used in crossplots and ternary diagrams (See corresponding figures for details)

<p>(TPI-GI Crossplot, Figure 33, Page 61) TPI = (Telo+Gelo+Semi+Fusi+Sclerotinite)/(Detro+Gelo+Inerto+Macrinite+Micrinite) GI = (Vit+Mac)/Other Inertinite</p>
<p>A = Sporinite+Detrovitrinite+Inertodetrinite (Double Triangle, Figure 34, Page 65) B = Sclerotinite+Fusinite+Semifusinite C = Cutinite+Resinite+Suberinite+Telovitrinite+Gelovitrinite D = Macrinite+Inertodetrinite+Mineral Matter If <20% D = Upper Triangle If >20% D = Lower Triangle</p>
<p>D = (Detrital) = Sporinite + Inertodetrinite (DTF Facies Diagram, Figure 35, Page 66) T = Telovitrinite F = Fusinite+Semifusinite</p>
<p>R = Remaining Macerals (RWD Facies Diagram, Figure 36, Page 67) W = (Wood) = Fusinite+Semifusinite+Telovitrinite D = (Detrital) = Sporinite + Inertodetrinite</p>
<p>A = Telovitrinite+Semifusinite+Fusinite (ABC Facies Diagram, Figure 37, Page 68) B = Detrovitrinite+Macrinite C = Minerals+Inertodetrinite</p>
<p>(GWI-VI Crossplot, Figure 41, Page 73) GWI = Gelovitrinite+Mineral Matter/Telovitrinite+Detrovitrinite VI = Telovitrinite+Fusinite+Semifusinite+Sclerotinite+Resinite/Detrovitrinite+Inertodetrinite+Sporinite+Cutinite</p>

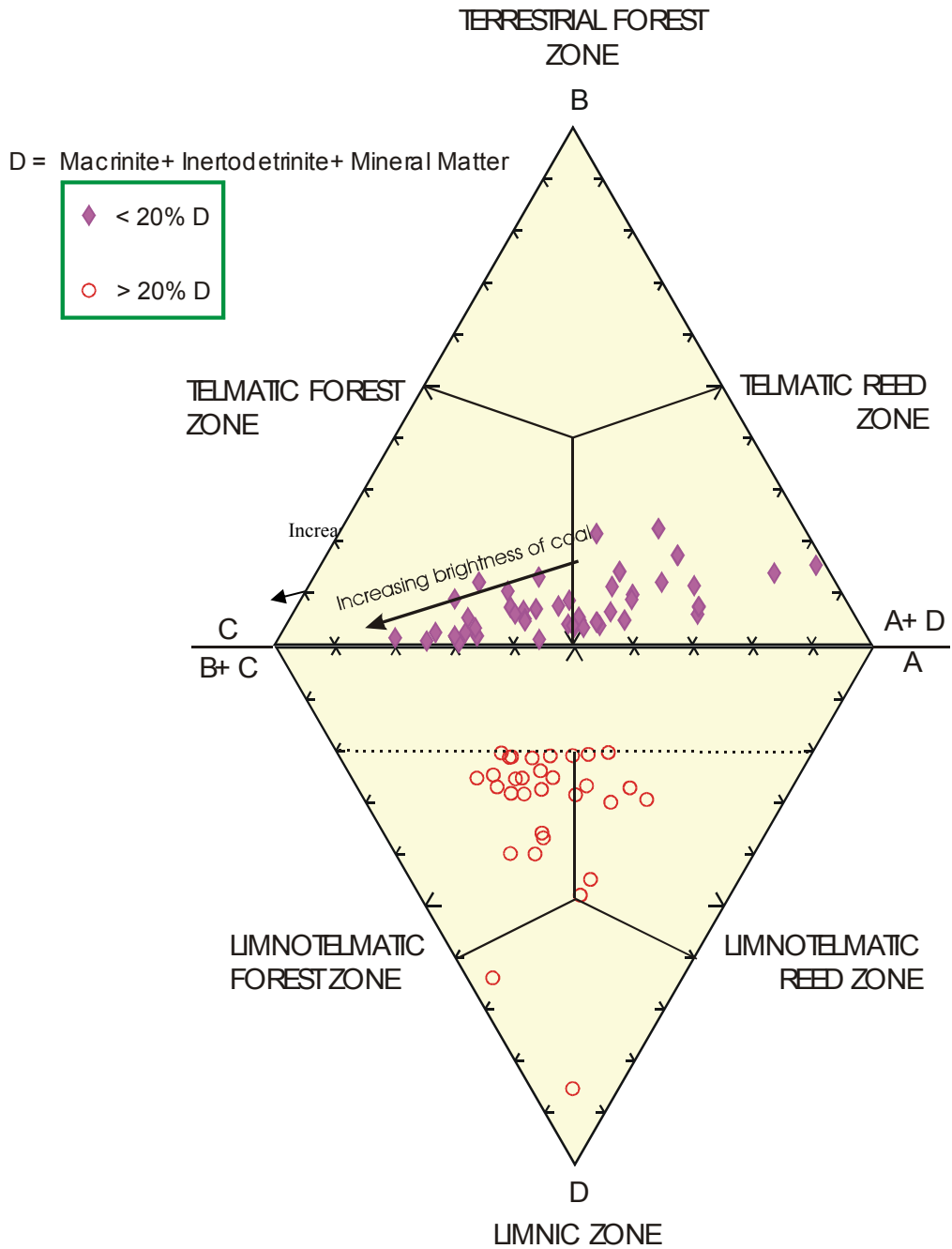


Figure 34: Modified Hacquebard's Double Triangle, based on maceral groups (After Hacquebard et al., 1964) (See Table 16 for details and text for explanation)

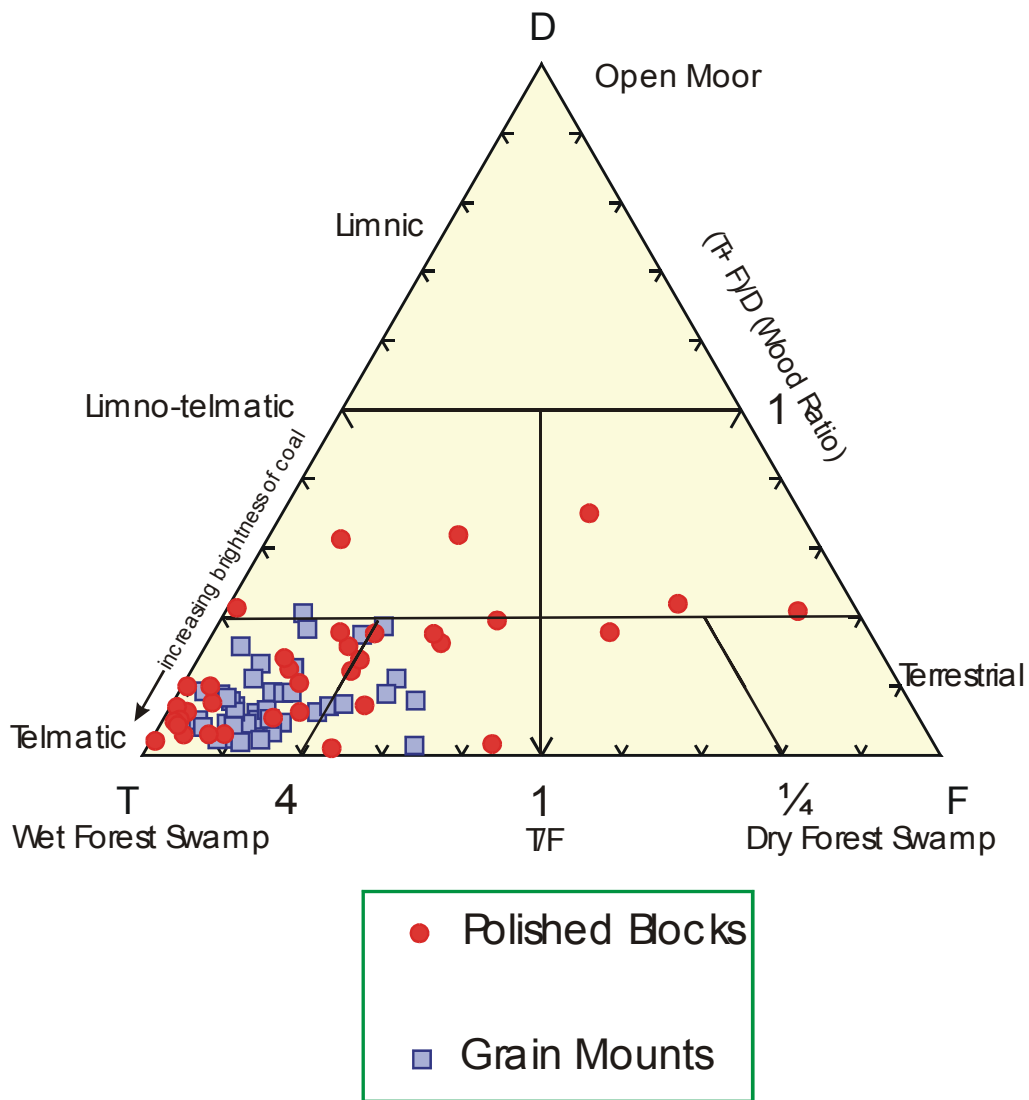


Figure 35: DTF Facies Diagram (D = (Detrital) = Sporinite + Inertodetrinite, T = Telovitrinite, F = Fusinite + Semifusinite) (After Diessel, 1982; Kent, 1995)

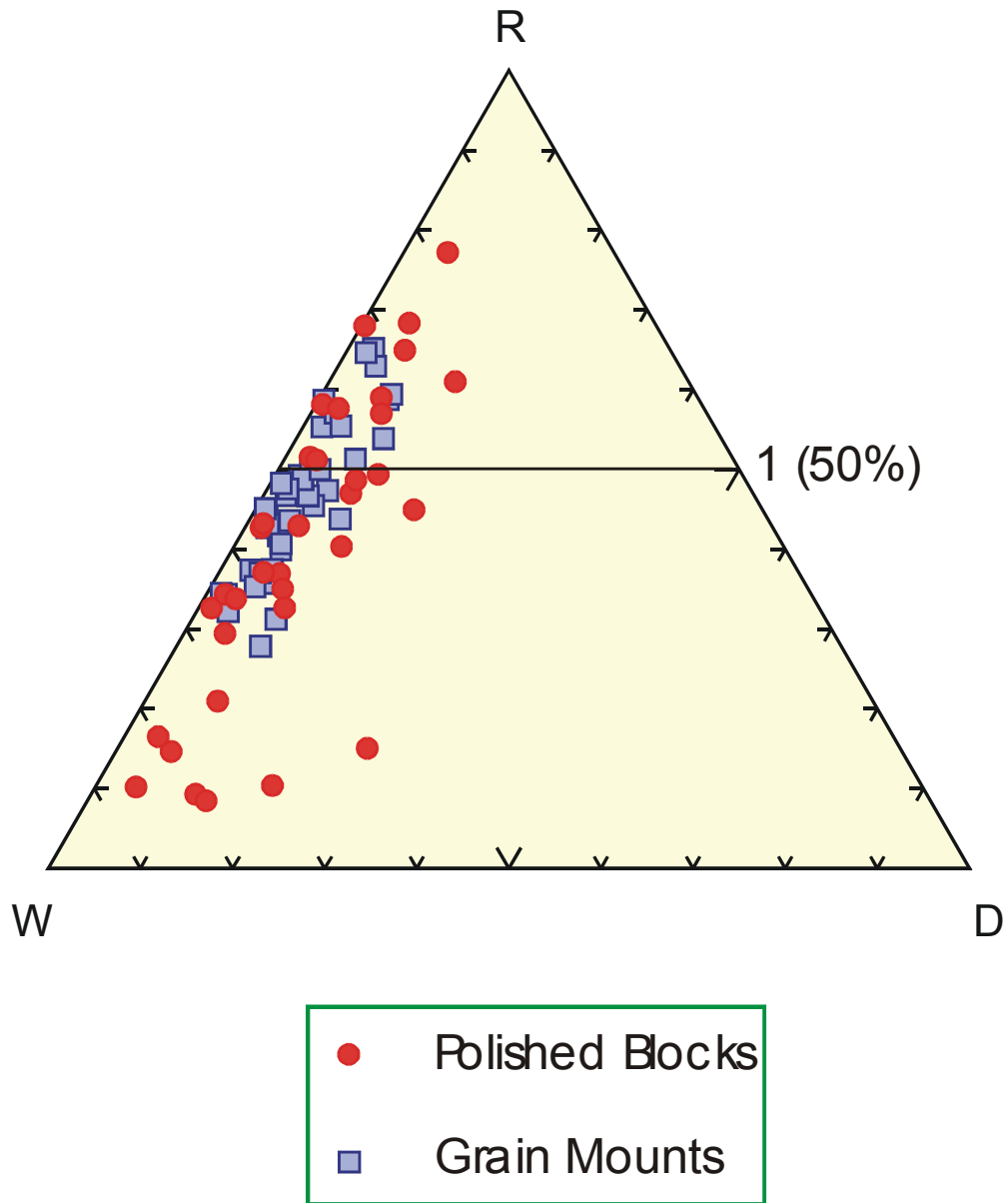


Figure 36: RWD Facies Diagram (R = Remaining Macerals, W = (Wood) = Fusinite + Semifusinite + Telovitrinite, D = (Detrital) = Sporinite + Inertodetrinite) (After Diessel, 1982)

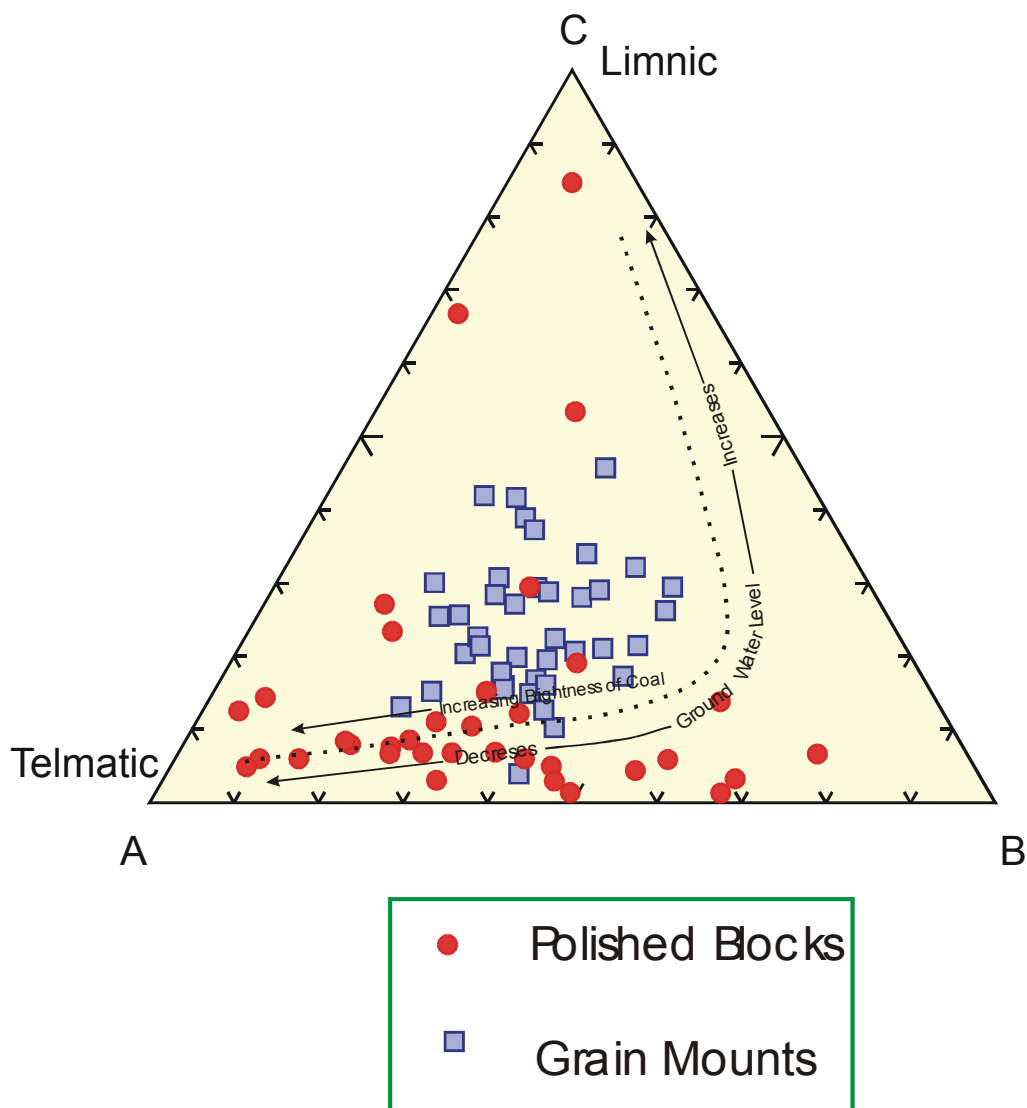


Figure 37: Depositional environments for coal lithotypes in relation to groundwater level, based on maceral associations and mineral matter contents (After Kalkreuth et. al., 1991) (A = Telovitrinite + Semifusinite + Fusinite, B = Detrovitrinite + Macrinite, C = Mineral Matter + Inertodetrinite)

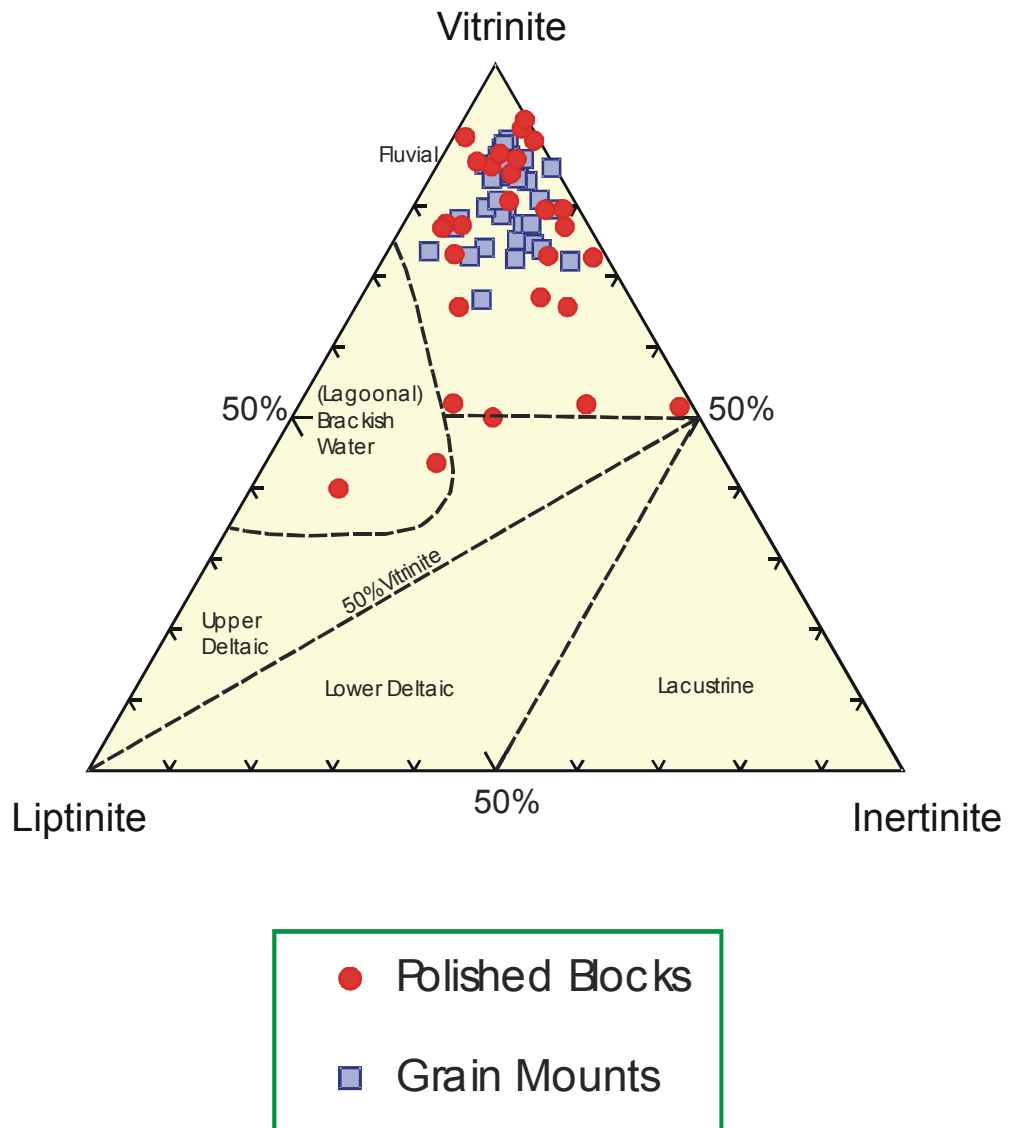


Figure 38: Maceral compositions of Ipswich coal in relation to depositional environments, microlithotypes used in Smyth (1984) have been replaced by main maceral groups in three apices (see text for details) (Modified from Smyth, 1984)

Calder et al. (1991) produced a facies model based on Groundwater Influence (GWI) and Vegetation Index (VI). The parameters used in the reconstruction of peat forming depositional environments are the degree of groundwater influence, relative rainfall, changes in groundwater level, vegetation, mineral matter content and degree of preservation of maceral precursor.

$$\text{Groundwater Influence Index (GWI)} = \frac{\text{Gelovitrinite} + \text{Mineral Matter}}{\text{Telovitrinite} + \text{Detrovitrinite}}$$

$$\text{Vegetation Index (VI)} = \frac{\text{Detrovitrinite} + \text{Inertodetrinite} + \text{Sporinite} + \text{Cutinite}}{\text{Telovitrinite} + \text{Fusinite} + \text{Semifusinite} + \text{Sclerotinite} + \text{Resinite}}$$

Moore and Shearer (2002) investigated four bogs in New Zealand to understand the relationship between peat type (coal type) and depositional environment. They concluded that no diagnostic coal types from four bogs could be used to distinguish particular depositional settings. However, they indicated that the level and variability of water table did have a correlation with coal types. This suggests the importance of groundwater influence on peat formation.

Figure 41 shows the development of palaeoenvironments under various hydrological regimes as suggested by the maceral analyses of Ipswich coal.

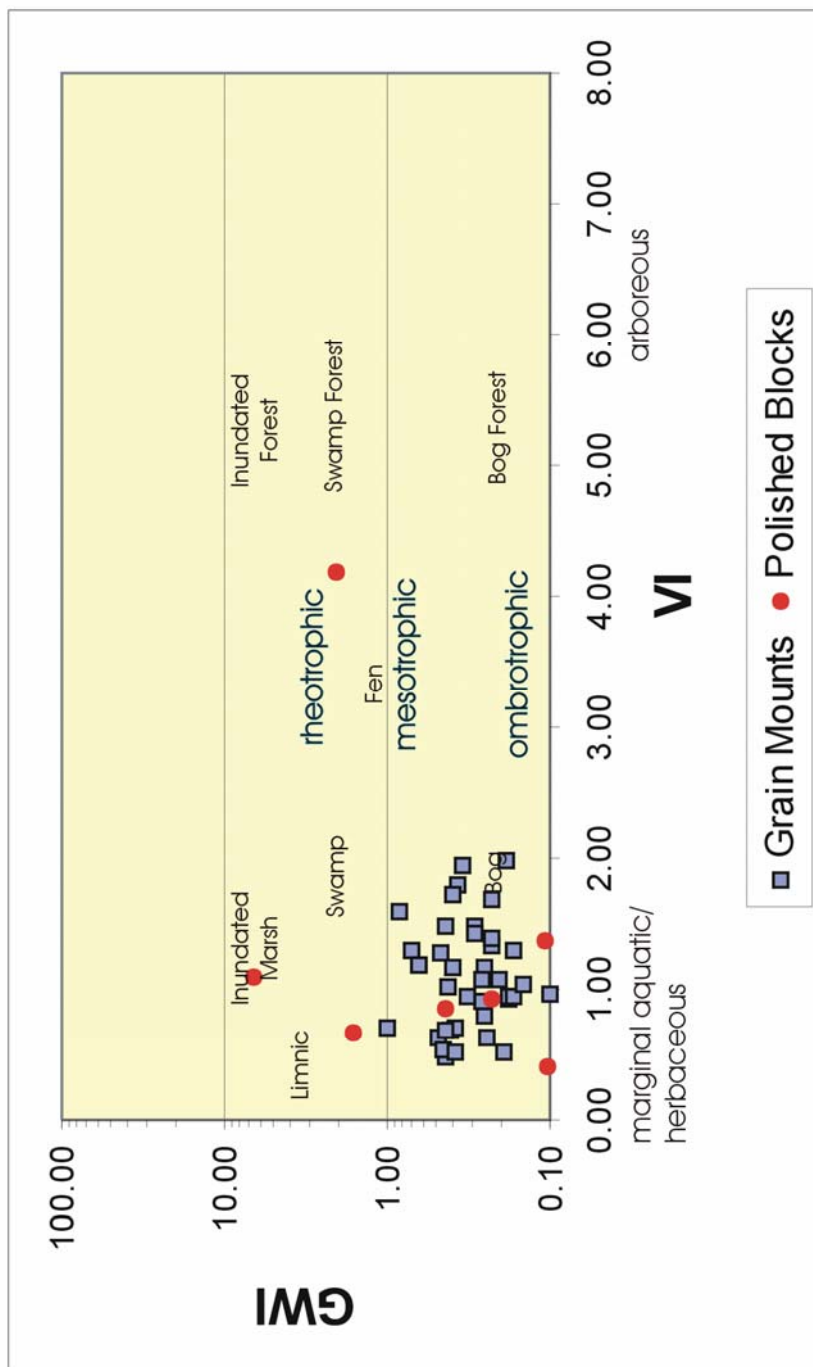


Figure 41 : GWI - VI Crossplot showing mire palaeodepositional environments in relation to various hydrological regimes (after Calder et al., 1991) (See text for details)

Coal Lithotypes vs Maceral Groups

The correlation of coal lithotypes based on brightness profiles and maceral groups has been established (as shown in Table 17) to study the variation between macroscopic and microscopic components.

Table 17: Brightness profile ranking (Codes in brackets are used in borehole profile logs) (Source: AS2519 – 1993)

This table is not available online. Please consult the hardcopy thesis available from the QUT library

Thirty-four highwall samples (polished block samples) were used to develop a relationship between lithotypes and maceral groups (Figures 42A/B and 43A/B). Individual lithotypes were point-counted to 300 points to obtain adequate sample coverage. Two lithotype categories, D and Dmb (duller components of profile), were excluded from the study because insufficient amount of the dull lithotypes were available for an adequate study (see Table 5 and Figures 20 to 31 for brightness profiles). Lithotypes were generally divided into three groups, including the Bright (roughly equivalent to B with minor Bd), Intermediate (roughly equivalent to Bd and DB) and Dull (roughly equivalent to Db with minor DB). Lithotypes Bd and DB were combined to form the Intermediate Group because these two middle-ranked-brightness lithotypes were difficult to differentiate in the field partly due to extreme weathering, lustre changes caused by density variations, lithotype changes (eg. heterogeneous and homogeneous lithotypes), and the friable nature of coal which gives variable brightness characters. Furthermore, the Bright Group contains minor Bd and the Dull Group contains minor DB because field identification of some lithotypes were extremely difficult. However, major grouping of lithotypes gives reasonable results for correlation purposes. Due to combination of lithotypes and formation of major groups, the Bright Group will contain 70 to 90% bright, the Intermediate Group will contain 60 to 70% bright and the Dull Group will contain 50 to 60% bright. It should be noted that the very dull components (ie. D and Dmb) were not included in the Dull Group. Samples containing more than 30% mineral matter were also used in analyses because the Ipswich coal contains high mineral contents, and thus, excluding >30% mineral matter samples may result in inadequate sample numbers for data analyses.

Figure 42A, Lithotype vs. Vitrinite, shows that vitrinite content is highest in bright coal as would be expected, and lowest in the dull lithotype. It shows the linear relationship between the vitrinite content and lithotype brightness.

Lithotype vs. Liptinite in Figure 42B shows that the intermediate coal contains the highest liptinite content, whereas the lowest liptinite content is found in the dull coal. It shows no particular trend or linear relationship.

Figure 43A, Lithotype vs. Inertinite, indicates that the bright coal contains the lowest inertinite content but the intermediate coal contains slightly higher inertinite content than the dull coal. The higher contents of both inertinite and liptinite macerals in the intermediate coal suggest that both macerals were produced under similar depositional conditions. The common association of liptinite and inertinite is a characteristic of Ipswich coal. The inertinite content is slightly variable as expected in continental coal basins. However, in general, bright coal contains lower inertinite content.

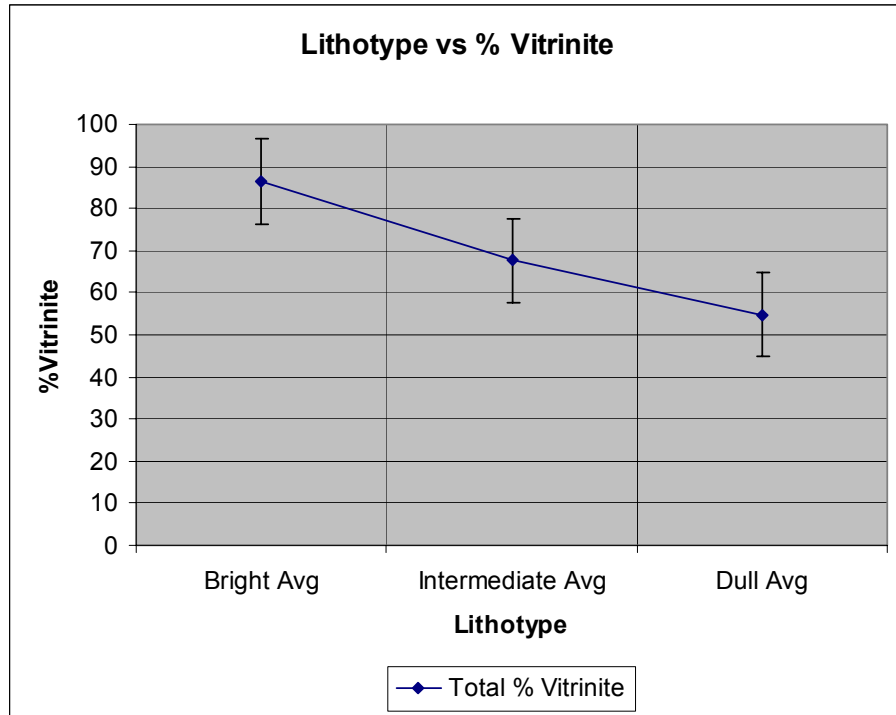
Figure 43B, Lithotype vs. Mineral Matter, shows a decreasing mineral matter content with increasing brightness. This indicates that bright coal lithotypes formed in quieter depositional environments with no significant fluvial incursion in the peat-mire.

In addition, block samples were used to produce a linear relationship graph of telovitrinite and detrovitrinite against lithotypes (Figure 44). Five lithotypes, including B, Bd, DB, Db and Dmb, were used to compare the amount (percentage) of two main vitrinite macerals in each lithotype. The detrovitrinite percentage generally increases with brighter coal components except Db which shows the high detrovitrinite content. This may be due to high inertinite macerals associated with detrovitrinite groundmass in Db. On the other hand, telovitrinite percentages vary but are lowest in the dull component. Some telovitrinite percentages display slightly higher values in the duller components than in the brighter components but total vitrinite content (telovitrinite+detrovitrinite) is still highest in the bright coal.

The relatively high telovitrinite contents in intermediate-ranked-lithotypes is partly due to friable thin lenses in dull coal which tend to produce brighter luster. Furthermore, an increase in density is usually accompanied by a decrease in lustre due to high mineral matter contents. Coals with homogenous lithotypes tend to develop even fractures and this leads to an even light reflection which gives a brighter appearance (eg. vitrain bands in coal). In contrast, lithotypes of heterogeneous composition such as those containing mixtures of macerals (eg. detrovitrinite and liptinite) display an irregular fracture patterns with the concomitant diffuse reflection of light. This results in a dull appearance of coal.

Furthermore, selecting different scales in brightness profile logging may produce variations in lithotype brightness characters. Thin bright bands in dull coal may be excluded from the profile if the scale is too large to produce detailed brightness characters. Oscillating patterns (alternative bright and dull bands) are produced by inertinite macerals in telovitrinite and detrovitrinite groundmass. In addition, very fine dull and bright bands and friable nature of the coal create difficulties in collecting a sample generally representing an identified lithotype interval. Another problem associated with using block samples is that only a small piece of sample is required to make a polished block which may not be a true representative of that lithotype on a brightness profile.

Figures 42 and 43 show plots of macerals versus lithotypes from polished block samples selected from various lithotype layers.



Figures 42A (vertical lines represent error bars)

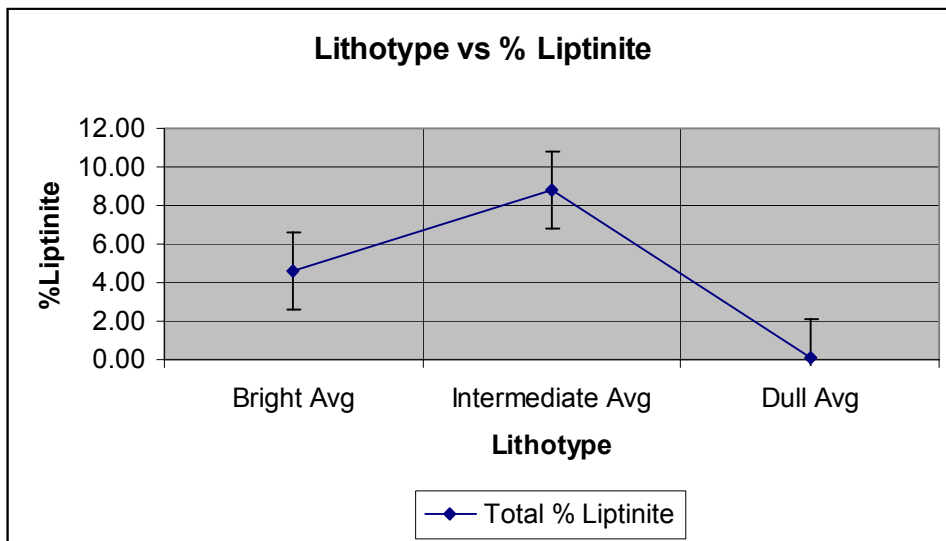


Figure 42B (vertical lines represent error bars)

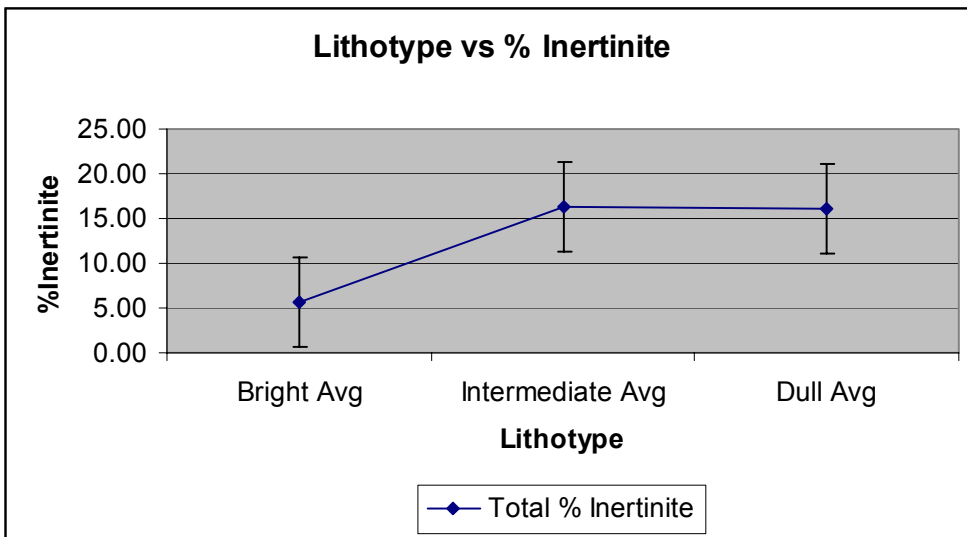
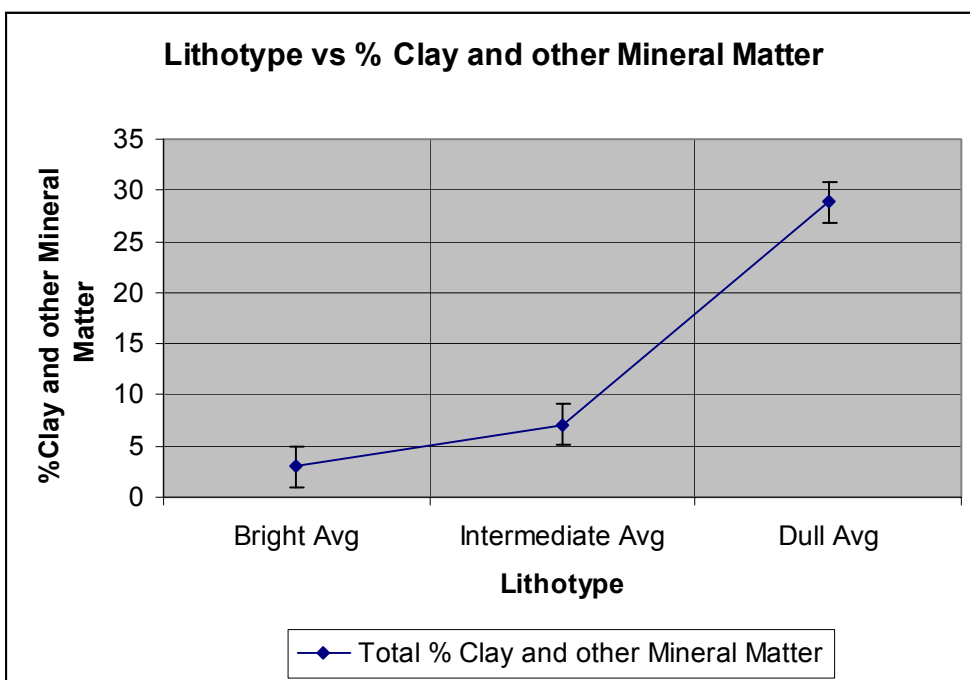


Figure 43A (vertical lines represent error bars)



Figures 43B (vertical lines represent error bars)

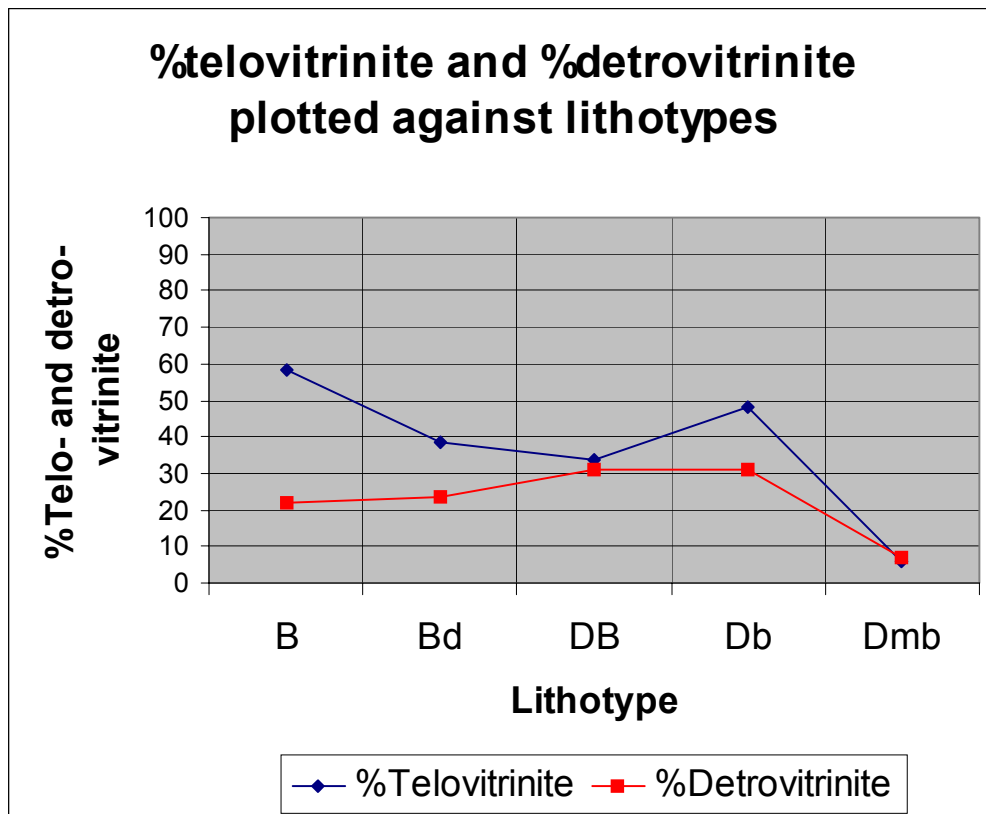


Figure 44: Percentages of telovitrinite and detrovitrinite plotted against lithotypes

The correlation of lithotypes and maceral groups gives mixed results. The vitrinite and mineral matter contents are roughly proportional to the brightness of coal. In general, the vitrinite content increases with brighter coals, while the mineral matter content decreases. The liptinite content and shows no obvious relationship to the brightness of coal. The higher liptinite content found in the intermediate coal is probably due to its association with inertinite. The intermediate coal also contains the highest inertinite content but the bright coal contains the lowest inertinite content. The high liptinite content, in general, is associated with high inertinite content. The cuticles of plants have normally high resistance to decay while the internal structures of leaves are less resistant and hence decompose during the peat formation. Relatively low water levels in the peat swamp generally favour the preservation of leaf tissues, while very wet or completely submerged conditions produce decay especially if the pH level is high. In general, low

pH (ie. acidic condition) favours preservation of plants due to less bioturbation. Furthermore, coals with high inertinite and relatively high liptinite contents could form under drier conditions but liptinite-rich rocks such as oil shales usually form under very wet conditions. The high cutinite content found in Ipswich coal may be due to following reasons:

- ◆ The very high resistance of waxy leaves and thick cuticles
- ◆ No permanent water cover in at least parts of the peat swamp (water level was probably oscillating)
- ◆ Relatively low pH level, and
- ◆ Abundant leaves produced by *Dicroidium* flora

The relationship between coal lithotypes and maceral groups is shown in Figures 42A/B to 43A/B. The total percentages of telovitrinite and detrovitrinite against lithotypes graph is shown in Figure 44 (See Appendix II, Tables 18 and 19 for selected samples used in Figures 42 to 44).

For Table 18 (Appendix II), samples were chosen at random to compare with other maceral groups. It contains all maceral groups including vitrinite, liptinite, inertinite and mineral matter. Whereas in Table 19 (Appendix II), sample values chosen for averages were selected to avoid extreme values which could skew the results. It only includes the telovitrinite and detrovitrinite macerals. Therefore, the averages in Tables 18 and 19 are different but they were used for different purposes. Samples are as received (a.rd) and contain mineral matter.

Both telovitrinite and detrovitrinite show different trends in relation to lithotypes. The graph indicates divergence of two lithotype trends in the bright coal (B) but two trends converge in the dull coal (Dmb). The detrovitrinite content is highest in the bright coal but telovitrinite content in the bright coal is lower than in other lithotypes except Dmb. However, the combined vitrinite content (detrovitrinite+telovitrinite) is highest in the bright coal. The high percentage of detrovitrinite in the bright coal (B) may be partly due to the higher detrital material in the coal which is indicated by friable nature of coal lithotype. In general, the bright coal contains the highest vitrinite content and the dull coal contains the lowest vitrinite content.

Patterns of Coal Seam Accumulation

In contrast to paralic basins, the patterns and distribution of coal and clastic sediments in continental coal basins are largely controlled by tectonism which causes basement tilting, modification in fluvial discharge and changes in sediment supply (Allen et al., 1996). Although climate and sediment source are important, the tectonic subsidence and tilting of the fluvial profile produce the greatest influence on the sediment distribution and packaging. The ratio between the rate of sediment supply and the rate of subsidence-controlled accommodation usually determines changes in the style of non-marine sediment packing patterns. Depending on the value of this ratio, two end members of a spectrum of stacking patterns develop. If the ratio is high (ie. little or no subsidence, and therefore no significant increase in fluvial accommodation) a lateral amalgamation of the fluvial channel will result forming a thick widespread sand sheet. On the other hand, if the ratio is low (ie. very low sediment influx and relatively high subsidence) a lacustrine system will develop. A rapid decrease in the ratio results in the development of a lacustrine “flooding surface”, which usually overlies fluvial deposits. When the ratio reaches its lowest value, a lacustrine “maximum flooding surface” will result. This maximum flooding surface usually contains coal measures and forms a relatively widespread correlation marker (Allen et al., 1996). Diessel (1992) suggested that the tectonic settings of a coalfield exert a strong influence on the chemical and mechanical properties of coal. The eustatic and relative sea level changes have no influence on continental basins, but tectonism together with seasonal variations and basin physiography largely control sediment accumulation and distribution. Furthermore, Smyth (1989) pointed out that these major controlling factors could be overridden by unique events and/or depositional conditions such as drought, flooding, volcanism and introduction of new flora. The dulling upward successions commonly found in brightness profiles indicate water level variations. Groundwater table level and degree of fluctuation in the peat swamp are main controlling factors on coal types. Some of the important events defined by Stach et al. (1982) include evolutionary development of flora, climatic changes mainly due to volcanism, geographical and structural position of the basin and the hydrology.

Results

A total of **1231** boreholes was used to study the distribution of coal seams and define the structures which controlled the coal sedimentation in the basin.

Figure 45 shows the surface contour map of the Ipswich Basin using borehole collar data (R.L). The borehole collar data were used to calculate

coal seam depths in relation to the surface topography. Seam thickness contour maps were generated for each major coal seam to define the depocentres of the Blackstone and Tivoli Formations. Seam roof contour maps show the overburden thickness and seam depths of all main coal seams. Seam split maps were also produced to study the splitting patterns and position of seam splits in relation to depocentres. The total thickness contour map (including coal and clastic sediments) of the Blackstone Formation and total coal thickness contour maps of the Blackstone and Tivoli Formations were produced to study the sedimentation patterns within the basin. The results are discussed in the following section from the oldest coal seam (Waterworks) to the youngest coal seam (Thomas).

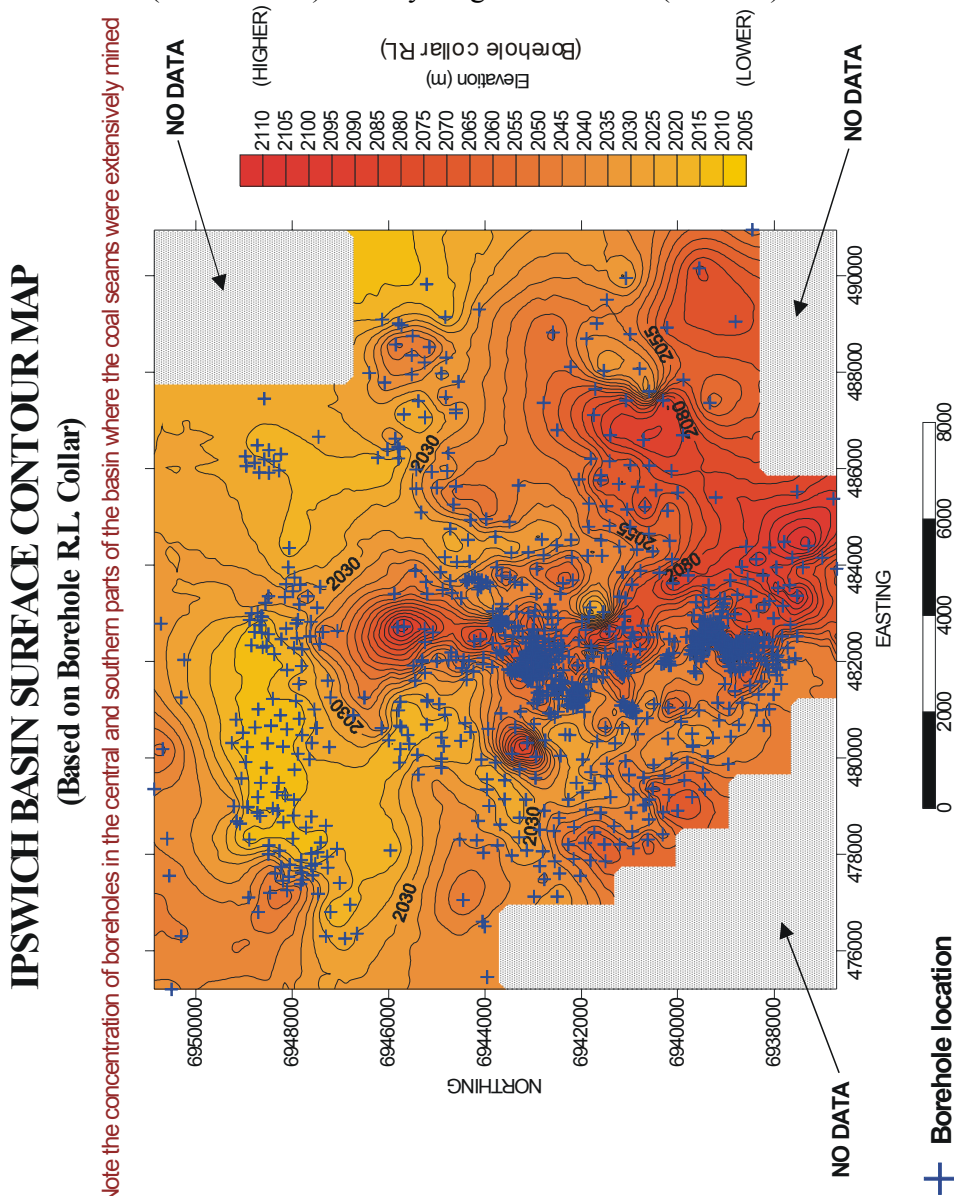


Figure 45: Ipswich Basin Surface Contour Map

Seam Contour Maps and Seam Split Maps

Contour maps were produced to study the seam thickness distributions and seam roof structures. Statistical analyses were performed on each seam and the data were used in conjunction with petrographic study to produce a depositional model.

Contour maps of all main seams and the Striped Bacon-Rob Roy interval have been produced for the Blackstone Formation. Unnamed, CL, Hillier, Unnamed 2, Francis and Morris seams have been excluded from the Tivoli Formation as they are relatively small.

Major seam split maps were produced to define seam splitting patterns. Seam splits show progressive splitting patterns and some seam splits coincide with depocentres (eg. Thomas Top, Bluff Top, Fourfoot Bottom, Cochrane Top and Tantivy Top). Two main types of seam splitting have been observed. In general, tectonic splitting is caused by rapid fault-controlled subsidence and/or movement such as uplift and tilting, whereas sedimentary splitting is produced by channel switching and avulsion and it shows random split distribution (see 'Discussion' section and Appendix V - Large Cross-sections for details). Tables 20 (Tivoli Formation) and 21 (Blackstone Formation) describe the summary of seam thicknesses, structures and splits.

Tivoli Formation

Waterworks Seam

This seam is the lowest in the stratigraphic sequence of the Brassall Subgroup. The seam is relatively thicker in the northeastern part where it is shallower (Figure 46) and dipping to the south (Figure 47).

Benley Seam

The Benley seam thickness contour map shows that the seam is thicker in the northwestern part (Figure 48). It may also be due to the closer borehole spacing in the northwest. The seam dips to the south (Figure 49).

Eclipse Seam

The Eclipse seam appears to be relatively thicker in the western part (Figure 50). However, like Benley seam, it may be due to closer borehole spacing in the west and very sparse boreholes in the east. The seam dips to the south and a synclinal structure was shown in the western part (Figure 51).

Poverty Seam

The Poverty seam is thicker in the southwestern part where it is also deeper (Figure 52) and dips to the southwest (Figure 53).

Tivoli Seam

The Tivoli seam appears to be thicker in the western part (Figure 54). The seam appears to be thicker on structure highs. The seam dips to the south (Figure 55).

Waterstown Seam

The Waterstown seam is thicker in the northeast (Figure 56) where the seam is shallower but there is no definite relation of structure to thickness. The roof structure contour map shows multi-directional dipping, but generally dips to the south. A synclinal structure is also observed in the western part (Figure 57).

Fiery Seam

The seam thickness contours are variable but mainly thicker in the western and southeastern parts (Figure 58). Thicker coal is mainly in deeper parts (in central and southern parts) but seam splitting occurs in shallower parts of the seam. The seam dips to the south (Figure 59). The Fiery seam splits into top, bottom and main seams (Figure 60).

Tantivy Seam

The seam thickness contour map shows that the seam is mainly thicker in the central and eastern parts (Figure 61). Thicker coal roughly coincides with deeper structure. The seam is generally dipping to the south (Figure 62). Tantivy seam splits into top, bottom and main seams. The seam splitting occurs in the structure high central part (Figure 63).

Westfalen Top Seam

The Westfalen Top seam appears to be thicker in the south (Figure 64). Coal is thicker in the deeper parts of the structure. The seam is steeply dipping to the west and south (Figure 65).

Garden Seam

The Garden seam thickness contours are varied but thicker in the central and eastern parts (Figure 66). The roof structure contour map shows steep dipping to the south and south-west (Figure 67).

Swanbank Area Seams

The Matthews, Livermore, Taylor, and Ritchie are all localised seams found only in the Swanbank Lagoon mining area (Figures 68 to 75). Thicker coal is in the deeper part of the structure but reverse is applied for the Taylor and probably the Livermore seam.

Cochrane Seam

The Cochrane seam thickness contour map shows variable thicknesses but mainly thicker in the southwest (Figure 76). The seam is dipping to the east and southeast (Figure 77). The seam splitting occurs in the southern and eastern parts. Splits occupy areas of structural low. The seam splits into top, bottom and main seams (Figure 78).

Table 20: Tivoli Formation seam thickness and structure description - Summary

Seam	Thickness and Structure Description	Split
Cochrane	This is the only seam in the Tivoli Formation deposited in the southern part of the basin. Steep dipping to the south of Bundamba Anticline. Structural deformation occurs just SE of the anticline. Thinner coal deposition at Bundamba Anticline.	Both top and bottom splitting occur at the anticline. Top split is in the west whereas bottom split is in the east.
Ritchie	Localised seam in the Swanbank area. Thicker coal in the deeper area in the south. Dips to the south.	No notable split.
Taylor	Localised seam in the Swanbank area. Taylor has thicker coal in the north where it is shallower. Dips to the south.	No notable split.
Livermore	Localised seam in the Swanbank area. Roughly thicker in the intermediate zone (east) where the dip is steeper. Dips to the south.	No notable split.
Matthews	Localised seam in the Swanbank area. Seam is thicker in the deeper area (north). Dips to the south.	No notable split.
Garden	Formed in the northern part of basin. Thicker in the north-eastern part. Dips to the south.	No notable split.
Westfalen-Top	Formed in the north. Thicker towards south-west and central east. Dips to the south-west.	No notable split.
Tantivy	Formed in the north. Central and eastern parts are thickest. Dips to the south-central part.	Minor split occurs in the centre on the steep slope.
Fiery	Formed in the north. Two thickness anomalies, larger one is in south-east and smaller one is in central-west. Dips to the south.	Seam splits mostly where the coal is thinner and shallower.
Waterstown	Formed in the north. Thicker in central and east where it is shallower. Dips to the south-west.	No notable split.
Tivoli	Formed in the north. Thicker in central-west. Seam dips to the south.	No notable split.
Poverty	Formed in the north. Thicker to the south-west. Also dips to the south.	No notable split.
Eclipse	Formed in the north. Relatively thicker in the north-west. Dips to the south.	No notable split.
Benley	Formed in the north. Thicker to the north-west. Dips to the south.	No notable split.
Waterworks	Formed in the north. Thicker to the north-east. Dips to the south.	No notable split.

All seams in the Tivoli Formation generally dip to the south. Only the Cochrane seam is formed in the southern part of the basin. Seam splitting is relatively less common than the Blackstone Formation. However, some seam splits were probably named as separate seams, such as those seams in the Swanbank area.

Blackstone Formation

Rob Roy Seam

The Rob Roy seam is generally thicker in the southwest (Figure 79). The roof structure contour map shows multi-directional dip, but generally to the southwest and southeast (Figure 80). The seam splitting occurs in a structural high area where the Bundamba Anticline develops. The Rob Roy splits into top and main seams (Figure 81).

Striped Bacon-Rob Roy Interval

This interval is thicker in the south-west (Figure 82). The seam roughly dips to the west and south-west (Figure 83). Figure 84 shows the Striped Bacon-Rob Roy interval with boreholes that intersected this interval.

Striped Bacon Seam

The Striped Bacon seam is thicker in the southwest (Figure 85). The seam is dipping to the west and east (Figure 86). A small bottom split is found in a central structure high area where the seam is thinner (Figure 87).

Bergin Seam

The Bergin seam is thicker in the central part but it shows variable thickness anomalies on both sides of the Bundamba Anticline (Figure 88). The roof structure contour map shows similar folded structure to the Fourfoot and Bluff seams (Figure 89). The seam splitting occurs in the south-central part and it splits into top, bottom and main seams (Figure 90).

Fourfoot Seam

The Fourfoot seam is relatively thicker in the west and splitting occurs in the south (Figure 91). The Fourfoot-Bergin interval was also included in the Fourfoot total thickness as it is mainly a Fourfoot split. The roof structure contour map shows dipping is slightly folded away from the centre where the Bundamba Anticline develops. (Figure 92). The seam splits into top, bottom and main seams across the Bundamba Anticline (Figure 93).

Bluff Seam

The Bluff seam is thicker on the northwestern side of the area and thinner when it forms a subcrop in the centre (Figure 94). The roof structure contour map (Figure 95) indicates that seam dip is slightly folded away from the subcrop area like the Fourfoot seam. The Bluff-Fourfoot interval was also found below the Bluff main seam and included in the Bluff total thickness

as it is essentially a Bluff split. Splitting mainly occurs in the central part of the area covered by the Bluff seam, but the Bluff-Fourfoot interval is present on the eastern side. The seam splits into top, bottom and main seams (Figure 96).

Aberdare Seam

Figure 97 shows that the Aberdare seam is relatively thicker in the northern part but a small thickness anomaly is found in the south-central part. The seam is also dipping southwest (Figure 98). Splitting occurs in the central and southern parts (Figure 99). The seam splits into top, bottom and main seams.

Thomas Seam

Figure 100 shows that the Thomas seam is thicker in the west. The roof structure contour map (Figure 101) shows that the seam is steeply dipping to the southwest direction. Seam splitting occurs in the west. The seam split map indicates splitting occurs around the depocentre (Figure 102). The seam splits into top and main seams.

Table 21: Blackstone Formation seam thickness and structure description - Summary

Seam	Thickness and structure Description	Split
Thomas	Coal is on the western side of the Bundamba Anticline and structure contours dip to the west where it is also thicker.	Split occurs in or around the depocentre where the dip is steeper and deeper.
Aberdare	Thickness contours show no relation to the Bundamba Anticline but thicker in the north. Structure contours roughly follow the Bundamba Anticline.	Southern part of the Bundamba Anticline.
Bluff	Coal is mostly on the Western side of the Bundamba Anticline. Structure contours roughly follow the anticline. It is generally thicker in deeper areas, especially in the west.	The Bluff seam splits on the anticline where the dip is relatively flat. Other seam splits coincide with steep structure contours.
Fourfoot	Depocentres on both sides of anticline. Structure contours roughly follow the anticline. The seam is thick on both sides of the anticline but thicker on the west side.	Splits mostly occur on the Bundamba Anticline but also across it.
Bergin	Depocentres are roughly on the both sides of anticline. Structure contours roughly follow the anticline.	Seam splits across the anticline but mostly on the anticline.
Striped Bacon	Thick on the west side of anticline. Structure contours roughly follow the anticline.	Small but on the anticline.
Rob Roy	Slightly thicker on the south-west of anticline. Structure contours roughly follow the anticline.	Splits along the anticline.

From Rob Roy to Bluff structure contours show progressive anticlinal structure reflecting the Bundamba Anticline, but Aberdare and Thomas seams structure contours only show a monoclinical structure.

The sedimentation patterns show that when coal was deposited at one place the available accommodation was significantly reduced so that better accommodation was available elsewhere. The coal accumulation began in the north-east of the basin and then went to north-west, west, east, north-east and finally south due to gradual tilting of the basin basement.

Following figures, Figures 46 to 102, display seam thickness contour maps, seam roof structure maps and seam split maps. Seam thickness maps and seam roof structure maps were drawn in the same scale for comparison. Seam split maps, on the other hand, were drawn in smaller scales to show where they occur and how they relate to major structures in the basin. Seam split lines were drawn on the thickness contour maps and then posted onto the Ipswich Basin basemap to investigate the overall splitting patterns.

All contour maps were generated from Surfer V.7 software package.

All Easting and Northing values are in meters.
Seam depth and thickness values are also in meters.

WATERWORKS SEAM THICKNESS CONTOUR MAP

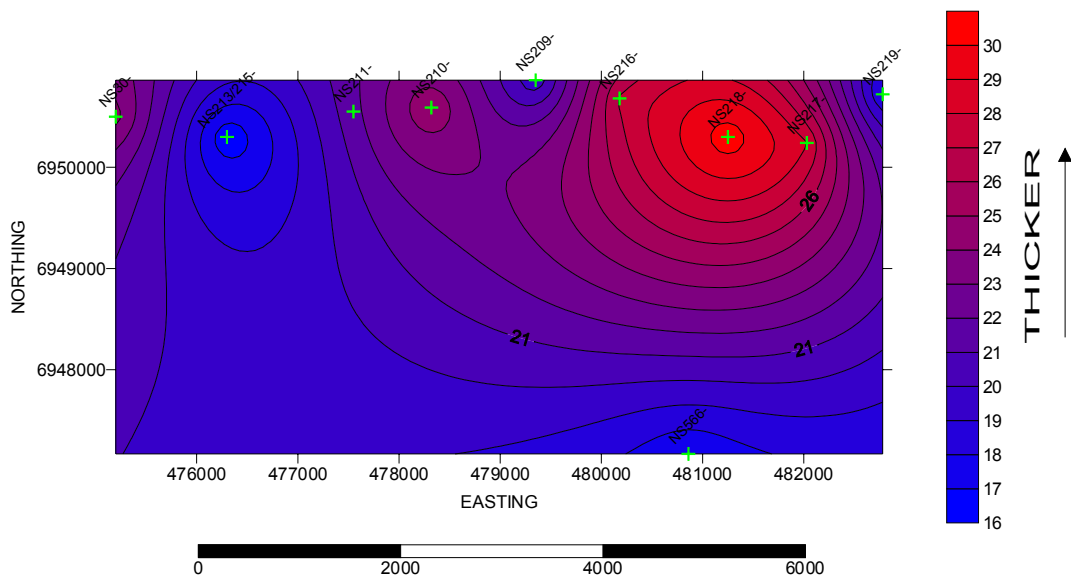


Figure 46

WATERWORKS SEAM ROOF CONTOUR MAP

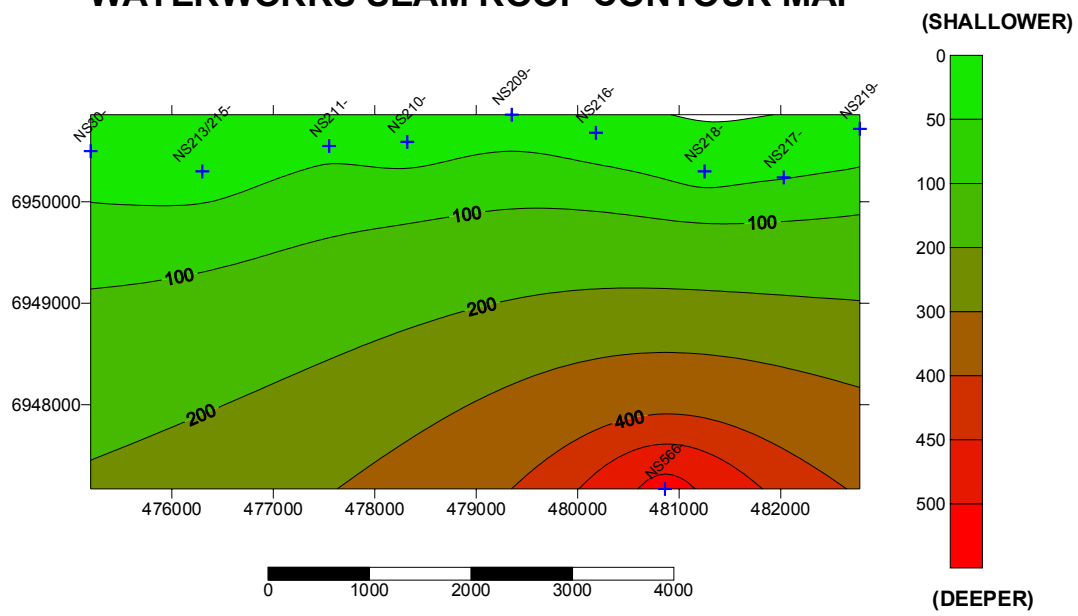


Figure 47

ECLIPSE SEAM THICKNESS CONTOUR MAP

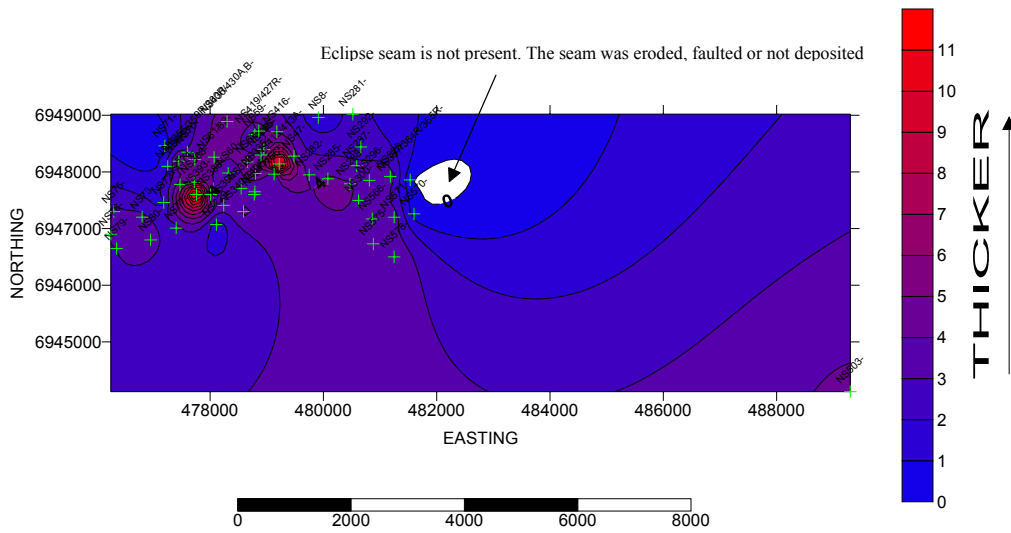


Figure 48

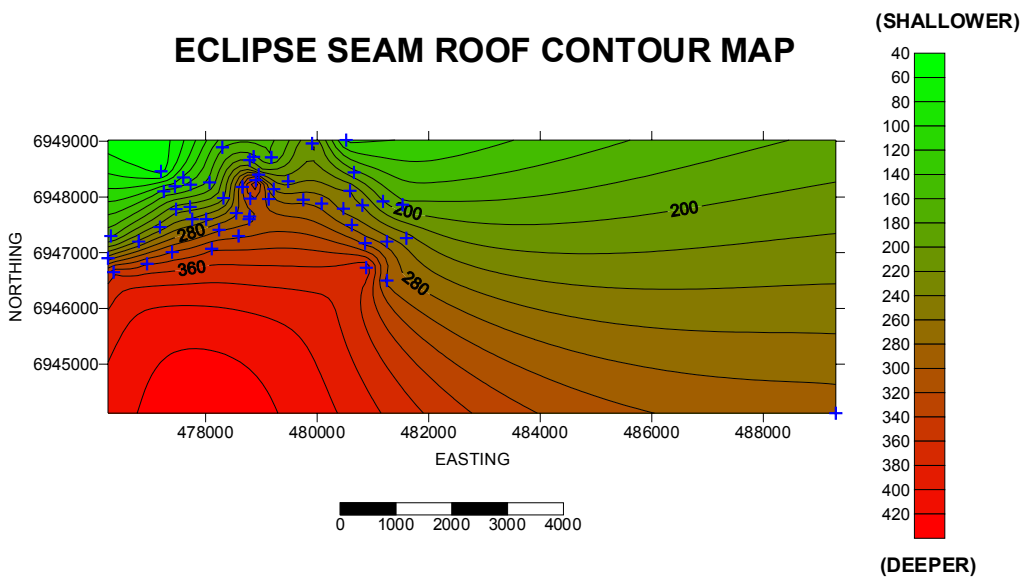


Figure 49

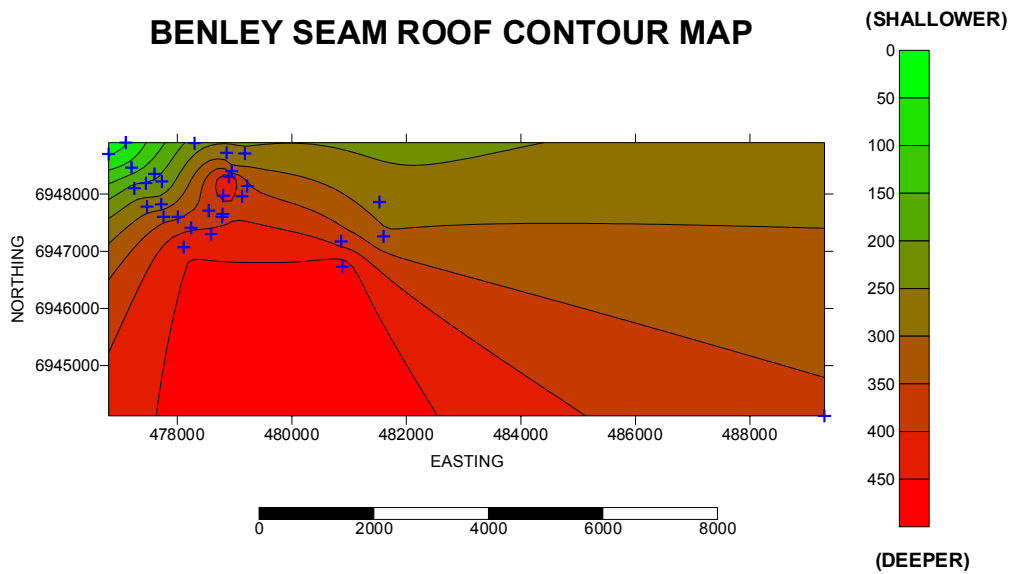


Figure 51

POVERTY SEAM THICKNESS CONTOUR MAP

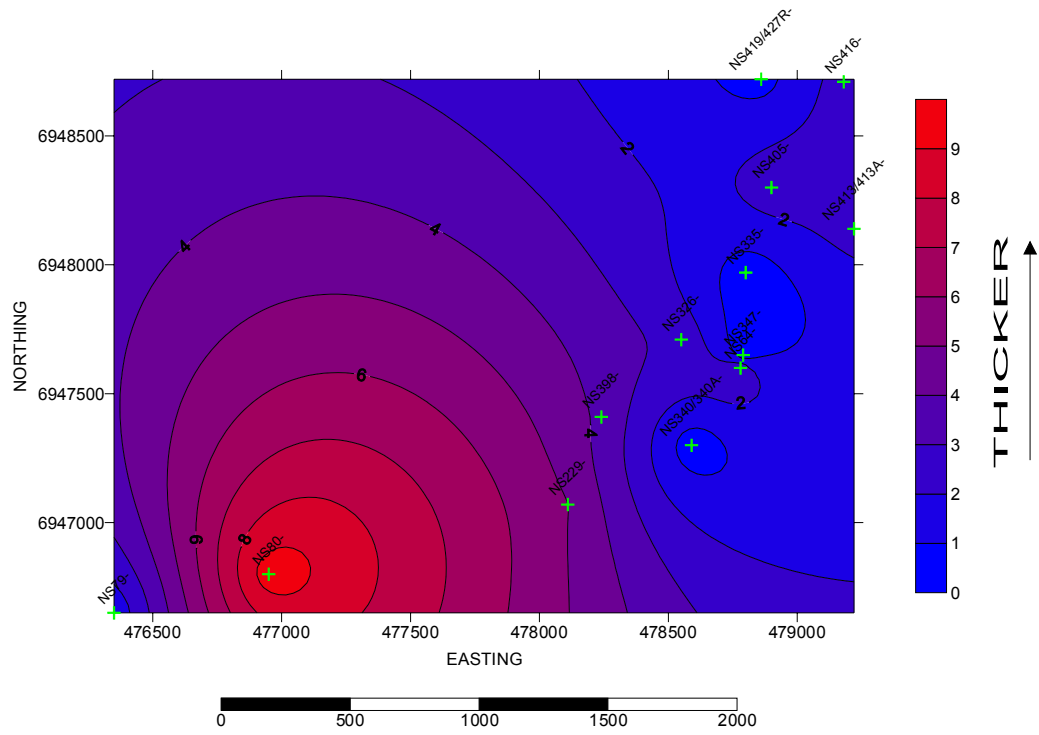


Figure 52

POVERTY SEAM ROOF CONTOUR MAP

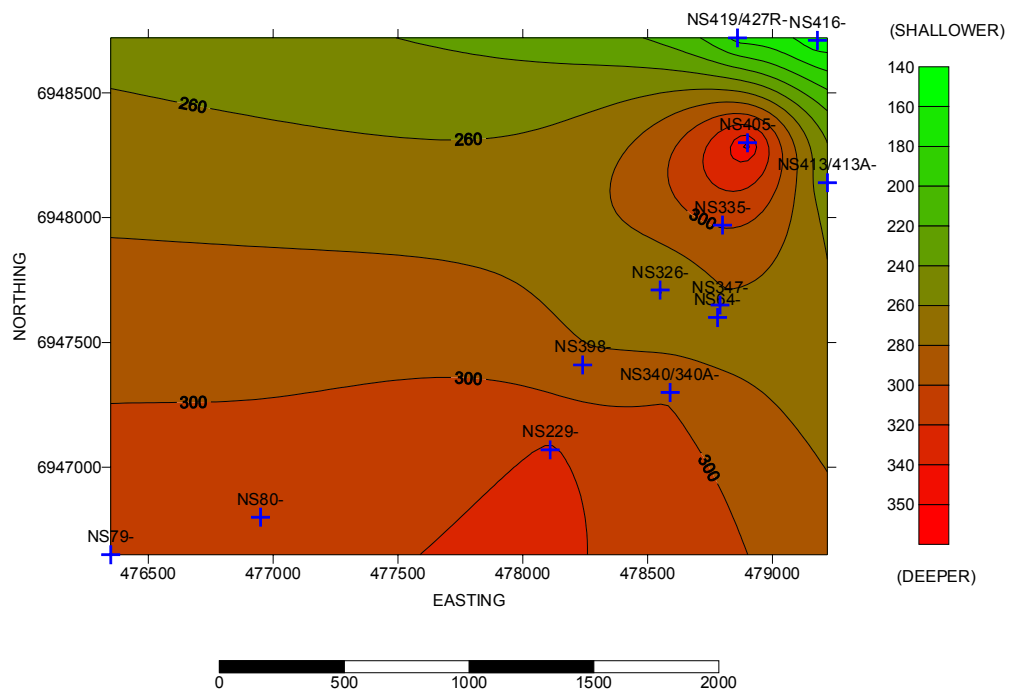


Figure 53

TIVOLI SEAM THICKNESS CONTOUR MAP

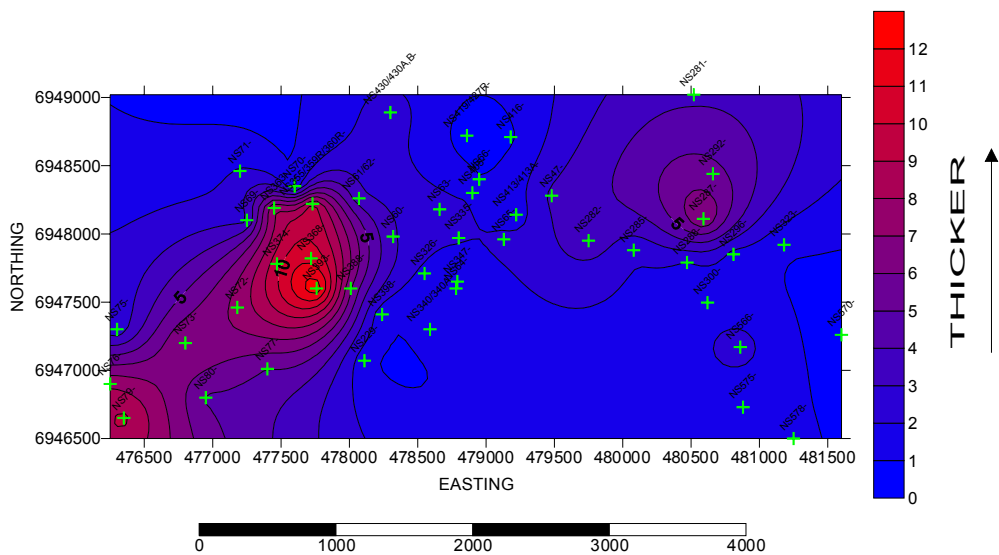


Figure 54

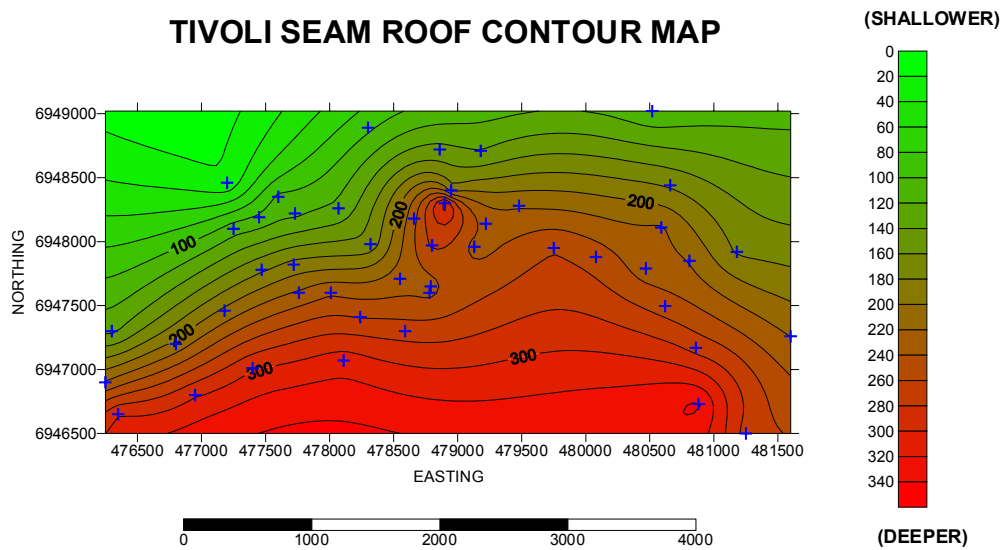


Figure 55

WATERSTOWN SEAM THICKNESS CONTOUR MAP

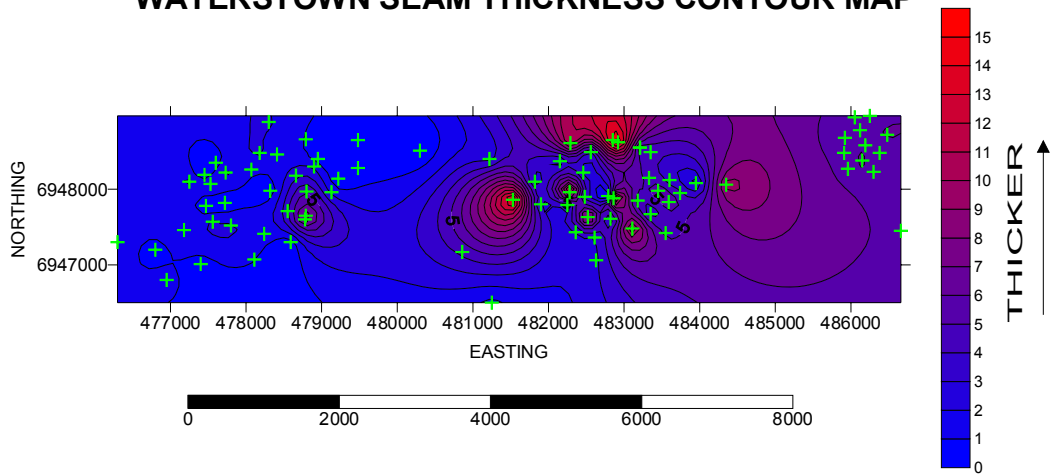


Figure 56

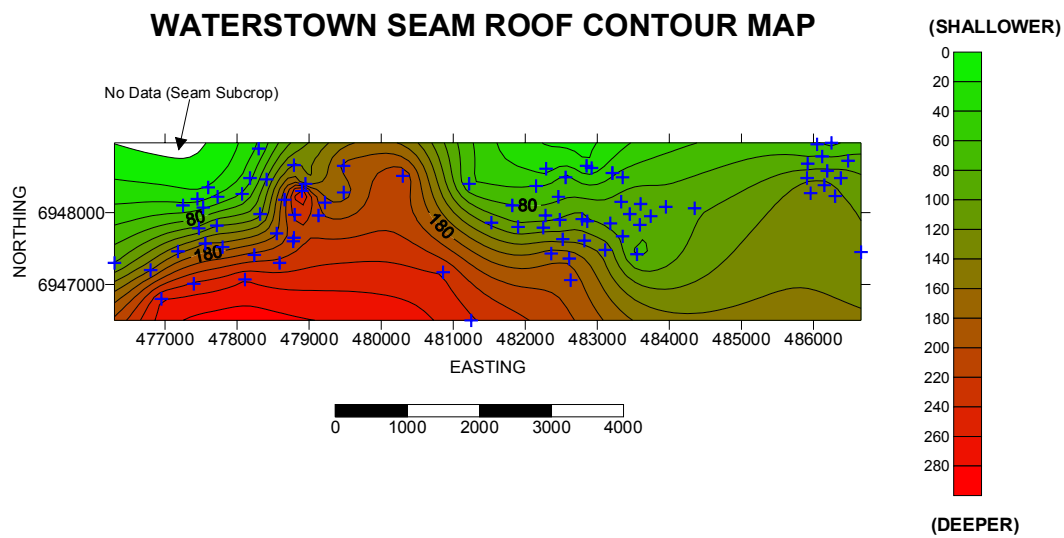


Figure 57

FIERY SEAM THICKNESS CONTOUR MAP

Eclipse seam is not present. The seam was eroded, faulted or not deposited

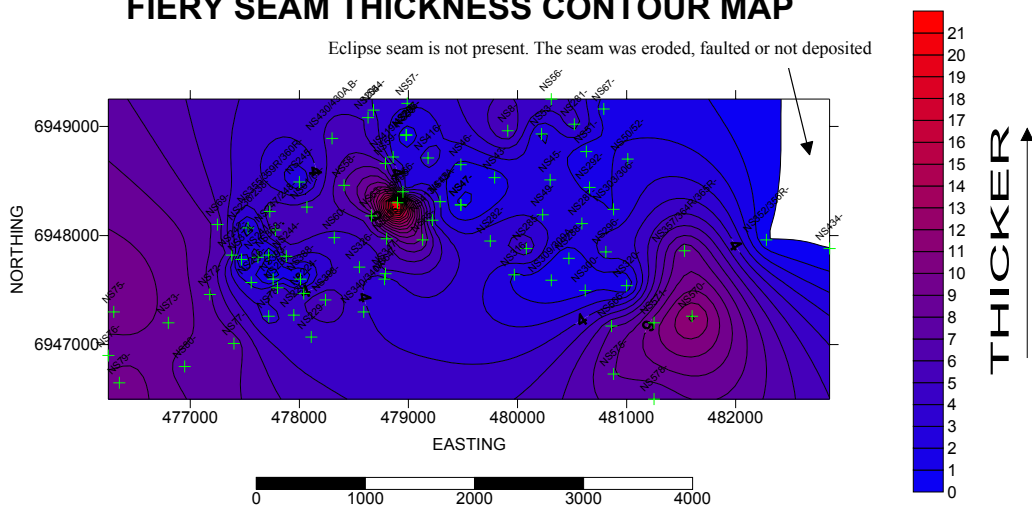


Figure 58

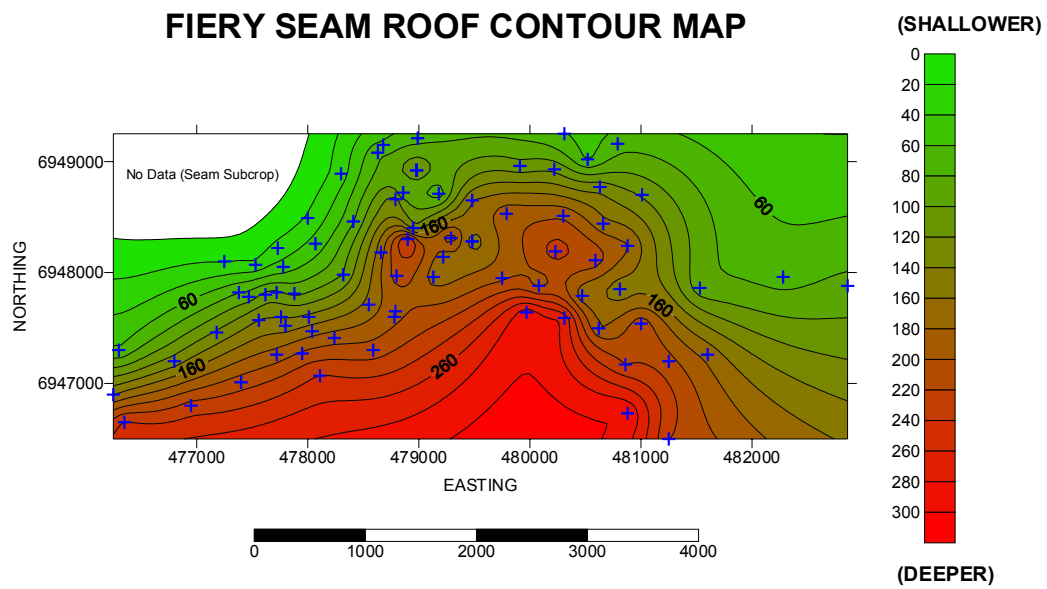


Figure 59

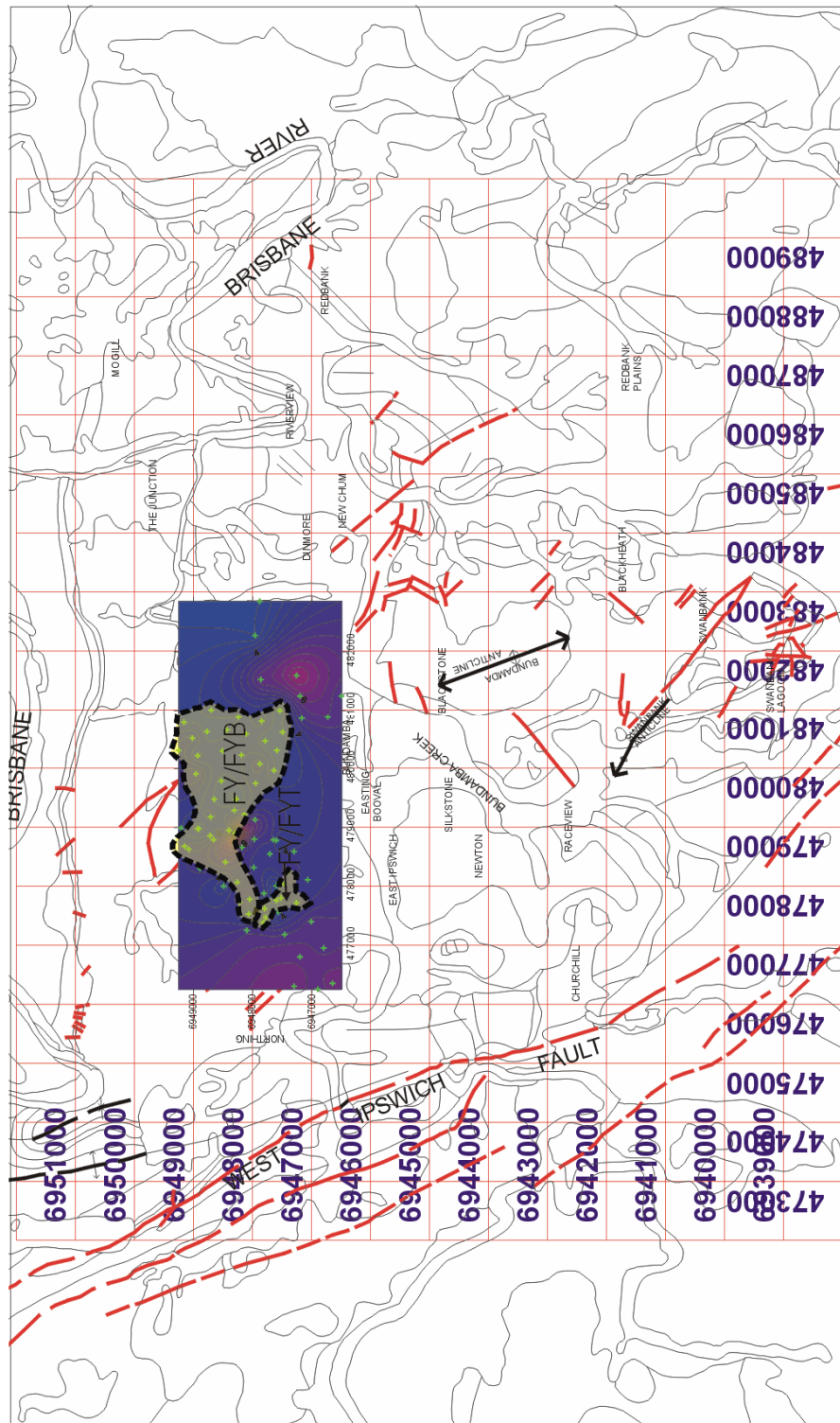


Figure 60: Fiery Top (FYT) (small) and Bottom (FYB) Splits
 (See Figure 58 for detailed thickness contour map)

Light-yellowish grey shaded areas with dotted lines in **split maps** represent areas of seam split (eg. FYT = Fiery Top Split, FYB = Fiery Bottom Split).

TANTIVY SEAM THICKNESS CONTOUR MAP

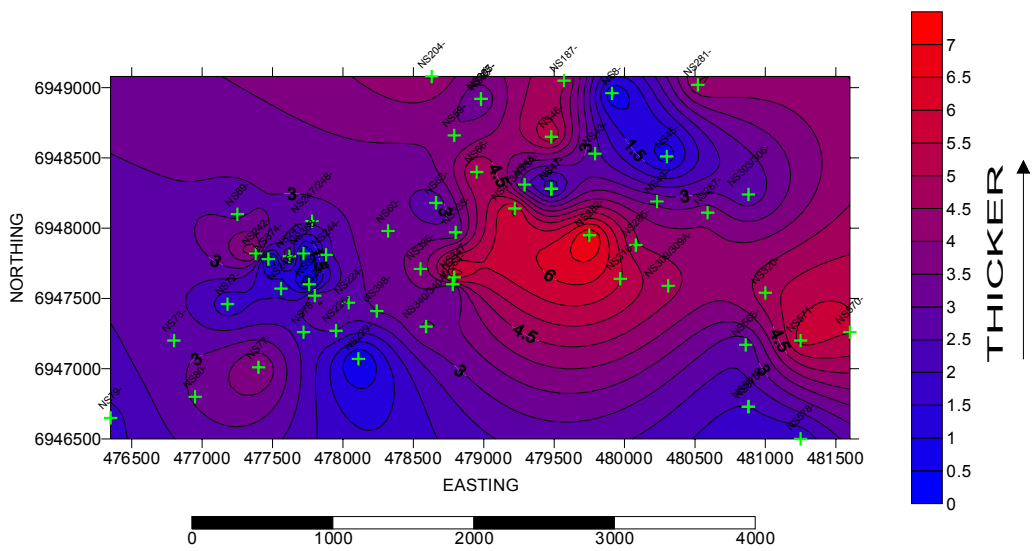


Figure 61

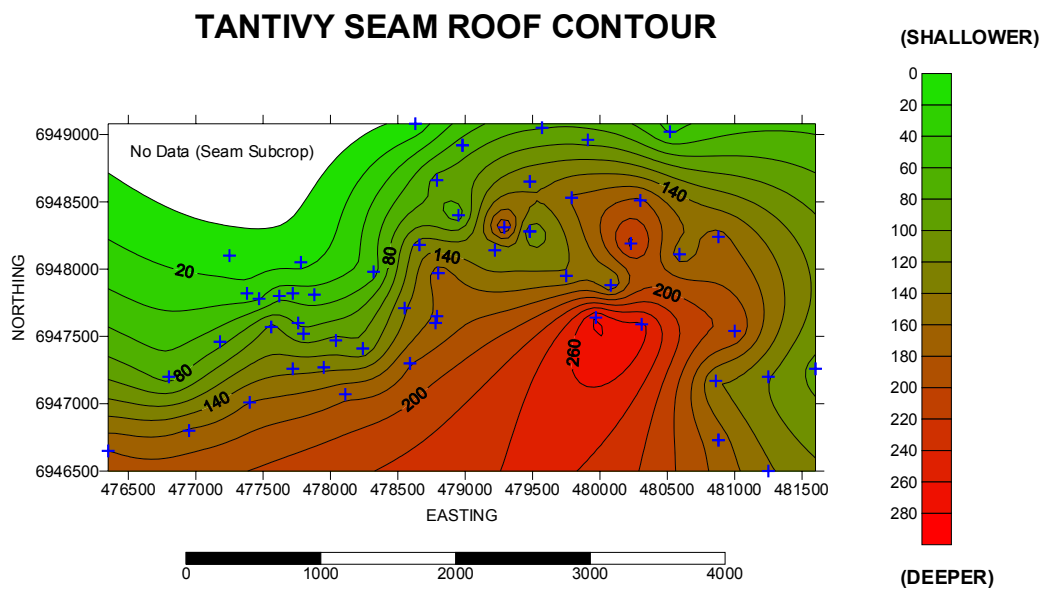


Figure 62

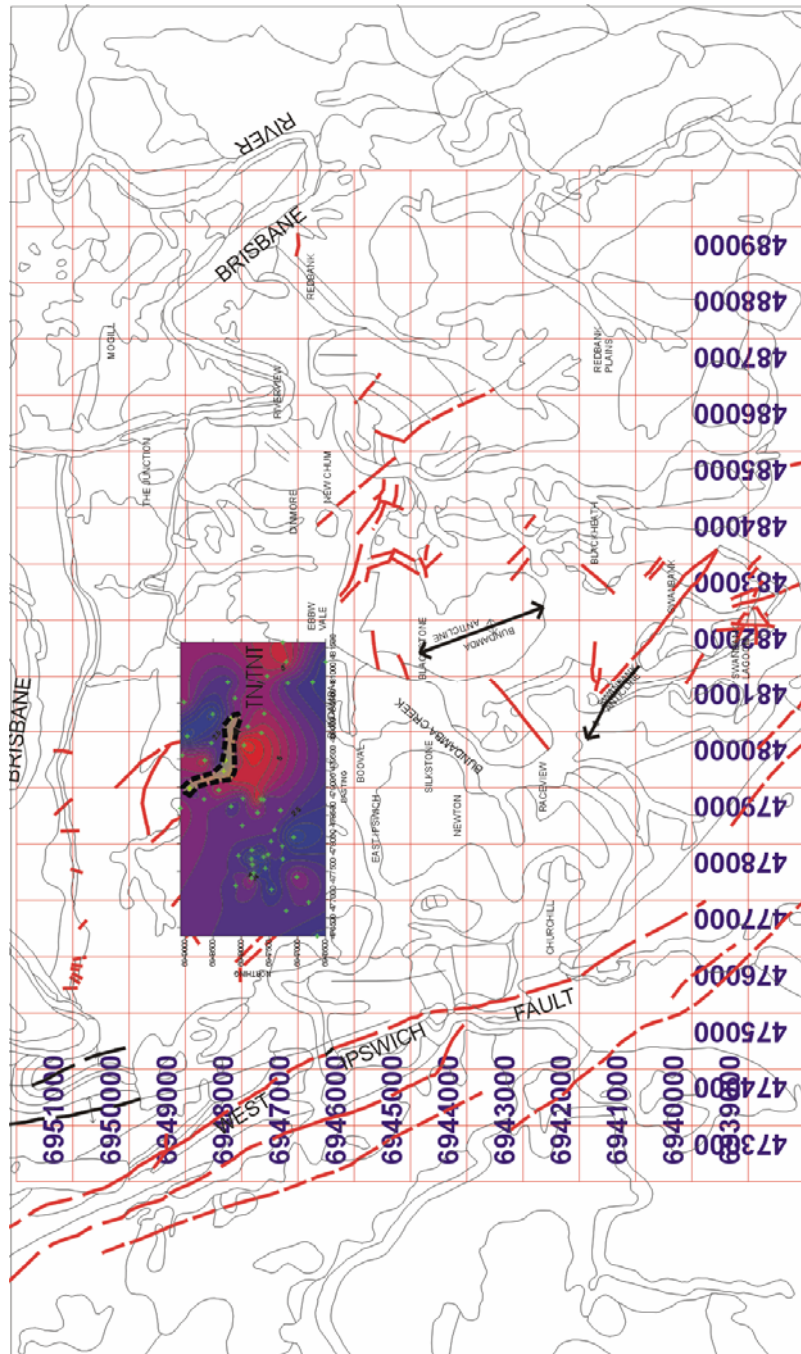


Figure 63: Tantivy Top (TNT) Split (a small split)
 (See Figure 61 for detailed thickness contour map)

WESTFALEN TOP THICKNESS CONTOUR MAP

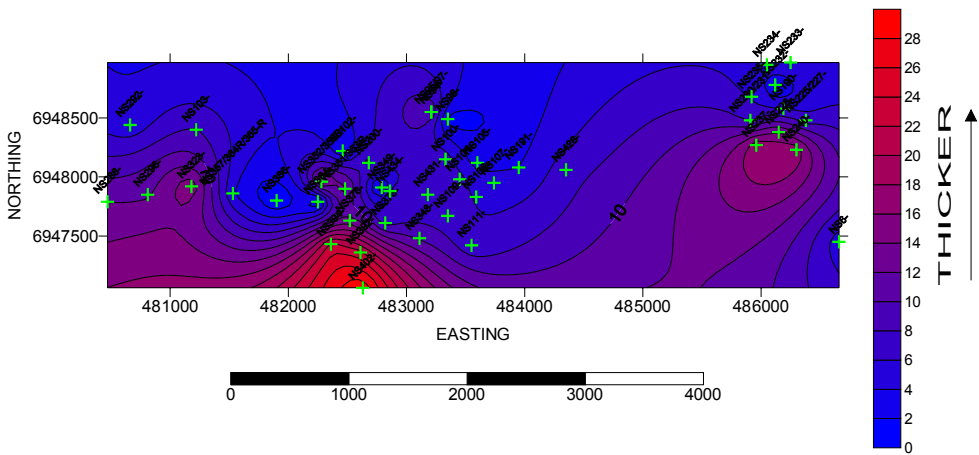


Figure 64

WESTFALEN TOP SEAM ROOF CONTOUR MAP

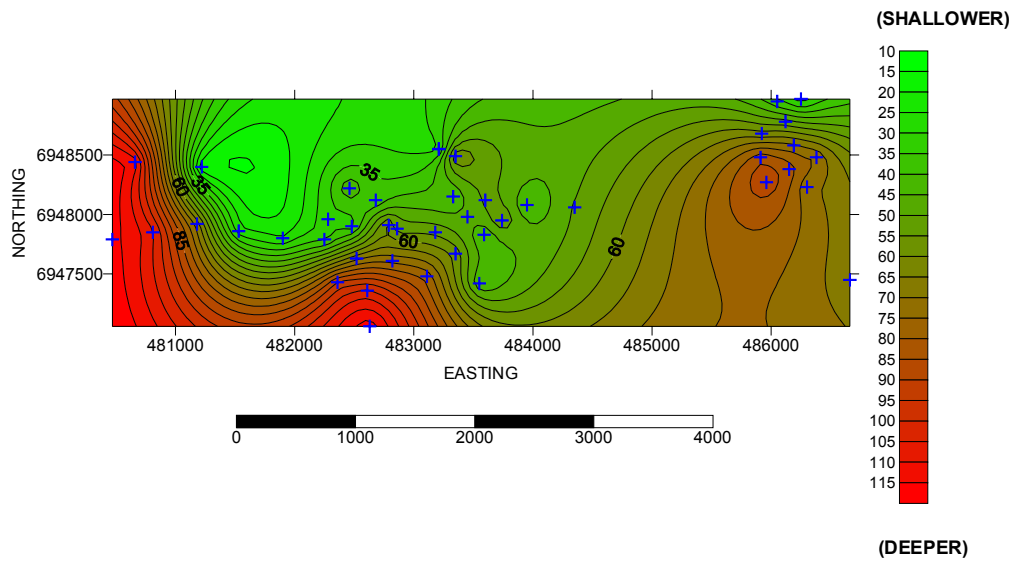


Figure 65

GARDEN SEAM THICKNESS CONTOUR MAP

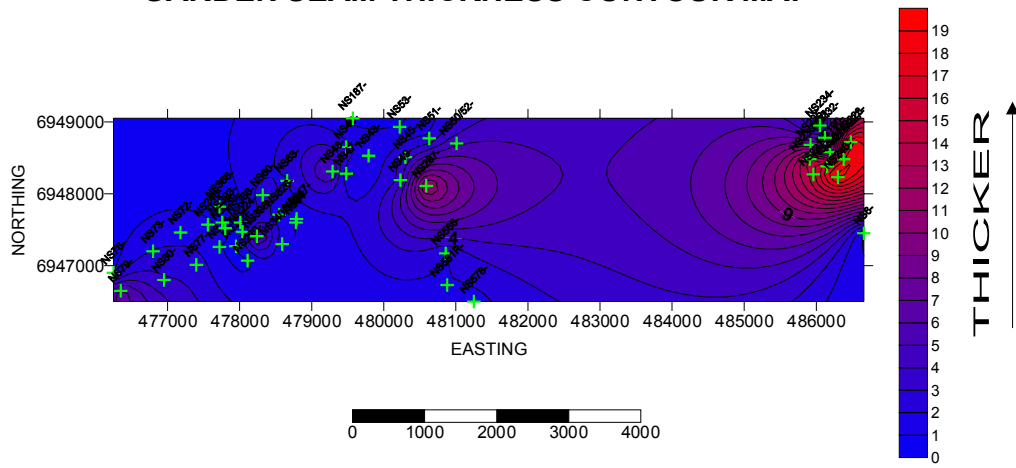


Figure 66

GARDEN SEAM ROOF CONTOUR MAP

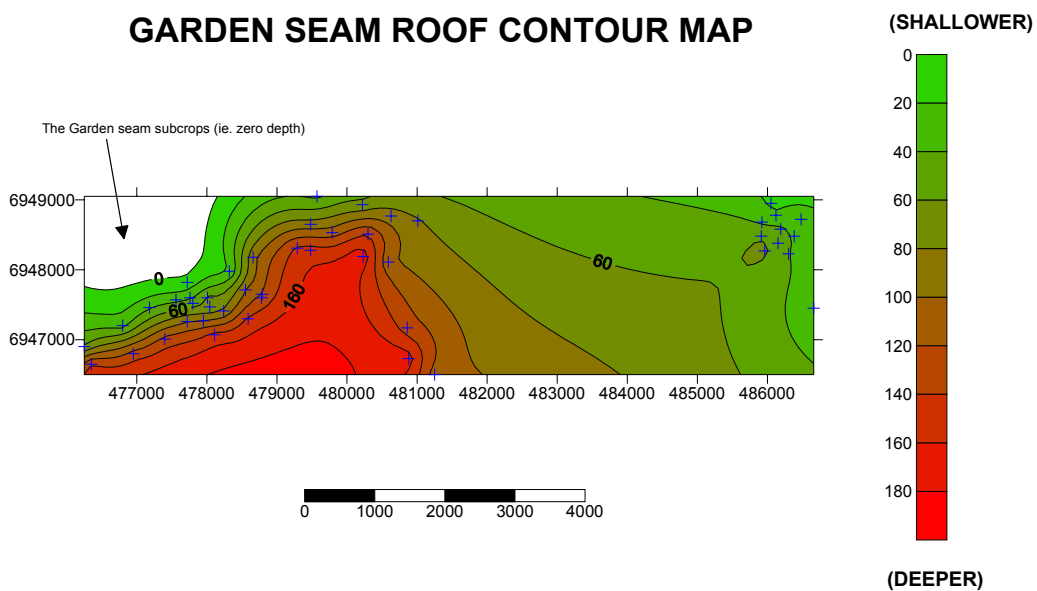


Figure 67

MATTHEWS SEAM THICKNESS CONTOUR MAP

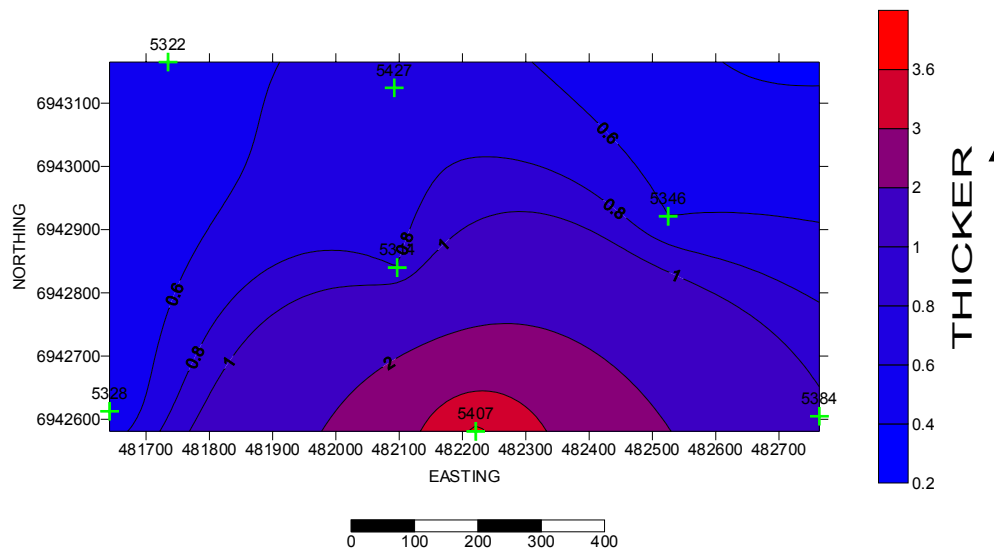


Figure 68

MATTHEWS SEAM ROOF CONTOUR MAP

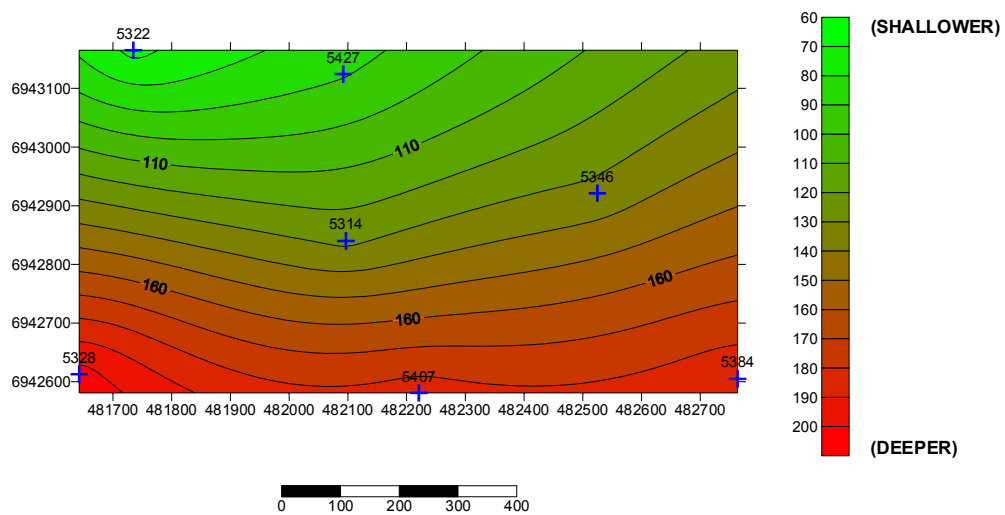


Figure 69

LIVERMORE SEAM THICKNESS CONTOUR MAP

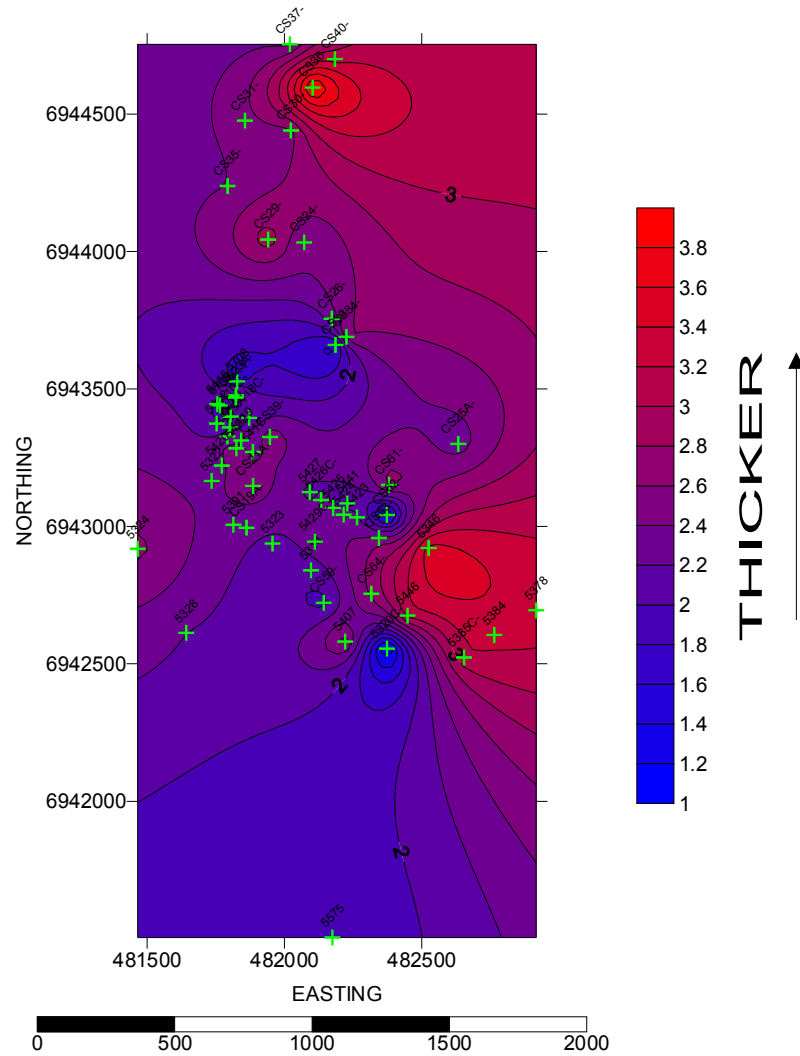


Figure 70

LIVERMORE SEAM ROOF CONTOUR MAP

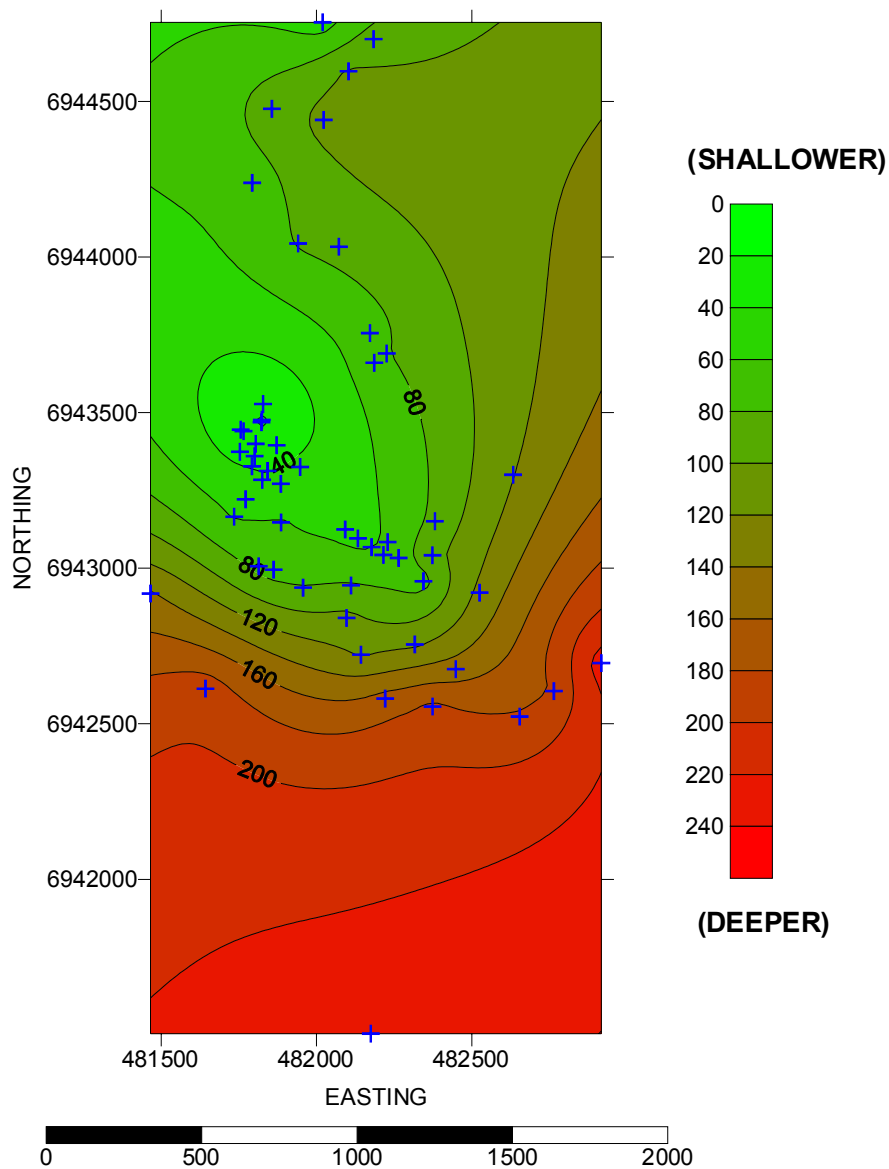


Figure 71

TAYLOR SEAM THICKNESS CONTOUR MAP

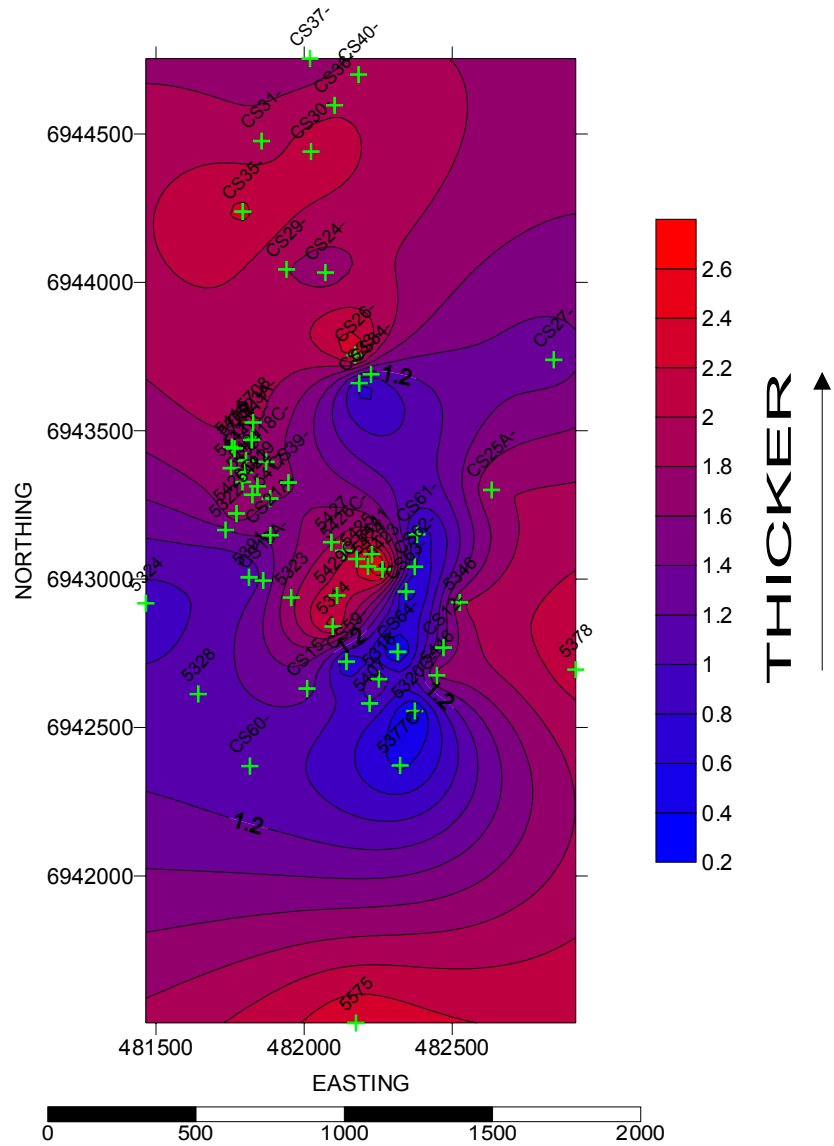


Figure 72

TAYLOR SEAM ROOF CONTOUR MAP

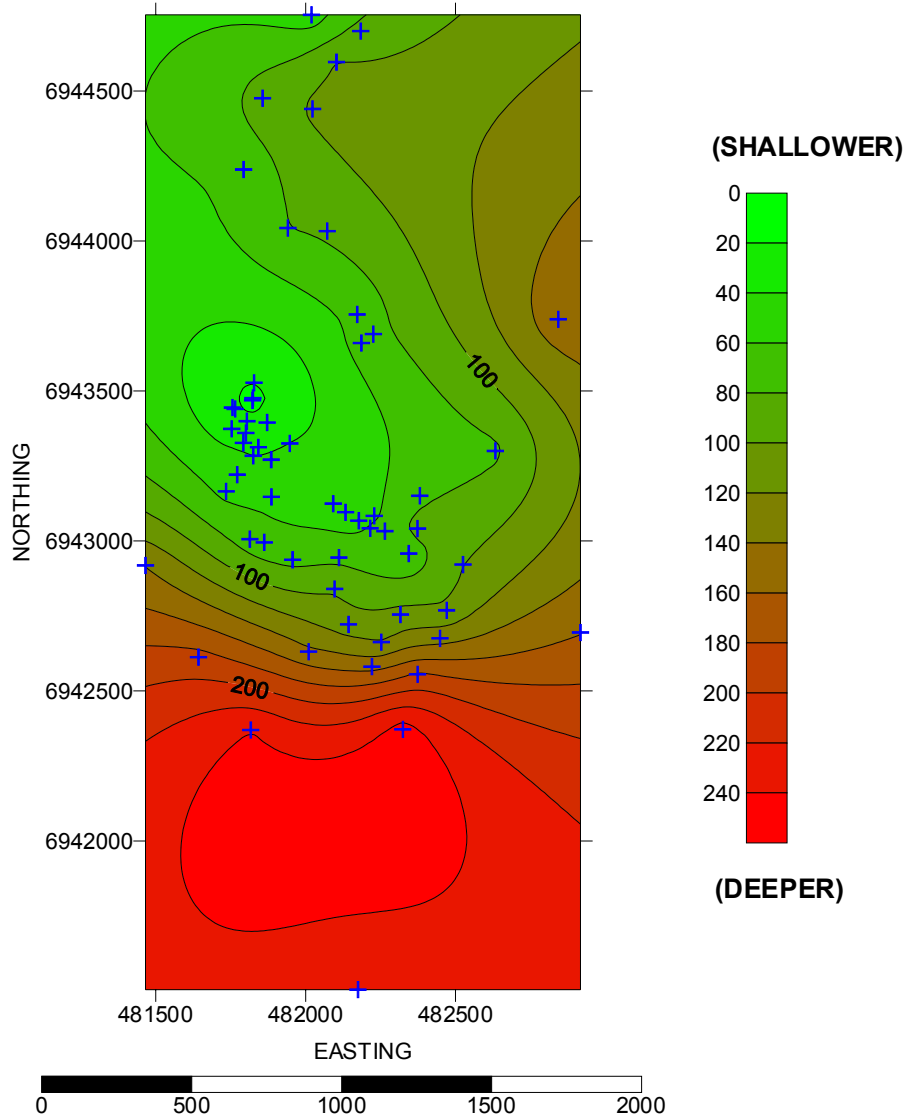


Figure 73

RITCHIE SEAM THICKNESS CONTOUR MAP

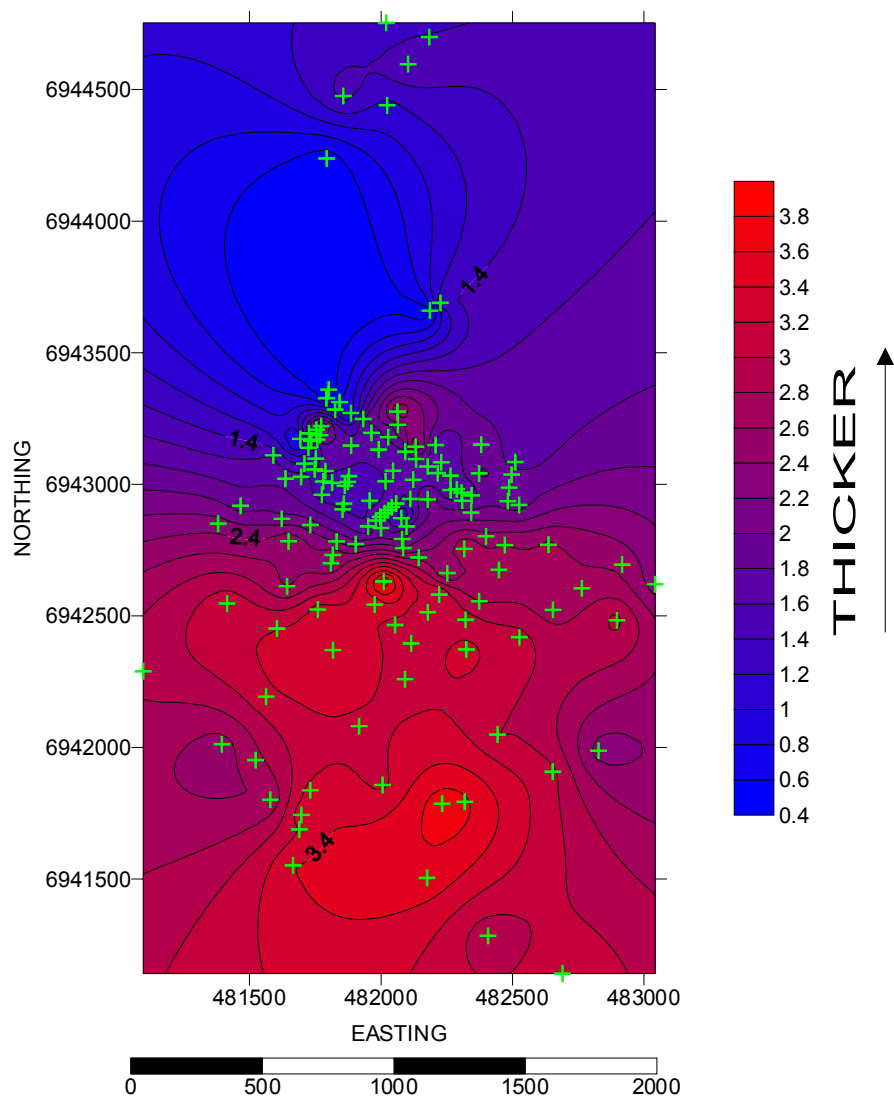


Figure 74

RITCHIE SEAM ROOF CONTOUR MAP

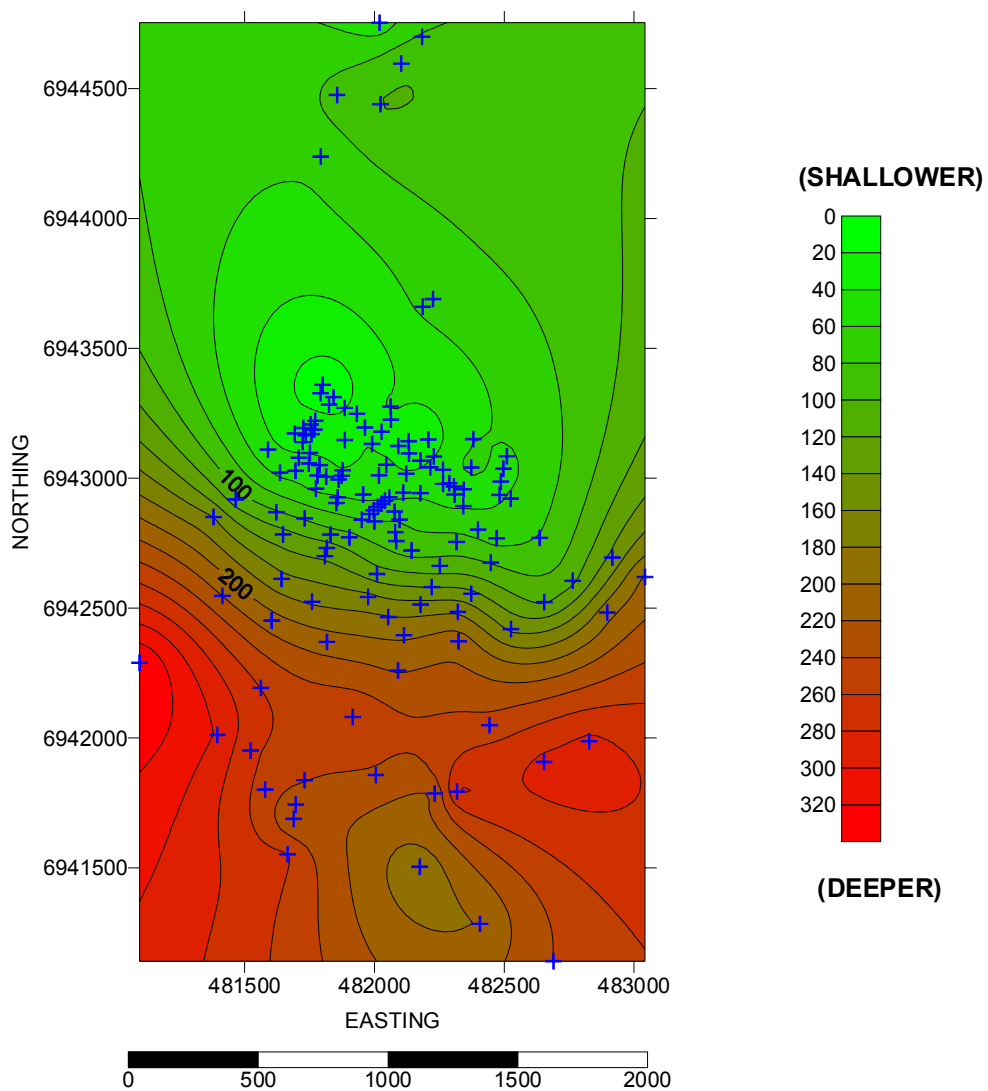


Figure 75

COCHRANE SEAM THICKNESS CONTOUR MAP

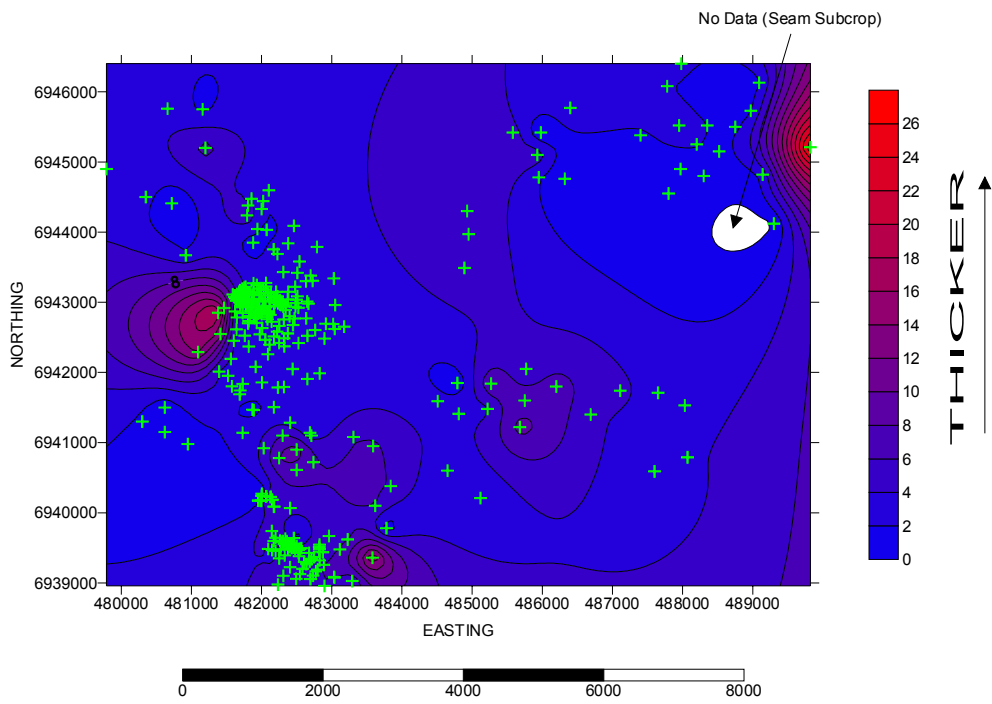


Figure 76

COCHRANE SEAM ROOF CONTOUR MAP

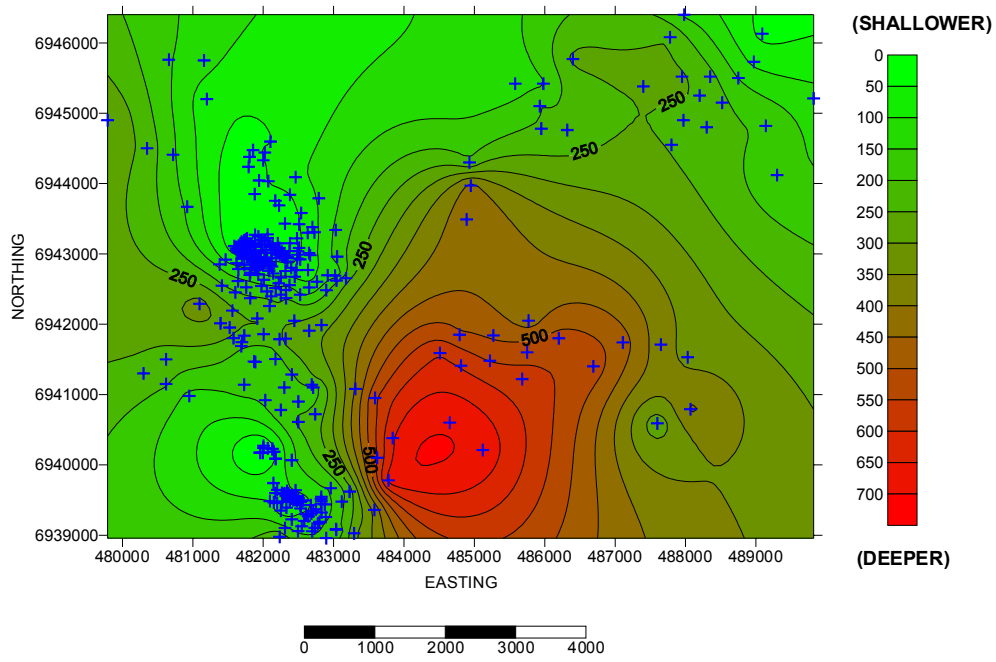


Figure 77

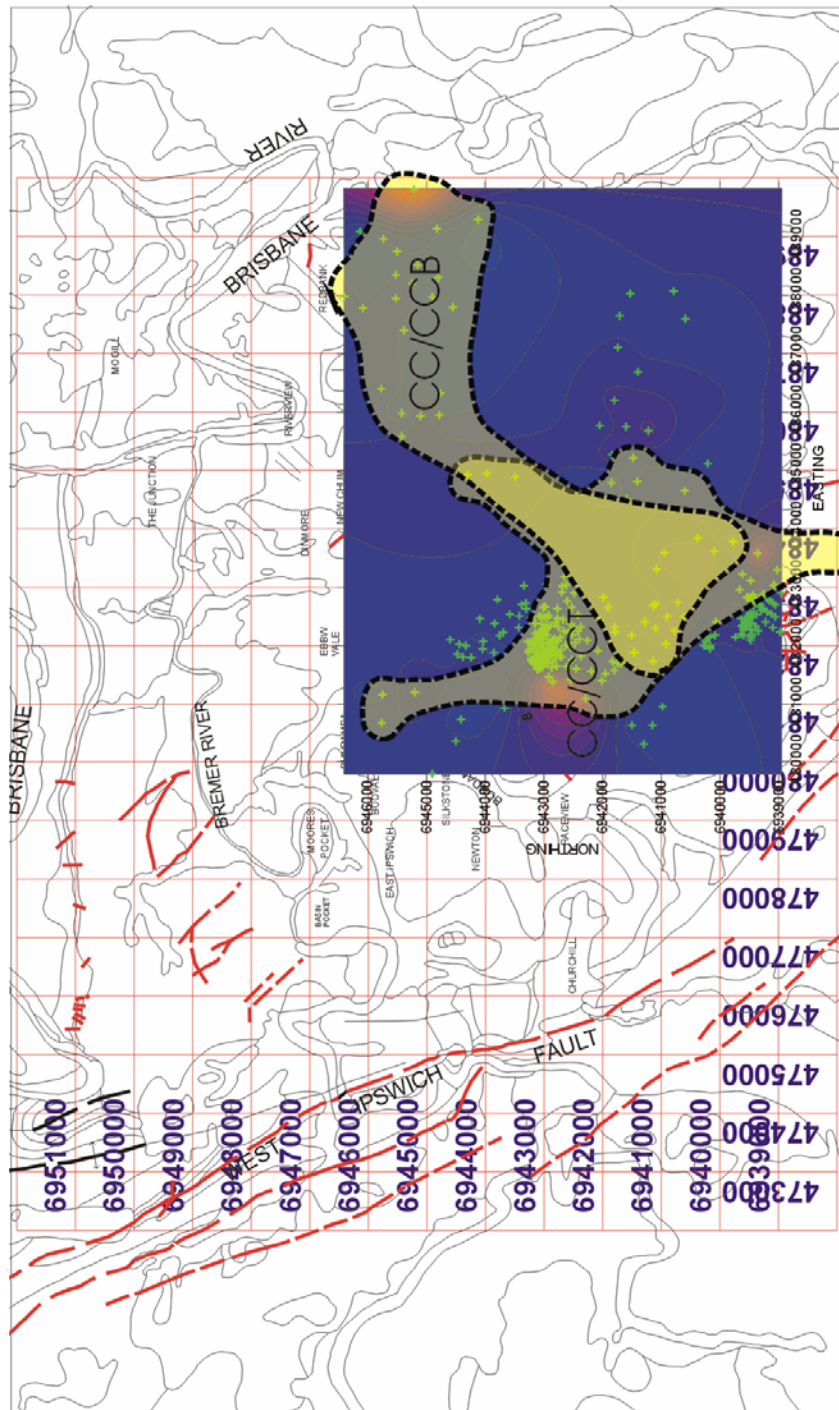


Figure 78: Cochrane Top (CCT) and Bottom (CCB) Splits (See Figure 76 for detailed thickness contour map)

ROB ROY SEAM THICKNESS CONTOUR MAP

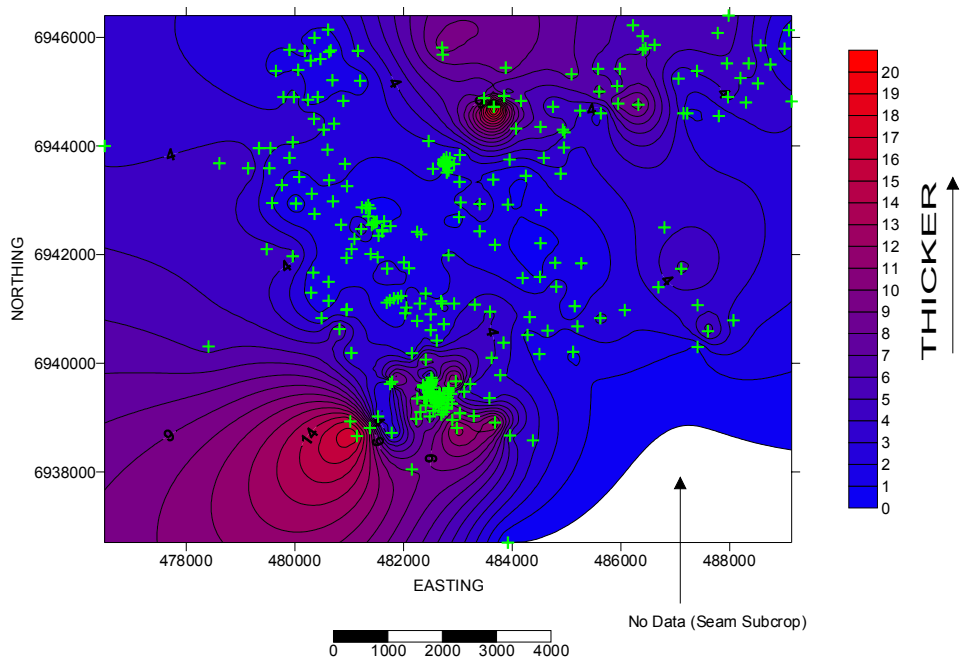


Figure 79

ROB ROY SEAM ROOF CONTOUR MAP

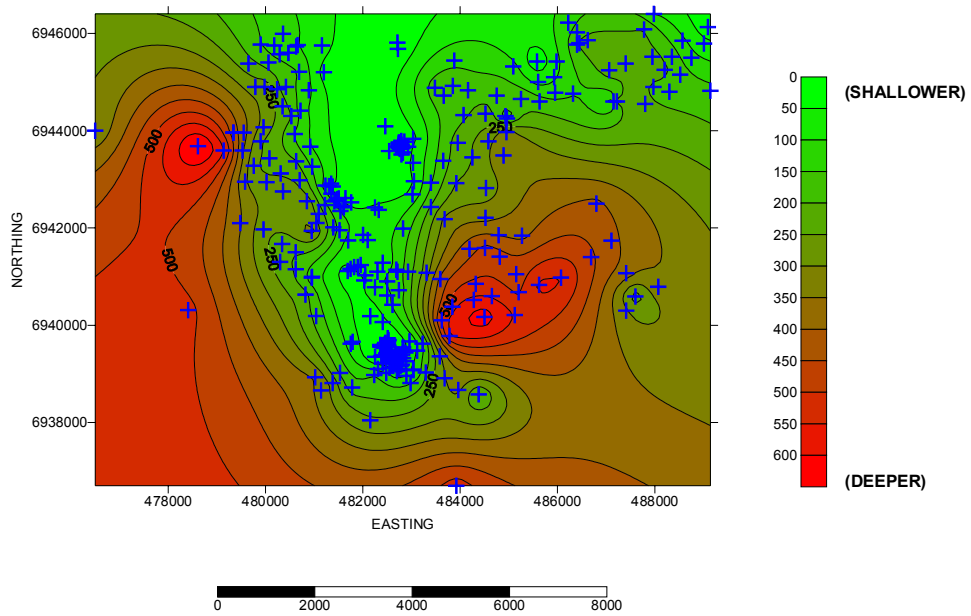


Figure 80

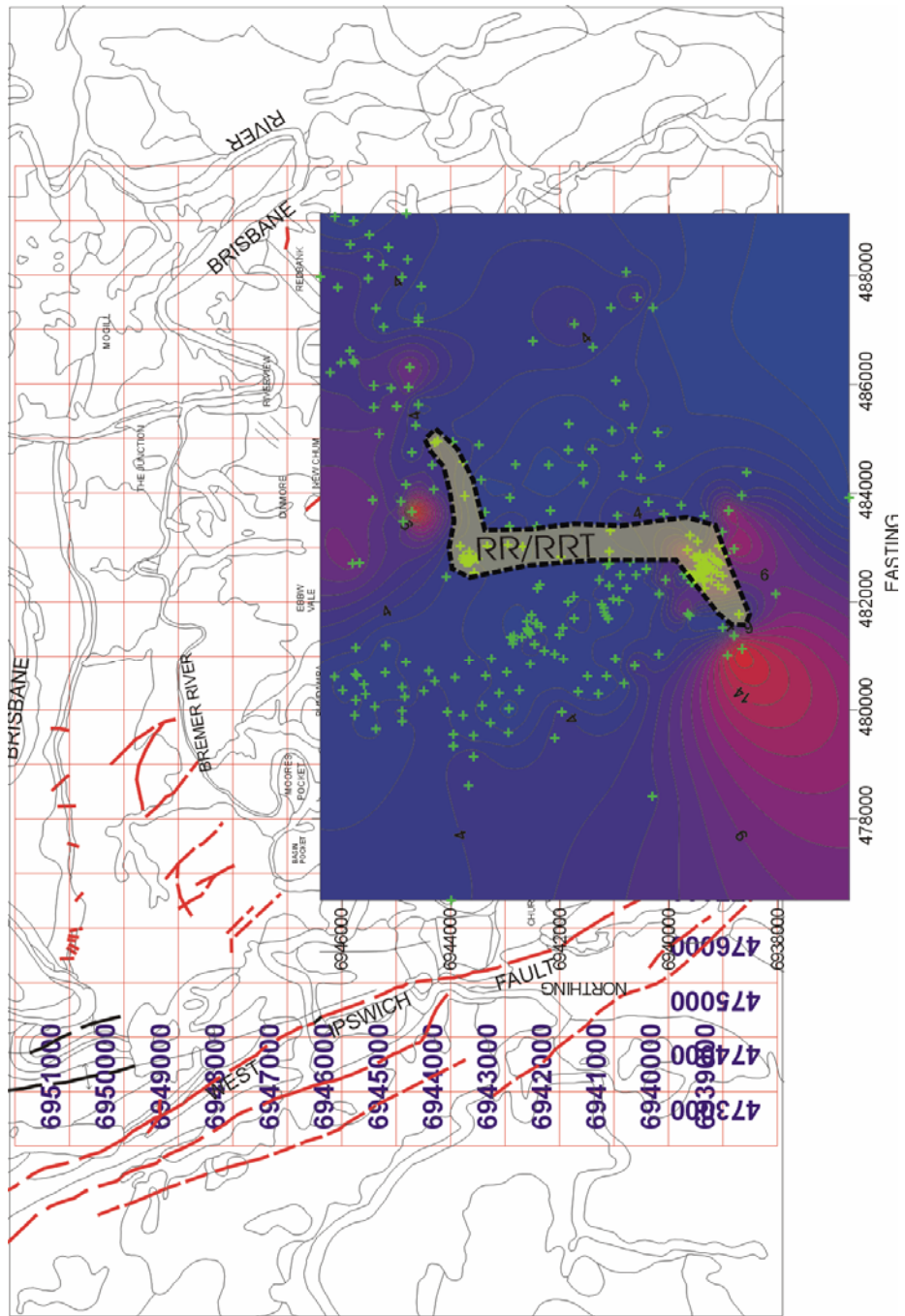


Figure 81: Rob Roy Top (RRT) Split
 (See Figure 79 for detailed thickness contour map)

STRIPED BACON-ROB ROY THICKNESS CONTOUR MAP

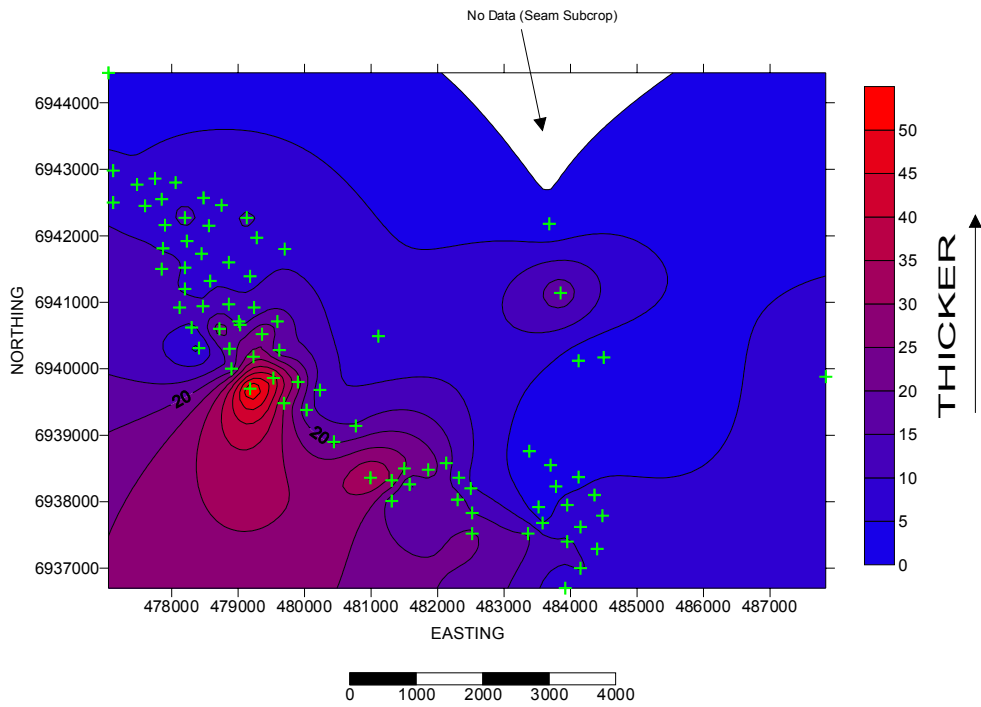


Figure 82

STRIPED BACON-ROB ROY ROOF CONTOUR MAP

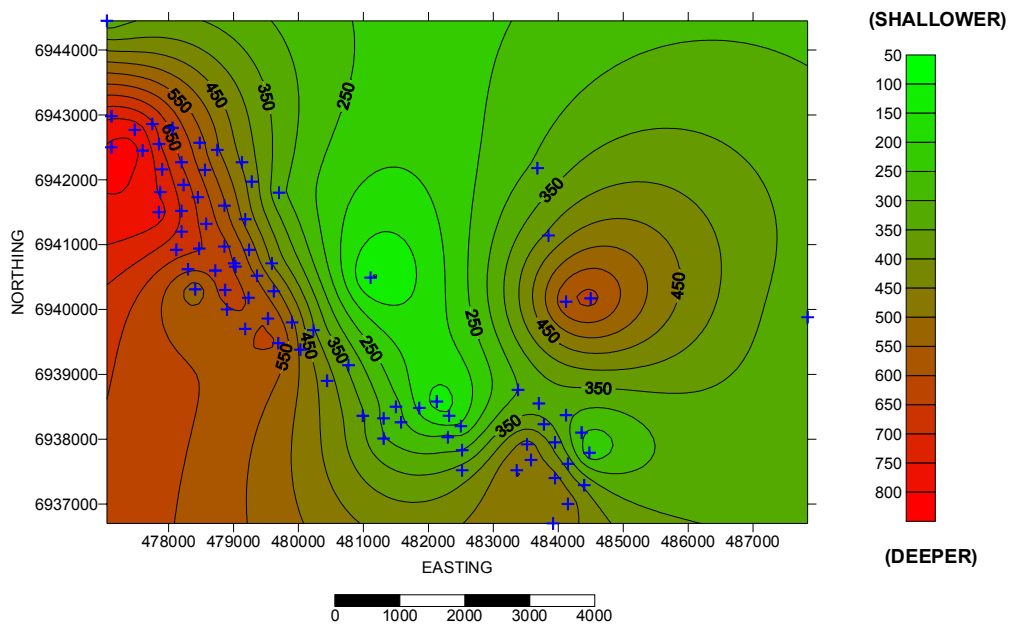
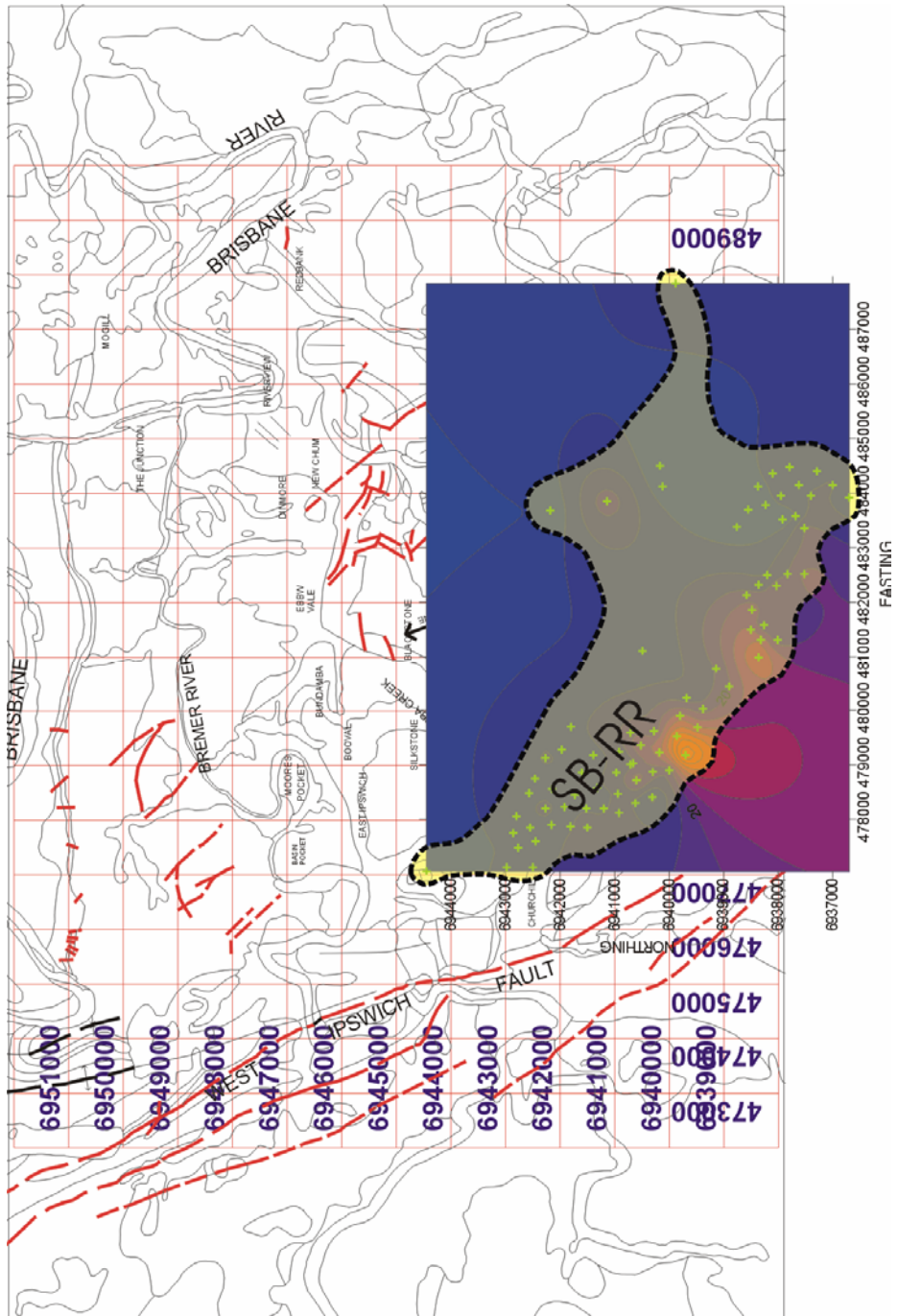


Figure 83



**Figure 84: Striped Bacon – Rob Roy Interval
(See Figure 82 for detailed thickness contour map)**

STRIPED BACON SEAM THICKNESS CONTOUR MAP

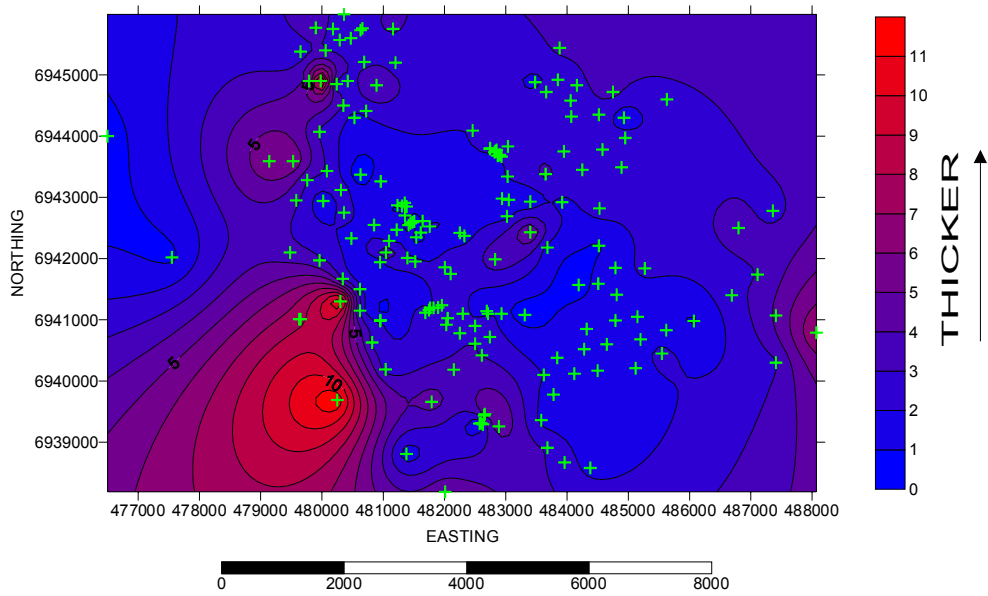


Figure 85

STRIPED BACON SEAM ROOF CONTOUR

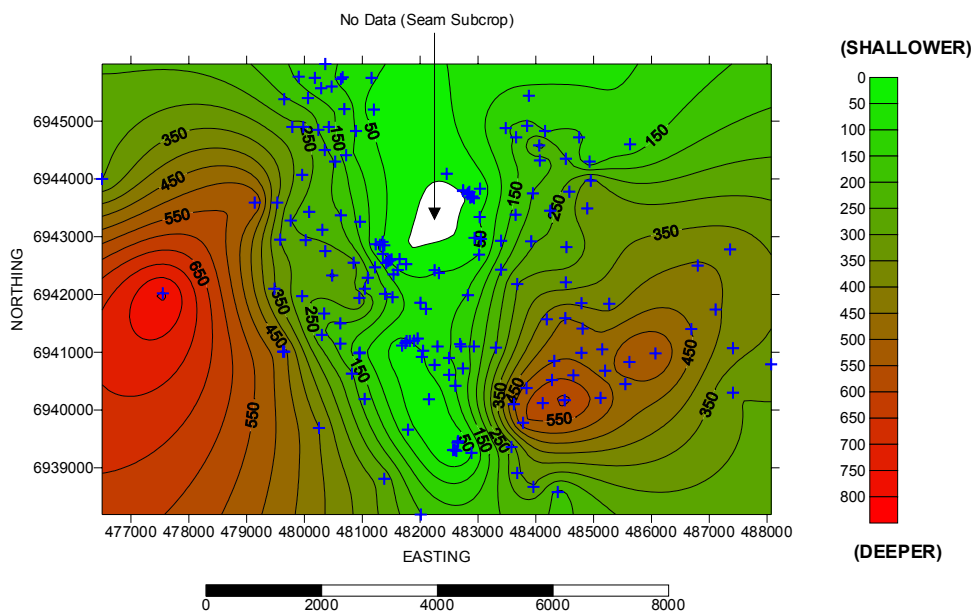
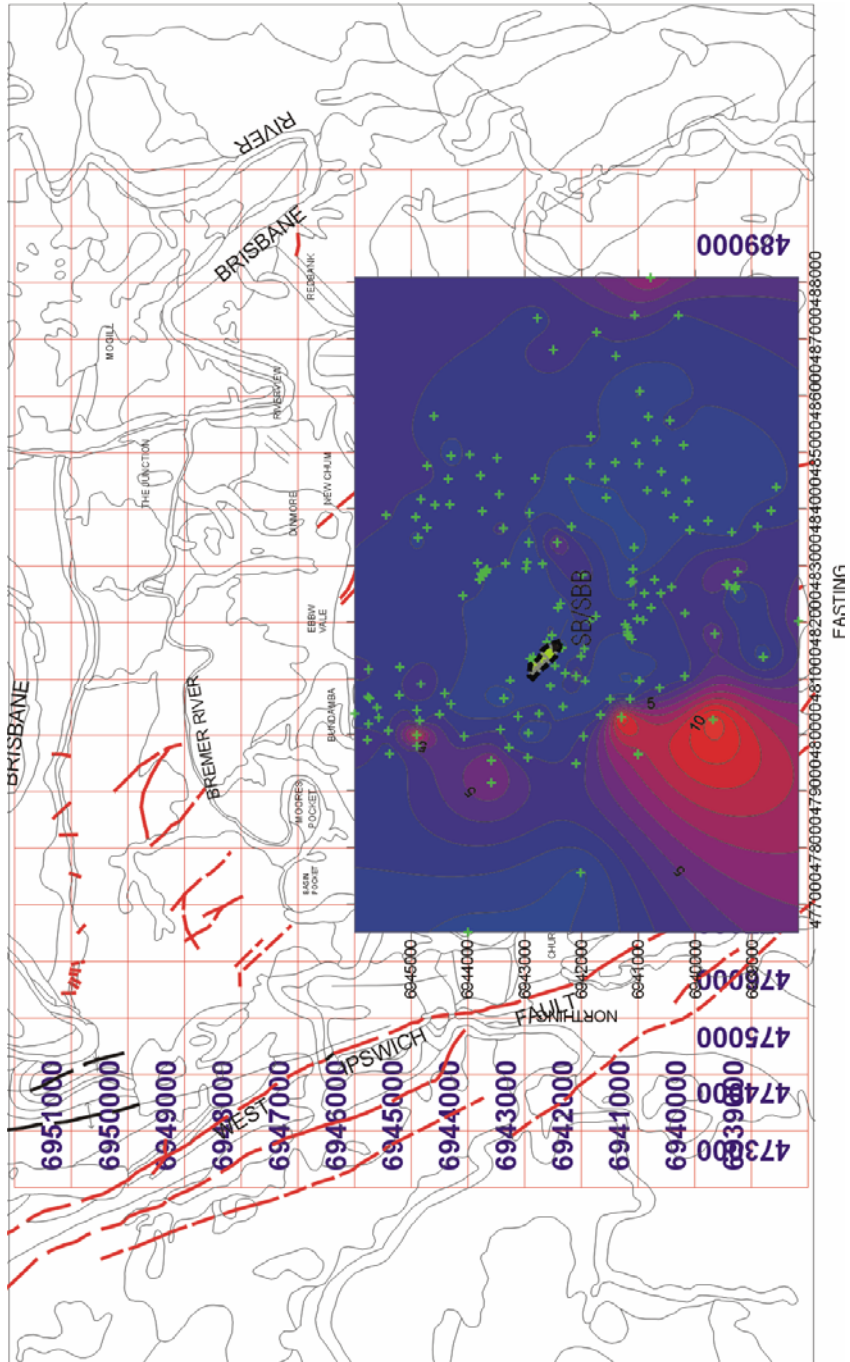


Figure 86



**Figure 87: Striped Bacon Bottom (SBB) Split (very small)
(See Figure 85 for detailed thickness contour map)**

BERGIN SEAM THICKNESS CONTOUR MAP

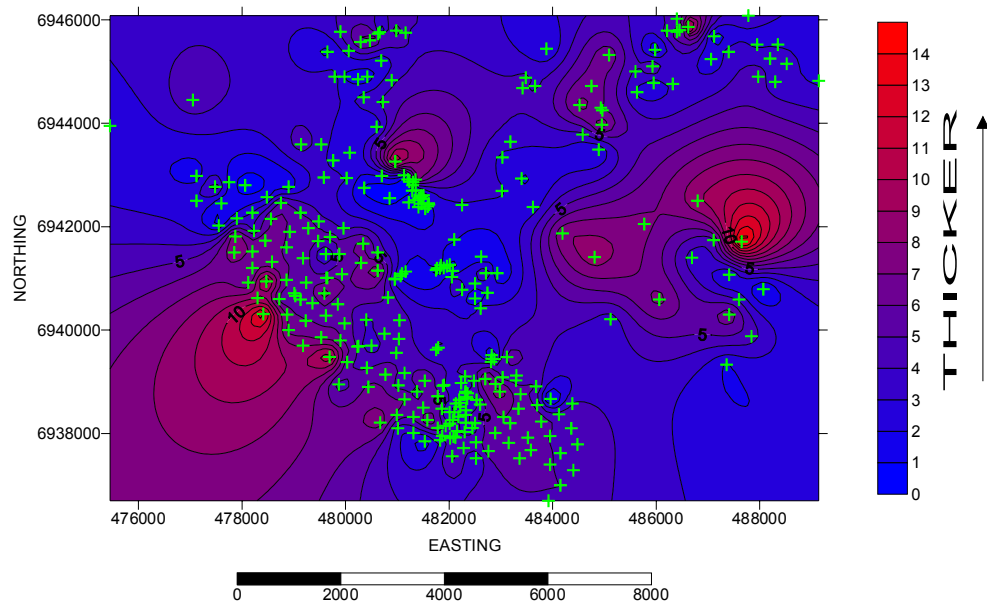


Figure 88

BERGIN SEAM ROOF CONTOUR MAP

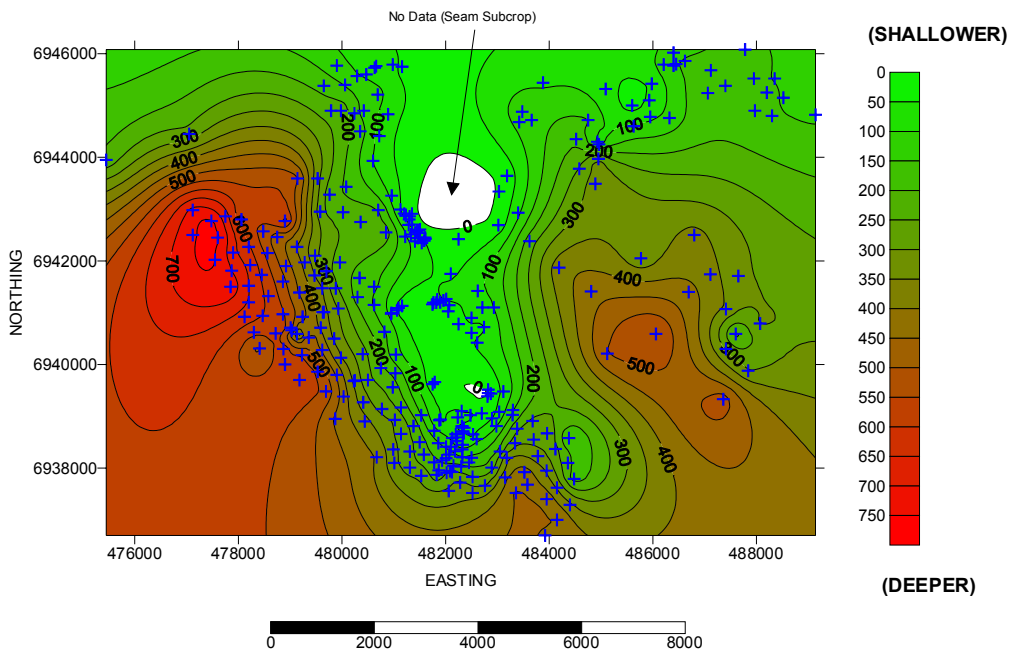


Figure 89

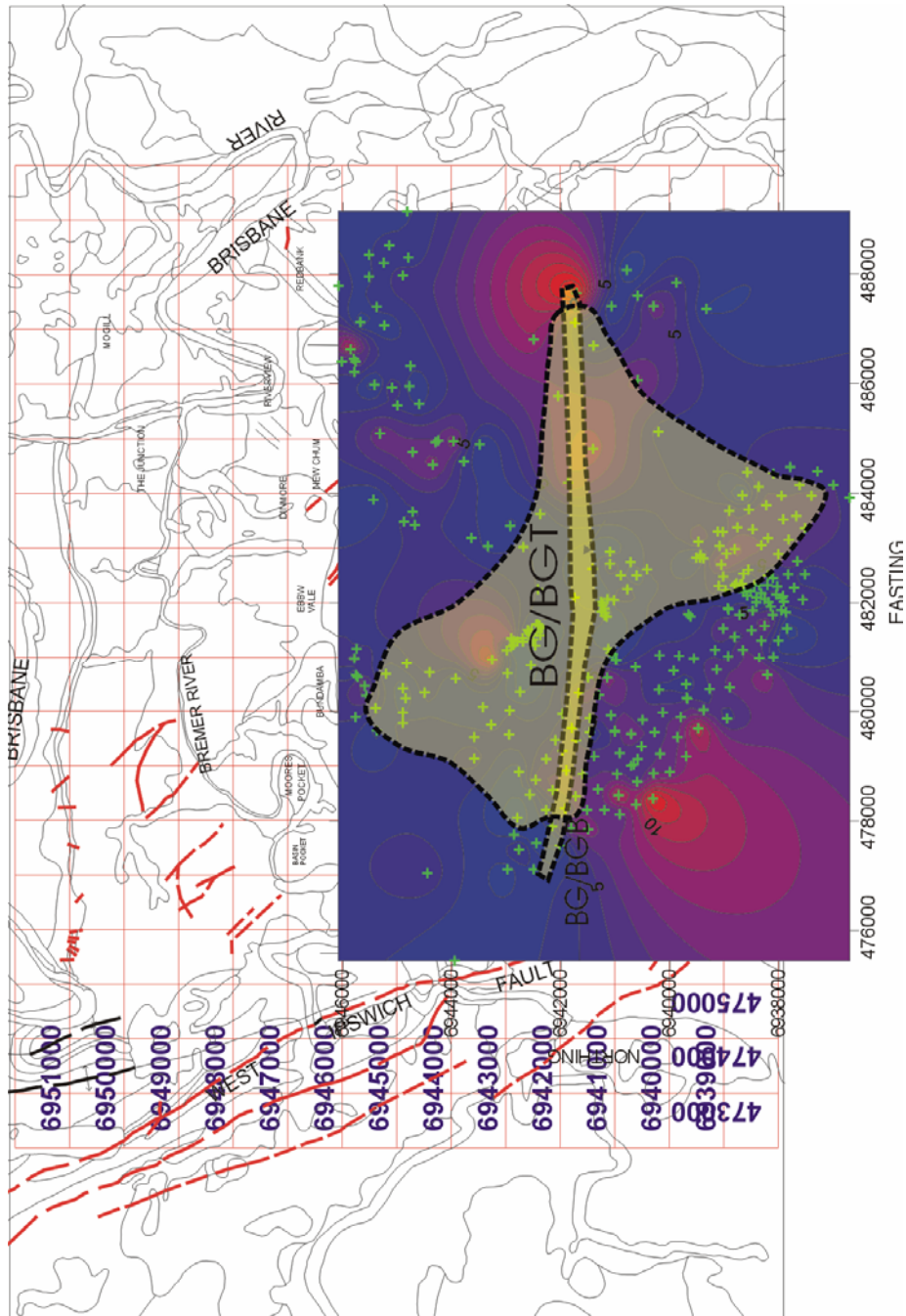


Figure 90: Bergin Top (BGT) and Bottom (BGB) Splits
 (See Figure 88 for detailed thickness contour map)

FOURFOOT SEAM THICKNESS CONTOUR MAP

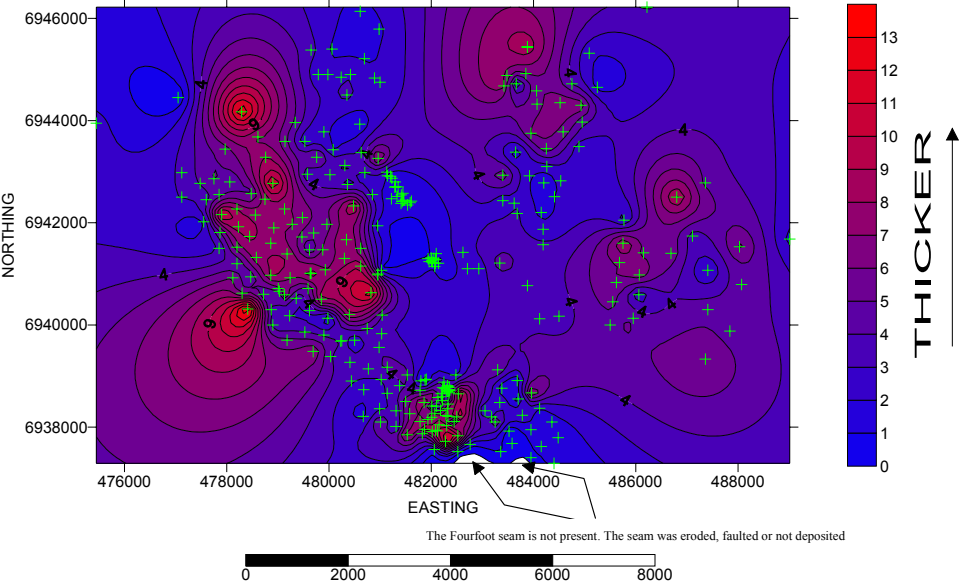


Figure 91

FOURFOOT SEAM ROOF CONTOUR MAP

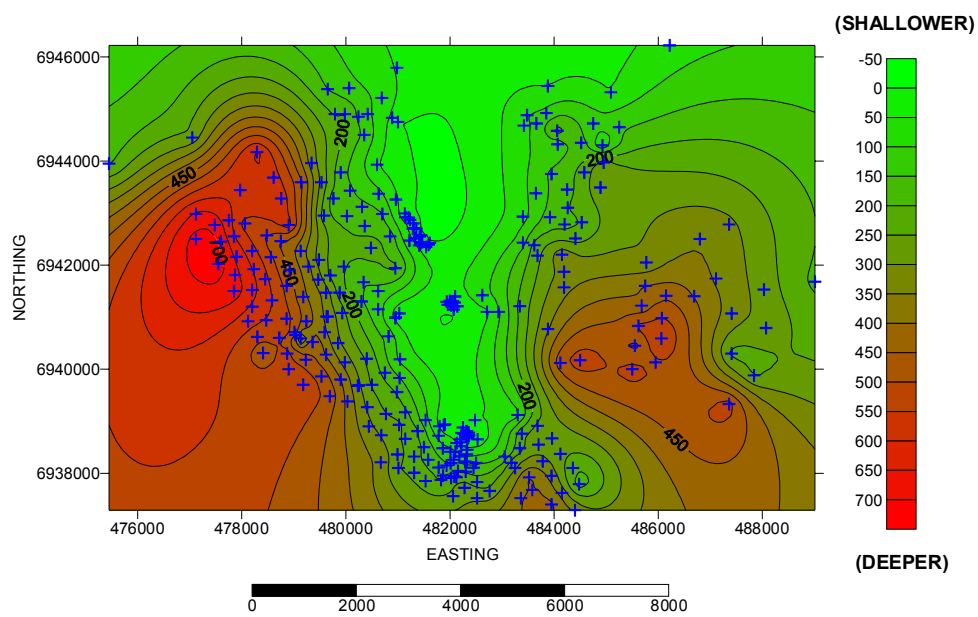


Figure 92

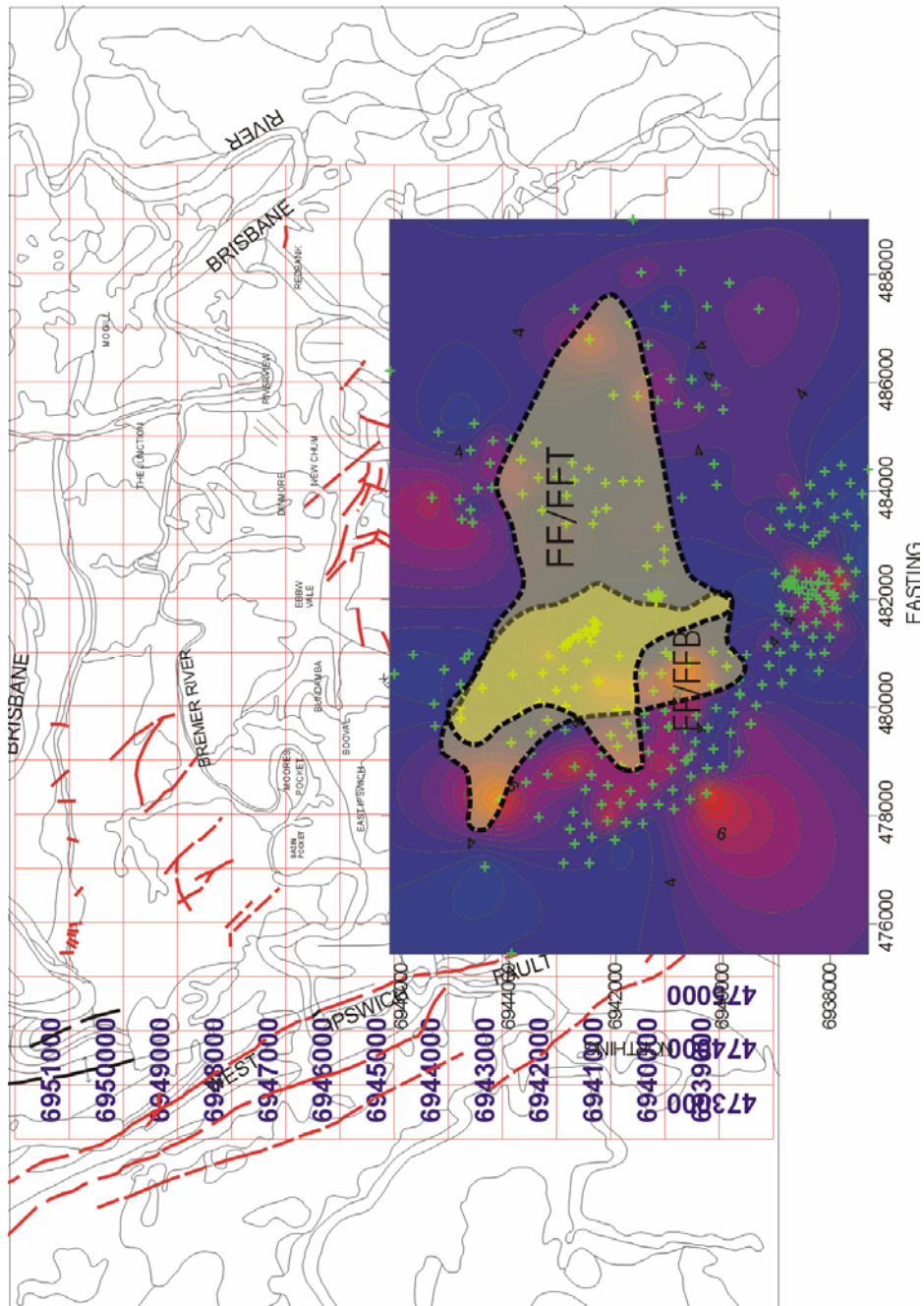


Figure 93: Fourfoot Top (FFT) and Bottom (FFB) Splits
 (See Figure 91 for detailed thickness contour map)

BLUFF SEAM THICKNESS CONTOUR MAP

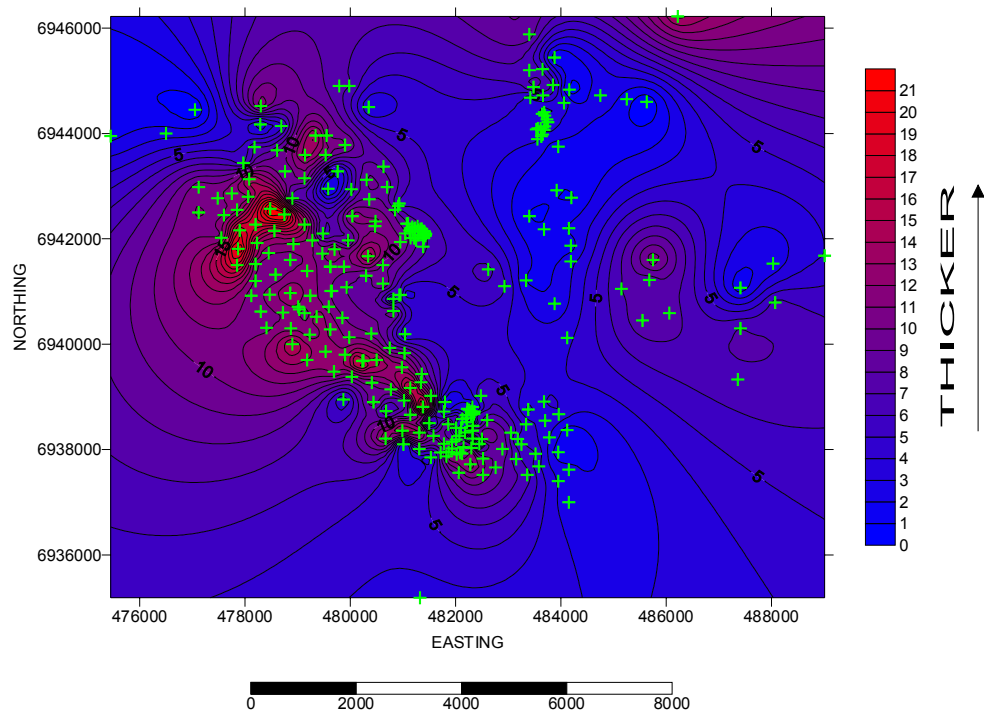


Figure 94

BLUFF SEAM ROOF CONTOUR MAP

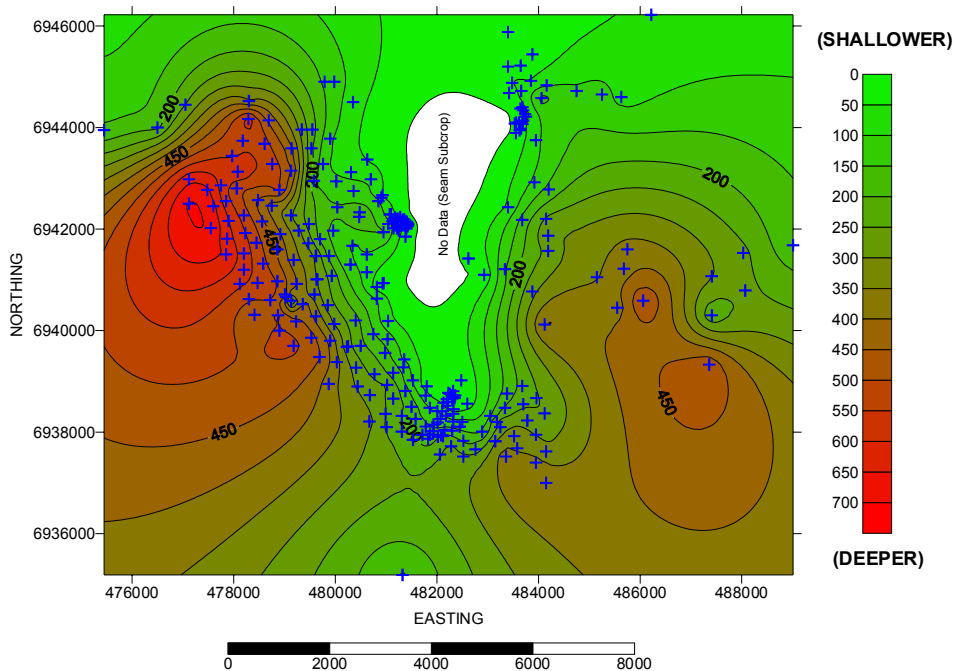
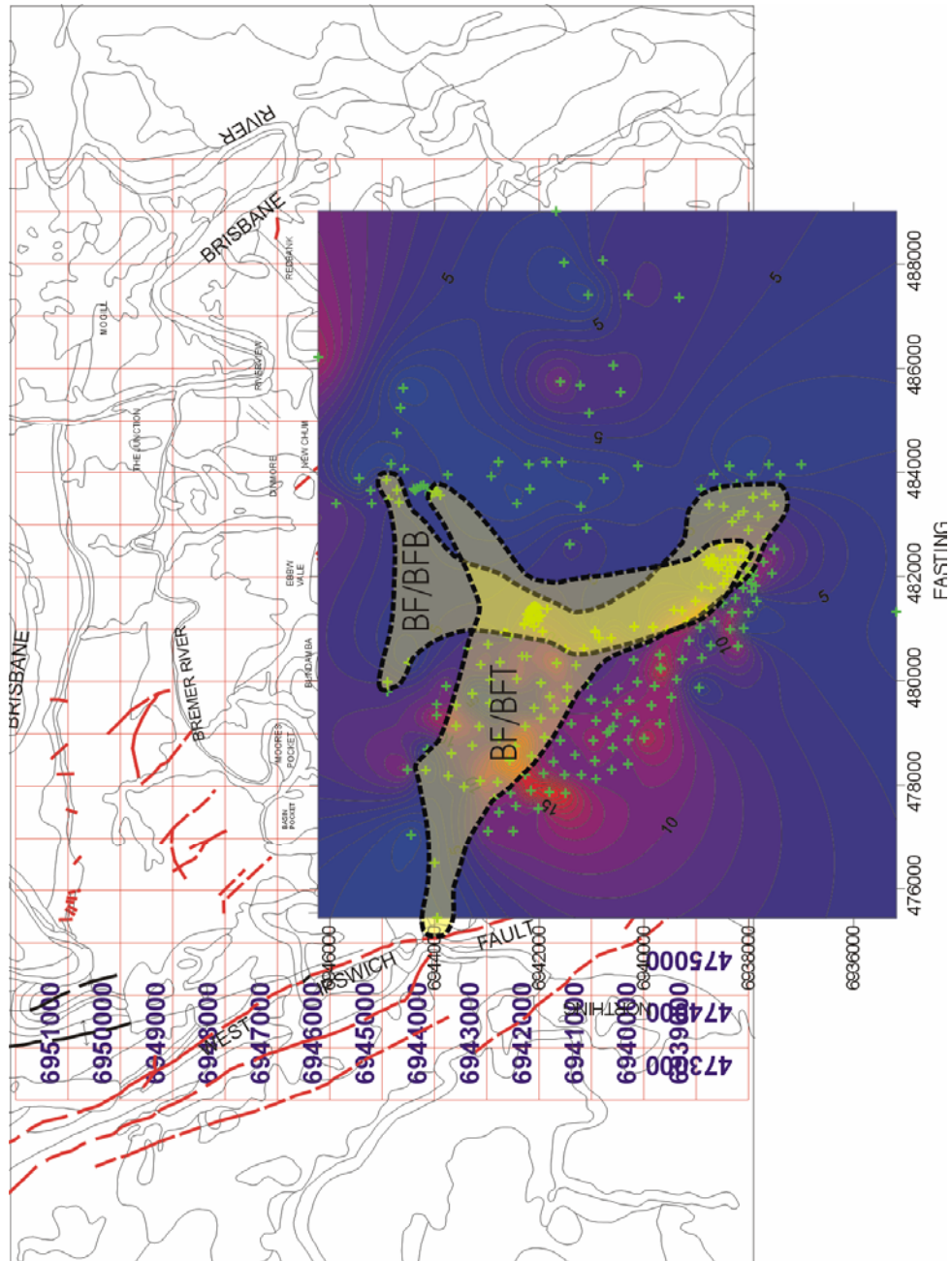


Figure 95



**Figure 96: Bluff Top (BFT) and Bottom (BFB) Splits
(See Figure 94 for detailed thickness contour map)**

ABERDARE SEAM THICKNESS CONTOUR MAP

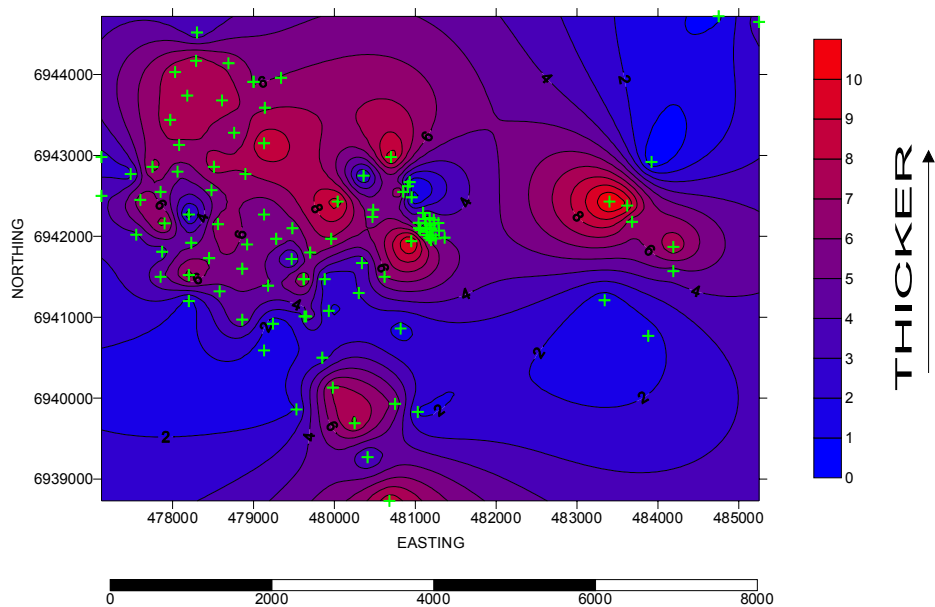


Figure 97

ABERDARE SEAM ROOF CONTOUR MAP

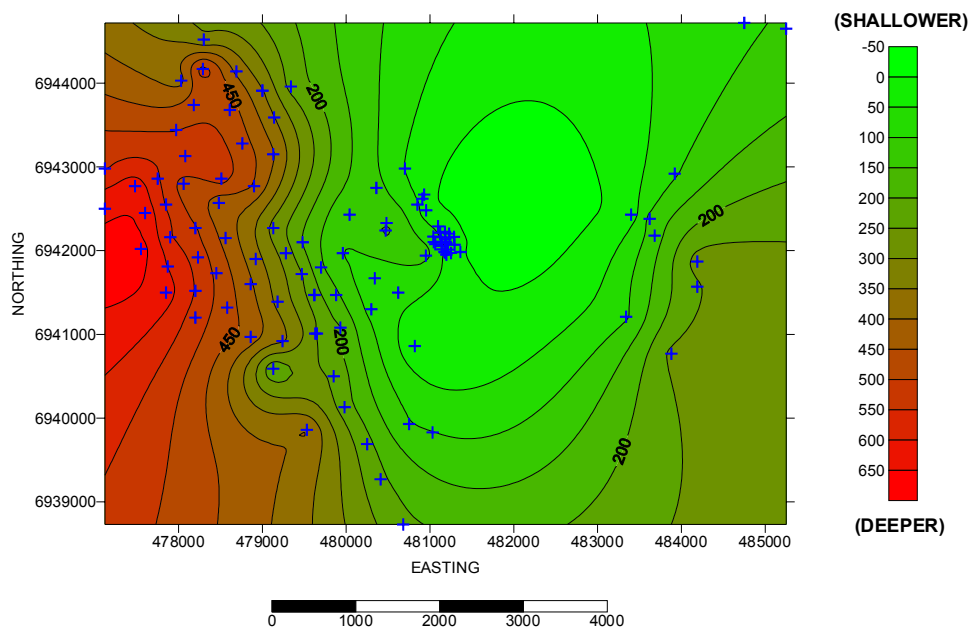


Figure 98

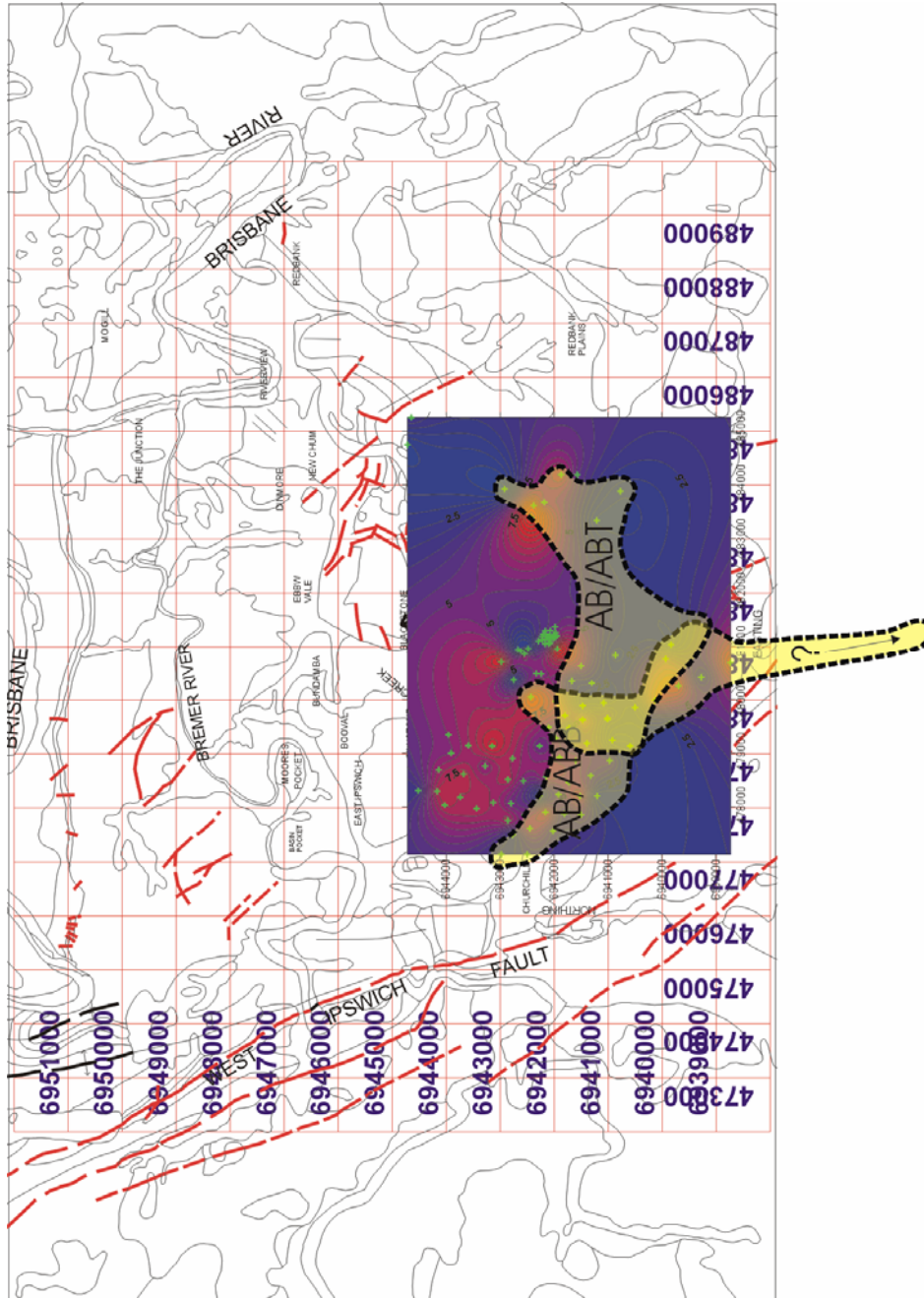


Figure 99: Aberdare Top (ABT) and Bottom (ABB) Splits
 (See Figure 97 for detailed thickness contour map)

THOMAS SEAM THICKNESS CONTOUR MAP

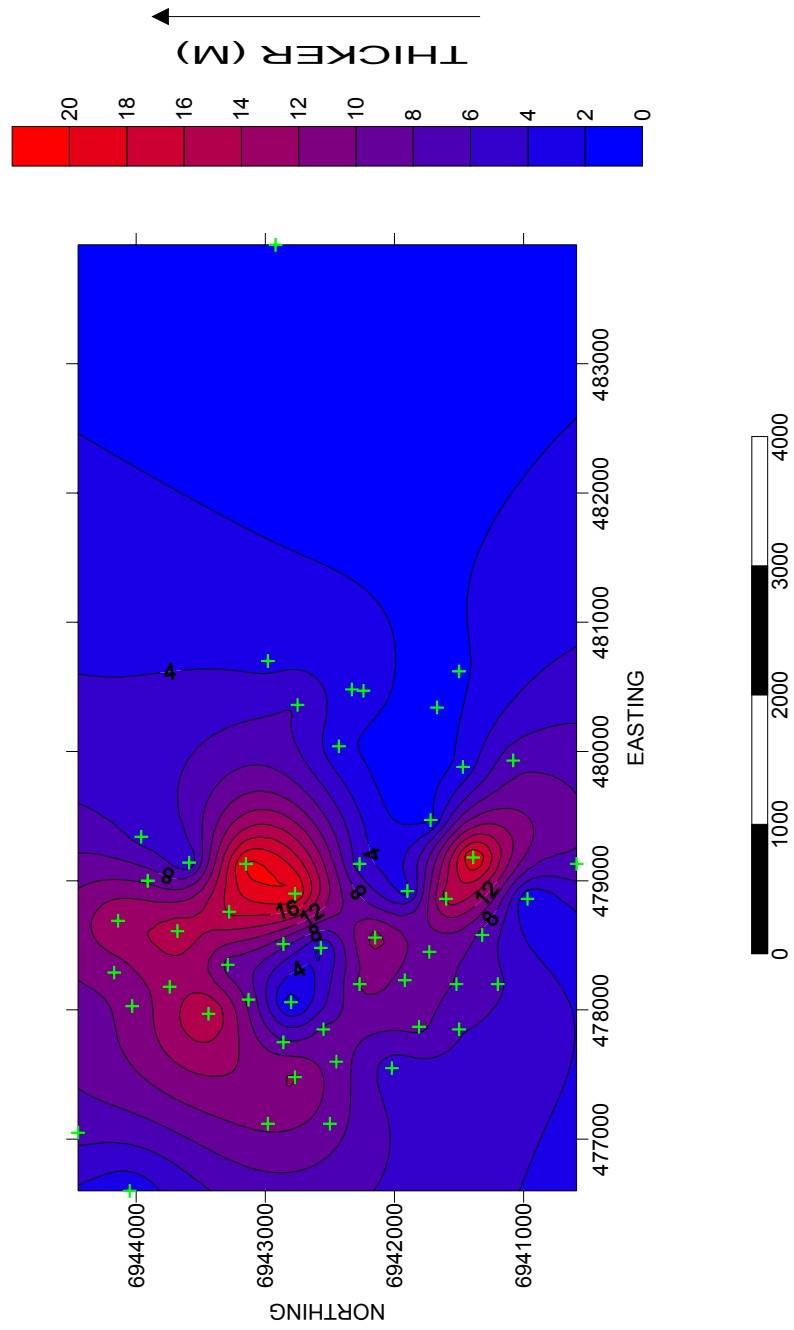


Figure 100

THOMAS SEAM ROOF CONTOUR MAP

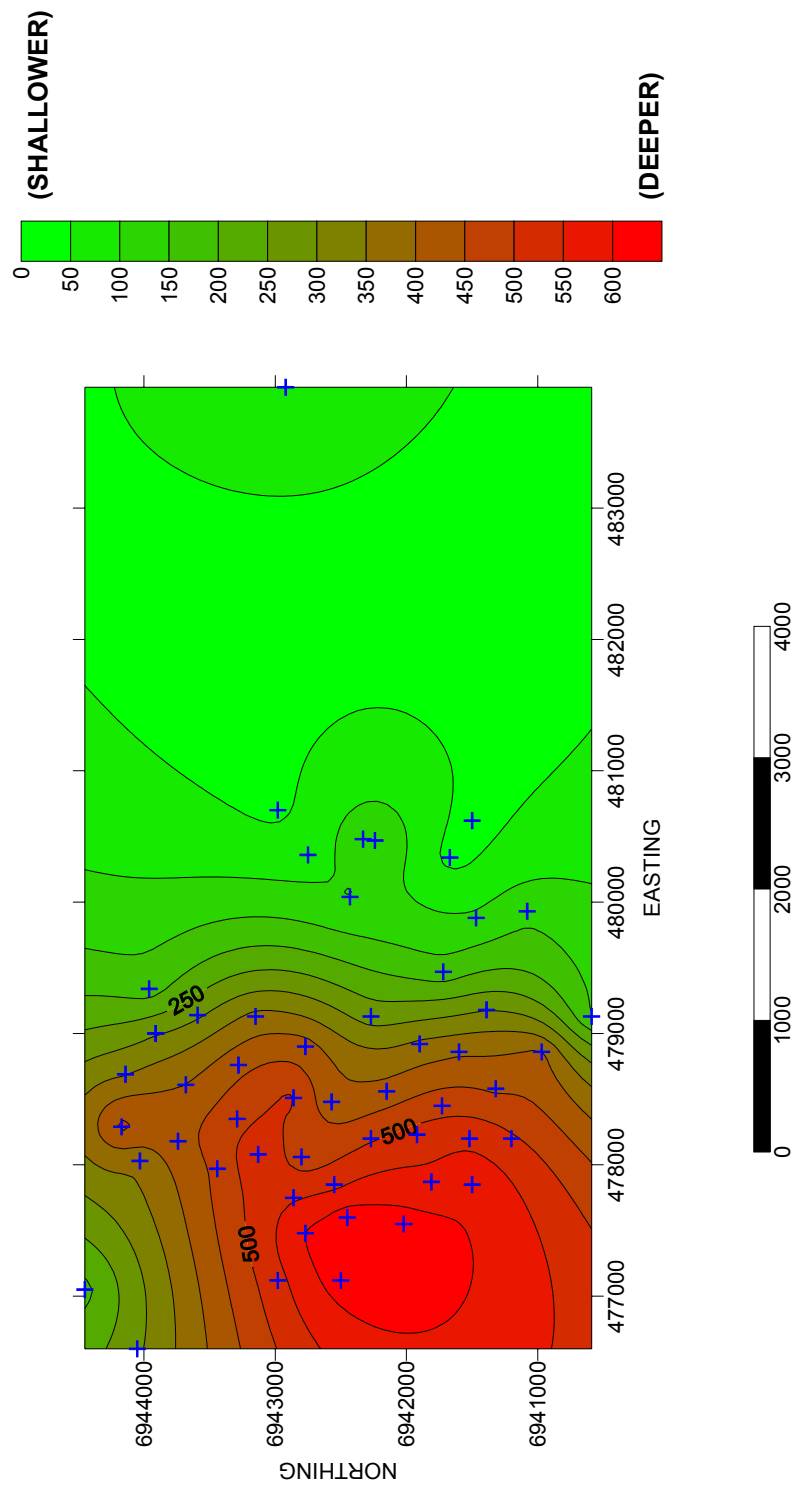


Figure 101

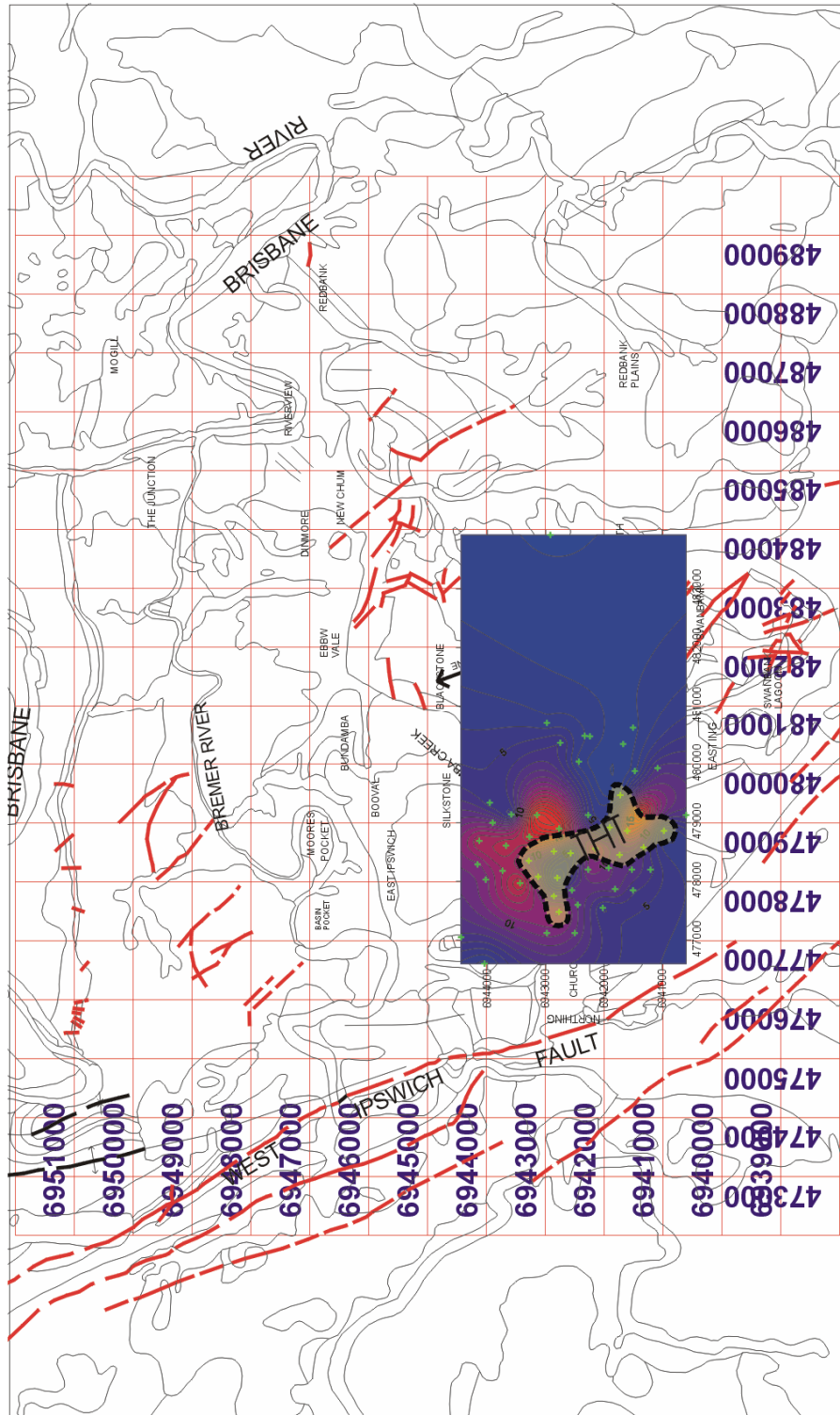


Figure 102: Thomas Seam Top Split (THT)
 (See Figure 100 for detailed thickness contour map)

Total Thickness Contour Maps

The Tivoli Formation accumulated mainly in the northern part of the basin except for the Cochrane seam which was deposited in the southern part adjacent to the Bundamba Anticline (Figure 103). The Blackstone Formation total thickness contour map, which includes coal and non-coal units, shows thick sedimentary accumulations on both sides of the Bundamba Anticline. They are marked as Depocentre 1 and Depocentre 2 in Figure 104. However, the Blackstone Formation coal thickness contour map (Figure 105) shows only Depocentre 1 on the western side of Bundamba Anticline contains the significant coal thickness. The sand-rich Depocentre 2 on the eastern side of the anticline was susceptible to higher fluvial activity such as flooding, and thus, contains less coal. On the other hand, depositional environments in the Depocentre 1 were more stable and therefore, favoured peat accumulation. The West Ipswich Fault may have also acted as a barrier to protect any fluvial incursion into the peat-mire in Depocentre 1.

(See following Figures for Tivoli Formation Total Coal Thickness Contour Map, Blackstone Formation Thickness Contour Map and Blackstone Formation Total Coal Thickness Contour Map).

Major coal accumulation is restricted to palaeo-low areas in the central-north and north-west parts of the basin.

Tivoli Formation Total Coal Thickness Contour Map
(Including main and split seams)

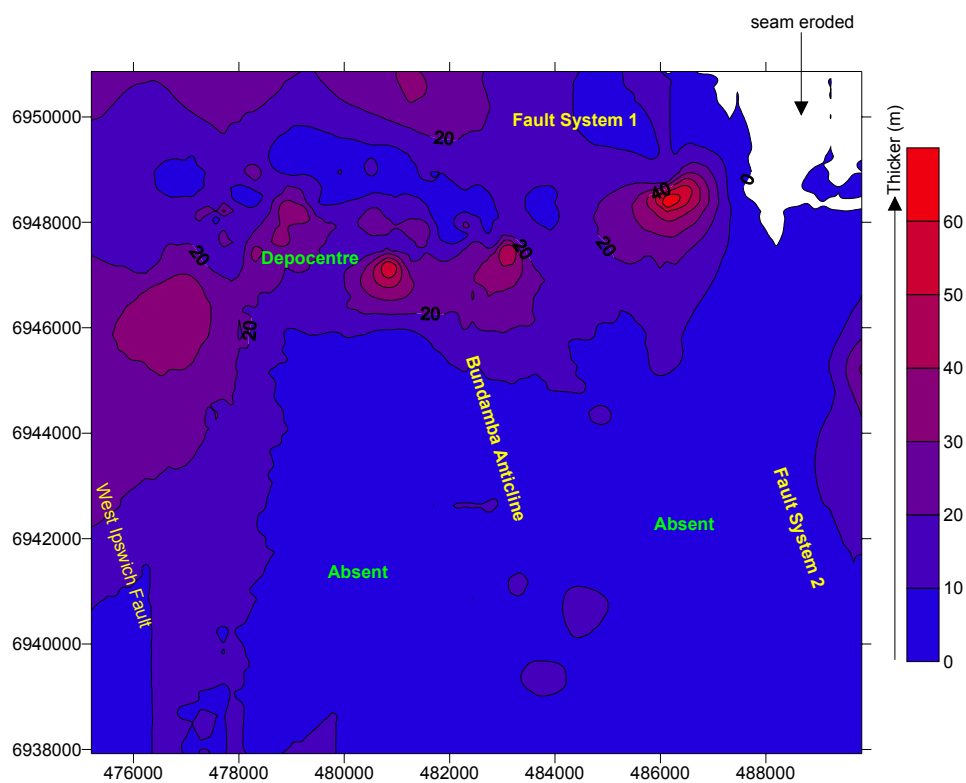


Figure 103

Blackstone Formation Thickness Contour Map
(Thickness includes coal and non-coal sedimentary rocks)

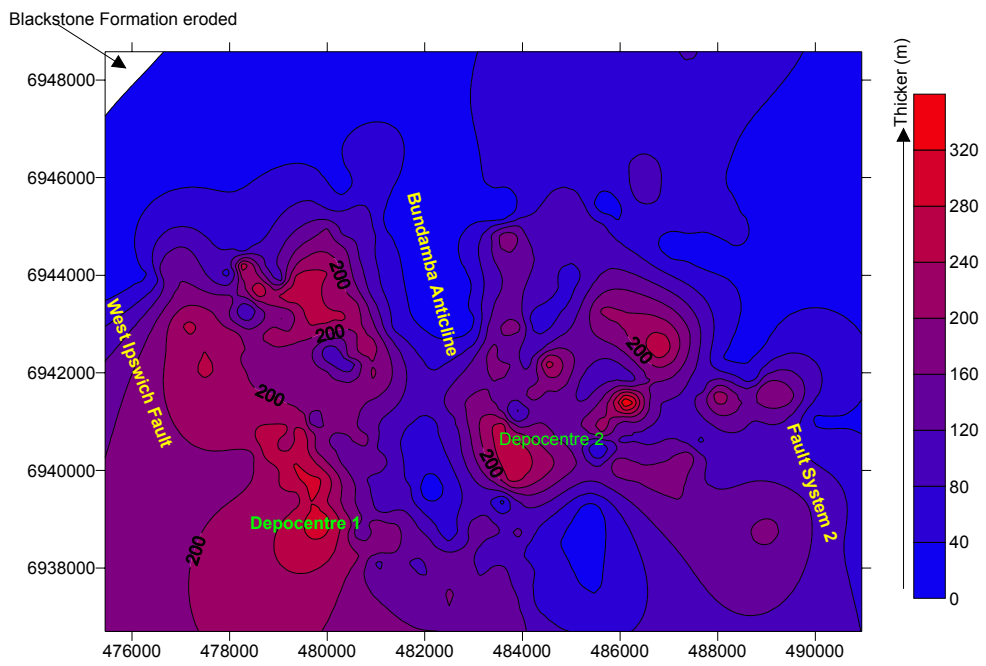


Figure 104

Blackstone Formation Total Coal Thickness Contour Map
(Including main and split seams)

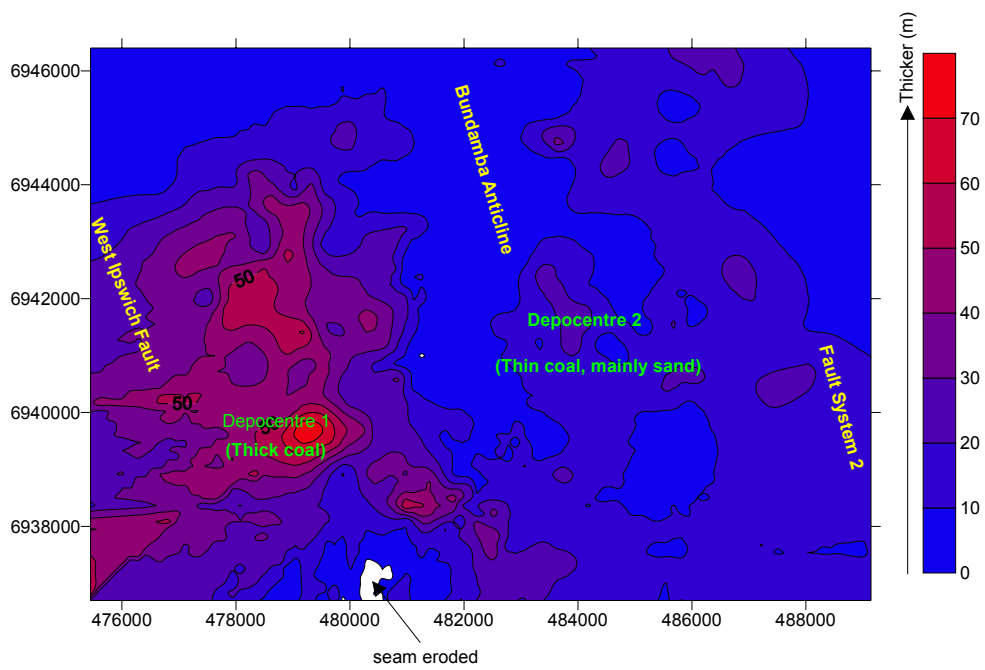


Figure 105

Area versus Thickness

A digital planimeter (Planix 7 from Tamaya and Company Limited, Tokyo) was used to measure the aerial extent of coal seams with cut-off limits at one-meter and four-meter thickness contour intervals. Each contour interval was measured three times and average values were taken to use in the “Thickness versus Aerial Extent” graphs (shown in Figures 106 and 107). A manual planimeter (compensating polar planimeter from Kent Limited) was also used for preliminary measurements but not used for final measurements due to its significantly high inaccuracy. Over thirty years of wear and tear may account for mechanical discrepancies with the manual planimeter. Table 22 shows the results of all measurements. One-meter thickness interval was used for seams which have a mean thickness of less than four meters and for preliminary seam grouping. They are, however, not as accurate as four-meter interval as borehole data are very sparse for that interval. Four-meter interval was used for final grouping of seams which have the mean thickness of more than four meters.

Table 22: Aerial extents for 1m and 4m seam thickness intervals

Formation	Seam Name	Planix 7 Digital Planimeter		Compensating Polar Planimeter	
		1 meter cut-off	4 meters cut-off	1 meter cut-off	4 meters cut-off
Blackstone Formation	Thomas	11531	2441	29530	6970
	Aberdare	12276	2967	9390	2286
	Bluff	35977	21021	40600	23280
	Fourfoot	27445	6653	21210	5510
	Bergin	41530	12023	42260	13390
	Striped Bacon	23742	5605	36140	8040
	Rob Roy	30862	16876	37880	11800
Tivoli Formation	Cochrane	19630	8587	9598	3506
	Ritchie	3785	NA	3235	NA
	Taylor	1706	NA	1568	NA
	Livermore	2111	NA	1812	NA
	Matthews	52	NA	73	NA
	Garden	6824	1817	3638	978
	Westfalen Top	5061	4236	8200	6118
	Tantivy	4190	596	5450	794
	Fiery	5914	3823	7146	4330
	Waterstown	6802	3189	3602	1702
	Tivoli	5004	611	7660	884
	Poverty	1657	337	1248	244
	Eclipse	21312	322	22690	350
	Benley	9086	3679	12310	5580
	Waterworks	13914	12111	11970	10566

All values are in m².

Mean Thickness versus Depth Graph

Figure 108, on the other hand, was used to demonstrate how economical the coal seams are to mine. It should be noted that seam depths are not related to stratigraphic order as they have been taken from drillhole intersections with coal seams at various locations. The coal seams are roughly divided into four groups, High Thickness-Shallow Depth, High Thickness-Deep Depth, Low Thickness-Shallow Depth and Low Thickness-Deep Depth. The

High Thickness-Shallow Depth contains only one seam and it is apparently the most economical seam whereas the Low Thickness-Deep Depth seams are the least economical seams (see Appendix II, Table 23).

- Group 1A = Very High Mean Thickness to Aerial Extent**
- Group 1B = High Mean Thickness to Aerial Extent**
- Group 1C = Low Mean Thickness and Aerial Extent**
- Group 2 = Moderate Aerial Extent to Mean Thickness**
- Group 3 = High Aerial Extent to Mean Thickness**

(NB: The relationship is only based on borehole data. All classifications such as very high and high are relative)

Mean Thickness vs Aerial Extent (1m Thickness Contour Cut-off Limits)

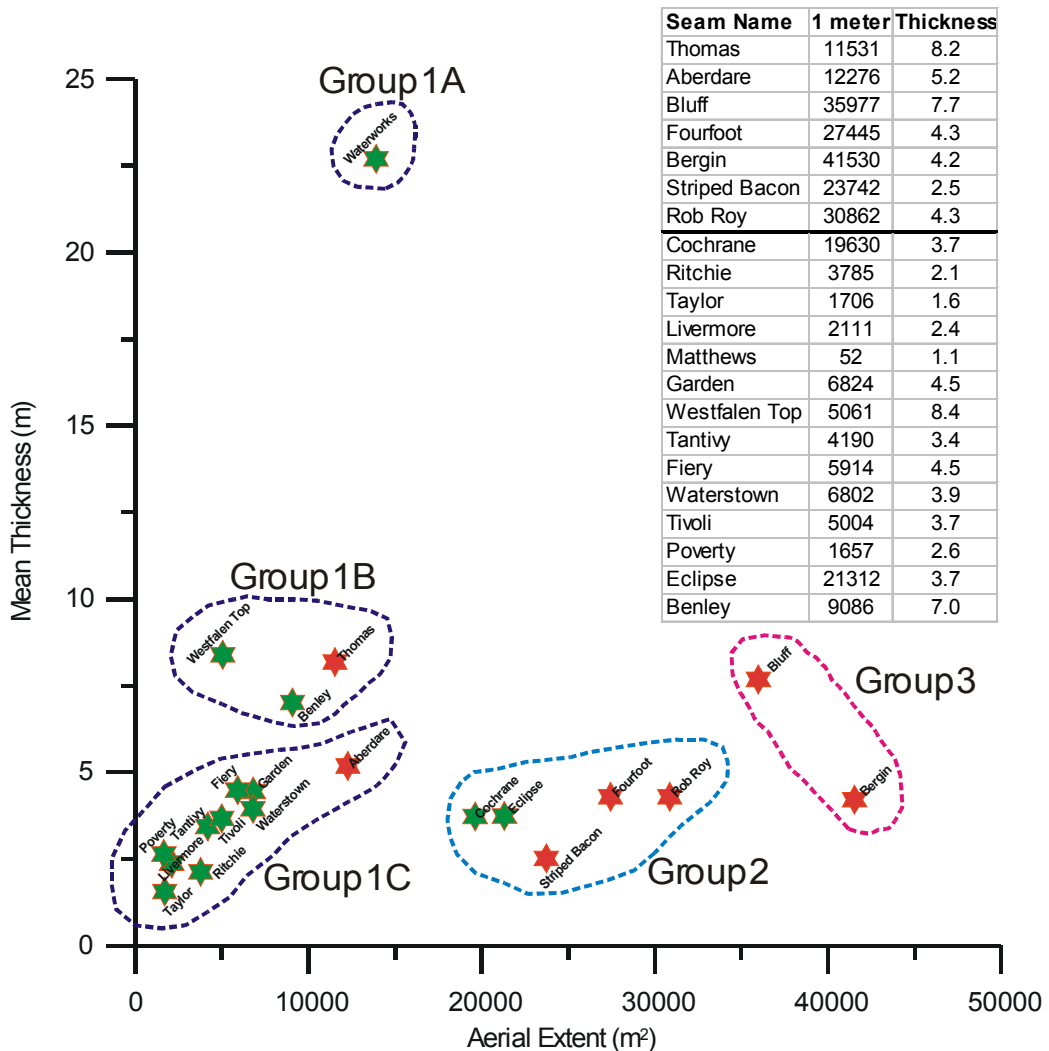


**Figure 106: Mean Thickness vs Aerial Extent (1m contour interval)
(Green = Tivoli Formation, Red = Blackstone Formation) (This graph was used for general grouping)**

Group 1A = Very High Mean Thickness to Aerial Extent

Group 1B = High Mean Thickness to Aerial Extent

Group 1C = Low Mean Thickness and Aerial Extent

Group 2 = Moderate Aerial Extent to Mean Thickness

Group 3 = High Aerial Extent to Mean Thickness

(NB: The relationship is only based on borehole data. All classifications such as very high and high are relative)

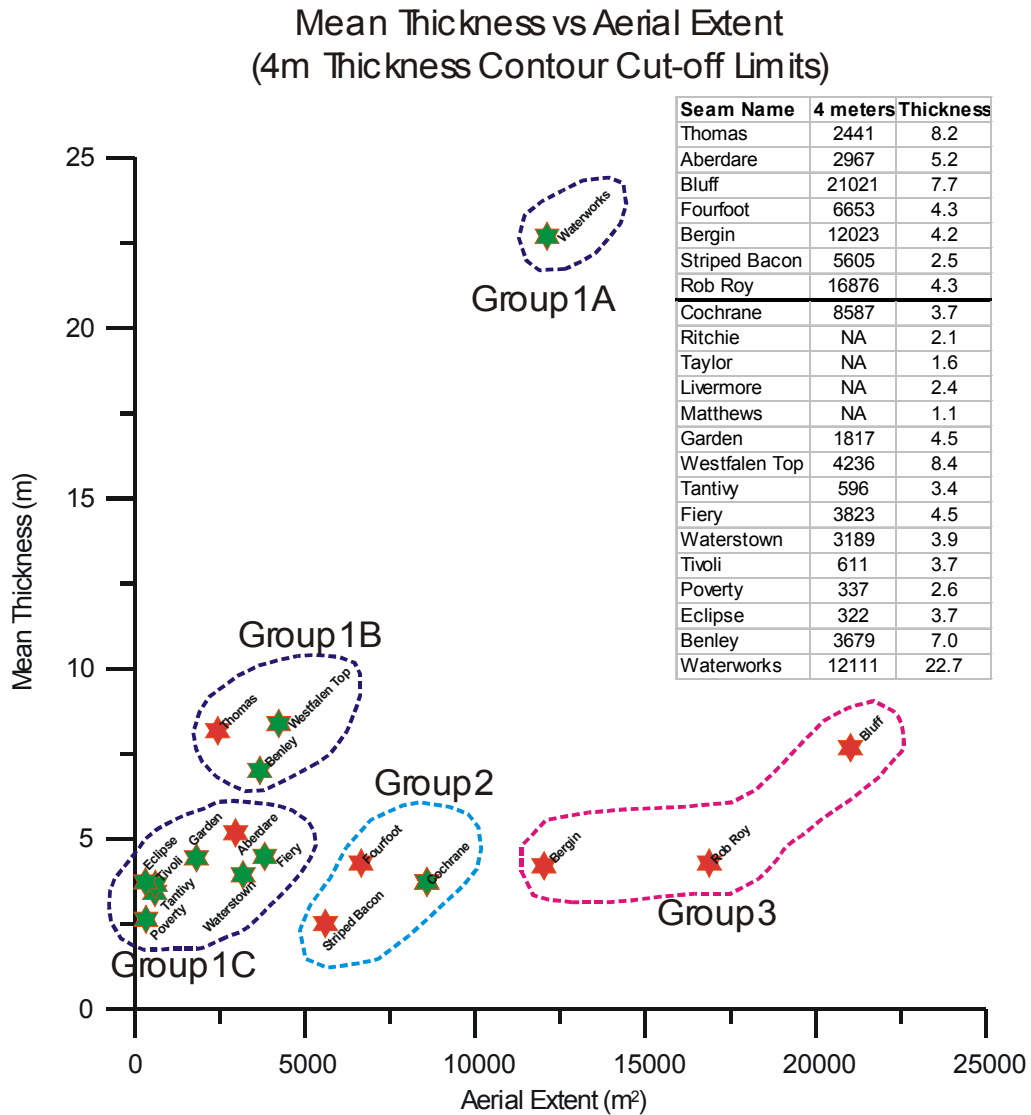
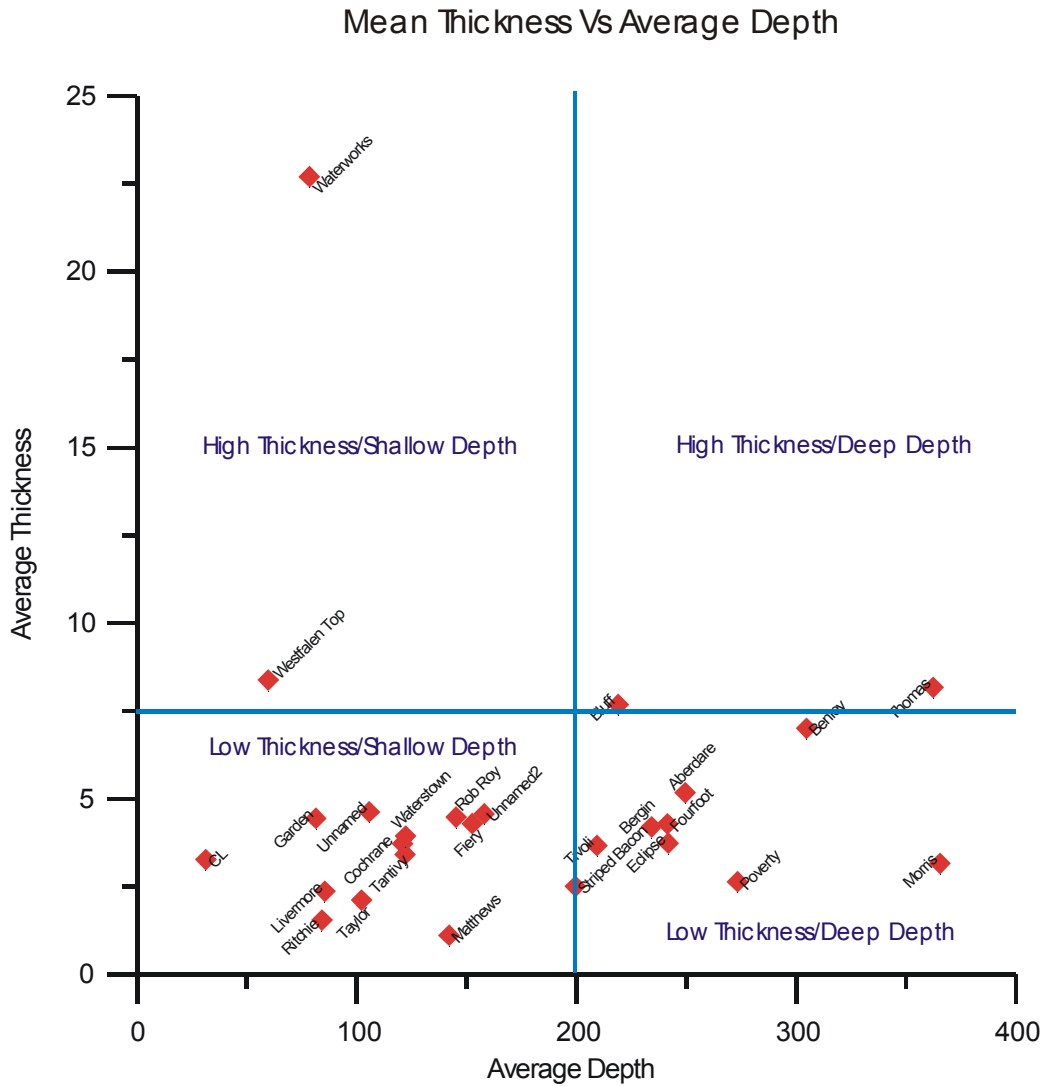


Figure 107: Mean Thickness vs Aerial Extent (4m contour interval) (Green = Tivoli Formation, Red = Blackstone Formation) (This graph was used for final grouping)



(Note: Average depths were calculated from borehole intersections with coal seams and hence, seam depths may not follow the stratigraphic order. For example, Rob Roy seam depth is shallower than Bluff seam because more boreholes have intersected Rob Roy seam at shallow depths. Therefore, average seam depth is relative to borehole location. This graph is only to demonstrate the overall relationship between depth and thickness).

Figure 108: Mean Thickness Vs Average Depth
 (The main use of this graph is to show how economic the seams are to mine. It should be noted that an aerial extent of a seam is also important in terms of determining the economic viability of a mine) (Also see Appendix II – Table 23).

Geophysical Map Interpretation

The gravity (bouguer anomaly) and airborne magnetic maps (Figures 109 and 112) were used to interpret the broad basal geometry and gross configuration of the basin. Two gravity profiles, northern and southern profiles (Figures 110 and 111), were also drawn to delineate the basement topography.

Figure 109, the bouguer gravity map, shows the significant thickness change in sedimentary accumulation within the basin. The north-eastern side of the study area shown in Figure 109 is interpreted as up-thrown side of the fault (Fault System 2, Figure 113) and it contains much thinner sedimentary accumulation (red = high density). Whereas south-western down-thrown side of the fault shows thicker sedimentary accumulation (blue = low density). Figures 110 and 111, the northern and southern gravity profiles, display steep curves caused by sudden change in gravity values across the interpreted fault line (F2). The narrow gravity high zone, which is between 6000m and 8000m distance on the northern profile and between 5000m and 10000m distance on the southern profile, indicates high sedimentary accumulation associated with subsidence created by the West Ipswich Fault (Fault System 3). Figure 112, the magnetic map, shows the northwest-southeast trending major basement fault system across the study area.

Figure 113 shows the patterns of gravity value variation within the basin. Three major fault systems (F1, F2 and F3) were interpreted from geophysical data and geological information (see “**Discussion**” section). Fault 1 system roughly follows the course of Brisbane River and controls sedimentation in the northern part of the basin. The earlier accumulation of the Tivoli Formation appears to conform to the configuration of the F1 system. The sedimentary accumulation is slightly thinner on the northern up-thrown side of F1. Fault 2 system, which largely controls the overall sedimentary accumulation within the basin, separates the much thinner sedimentary strata on the north-eastern side from progressively thicker sedimentary strata on the south-western side. Fault 3 system, the West Ipswich Fault, limits the deposition of coal-bearing Tivoli and Blackstone Formations to the west. The gravity map shows a low density anomaly on the western side of F3. This is due to the rejuvenation of F3 in the early Jurassic causing the western side to drop down (Day et al., 1974). However, there is no significant occurrence of coal accumulation on the western side of the West Ipswich Fault in the study area.

Figure 114 shows the depocentres of the Tivoli and Blackstone Formations together with the interpreted fault systems. The depocentre map was produced from combining depocentres of each coal seam shown in thickness contour maps (see “**Seam Contour Maps and Seam Split Maps**” section). This depocentre map can be studied in conjunction with total coal

thickness isopach maps for the Tivoli and Blackstone Formations (Figures 103 to 105). Figures 103 and 104 were produced by adding up thicknesses of all coal seams intersected in each borehole for the Tivoli and Blackstone Formations. The isopach maps indicate that the distribution of depocentres followed the patterns of major fault systems. The eastern and northern parts are limited by F1 and F2 systems, while F3 marks the western edge of the basin. However, the southern part of the basin is covered by the younger Moreton Basin sedimentary rocks and no significant fault system has been noted. The southern part of the Ipswich Basin probably extends in an attenuated fashion to other Triassic sedimentary basins in the south to Evans Head, Red Cliff and Nymboida (see Figure 11). The eastern boundary also probably extends in an attenuated fashion to Salisbury and Nundah.

It should be noted, however, that apart from the West Ipswich Fault (F3), the other fault systems (F1 and F2) are basement structural faults of Palaeozoic age and hence, they may not be directly related to the control on the sedimentation patterns of the younger Brassall Subgroup of Late Triassic Epoch (see Table 1 – Stratigraphic Succession). The Ipswich Coal Measures only occupies the higher stratigraphic position in the Ipswich Basin and it is unlikely to have any direct structural influence of the deep basement fault systems F1 and F2. However, the overall sedimentation patterns of the Ipswich Coal Measures conform to the patterns of these major faults which suggests the fault systems had a role in the formation of the Ipswich Basin.

(See following Figures for Gravity Map, Gravity Profiles, Magnetic Map, Major Fault Systems and Depocentres).

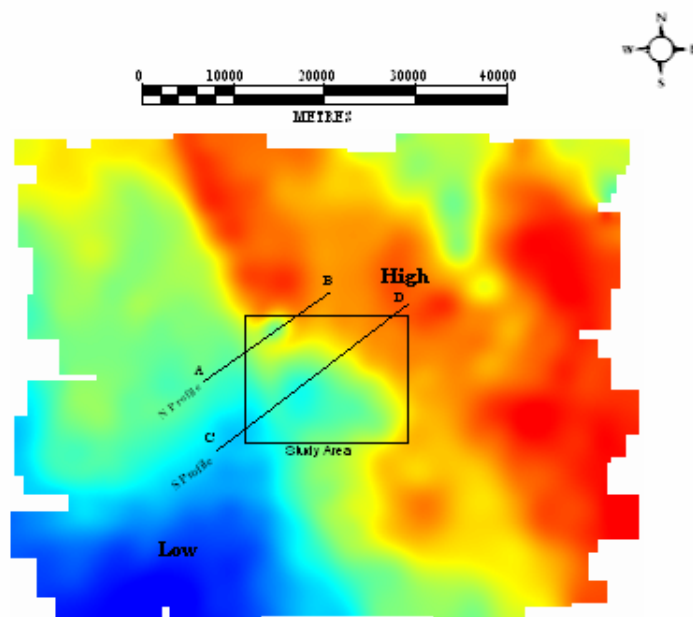
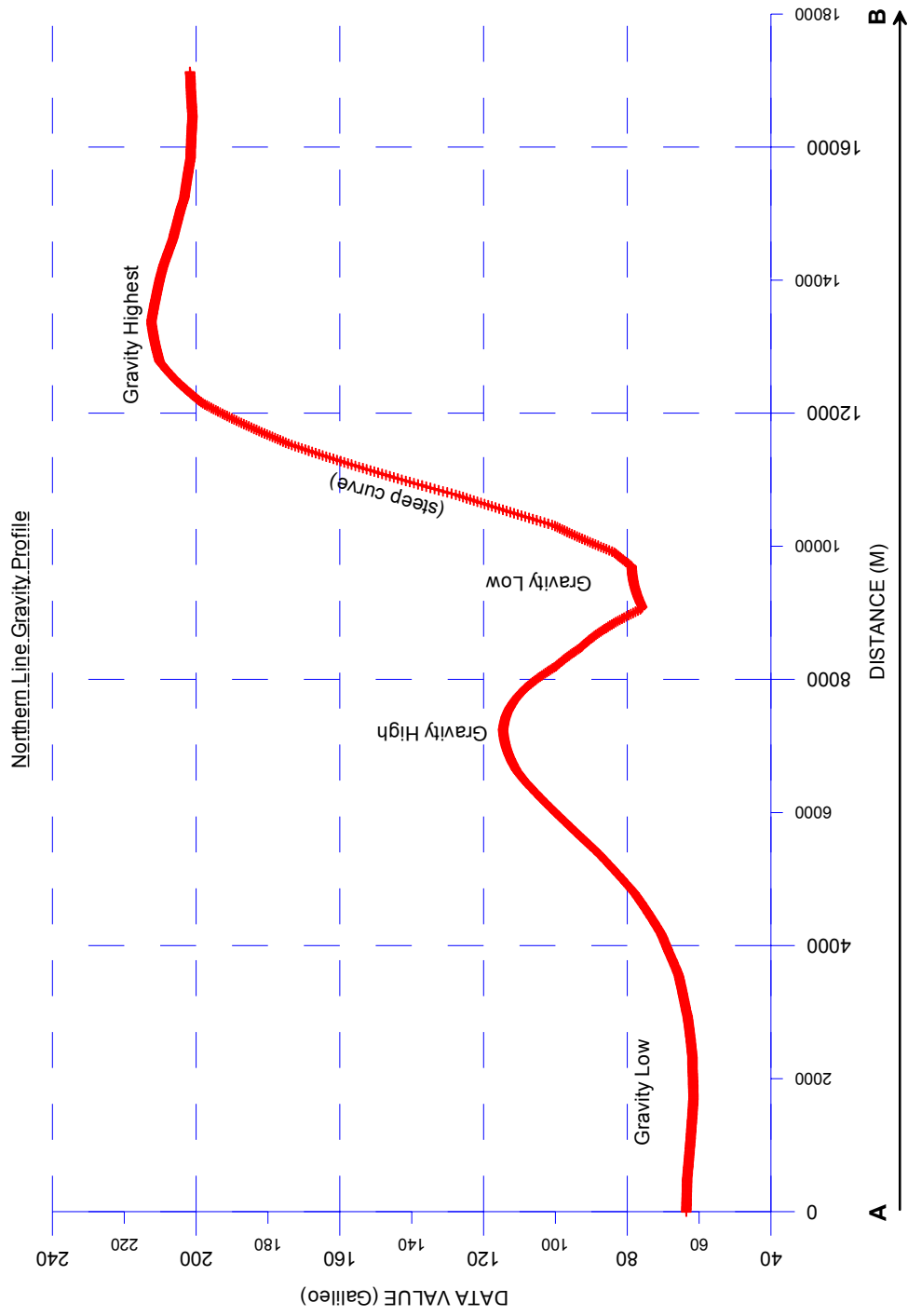
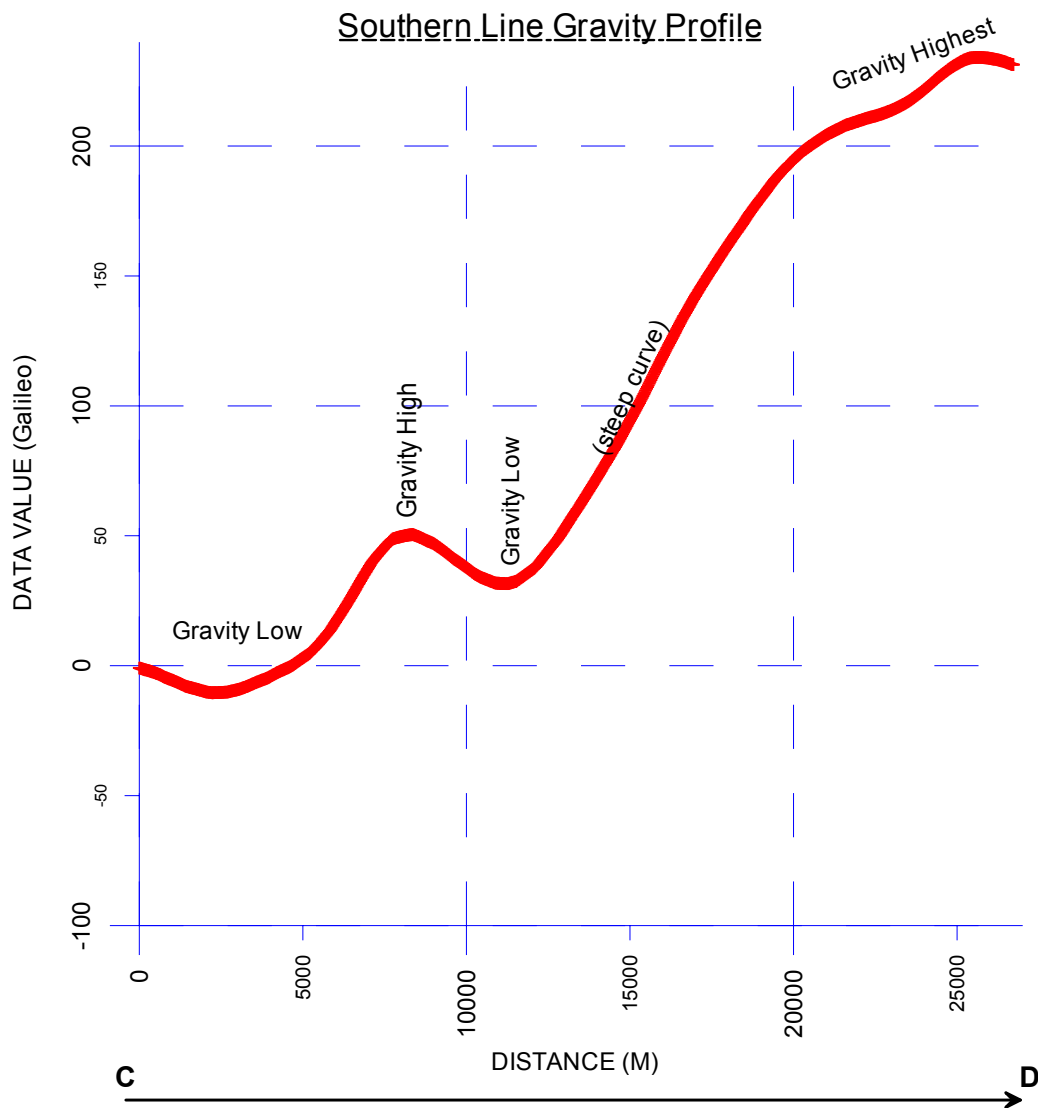


Figure 109: Gravity Map (blue shaded areas denote low density or thick sedimentary accumulation and red areas represent high density or thin sedimentary accumulation. The gravity anomalies are indicative of significant thickness of low density material, typically thick sedimentary strata, which reflects fault-bounded depositional basins. (Gravity data courtesy of Queensland Department of Mines and Energy)



**Figure 110: Northern Gravity Profile (see Figure 109 for location)
(Gravity data courtesy of Queensland Department of Mines and Energy, 2002)**



**Figure 111: Southern Gravity Profile (see Figure 109 for location)
 (Gravity data courtesy of Queensland Department of Mines and energy,
 2002)**

This image is not
available online.
Please consult
the hardcopy
thesis available
from the QUT
library

Figure 112: Magnetic map showing the major basement fault structure across the basin with up and down throw sides. (Note the relatively weaker pattern in the study area probably due to faulting, erosion and later high sedimentation) (Magnetic map courtesy of Queensland Department of Mines and Energy)

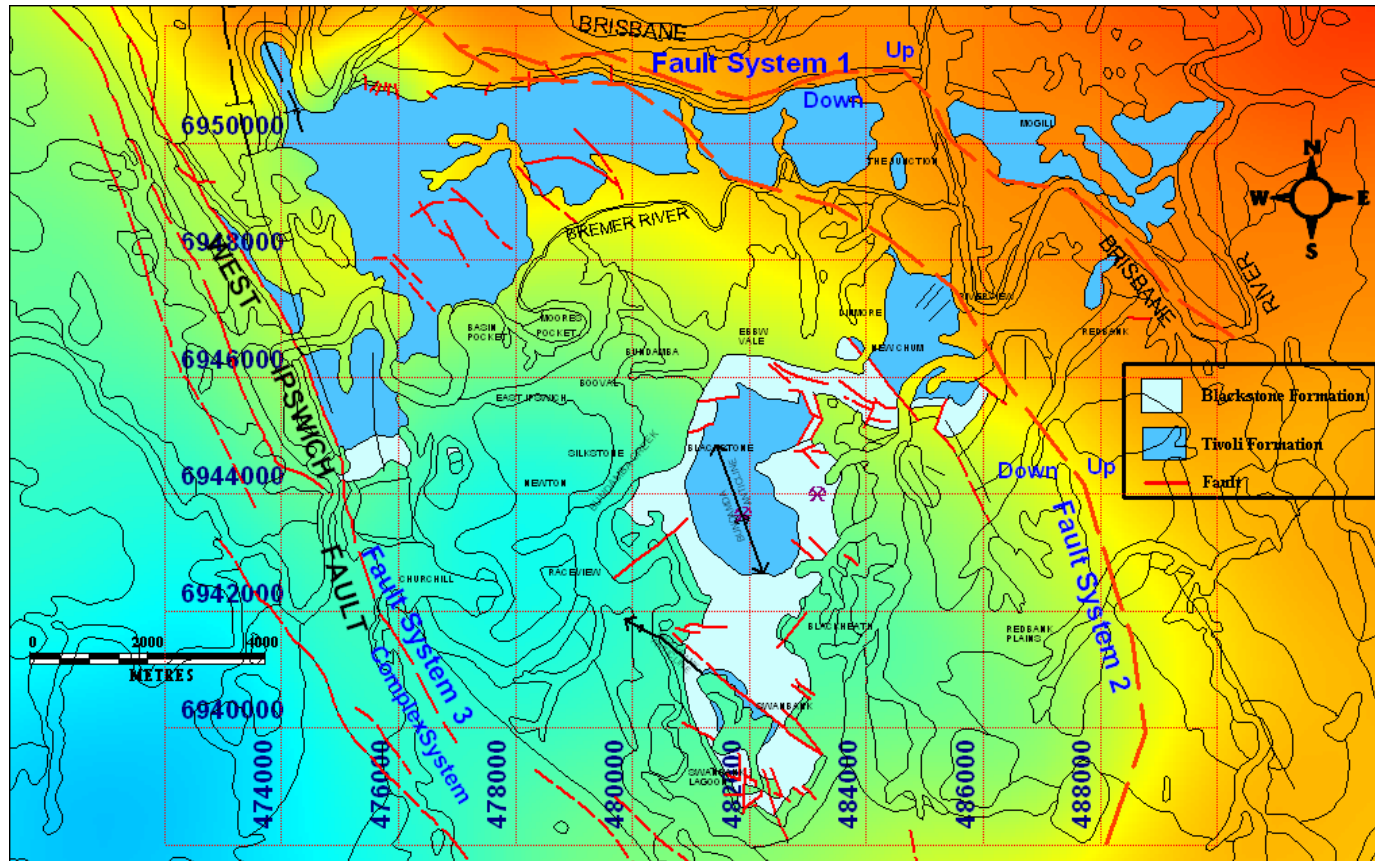


Figure 113: Ipswich Basin major fault systems 1, 2 and 3 (red thick broken lines). Red to blue background colour indicates high to low density.

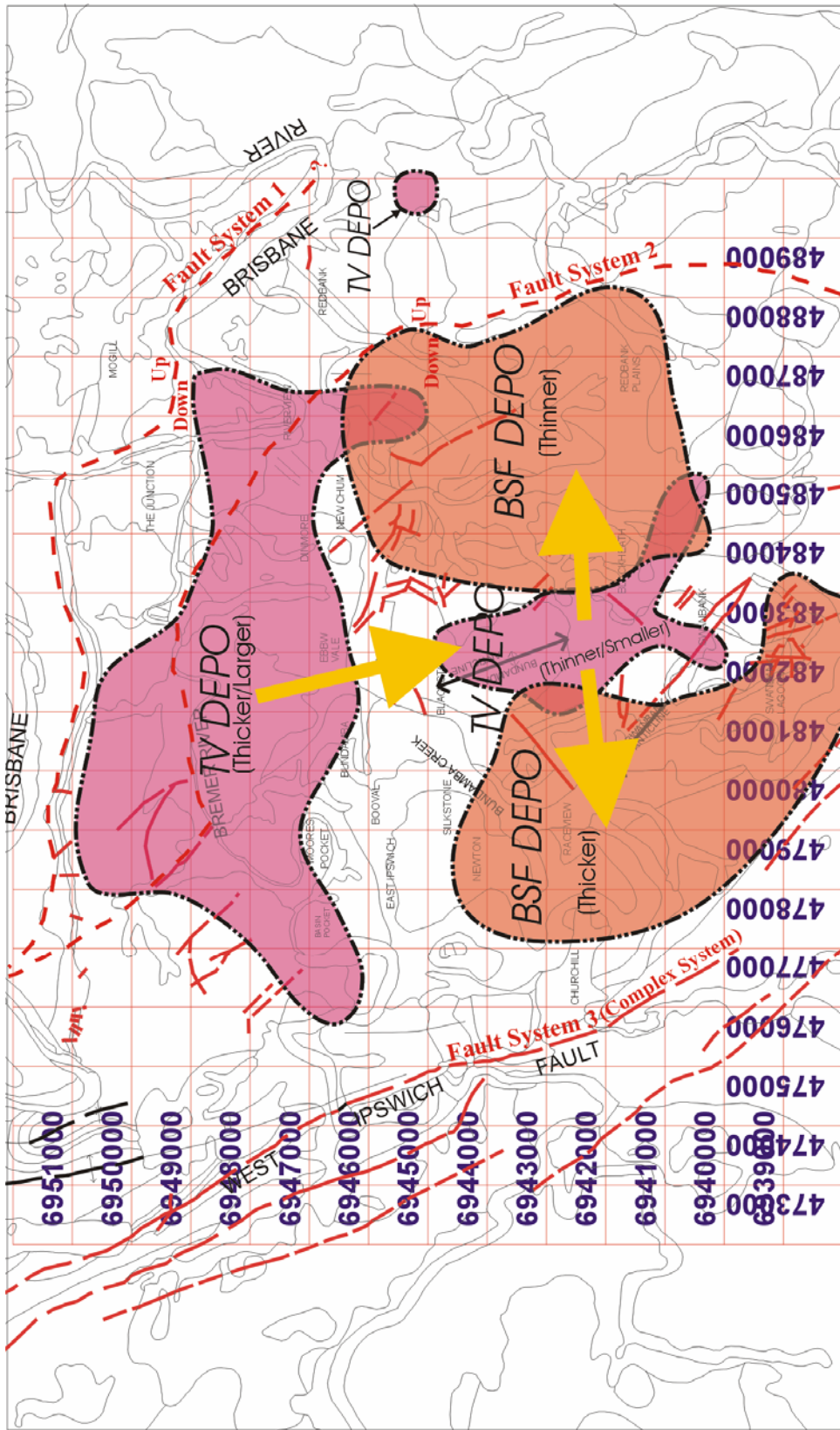


Figure 114: Depocentres for the Blackstone Formation (BSF DEPO) and Tivoli Formation (TV DEPO)-Coal thickness only
 Large yellow coloured arrows indicate depocentre shift

Basement Structural Cross-sections

Three structural cross-sections were drawn across the Ipswich Basin to delineate the basement structure and faulting patterns of the basin (see Figure 115 for Location Map and Figures 116 to 118 for Cross Sections). There are, however, no available borehole data to draw basement structural sections across the coalfield to include both Tivoli and Blackstone Formations on one cross-section, because all boreholes in the area are shallower than the base of Tivoli Formation. These shallow boreholes were used to produce fifty cross-sections for coal seam correlation purposes (see Appendix IV). In addition, three large cross-sections, including one north-south cross-section and two east-west cross-sections, were produced to correlate coal seam across the basin and study the general seam splitting patterns (see Appendix V).

Seven deep structural drillholes, including GSQ Ipswich series drillhole numbers 1, 2, 7, 16, 18, 25 and 26, were used to interpret the palaeotopography prior to coal sedimentation in the Ipswich Basin. All cross sections show a steep rise of basin basement to the east. This is consistent with gravity and magnetic maps which show the high density in the northeast and low density or bouguer gravity anomalies in the southwest. The sudden change in base level in a relatively short distance (<1km) was possibly due to tectonic subsidence in the basin, the configuration of which is largely related to basement fault systems F1, F2 and F3. The basin subsidence occurred prior to and during the formation of Ipswich Coal Measures, and hence, coal seams were deposited in the subsided areas where the accommodation was the highest (see Figures 103 to 105). This formed the basis for the movement of depocentres and sedimentation patterns in the basin.

(See following Figures for Cross-section Locations Map, Cross-sections 1, 2 and 3)

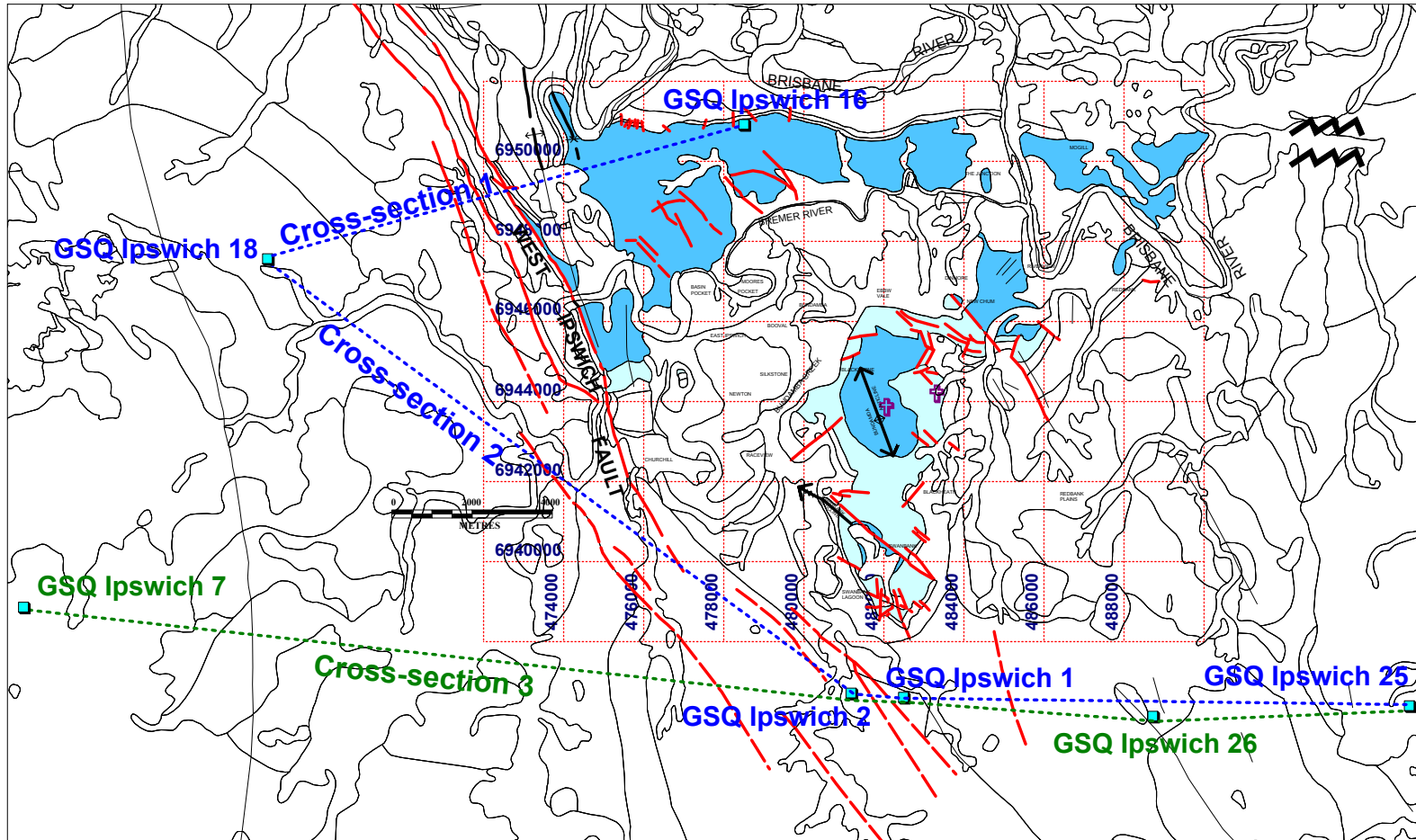


Figure 115: Base Map Showing GSQ Ipswich Borehole Cross-sections (structural cross-sections used to study basin basement structures) (Modified from Queensland Department of Mines and Energy, 1999)

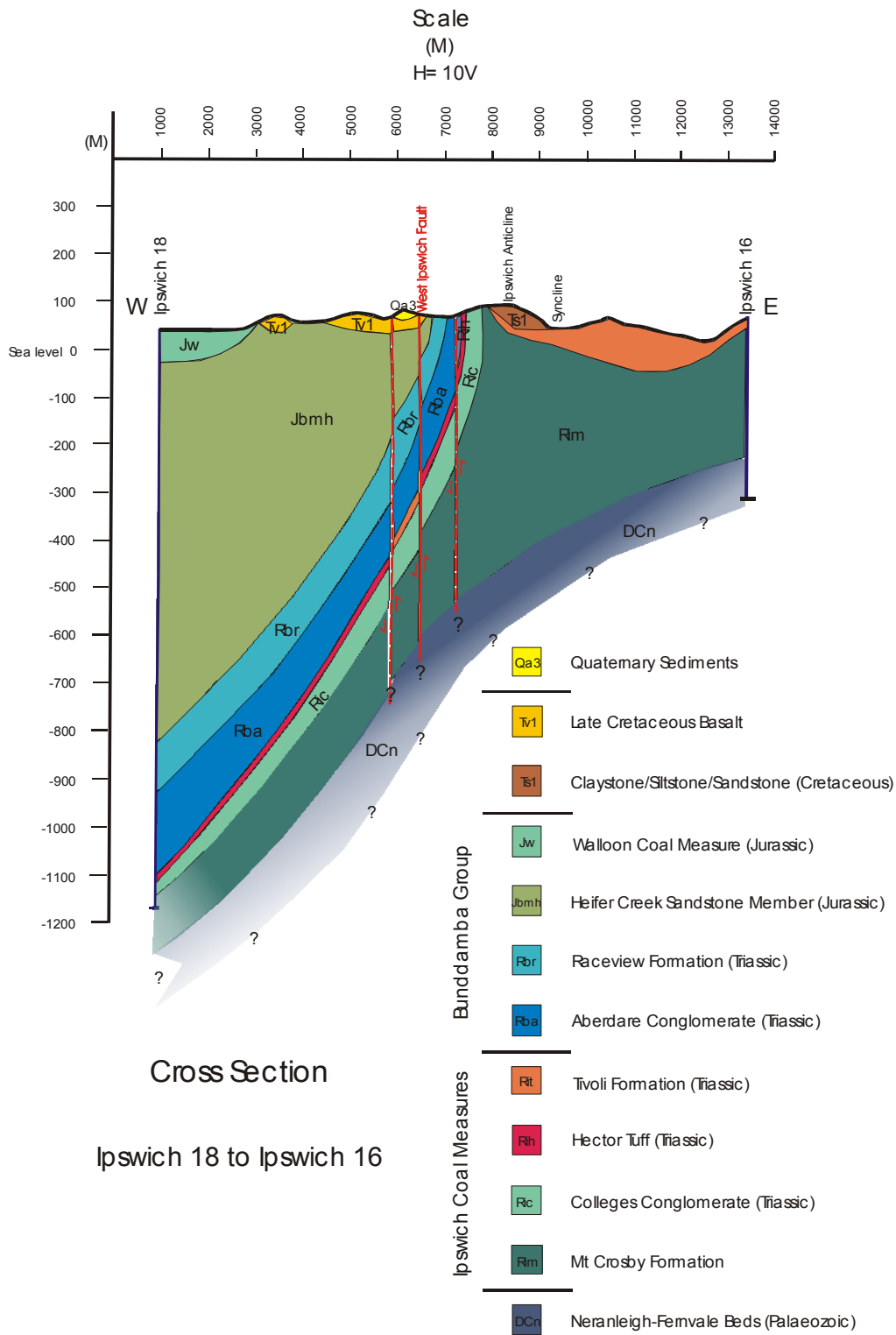


Figure 116: Cross-section 1 (After Allen, 1972; Gray, 1975; Russett, 1986; Cranfield, et al., 1989)

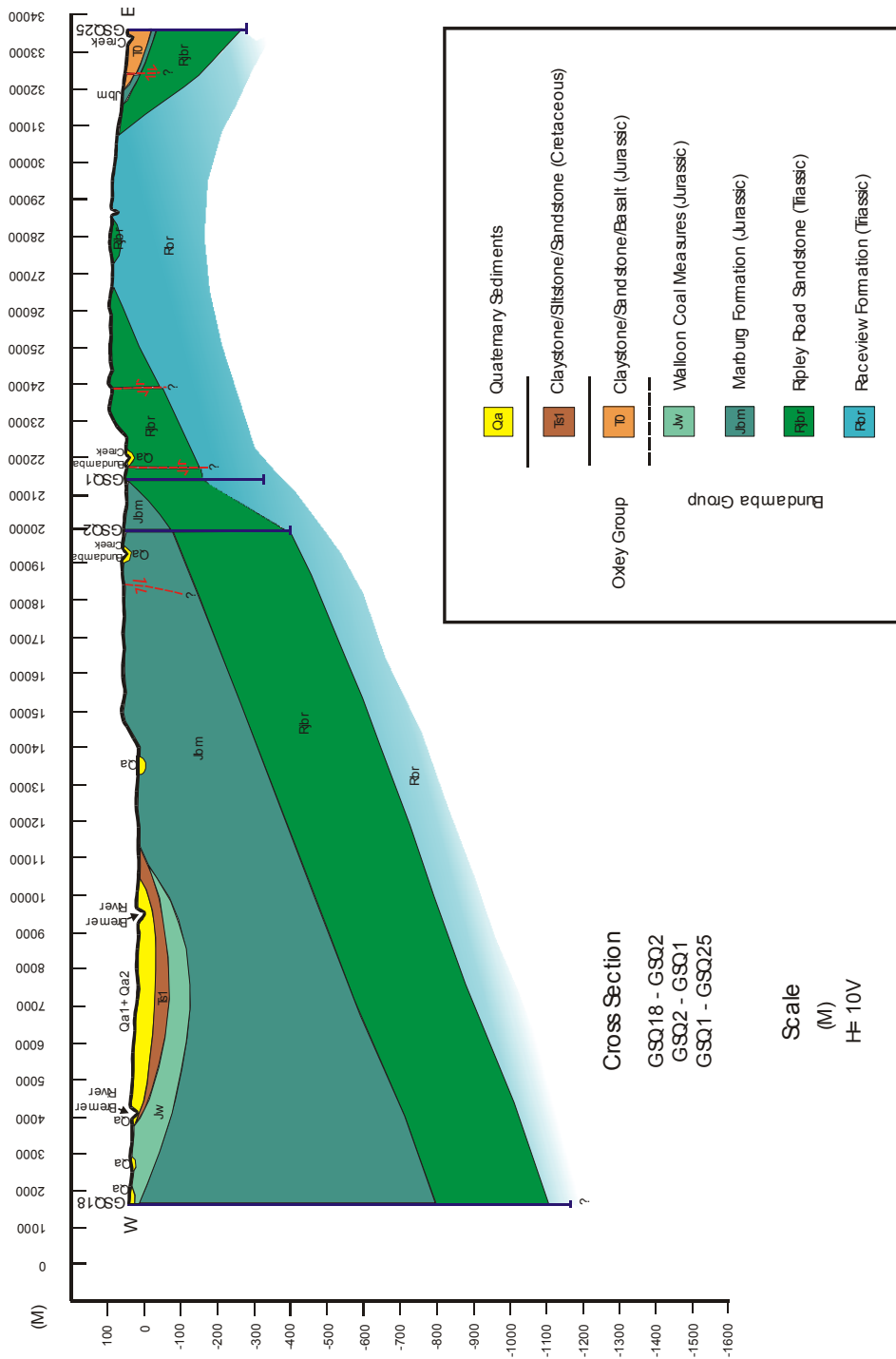


Figure 117: Cross-section 2 (After Allen, 1972; Gray, 1975; Hawkins, 1975; Almond, 1982; Cranfield, 1976, 1981, 1984; Russett, 1986; Haselwood, 2002)

This image is not available online. Please consult the
hardcopy thesis available from the QUT library



Figure 118: Cross-section 3 (Tiv = Tivoli Formation, Black = Blackstone Formation, Source: Arrow Energy N. L., 2002)

Discussion

The maceral data analysis in conjunction with the study of tectonic processes and distribution patterns of sedimentary rocks to interpret the coal forming depositional environments in the Ipswich Basin.

All coal seams have been grouped according to their mean seam thickness and aerial extent ratio (eg. Group: 1A, 1B, 1C, 2 and 3) (Figures 106 and 107). Two “Mean Thickness versus Aerial Extent” graphs were produced using 1m and 4m thickness contour interval cut-off limits (Table 22). Two graphs give similar results. However, the very sparse drillhole data do not allow the production of accurate one metre contours and thus the areas stated at that contour interval are estimates only. The one meter contour graph is only used for seams which have the average thickness of less than 4m and for preliminary seam grouping. Major fault systems, which shaped the basin configuration, were also classified as Fault System 1 (F1), Fault System 2 (F2) and Fault System 3 (F3), based on their structural relation to basin subsidence and sedimentation, with F1 being the oldest and F3 being the youngest (see Figure 129). The average seam thickness to depth relationship has been classified as four groups, including low thickness-shallow depth, low thickness-deep depth, high thickness-shallow depth and high thickness-deep depth, according to the general grouping patterns of seams on the graph (Figure 113).

Evolution of Coal Sedimentation Patterns

The coal forming depositional processes are discussed below from the oldest seam (Waterworks) to the youngest seam (Thomas) to give an indication of the progressive change in depositional conditions with time.

Tivoli Formation

The very high mean thickness to aerial extent ratio (Group 1A) of the Waterworks seam (Figure 106) suggests that basin subsidence had occurred just prior to coal accumulation. According to Denmead (1954) a sustained period of basinwide subsidence in the Late Triassic Epoch initiated the formation of Kholo Conglomerate (=Colleges Conglomerate). This was followed by a renewal of tectonic activity in the line of the Brisbane Valley. It may have been caused by the transpressional movements in the Late Triassic Epoch in eastern Australia which followed the configuration of the basin basement fault (F1). Figure 113 shows the F1 system with small subsidiary faults roughly parallels the Brisbane River. Willmott and Stevens (1992) stated that the Brisbane River existed as early as Late Triassic Epoch as a stream or streams draining the hinterland through the Ipswich – Brisbane corridor while the Ipswich Coal Measures formed in a series of

rivers, swamps and lakes between the older mountains. The subsidence created accommodation or space for sediment accumulations to occur on the southern down-thrown side of the fault (F1), which is located in the northern part of the basin. The bouguer anomaly Gravity Map (Figure 109) shows the low density, ie. higher sedimentary accumulation, on the southern downthrown side of the basement structure F1. Due to rapid fault controlled subsidence the Waterworks seam is thick but aerially limited. The clastic influx was also high because of high accommodation created by rapid subsidence, and as the coal contains numerous clastic bands. The depocentre of coal accumulation was in the north of the basin (Figure 114).

After the deposition of Waterworks seam, the coal displays a moderately high thickness to aerial extent ratio (Group 1B) typified by the Benley seam. This suggests vertical growth of peat-mire occurred in the basin probably due to continuous accumulation and prolonged existence of peat-mire, which maintained balanced relative water level. This prevented oxidation of peat and drowning of the peat swamp. In addition, water level in the peat-mire was increased by seasonal flooding and/or water level fluctuations which may have helped to spread nutrients and fresh water across the basin, and the slow compaction of lower strata caused by sediment loading may have created accommodation and given time for the peat-mire growth.

However, low mean seam thickness and aerial extent (Group 1C) shown by the Eclipse, Poverty, Tivoli, Waterstown, Fiery and Tantivy seams indicates that further fault-controlled differential subsidence occurred in the northern part of the basin. Coal accumulation was restricted to areas where the subsidence rates were high, and coal seams were isolated and rapidly buried by terrigenous influx before they could gradually expand. Coal accumulation was still limited to the northern part of the basin.

This was followed by the deposition of Westfalen Top seam. Relatively high mean thickness to aerial extent ratio (Group 1B) of the Westfalen Top seam suggests lower clastic influx and continued subsidence which favoured peat-mire aggradation (vertical growth). The coal accumulation kept pace with subsidence rates in the basin. This type of coal facies is described as terrestrial origin resulted from undisturbed peat which grew *in situ* (Stach et al., 1975). Peat may have continued to accumulate as an ombrogenous high moor after the water body became silted-up. Diessel (1992) defined this type of peat-mire expansion as 'Terrestrialisation'. Coal accumulation occurred only in the north of the basin on the southern down-thrown side of the F1 basement fault.

However, the Garden seam shows low mean thickness and aerial extent (Group 1C). This may have been caused by the further tilting or subsidence of the basement to the south. The subsidence appears to conform to the configuration of the earlier basement fault system (F2), which parallels the

West Ipswich Fault (F3) (Cranfield, Hutton and Green, 1989). The coal accumulations and depocentres of the following seams shifted to the south-central part of the basin (Figure 130).

The small isolated seams, including Matthews, Livermore, Taylor and Ritchie seams, show both low mean thickness and aerial extent (Group 1C), possibly due to fault-controlled rapid subsidence. The rate of peat formation did not keep pace with the high subsidence rate and thus, the peat swamp was terminated before it could expand. Coal accumulations, on the other hand, were restricted to the south-central part of the basin (Figure 114).

The Cochrane seam, which is the highest in the stratigraphic order of the Tivoli Formation, was deposited in the southern part of the basin across the Bundamba Anticline. The moderately high aerial extent to mean thickness ratio (Group 2) of Cochrane seam suggests another peat-mire expansion or progradation occurred probably as a result of relatively shallower accommodation, which prevented high clastic influx into the peat swamp. This was followed by minor flooding in the areas adjacent to peat-mire which may have led to peat-mire encroachment upon surrounding areas. This type of peat formation is commonly known as paludification, which is a replacement of dry land by a mire usually as a result of rising groundwater table.

The isopach maps show that the second depocentre of the Tivoli Formation which formed in the south-central part of the basin appears to be much shallower and more restricted than the first depocentre formed in the north of the basin (Figure 103). This suggests relatively slower subsidence and quieter tectonic activity near the end of the Tivoli Formation. However, the bouguer anomaly gravity map shows thicker sedimentation on the southern part of the basin. This indicates higher clastic influx in the basin with little coal accumulation. Another very small thickness anomaly of the Tivoli Formation in the east of the basin was probably caused by minor subsidence associated with the sediment compaction.

Following the deposition of Cochrane seam, the Ipswich Basin was inundated with clastic sediments transported from higher surrounding source areas. This ended the deposition of Tivoli Formation.

Blackstone Formation

The Blackstone Formation overlies the Tivoli Formation. Coal accumulation in the Blackstone Formation resumed in the basin after a period of non-deposition and erosion. The Blackstone Formation depocentres shifted simultaneously to both east and west. This created the peculiar shape of the basin (Figure 114). The depocentre shift was probably associated with an uplift caused by flexural movements. The east side down movement of the

West Ipswich Fault (F3) together with west side down movement of the possible fault (on the eastern side of the basin) may have caused compression that produced the Bundamba Anticline. Figure 105 shows progressive thinning of the Blackstone Formation towards the Bundamba Anticline. The thinner coal accumulation which occurred around the Bundamba Anticline suggests that the anticline was initiated prior to or during the time of coal deposition. The east block-down movement of F3 created subsidence in the west close to the West Ipswich Fault and subsequent uplift in the east away from the fault due to flexural movements in the basin. The uplift initiated the Bundamba Anticline which forms one of the major structures in the Ipswich Basin. Figures 105 and 114 show thicker coal accumulation of the Blackstone Formation on the western side of the Bundamba Anticline close to the West Ipswich Fault (F3). The depocentre of the Blackstone Formation on the eastern side of the Bundamba Anticline appears to be thinner due to reduced subsidence away from the West Ipswich Fault (F3). Figure 119 illustrates the tectonic movements initiated by F3.

The lower seams of the Blackstone Formation, including the Rob Roy, Striped Bacon, Bergin and Fourfoot seams show moderate and high aerial extent to mean thickness ratios (Group 2 and Group 3) indicating the widespread coal distribution in the basin. This peat-mire expansion was probably due to wetter environments with sufficient accommodation available for peat accumulation. This is indicated by the bright nature of coal lithotypes. Petrographic study suggests a telmatic (wet forest swamp) depositional environment. The oscillating water level is shown by alternating high and moderate aerial extents (Group 3 and Group 2) of coal seams. The Rob Roy and Striped Bacon seams contain numerous tuffaceous claystone bands (tonstein). This suggests that peat-mire was affected by volcanism, which may have also contributed to the widespread coal accumulation in the basin.

The Bluff seam shows the highest aerial extent and mean thickness (Group 3) indicating the possible maximum flooding level, which coincided with peat-mire that reached its maximum expansion. The relatively quieter and more stable conditions with limited fluvial sediment influx favored the widespread accumulation of coal in the basin.

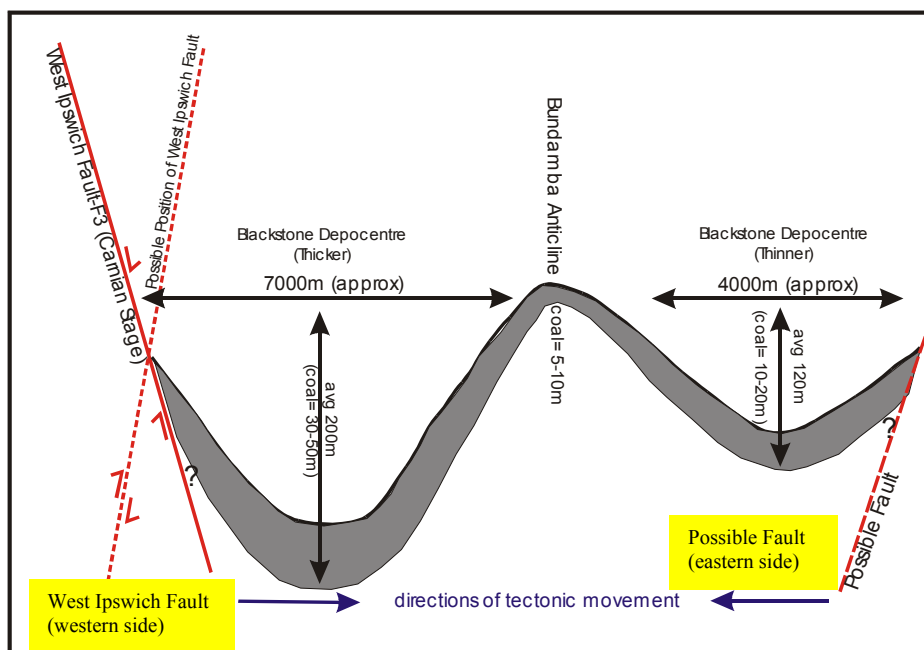


Figure 119: Cartoon illustrating the 'Flexural Movements' of F3 system (diagrammatic only, not to scale)

The Aberdare seam shows low aerial extent and mean thickness (Group 1C), suggesting peat-mire retreat probably due to the movements of fault system F3 (West Ipswich Fault). The Aberdare is the only seam in the Blackstone Formation included in Group 1C. Cranfield et al. (1989) stated that the major movement on the West Ipswich Fault during the deposition of the Ipswich Basin was east-block-down. Falkner (1986) also indicated that the West Ipswich structure appeared to be a complex fault zone which was downthrown to the east during the Carnian and downthrown to the west from the Rhaetian onward. The geological and palynological evidence from the Ipswich area indicates that the Ipswich Coal Measures were deformed in the Late Triassic (Norian) (Allen et al., 1960; de Jersey, 1970). The Thomas seam, which has the relatively high mean thickness to aerial extent ratio (Group 1B), was deposited after the fault-controlled subsidence. McCabe (1984) stated that if an ombrotrophic peat accumulation continued to outstrip the rate of subsidence, the formation of thick and clean coal would occur. The Thomas seam is aerially restricted but thick and produces relatively clean coal with few intraseam clastic bands. Day et al. (1974) stated that the asymmetric Ipswich Anticline in the northwestern corner of the Ipswich Basin was truncated on its western side by the western downthrow movement of the West Ipswich Fault in the Early Jurassic Epoch after the deposition of the Thomas seam. This caused the West Ipswich Fault to move the west block down.

Effects of Faulting

The western downthrow movement of the West Ipswich Fault, which occurred after the deposition of the Ipswich Coal Measures, was probably as a result of reverse faulting. Haselwood (2003) in his study of the Clarence-Moreton Basin produced thermal maturity maps using vitrinite reflectance data (%R_{omax}) and showed that the thermal maturity increased towards the east (Figures 120 and 121). The vitrinite reflectance maps showed that the R_{omax} pattern was independent of the West Ipswich Fault. This suggests that coal matured after faulting in the basin. It can be interpreted that coal formation was not directly influenced by basement fault systems. There is, however, no available information regarding the displacement of the West Ipswich Fault as it is a very complex fault system and no proper study has been carried out to measure the extent of fault displacements. Furthermore, the gravity map shows lower density anomalies or thicker sedimentary accumulation in the east of the West Ipswich Fault suggesting that the fault was east block down during sedimentation in the basin. The narrow gravity high zone recorded on the northern and southern profiles (see '**Geophysical Map Interpretation**' section) indicates high sedimentary accumulation as a result of subsidence created by the West Ipswich Fault (F3). The gravity profiles (Figures 110 and 111) and basement structural cross-sections (Figures 116 to 118) show a steep basement rise to the east and northeast. The dominant fault trend in the basin is northwest-southeast and this is well illustrated in the Magnetic Map (Figure 112). Allen, Staines and Wilson in Hill and Denmead (1960) noted a few reverse displacements and some overthrusting based on surface geological data interpretation.

This image is not available online. Please consult the hardcopy thesis available from the QUT library .

Figure 120: Thermal maturity patterns driven from vitrinite reflectance data at the top of the Tivoli Formation (Source: Haselwood, 2003)

This image is not available online. Please consult the hardcopy thesis available from the QUT library

Figure 121: Thermal maturity pattern at the top of the Ipswich Basin, using the vitrinite reflectance data from the Woogaroo and Brassall Subgroups (Source: Haselwood, 2003)

Two common tendencies are rapid lateral variation in displacement and bifurcation into smaller faults which gradually die out. It was also stated that two predominant NW-SE trending faults developed north of Bremer River (probably F1) and southern end of Bundamba Anticline (probably F2). Tucker (1949) noted a fault system (possibly F1) that followed the course of the Brisbane River and threw down the Ipswich Coal Measures against older metamorphic rocks of Palaeozoic age. The western margin of the Ipswich Basin is marked by steeply dipping strata of various ages. They are traceable for several kilometers to the north and south and shown as the West Ipswich Fault. Cameron (1906 and 1923) interpreted this structure as a monoclinal fold, which developed to a normal fault. Denmead (1955) considered "that the Bundamba beds were first up-ended as a result of large-scale down-warping over a wide area and that the adjacent Ipswich beds were subsequently squeezed against the relatively stable mass of steeply dipping sandstones and as a result were locally folded and faulted". Wilson (unpublished thesis, 1958) noted that the dominant structure was the fractured axis of an asymmetrical anticline and this occupied approximately the same position as Denmead's West Ipswich Fault. The West Ipswich structure and the Bundamba Anticline are probably contemporaneous in origin and development. This is uncertain but this study suggests that the Bundamba Anticline may have formed prior to and during the time of coal deposition. Regionally, the Bundamba Anticline is a subsidiary fold on the eastern flank of the West Ipswich structure (see Figure 119).

Following the deposition of the Blackstone Formation, the Ipswich Coal Measures were slightly uplifted and partially eroded, before the Aberdare Conglomerate was deposited. Later in the Mesozoic Era, the Triassic and Jurassic sedimentary rocks were folded and faulted. These events obscured the earlier structural patterns of the Bundamba Anticline and West Ipswich Fault. During the Mid or Late Tertiary Epoch, the preexisting folds were accentuated and the Tertiary sediments were down-warped in the Booval Syncline to below present sea level (Allen et al., 1960).

Compaction

The typical thickness of the Brassall Subgroup, including the Blackstone and Tivoli Formations, is about 720m. The combined average seam thickness of the coal measures is about 129.69m or 18% of the total thickness (including Swanbank seams), and 117.88m or 16% (excluding Swanbank seams), of the Brassall Subgroup (Tables 1 and 4). A minimum 10% of coal is required to give significant compaction (Ryer and Langer, 1980). Therefore, the compaction plays an important role in sedimentation within the basin. However, the variations in seam thickness and distribution appear to be largely controlled by basin subsidence associated with tectonic movements. Depocentre shift, from north to south (Tivoli Formation) and

later to east and west (Blackstone Formation), also indicates tilting or subsidence of the basement that roughly conform to the F1 and F2 systems configuration. The southerly dipping of seams in Tivoli Formation suggests down-thrown sides of faults are generally to the south. Denmead (1955a) also noted the southerly dipping of strata in the Ipswich Coalfield. Gravity and magnetic maps in Figures 109 and 112 clearly show the overall sedimentation patterns were controlled by the basement structural configuration.

The Unamed seam, City Lower (CL) seam, Hillier seam, Unnamed 2 seam, Francis seam, Poverty seam and Morris seam have not been taken into account due to inadequate amount of drillhole data. These seams are generally insignificant and nothing to suggest that they would differ from others. They are, therefore, unlikely to change the overall picture.

Depositional Environments and Associated Sedimentation Patterns

Application of sequence stratigraphy mainly focuses on basins which are associated with marine or coastal environments. Therefore, it is generally accepted that sequence stratigraphy is not applicable to cratonic interior basins such as intermontane basins, because these basins do not have any direct influence of sea-level fluctuation or eustacy. However, basic concepts of sequence stratigraphy can be used in conjunction with petrographic study to interpret the facies changes and depositional environments of continental basins (Allen, 1996; Boyd et al., 1996; Diessel, 1992).

In a fluvial system, basic controls on accommodation and modification of equilibrium profile are caused by tectonic subsidence and tilting, modification in fluvial discharge and changes in the sediment supply (Allen, 1995). The relationship between the rate of sediment supply and the rate of subsidence-controlled-accommodation usually determines changes in the style of non-marine sedimentation patterns. Furthermore, continental peat accumulation largely depends on a delicate balance among subsidence, aggradation and maintenance of a slow but continuous rise of groundwater level to keep pace with peat growth (Galloway, 1983). The dominance of either bright or dull lithotypes depends on the position of the groundwater level in relation to the peat surface. If a slow subsidence occurs, peat accretion can usually cope with the subsidence. On the other hand, if the rate of peat vertical growth exceeded the slow subsidence rate, the peat surface may be raised high above the groundwater level leading to a change in depositional conditions and dulling upward sequences would be produced. In addition, the climatic conditions and sediment source play an important part. The significant change in climatic conditions may modify the depositional environments and sediment source which normally determines the type of basin fill. On the other hand, Jones and de Jersey

(1947) pointed out that the Ipswich Basin is comparatively aerially limited (ie. less than 700Km² for the whole basin and less than 300km² for the coal measures) and thus, variations of climate and depositional environment within the basin are likely to be minimal. The unique event of volcanism plays a part in terms of producing tuffaceous claystone bands (tonstein) and modifying coal seam architecture. According to Falkner (1986) tonstein bands are kaolinite rich rocks or reworked tuff produced from alteration of primary volcanic material after deposition. They primarily formed from the fallout of volcanic tephra ash clouds over the coal swamp. They are generally thin (<10cm) but laterally persistent and homogeneous. On the other hand, sedimentary lutite bands are lenticular and generally darker (eg. carbonaceous mudstone and shale). Other sedimentary intraseam clastic bands include siltstone and fine-grained sandstone. They display some sedimentary structures such as parallel and cross lamination.

Coal Petrology

The petrographic study shows relatively high percentage of mineral matter content (average 20.42% in grainmount samples) (Tables 15A and 15B). This is possibly due to frequent fluvial incursion (eg. crevasse splay deposits and overbank fines). The ash content is high, averaging 22.5% in the Blackstone Formation and 22.8% in the Tivoli Formation (Cook, 1975). Vitrinite is the most dominant maceral group indicating the wet forest type and telmatic zone (average 64.54% in grainmount samples). The relatively high liptinite content (average 6.37% in grainmount samples) is due to the high cutinite content in the coal. It suggests the domination of leafy *Dicroidium* flora in the peat-mire. However, *Dicroidium* leaves and conifers are more resistant to decay, and thus, they may be over-represented in the coal relative to their prominence within the peat swamp. Furthermore, in a subaqueous environment, reeds and non-arborescent vegetation decompose readily which results in a concentration of more resistant waxy leaves and cuticles. Compared to other continental coals the inertinite content in Ipswich coal is low (8.35% in grainmount samples) due to wetter depositional environments. The inertinite macerals were probably produced by occasional fires, seasonal low water level and drying out of peat surface which lead to oxidation. The high preservation of woody or structured macerals suggests that coal is autochthonous and formed in a cool climate with minimal biodegradation. The average percentage of telovitrinite is 34.15% in grainmount samples, whereas detrovitrinite percentage is 30.12% in grainmount samples (see Appendix II, Tables 13 and 14). The high content of telovitrinite, which formed from woody tissues such as stems, branches and roots, indicates forest swamp environment.

The brightness profiles show no obvious trend or significant relationship with respect to stratigraphic sequence. In general, they are highly variable reflecting the dynamic depositional systems within the basin. However,

seventeen brightness profiles, including six highwall profiles and eleven core sample profiles, show small scale oscillating patterns caused by water level fluctuations. The water level in the peat-mire was largely controlled by rates of subsidence and seasonal variations. On the other hand, sixteen 'dulling upward' successions, including six highwall profiles and ten core sample profiles, indicate drying out of the peat-mire due to low water levels and drier seasons. These dulling upward profiles also suggest cyclic patterns of coal sedimentation. Deposition of coal seams was initiated by wetter environments but drier conditions were more dominant in the later part of coal sedimentation (see Appendix I, Drillhole Brightness Profiles). Rates of subsidence in the basin may have been slow at that time. This slow subsidence was followed by abrupt change in rates of subsidence which brought clastic sediments into the peat swamp. High sediment influx produced high mineral matter in the coal. Coal sedimentation eventually ended due to high clastic influx in the peat-mire. In addition, seven brightening upward profiles, including three highwall profiles and four core sample profiles, were recorded. They suggest progressively wetter depositional conditions in parts of the peat swamp during coal sedimentation (see Table 24 for details).

Most coal lithotypes are consistent with micro-petrographic results (eg. bright coals containing the highest vitrinite content and low mineral matter content). On the other hand, liptinite content (mainly cutinite) is the highest in the intermediate coal and second highest in the bright coal. This reflects the source of the vitrinite which was leaves as also noted by Falkner (1986). The high concentration of cutinite in coal is due to waxy and thick leaf cuticles which are resistant to decay and protected the vitrinite they enclosed. The relatively high inertinite content in the intermediate lithotype is probably as a result of inertinite macerals associated with detrovitrinite matrix (Appendix III – Coal Atlas). In addition, the common association of inertinite macerals with liptinite macerals is a characteristic of the Ipswich coals. It suggests that these two maceral groups formed under similar depositional conditions.

Minor inconsistencies such as high vitrinite contents in intermediate lithotypes, found in some polished block samples are possibly caused by following reasons:

- Extreme weathering of exposed coal seams and outcrops.
- Large scale logging of brightness profiles due to difficulties in accessing highwall and outcrop exposures.
- Block samples may not be statistically reliable as shown in maceral analysis.
- Complex internal coal seam architecture due to post-depositional deformation.

- Badly damaged coal faces, outcrops and highwall exposures caused by excavation (eg. blasting and scaling).
- Friable nature of coal which gives brighter appearance.
- Difficulties in sampling and handling friable coal.
- Decrease in lustre due to increase in density caused by high mineral matter contents.
- Homogeneous lithotypes produce brighter appearance due to even light reflection, and
- Heterogeneous lithotypes usually cause duller appearance owing to irregular fracture patterns which give dispersed reflection.

Table 24: Highwall and core sample brightness profile patterns

Figure No.	Brightening Upward	Dulling Upward	Oscillation (no trend)	Comments
Highwall brightness profiles				
Figure 20		Y		Intermediate brightness at bottom, bright middle and dull top
Figure 21			Y	
Figure 22		Y		Figure 22 has 2 profiles
Figure 23			Y	Figure 23 has 3 profiles
Figure 24-1	Y			
Figure 24-2		Y		
Figure 24-3	Y			
Figure 25		Y		Dulling upward sequences
Figure 26		Y		Not obvious but slightly dulling upward
Figure 27			Y	
Figure 28-1			Y	
Figure 28-2		Y		Contains 2 dulling upward sequences
Figure 29			Y	
Figure 30	Y			Figure 30 has 2 profiles
Figure 31			Y	Figure 31 has 3 profiles, numerous claystone bands
Core sample brightness profiles				
Appendix I Figure 1		Y		Generally shows dulling upward pattern
Appendix I Figure 2		Y		Generally shows dulling upward pattern
Appendix I Figure 3	Y			
Appendix I Figure 4	Y			Not obvious, but slightly brighter at top
Appendix I Figure 5			Y	Generally bright
Appendix I Figure 6		Y		
Appendix I Figure 7	Y			Dulling upward bottom unit with bright top unit
Appendix I Figure 8	Y			

Appendix Figure 9	I			Y	
Appendix Figure 10	I			Y	Bright at top and bottom, middle unit is dull and stoney
Appendix Figure 11	I			Y	
Appendix Figure 12	I		Y		
Appendix Figure 13	I		Y		
Appendix Figure 14	I		Y		Contains generally dulling upward successions
Appendix Figure 15	I			Y	
Appendix Figure 16	I		Y		
Appendix Figure 17	I			Y	Very slightly dulling upward, but generally oscillating
Appendix Figure 18	I		Y		
Appendix Figure 19	I			Y	No obvious trend, but bright in the middle
Appendix Figure 20	I			Y	A general oscillating pattern with slightly duller top unit
Appendix Figure 21	I		Y		Generally dulling upward successions
Appendix Figure 22	I		Y		
Appendix Figure 23	I			Y	
Appendix Figure 24	I			Y	
Appendix Figure 25	I	Y			
Appendix Figure 26	I			Y	
Appendix Figure 27	I	Y			Generally brighter top
Appendix Figure 28	I	Y			Generally brighter top

Clay Mineralogy

Chern (1997) stated that clay mineralogy is uniform throughout the coal measures. Kaolinite is the dominant clay mineral and illite is found in illite-smectite mixed layers. The acidic groundwater conditions may have aided the transition from illite to kaolinite. This is indicated by the presence of illite in the kaolinite-rich samples. However, according to Falkner (1986) illite is absent from most kaolinite-rich tonsteins and the presence of illite bearing mudstones adjacent to kaolinite-rich tonsteins does not favour the illite as a source rock of kaolinite. No petrographic evidence showing illite

being altered to kaolinite was observed. The occurrence of similar accessory mineral such as detrital quartz, suggests a common primary source.

The high kaolinite content in Ipswich coals is possibly as a result of the physiochemical alteration of tuffaceous material (Falkner, 1986). Acidic peat swamp conditions would have favoured the formation of kaolinite. Other reasons for kaolinite domination are either because no other clays came with it or they were altered. Furthermore, kaolinite forms the simplest and most stable of the clay mineral structure ($Al_2Si_2O_5(OH)_4$), which is commonly referred to as 1:1 layering. In addition to well crystallised kaolinite, which was formed by authigenic precipitation and/or as metasomatic replacement of other silicate rocks, the amorphous variety allophane is present (Chern, 1997). It occurred as an early precipitate in the still uncompact cell luman of telovitrinite.

Seam Splits

Major seam splitting mechanisms in the Ipswich Basin include differential subsidence, channel avulsion, and lateral channel migration. The channel avulsion is caused by high water discharge and this event rapidly covers the low lying peat surface with a crevasse splay deposit. Whereas, the lateral channel migration is a relatively slow encroachment on part of the peat-mire by a migrating river channel and its associated overbank deposits.

The Blackstone Formation has at least 18 seam splits (Figure 17) revealed by 596 drill holes but the Tivoli Formation has 6 to 10 splits (Figure 14) revealed by 513 drill holes, which suggests there are relatively more splits in the Blackstone Formation (see Appendix IV and V). The Blackstone Formation also appears to contain thicker seams than the Tivoli Formation (excluding the Waterworks seam). However, it may not be true because drilling records indicate that most drill holes did not go through the full sequence of the Tivoli Formation as this formation is deeper. Furthermore, some of the minor seams in the Tivoli Formation may be top or bottom splits of main seams (eg. Unnamed and CL seams). On the other hand, some thick but localised seams may have formed from coalescing of two thin seams (eg. Westfalen Top) (see Tables 20 and 21, and Figures 60, 63, 78, 81, 84, 87, 90, 93, 96, 99 and 102). Therefore, the Tivoli Formation contains thicker splits and more localised combined seams. This indicates higher tectonic activities in the basin during the deposition of Tivoli Formation. On the other hand, higher number of small seam splits found in the Blackstone formation suggests sedimentary seam splitting due to frequent fluvial incursion.

Two types of seam splitting occurred in the Ipswich Coal Measures. Tectonic splitting is as a result of differential subsidence associated with movement of the faults. It is characterised by single well defined epiclastic

wedges with little apparent alteration of the character of the coal plies, indicating rapid and restricted pulses of fluvial sedimentation (Warbrooke and Roach, 1986). Furthermore, the progressive splitting pattern, that is a large number of seam splits formed in the south-central part of the basin around depocentres, was associated with basin subsidence. According to Diessel (1992) tectonic splitting results from a relative increase in subsidence towards the depocentre. The axis of seam split marks a boundary between areas of different subsidence rates or different subsidence to sedimentation ratios. The differential subsidence may produce different zones to accommodate sedimentation. This usually produces seam splitting. The thicknesses of both split and main seams are maximum near the split axes, where subsidence, compaction and accretion rates are balanced. However, in the split zone, peat accretion associated with wetter conditions can only keep pace with subsidence rates and thus, produces thinner seams.

Sedimentary splitting or autosedimentational seam splitting, on the other hand, is the result of epiclastic material deposited in the coal swamp by long term fluvial processes active throughout seam deposition. These processes include avulsion, rapid covering of crevasse splay deposit in a low lying peat surface, and lateral channel migration. The temporary spread of lacustrine conditions across the basin may also produce seam splitting (Diessel, 1992). Repeated flooding of the coal swamp may result in intercalation of coal and clastic sediments and distinct changes in the nature of coal plies. This is indicated by a decrease in thickness of coal towards the split axis and in the split zone. The low cation levels and low pH level in sedimentary environments favour kaolinite formation. Chern (1996), in his study of the Blackstone Formation, performed X-ray diffraction analysis (XRD) on fifty-six clay and clay fractions of sandstone and siltstone samples. Most samples were collected from intraseam lutite bands, but several samples came from roof and floor of coal seams. All samples consistently show the presence of kaolinite. Bustin et al. (1983) referring to Berner (1971) stated "...fresh water swamps, with their low pH, tend to favour in situ alteration of smectite, illite and mixed layer clays to kaolinite". In general, illite is dominant in coals with marine influence, whereas kaolinite is dominant in non-marine coals. In the earlier stage of the basin development, the Ipswich Basin was a rapidly subsiding, poorly drained intermontane basin (Day et al., 1975). Then a better drainage system evolved as the basin filled, and muddy and sandy sediments were laid down by a meandering channel system. Most seam splits in the Tivoli Formation may have occurred as a result of rapid differential subsidence, especially where organic matter is greater than 10% of the total thickness of the sedimentary unit. They appear to have completely separated from the main seams and formed as individual seams. Whereas, seam splitting in the Blackstone Formation was largely due to frequent fluvial incursion. The common mudstone, siltstone and sandstone lamination in the coal was produced by channel migration and avulsion. More seam splitting in the

Blackstone Formation may have occurred due to active high-energy fluvial systems adjacent to coal swamp. However, seam split maps (see '**Seam Split Maps**' in '**Seam Contour Maps and Seam Split Maps**' section) show a progressive seam splitting pattern or seam splits formed in overlapping manner in and around depocentres of coal accumulation. This reflects that overall seam splitting is largely controlled by tectonic subsidence. In a rapidly subsiding basin, there is a little lateral facies shifting with time, and vertical stacking of facies is more common. In addition, coal seams formed in a rapidly subsiding basin are laterally discontinuous, contain more splays as a result of flooding and change facies over relatively short distances (Bustin et al., 1983). The complex coal seam architecture and impersistent nature of coal seams found in the Ipswich Coal Measures may have resulted from tectonism as well as fluvial influence, periodic volcanism and to the ratio of peat to clastic sediments.

Major seam splitting occurred probably due to subsidence (see split maps). However, common seam splitting is associated with minor sedimentary splits (see Appendix IV – Borehole Correlation, and Appendix V – Large Cross-sections).

CONCLUSIONS

Patterns of coal sedimentation in the Ipswich Basin were mainly controlled by tectonic subsidence which roughly conformed to the basement fault systems that shaped the basin configuration. Sediment compaction plays a significant role in terms of sediment distribution in the basin. Thick but aerially restricted coal seams were produced by fault-controlled rapid subsidence. The occasional peat-mire expansion was probably due to tectonically quiet and stable depositional conditions. The accumulation of organic matter in the peat-mire was interrupted periodically by the introduction of fine clastic sediments during floods. This produced the high mineral matter content in coal. Two types of peat-mire expansion have been noted. They occurred in different stages of peat formation and were largely controlled by changing depositional environments. The lateral expansion, or peat-mire progradation, which was associated with widespread coal accumulation, and vertical expansion, or peat-mire aggradation, which occurred as a result of tectonic subsidence and produced thick but aerially limited coal seams. The former type of peat formation may be related to paludification, while latter type is largely due to terrestrialisation.

The complex stratigraphy and higher components of brighter lithotypes in the Ipswich coal compared with other Australian Triassic coals suggest that peat was formed in a relatively wet depositional environment and dominated by active fluvial systems. Periodic volcanism, acid peat conditions, and rapid subsidence and burial may have also contributed to preserving peat and producing bright coal. Moderate groundwater level and cool to

temperate climatic conditions preserve structured or woody macerals such as telovitrinite and semifusinite. The abundant structured macerals such as vitrinite, fusinite and semifusinite in the coal also suggests autochthonous origin. Peat-mire may have risen above the ground surface (ie. peat-mire aggradation), which formed the limnetic forest swamp environment. This may have prevented the formation of allochthonous macerals. The high cutinite contents in the coal indicate that peat-mire vegetation was dominated by the leafy *Dicroidium* flora and pteridosperm (seed ferns) which characterize the Yabeiella Opel-zone.

The complex coal seam architecture is possibly related to high subsidence, volcanism and post-depositional deformation such as folding, faulting and shearing. Major seam splitting occurred mainly due to tectonism. However, minor partings and repetition of lithotype sequences were produced by repeated flooding, channel avulsion and lateral stacking of channel fill sequences. Correlation of coal seams was hindered by seam discontinuities and deformation. Coal seams coalesce and split in various combinations, suggesting the high tectonic and fluvial activity in the basin during the time of coal formation.

The global tectonic events during the Late Triassic Epoch produced similar patterns of basin development in eastern Australia. The little variation in climate and peat-mire vegetation between Ipswich, Tarong and Callide Basins would have had minor effect on coal characteristics. The climatic conditions of all these basins were cool to temperate with drier conditions except in the Ipswich Basin where wetter conditions prevailed. The differences in coal facies types appear to be related to unique events such as local tectonism and volcanism which created a variety of tectonic settings and depositional environments within the basin. The relative standing water level and sediment supply in the basin were determined by tectonic movements. The flexural subsidence and uplift associated with fault movements created change in sedimentological equilibrium profile and this produced different styles of sedimentary packing and distribution.

Furthermore, the movement of depocentres was controlled by compression and tectonic movements such as folding, faulting, subsidence and uplift. Formation of depocentres within the basin generally conformed to the basin configuration, which was shaped by major fault systems. In addition, when accommodation was reduced by sediment fill the depocentre moved to another more suitable area. This created the depocentres juxtaposing in the basin.

To sum up, the sedimentation patterns and coal characteristics in the intermontane Ipswich Basin is different to other coal basins firstly because of its geographic location in high latitude and cooler climatic conditions and the age, and secondly because of tectonic conditions and volcanism.

References

Allen, G. P., 1995, Facies Analysis and Identification of Depositional Environments in Fluvial, Coastal and Deltaic Settings, Queensland University of Technology Press.

Allen, G. P., et al., 1996, Application of Sequence Stratigraphy to Continental Successions: Implications for Mesozoic Cratonic Interior Basins of Eastern Australia, *In: Mesozoic 96*, Geological Society of Australia Inc. (Queensland Division), Extended Abstract No. 43, pp 22 – 26.

Allen, R. J., 1955, The Kholo Stage of the Ipswich Coal Measures, Honours Thesis, Unpublished, University of Queensland.

Allen, R. J., 1972, Petroleum Stratigraphic Core-drilling on the Ipswich 1:150,000 Sheet Area, 1968 – 71, Queensland Government Mining Journal, pp 453 – 456.

Allen, R. J., Staines, H. R. E. and Wilson, E. G., 1960, The Ipswich Basin, *In: The Geology of Queensland*, Hill, D. and Denmead, A. K. (editors), Journal of the Geological Society of Australia, Melbourne University Press, pp 252 – 262.

Almond, C. S., 1982, Stratigraphic Drilling Report – GSQ Ipswich 26, Queensland Government Mining Journal, November 1982, pp 514 – 523.

AS2519-1993, Guide to the Technical Evaluation of Higher Rank Coal Deposits, Australian Standard, Standards Association of Australia.

Beeston, J. W., 1987, Aspects of Inertinite Formation and Deposition in the Denison Trough, Queensland, Australian Coal Geology 7, pp 33 – 45.

Berner, R. A., 1971, Principles of Chemical Sedimentology, Mc Graw Hill, Toronto, Canada, 240pp.

Bowern, R., 1987, Authority to Prospect 427C - Redbank, exploration progress report and evaluation of detailed coal quality data, Queensland Geological Services for Westfalen Colliery Pty Ltd, Unpublished Company Report.

Boyd, R., et al., 1996, Terrestrial sediment response to changes in accommodation, *In: Geological Society of Australia, Abstract No. 41*, Australia.

Busby, C. J. and Ingersoll, R. V., 1995, Tectonics of Sedimentary Basins, Blackwell Science, Massachusetts, U.S.A.

Bustin, R. M., et al., 1983, Coal Petrology – Its Principles, Methods, and Applications, Short Course Notes Volume 3, Victoria 1983, Geological Association of Canada.

Calder, J. H., Gibbing, M. R., Mukhopadhyay, P. K., 1991, Peat formation in a westphalian B piedmont setting, Cumberland Basin, Nova Scotia: Implication for the maceral-based interpretation of rheotrophic and raised paleomires, Bulletin Society Geology France, 162, pp 283 – 298.

Cameron, J. B., 1969, Coal resources – West Moreton (Ipswich) coalfield, Rylance Abermain Nos 1 and 2 mine areas, Supplementary drilling, Haighmoor Extended mine area, Geological Survey of Queensland, Report 30, pp 1 – 8.

Cameron, W. E., 1906, Second Report on the West Moreton (Ipswich) Coalfield, with special reference to the Bundamba district, Publication of the Geological Survey of Queensland 204, pp 1 – 37.

Cameron, W. E., 1923, Geological Map of Ipswich and Bundamba Coalfield, Publication of the Geological Survey of Queensland 271.

Carr, A. F., 1966a, Coal resources – West Moreton (Ipswich) coalfield, Supplementary drilling P.D.T.S. No. 1, 2, and 3 mine areas Swanbank Lagoon, Geological Survey of Queensland, Report 13.

Carr, A. F., 1966b, Coal resources – West Moreton (Ipswich) coalfield, Supplementary drilling Edward S. Cornwall mine area, Geological Survey of Queensland, Report 15.

Carr, A. F., 1969, Coal resources, West Moreton (Ipswich) coalfield, Supplementary drilling Rhondda – Eastern extension, Geological Survey of Queensland, Report 25, pp 11 – 18.

Carr, A. F., 1970, Coal resources, West Moreton (Ipswich) coalfield, Ripley Road South area, Geological Survey of Queensland, Report 45.

Carr, A. F., 1972, Coal resources, West Moreton (Ipswich) coalfield, Blackstone area, Geological Survey of Queensland, Report 66.

Carr, A. F., 1977, Coal resources, West Moreton (Ipswich) coalfield, Redbank – Goodna area, Geological Survey of Queensland, Record 1977/14.

Chern, P. K., 1997, Coal Geology of the Blackstone Formation, Ipswich Coal Measures, Southeast Queensland, Honours thesis, Unpublished, Department of Natural Resource Sciences, Queensland University of Technology.

Cohen, A. D., 1973, Petrology of some Holocene peat sediments from the Okefenokee swamp-marsh complex of southern Georgia, Geological Society of America Bulletin 84, pp 3867 – 3878.

Cook, A. C., 1975 (editor), Australian Black Coal: Its occurrence, mining, preparation and use, Australasian Institute of Mining and Metallurgy (Illawarra Branch), New South Wales.

Coxhead, B. A., 2001, Queensland Coals (physical and chemical properties, colliery and company information), 13th edition, Natural Resources and Mines, Queensland Government.

Cranfield, L. C., Schwarzbock H. and Day, R. W., 1976, Geology of the Ipswich and Brisbane 1:250,000 Sheet Areas, Geological Survey of Queensland, Report 95.

Cranfield, L. C., 1981a, Stratigraphic Drilling Report – GSQ Ipswich 24 and 25, Queensland Government Mining Journal, October 1981, pp 468 – 487.

Cranfield, L. C., 1981b, The Ipswich Coalfield, *In: 1981 Field conference, Brisbane-Ipswich area*, Geological Society of Australia (Queensland Division).

Cranfield, L. C. and Green, P. M., 1983, Record Series (Record 1983/42), Compilation of Formation Intersections in Departmental Coal Exploration Bores (N. S. Series) in the Ipswich Coalfield, Queensland Department of Mines.

Cranfield, L. C., 1984, Stratigraphic Drilling Data – Ipswich, Brisbane and Gympie 1:250,000 Sheet Areas, 1972 to 1976, Geological Survey of Queensland, Record 1984/03.

Cranfield, L. C., Hutton, L. J. and Green, P. M., 1989, Ipswich (Sheet 9442) – Queensland, 1:100,000 Geological Map Commentary, 56p, Queensland Department of Mines, Queensland Minerals and Energy Centre, Brisbane.

Day, R. W., Cranfield, L.C. and Schwarzbock, H., 1974, Stratigraphy and structural setting of Mesozoic basins in southeastern Queensland and northeastern New South Wales, *In: The Tasman Geosyncline - A Symposium*, A.K. Denmead, G.W. Tweedale and A.F. Wilson (Editors), Geological Society of Australia, Queensland.

Day, R. W., et al., 1975, Queensland Geology: A companion volume to the 1:2,500,000 scale geological map, Geological Survey of Queensland, Publication 383.

De Jersey, N. J., 1964, Triassic spores and pollen grains from the Bundamba Group, Geological Survey of Queensland, Publication 321, 21p.

De Jersey, N. J., 1970, Triassic miospores from the Blackstone Formation, Aberdare Conglomerate and Raceview Formation, Geological Survey of Queensland, Publication 348, Palaeontological Papers No. 22.

De Jersey, N. J., 1975, Miospore Zones in the Lower Mesozoic of Southern Queensland, *In: Gondwana Geology (papers presented at the third Gondwana Symposium, Canberra, Australia, 1973)*, K. S. W. Campbell (Editor), Australian National University Press, Canberra, pp 159 – 172.

Denmead, A. K., 1954, Some Notes on Depositional Environment in the Ipswich Coal Basin, Unpublished address to A.N.K.A.A.S (?). Section C, Canberra 1954.

Denmead, A. K., 1955a, The West Moreton (Ipswich) Coalfield, Geological Survey of Queensland, Publication 279.

Denmead, A. K., 1955b, Coal Resources, West Moreton (Ipswich) Coalfield, Part 1, P.D.T.S. Nos 1, 2, and 3 mine areas, Swanbank Lagoon, Part 2, P.D.T.S. Nos. 7 and 8 mine areas, Bundamba, Geological Survey of Queensland, Publication 280.

Department of Mines and Energy - Queensland, South East Queensland Digital Maps in MapInfo™ and Corel Draw™ Formats.

Diessel, C. F. K., 1982, An appraisal of coal facies based on maceral characteristics, *In: Coal resources – origin, exploration and utilization in Australia*, Mallett, C. W. (editor), Australian Coal Geology, pp 474 – 484.

Diessel, C. F. K., 1984, Coal Geology, Workshop Course 282/84, Part 1 and 2, New Zealand, 17th – 23rd May 1984, Revised January 1985, Australian Mineral Foundation.

Diessel, C. F. K., 1986, The correlation between coal facies and depositional environments, *In: Advances in the Study of the Sydney Basin, Proceedings 20th Symposium*, University of Newcastle, pp 19 – 22.

Diessel, C. F. K., 1992, Coal Bearing Depositional Systems, Springer-Verlag, Germany.

ESSO Coal Australia Inc., 1974, Relinquishment Report of Authority to Prospect 131C Warrill Creek, Moreton Basin, Queensland, Company Report CR4789 (A and B).

Falcon, R. M. S. and Snyman, C. P., 1986, An introduction to coal petrography: Atlas of petrographic constituents in the bituminous coals of South Africa, Review Paper No. 2, February 1986, Geological Society of South Africa, Johannesburg, 27p.

Falkner, A. J., 1986, Sedimentology of the Blackstone Formation, Ipswich Coal Measures, Southeast Queensland, PhD thesis, Unpublished, Department of Geology and Mineralogy, University of Queensland.

Faure, K., et al., 1994, Late Permian global coal discontinuity and Permian – Triassic boundary events, *In: Geological Society of Australia, Abstracts No. 37*, 12th Australian Geological Convention, Perth.

Forsyth, S. M., 1989, Upper Parmeener Supergroup, *In: Geology and mineral resources of Tasmania*, C.F. Burrett and E.L. Martin (Editors), Geological Society of Australia, Special Publication 15, pp 309-334.

Galligan, A. G., 1979, The stratigraphy, exploration, and development of coal deposits in Queensland, Queensland Government Mining Journal, December 1979, pp 619-625.

Galloway, W. E. and Hobday, D. K., 1983, Terrigenous Clastic Depositional Systems: Application to Petroleum, Coal and Uranium Exploration, Springer-Verlag, New York.

GeoScape™, Scanned Aerial Photography, Regional Southeast Queensland, 1997 Version, Department of Natural Resources, Queensland Government.

Gould, R. and Shibaoka, M., 1980, Some Aspects of the Formation and Petrographic Features of Coal Members in Australia, with special reference to the Tasman Orogenic Zone, *In: Coal Geology*, Journal of the Coal Geology Group of the Geological Society of Australia, Volume 2, 1980, Part 1, pp 1 – 29.

Gray, A. R. G., 1975, Bundamba Group – Stratigraphic Relationships and Petroleum Prospects, Queensland Government Mining Journal, September 1975, pp 310 – 324.

Hacquebard, P. A., et al., 1964, Die Ablagerungsbedingungen des Fluzes Harbour im Sydney – Kohlengebiet von Neuschottland (Kanada), Fortschr Geol Rheinld Westf 12:331 – 356.

Hacquebard, P. A., Birmingham, T. F. and Donaldson, J. R., 1967, Petrography of Canadian Coals in Relation to Environment of Deposition, Symposium on the Science and Technology of Coal, Ottawa 1967, Published by the Department of Energy, Mines and Resources, pp 84 – 97.

Hallam, A., 1985, A review of Mesozoic climates, Journal of the Geological Society of London, v 142, pp 433-445.

Haselwood, R. F., 2002, The Hydrocarbon Potential of the Lockrose to Tamrookum Section of the Clarence – Moreton Basin, Southeastern Queensland, Master Thesis, Unpublished, Queensland University of Technology.

Hawkins, P. J., 1975, Appendix – Petrologic Analysis of Selected Core Samples from NS 272 and GSQ Ipswich 18, Queensland Government Mining Journal, September 1975, pp 325 – 328.

Houston, B. R., 1965, Triassic Volcanics from the Base of the Ipswich Coal Measures, Southeast Queensland, Geological Survey of Queensland, Publication 327.

Hunt, J. W., Brakel, A. T. and Smyth, M., 1986, Origin and distribution of the Bayswater Seam and its correlatives in the Permian Sydney and Gunnedah Basins, Australia, Australian Coal Geology, 6, pp 59 – 75.

Jones, O. A. and de Jersey, N. J., 1947, The flora of the Ipswich Coal Measures - morphology and floral succession, University of Queensland, Department of Geology Papers 3 (3), pp 1 - 88, plates 1 – 10.

Kailasham, L. N., 1976, Geophysical studies of the major sedimentary basin of the Indian Craton, their deep structural features and evolution, Tectonophysics, v 36, pp 225-245.

Kalkreuth, W. D., et al., 1991, The relationship between coal petrography and depositional environments from selected coal basins in Canada, International Journal of Coal Geology, 19 (1991), pp 21 – 76.

Karmasin, K. von, 1952, Deutung des Fazieswechsels in den Flözen Erda und Ägir auf Grund mikropetrographischer schlitzprobenuntersuchungen, Bergbau-Archiv 13, pp 74 – 100.

Kent, P. R., 1995, Coal Geology of the Walloon Coal Measures at Ebenezer Coal Mine, Southeast Queensland, Unpublished, Honours Thesis, Queensland University of Technology.

Lamberson, M. N., Bustin, R. M. and Kalkreuth, W., 1991, Lithotype (maceral) composition and variation as correlated with paleo-wetland environments, Gates Formation, Northeastern British Columbia, Canada, International Journal of Coal Geology, 18 (1991), pp 87 – 124.

Lyons, P. C., 2000, Funginite and Secretinite – two new macerals of the inertinite maceral group, International Journal of Coal Geology 44, pp 95 – 98.

McCabe, P. J., 1984, Depositional environments of coal and coal-bearing strata, *In*: Rahmani, R. A. and Flores, R. M. (editors), Sedimentology of coal and coal-bearing sequences, International Association of Sedimentologists, Special Publication 7, pp 13 – 42.

McElroy, C. T., 1962, The Geology of the Clarence-Moreton Basin, Geological Survey of New South Wales, Memoir 9.

McElroy, C. T., 1969a, Narrabeen Group sedimentation, *In: The Geology of New South Wales*, G.H. Packham (Editor), Journal of the Geological Society of Australia, 16, pp 439-443.

McElroy, C. T., 1969b, The Clarence-Moreton Basin in New South Wales, *In: The Geology of New South Wales*, G.H. Packham (Editor), Journal of the Geological Society of Australia, 16, pp 457-479.

Mackowsky, M-Th, 1953, Problems der Inkohlung, Brennstoff-Chemie, 34, pp 182 – 185.

Mengel, D. C., 1963a, Coal resources – West Moreton (Ipswich) coalfield, Supplementary drilling – Haighmoor mine area, Queensland Government Mining Journal, 64, pp 82 – 87.

Mengel, D. C., 1963b, Coal resources – West Moreton (Ipswich) coalfield, Scout drilling, Waterworks seam, North Ipswich, Queensland Government Mining Journal, 64, pp 291 – 298.

Mengel, D. C., 1975, Ipswich Coal Field, Queensland, *In: Economic Geology of Australia and Papua New Guinea, 2 Coal*, Traves, D. M. and King, D. (editors), Knight, C. L. (chief editor), The Australasian Institute of Mining and Metallurgy Monograph Series No. 6.

Mengel, D. C. and Carr, A. F., 1969, West – Moreton (Ipswich) coalfield, A correlation of coal seams and a revision of nomenclature in the Blackstone Formation, Geological Survey of Queensland, Report 36.

Mengel, D. C., 1970a, Coal resources – West Moreton (Ipswich) coalfield, Supplementary report, Southern Cross No. 9 mine area, Geological Survey of Queensland, Report 37.

Mengel, D. C., 1970b, Coal resources – West Moreton (Ipswich) coalfield, Supplementary report, Westfalen No. 2 mine area, Geological Survey of Queensland, Report 39.

Mengel, D. C. and Carr, A. F., 1972, Coal resources – West Moreton (Ipswich) coalfield, New Hope No. 5 mine area, Geological Survey of Queensland, Report 48.

Mengel, D. C. and Carr, A. F., 1976, Ipswich Coalfield, Queensland Department of Mines, Geological Survey of Queensland Report No. 94.

Miller, http://www.geo.utep.edu/class_notes/3102_Miller/Lectures/Lecture_20.html, Geology of the Mesozoic Era, Undated, Accessed 21/2/99, 4p.

Moore, T. A. and Shearer, J. C., 2003, Peat/coal type and depositional environment – are they related?, *In: International Journal of Coal Geology*, 56, pp 233 – 252.

New Hope Mines Ltd, Borehole Data and Digital Maps of Swanbank Mining Area.

Osvald, H., 1937, Myrar och Myrodling (Peatlands and their cultivation), Kooperative Förbundels Bikflörlag, Stockholm, Sweden.

Parrish, J. T., Zeigler, A. M. and Scotese, C. R., 1982, Rainfall patterns and the distribution of coals and evaporites in the Mesozoic Cenozoic, *Palaeogeography Palaeoclimate Palaeoecology* 40, pp 67 – 101.

Plumstead, E. P., 1966, The Story of South Africa's Coal, Optima, pp 187 – 202.

Queensland Department of Mines and Energy, Southeast Queensland Digital Map, Gravity and Magnetic Maps, and NS-series Drillhole Records.

Queensland Geological Services Pty Ltd, Confidential Company Reports.

Russeit, T. G., 1986, A Review of the Geology and Hydrocarbon Potential of Authority to Prospect 266P, Moreton, Ipswich and Esk Basins, Bligh Oil and Mineral N. L., Company Report, Unpublished.

Retallack, G. J., 1977a, Triassic palaeosols in the Upper Narrabeen Group of New South Wales, Part II: Classification and Reconstruction, *Journal of the Geological Society of Australia*, v 24, March 1977, pp 19 – 36.

Retallack, G. J., 1980, Late Carboniferous to Middle Triassic Megafossil Floras from the Sydney Basin, *In: A Guide to the Sydney Basin*, Chris, H. and Helby, R. (editors), Department of Mineral Resources, Geological Survey of New South Wales, Bulletin 26.

Retallack, G. J., 1997, Palaeosols in the upper Narrabeen Group of New South Wales as evidence of Early Triassic palaeoenvironments without exact modern analogues, *Australian Journal of Earth Sciences*, v 44, No. 2, Geological Society of Australia, pp 185 – 201.

Retallack, G. J., 1996, greg_retallack@ccmail.uoregon.edu, Recent research interests, <http://darkwing.uoregon.edu/~dogsci/retall/oldrsch.html>, 18/6/96, Accessed 21/2/99, 2p.

Read, J., 1997, Fossils in coal deposits at Callide mine and Ipswich, ESB602 QUT undergraduate project, Unpublished.

Rigby, J., 2004, personal communication, QUT research fellow.

Robinson, P. L., 1973, Palaeoclimate and continental drift, *In: Implications of continental drift to the earth sciences*, D. H. Tarling and S. K. Runcorn (Editors), v 1, Academic Press, London, pp 449 – 476.

Ryer, T. A. and Langer, A. W., 1980, Thickness changes involved in the peat to coal transformation for a bituminous coal of Cretaceous age in central Utah, *Journal of Sedimentary Petrology* 50, pp 987 – 992.

Saunders, B. J., 1983, Report to Biddleminster Pty Ltd on geological investigations ATP 392C - Redbank, for Westfalen Colliery Pty Ltd, Unpublished Company Report, Queensland Geological Services Pty Ltd.

Scott, A. C., 2002, Coal petrology and the origin of coal macerals: a way ahead, *International Journal of Coal Geology* 996 (2002) (article in press), 16p, Elsevier Science.

Scott, P. T., 1982, The Geology of the Evans Head – Balline Region, Master Thesis, Unpublished, Department of Geology and Geophysics, University of New England.

Smyth, M., 1979, Hydrocarbon Generation in the Fly-Lake-Brolga Area of the Cooper Basin, *Journal of Petroleum Exploration Association* 19, pp 108 – 114.

Smyth, M., 1980, Coal encounters of the third kind: Triassic, *Australian Coal Geology* 2, pp 161 – 178.

Smyth, M., 1984, Coal microlithotypes related to sedimentary environments in the Cooper Basin, Australia, *In: Sedimentology of coal and coal-bearing sequences*, Special Publication of the International Association of Sedimentologists No. 7, R. A. Rahmani and R. M. Flores (Editors), Blackwell Scientific Publications, Oxford, pp 333 – 348.

Smyth, M. and Mastalerz, M., 1991, Organic petrological composition of Triassic source rocks and their clastic depositional environments in some Australian sedimentary basins, *International Journal of Coal Geology*, 18 (1991), pp 165 – 186.

Stach, E., et al., 1975, Stach's Textbook of Coal Petrology, 3rd Revised and Enlarged Edition, Gebruder Borntraeger Stuttgart.

Smyth, M., 1989, Organic petrology and clastic depositional environments with special reference to Australian coal basins, *International Journal of Coal Geology*, 12 (1989), pp 635 – 656.

Staines, H. R. E., 1961, Coal resources – West Moreton (Ipswich) coalfield, Part 14, P.D.T.S. Nos. 11, 12, and 14 mine areas, Rhondda, Geological Survey of Queensland, Publication 298.

Staines, H. R. E., 1964, Coal resources – West Moreton (Ipswich) coalfield, Part 17, Rylance Abermain No. 2 and No. 1 mine areas, Geological Survey of Queensland, Report No. 5.

Staines, H. R. E., 1967, Coal resources – West Moreton (Ipswich) coalfield, Part 18, Silkstone area, Geological Survey of Queensland, Report 16.

Staines, H. R. E., 1969, Coal resources – West Moreton (Ipswich) coalfield, Ripley Road north area, Geological Survey of Queensland, Report 27.

Staines, H. R. E., Falkner, A. J. and Thornton, M. P., 1995, Ipswich Coalfield, *In: Geology of Australian Coal Basins*, C. R. Ward, et. al. (Editors), Geological Society of Australia Inc., Coal Geology Group, Special Publication No. 1, pp 455 – 464.

Taylor, G. H., Liu, S. Y. and Diessel, C. F. K., 1989, The cold climate origin of inertinite-rich Gondwana coals, *International Journal of Coal Geology* 11, pp 1 – 22.

Teichmüller, M., 1962, Die Genese der Kohle, C. R. 4 Congr. Internat. Geol. Carbon., 3, pp 699 – 722.

Teichmüller, M., 1989, The genesis of coal from the viewpoint of coal petrology, *In: Peat and coal: origin, facies, and depositional models*, P. C. Lyons and B. Alpern (Editors), *International Journal of Coal Geology*, 12 (1989), pp 1 – 87.

Ties, P., Shaw, R. D. and Geary, G. C., 1985, The petroleum prospectivity of the Clarence-Moreton Basin in New South Wales, *Australian Petroleum Exploration Association Journal*, 25 (1), pp 15-33.

Tucker, A. H., 1949, First Report on the Coal Industry of Queensland, Powell Duffryn Technical Services Limited (Volumes I, II and III), Queensland Premier and Chief Secretary's Department, Brisbane, Government Printer.

Veevers, J. J., Conaghan, P. J. and Powell, C. McA., 1994, Eastern Australia, *In: Permian-Triassic Pangean Basins and Foldbelts along the Panthalassan Margin of Gondwanaland*, J. J. Veevers and C. McA. Powell (Editors), Memoir 184, Geological Society of America, Colorado, U.S.A.

Warbrooke, P. R. and Roach, M. J., 1986, The Relationship between Seam Splitting, Coal Formation Environments and Coal Properties in the Newcastle Coal Measures, *In: Advances in the Study of the Sydney Basin*, Proceedings of the Twentieth Symposium, Newcastle Symposium, Department of Geology, University of Newcastle.

Ward, C. W., 1980, Why Tasmanian Coal?, Abstract of paper in coal geology sessions, Symposium on geology of north-eastern Tasmania, Launceston, Tasmania, 8 – 9, November 1980, *In: Coal Geology, Journal of the Coal Geology Group of the Geological Society of Australia*, v 2, 1980 Parts 3 and 4, pp 116 – 117.

Ward, C. W., 1984, Coal Geology and Coal Technology, Blackwell Scientific Publications, Victoria, Australia.

Webb, J. A. and McNaughton, N. J., 1978, Isotopic Age of the Sugars Basalt, Queensland Government Mining Journal, 79, pp 591 – 595.

Webb, J. A., 1980, Aspects of the palaeontology of Triassic continental sediments in southeast Queensland, plants and conchostraca, PhD thesis, Unpublished, University of Queensland.

White, M. E., 1990, The nature of hidden worlds, Reed Book Pty Ltd, New South Wales.

Willmott, W. and Stevens, N., 1992, Rocks and Landscape of Brisbane and Ipswich, Geological Society of Australia Inc., Queensland Division.

Wilson, E. G., 1958, The Bundamba Group in the Area Southeast of Ipswich, Honours Thesis, Unpublished, University of Queensland.

Yemane, K., 1993, Contribution of Late Permian palaeogeography in maintaining a temperate climate in Gondwana, Nature, v 361, 7 January 1993, pp 51 – 54.

Ziegler, P. A., 1977, Geology and hydrocarbon provinces of the North Sea, Geological Journal, v 1, pp 7-32.

Ziegler, P. A., 1978, Norht-western Europe: Tectonics and basin development, Geologie en Mijabouw, v 57, pp 589-626.

Ziegler, P. A., 1982, Faulting and graben formation in western and central Europe, Philosophical Transactions of the Royal Society of London, V A305, pp 114-143.

Ziegler, P. A., 1987, Late Cretaceous and Cenozoic intraplate comperssional deformations in the Alpine foreland - a geodynamic model, Tectonophysics, v 137, pp 389-420.

Ziegler, P. A., 1988, Evolution of the Arctic-North Atlantic and the western Tethys, AAPG Memoirs 43, 198p.

Ziegler, A. M., 1993, Models come in from the cold, Nature, v 361, 7 January 1993, pp 16 – 17.

APPENDICES

Appendix I: Drillhole Brightness Profiles

Appendix II: Tables

Appendix III: Coal Atlas

Appendix IV: Borehole Correlation

**Appendix V: Borehole Location Plan and
Large Cross-sections**

APPENDIX I

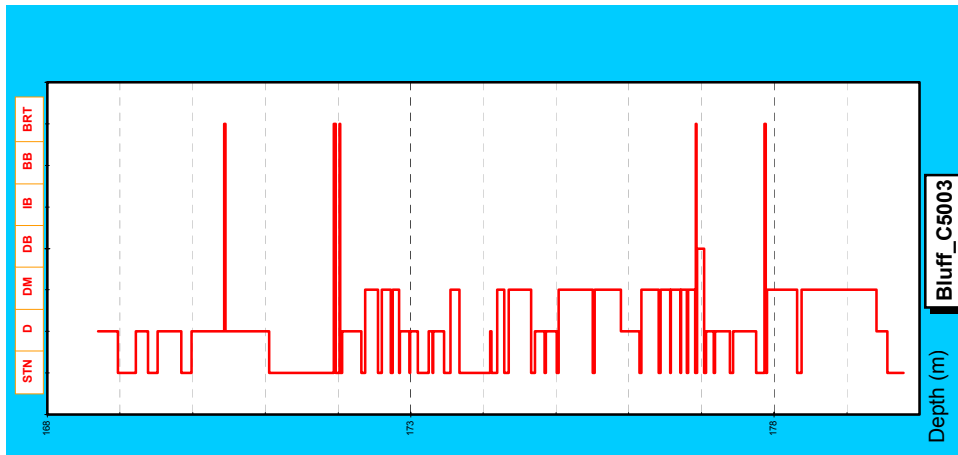
Drillhole Brightness Profiles

LEGEND

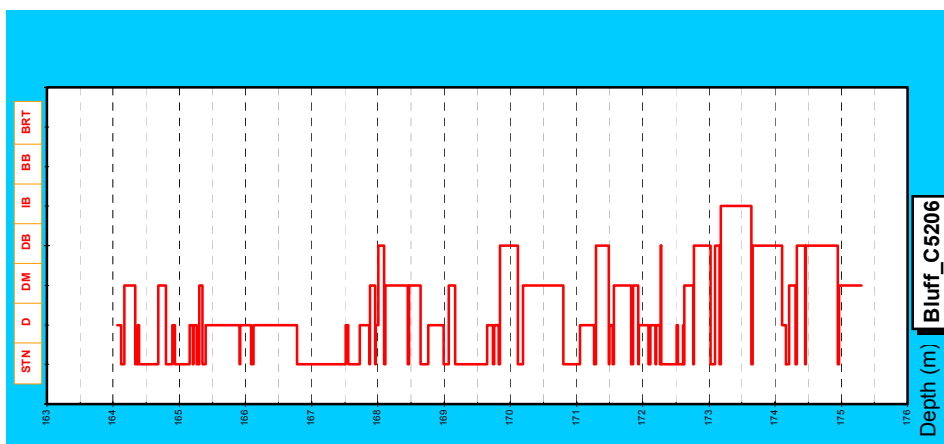
STN = stone band
D = <1% bright
DM = <10% bright
DB = 10 – 40% bright
IB = 40 – 60% bright
BB = 60 – 90% bright
BRT = >90% bright

These brightness profiles and statistical data (Table 5, Page 35) have been generated through an Excel macro written by Fernando Tapia-Vergara from CSIRO (Kenmore). See Figure 19 for brightness profile locations.

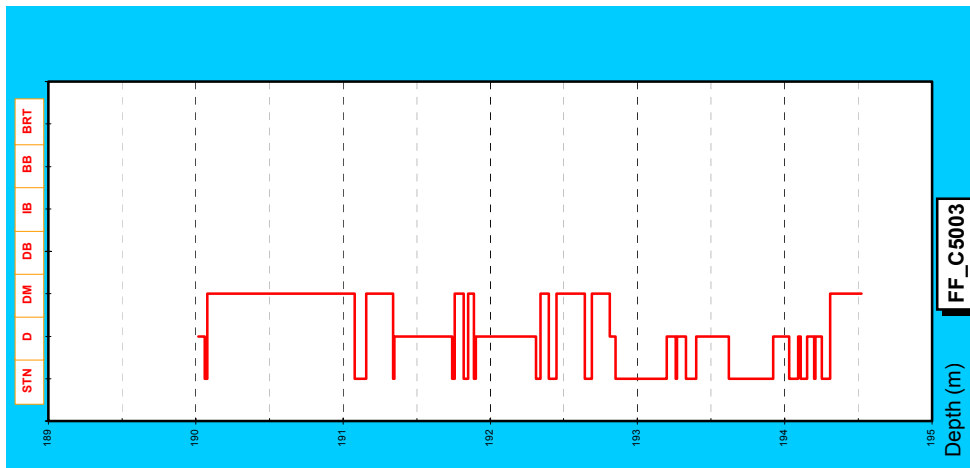
These brightness profiles and statistical data have been generated through an Excel macro written by Fernando Tapia-Vergara from CSIRO (Kenmore).



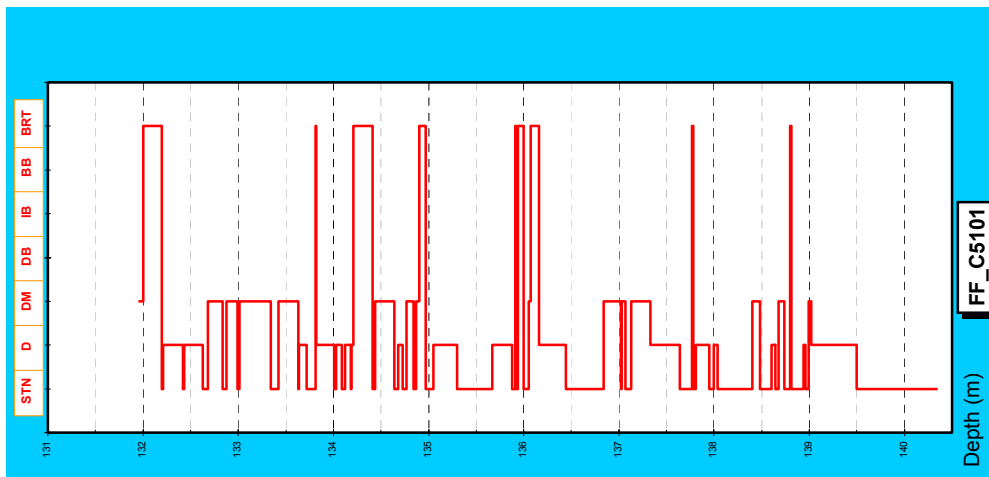
Appendix I - Figure 1: Brightness profile of the Bluff seam showing general dulling upward succession with high percentage of intraseam (STONE) bands, Hole No. C5003



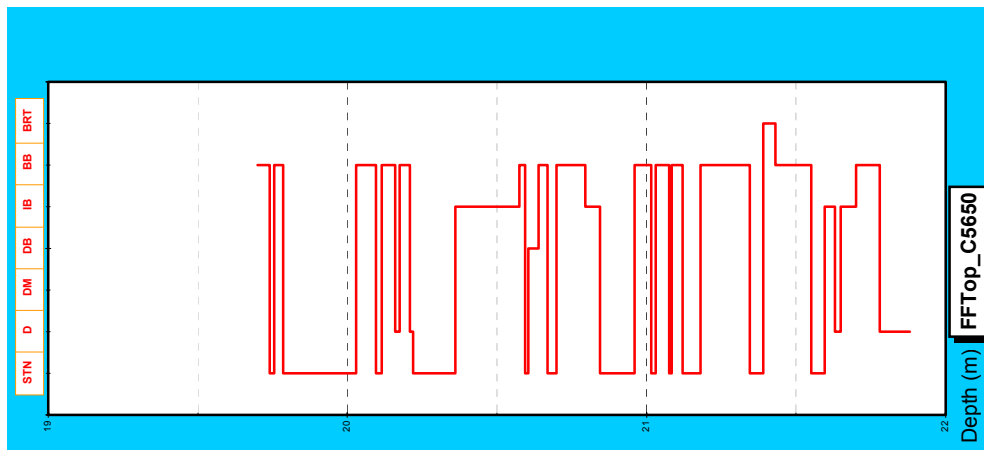
Appendix I - Figure 2: Brightness profile of the Bluff seam showing oscillating patterns but the whole profile is dulling upward, top unit is duller than bottom unit, Hole No. C5206



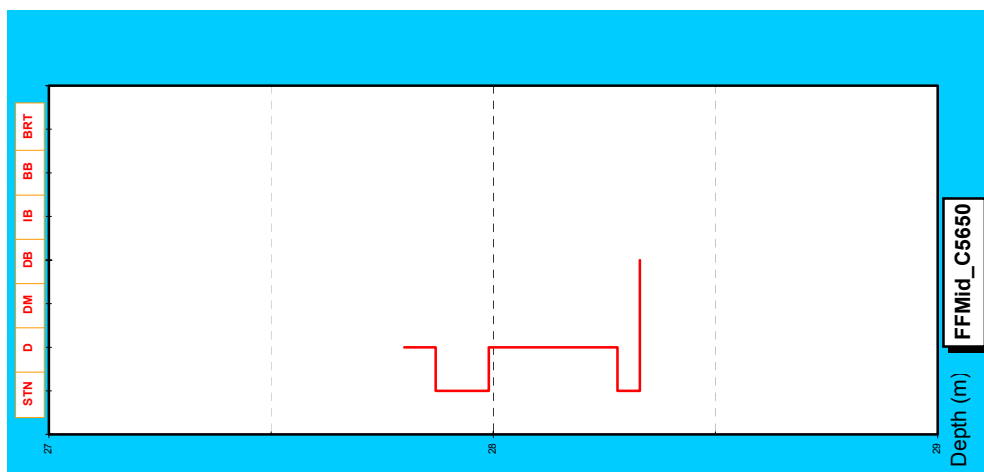
Appendix I - Figure 3: Brightness profile of the Fourfoot seam which is mainly dull but top unit is relatively bright, Hole No. C5003



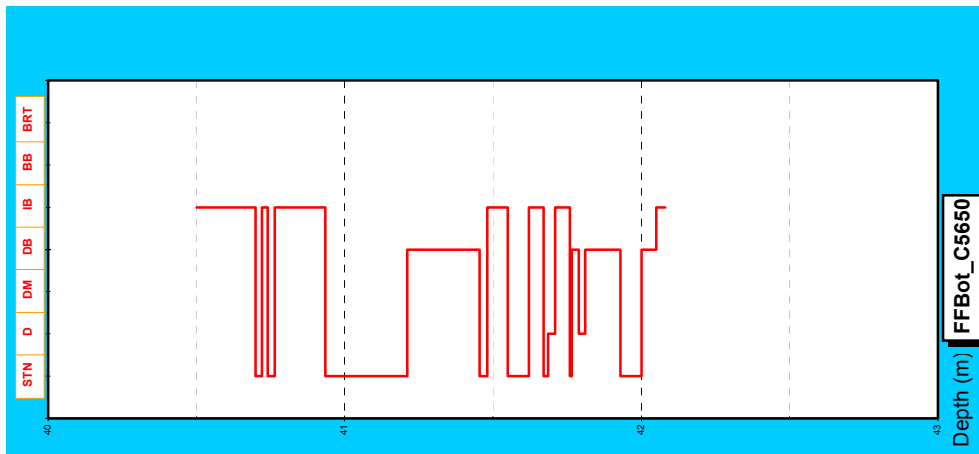
Appendix I - Figure 4: Brightness profile of the Fourfoot seam showing an oscillating pattern, Hole No. C5101



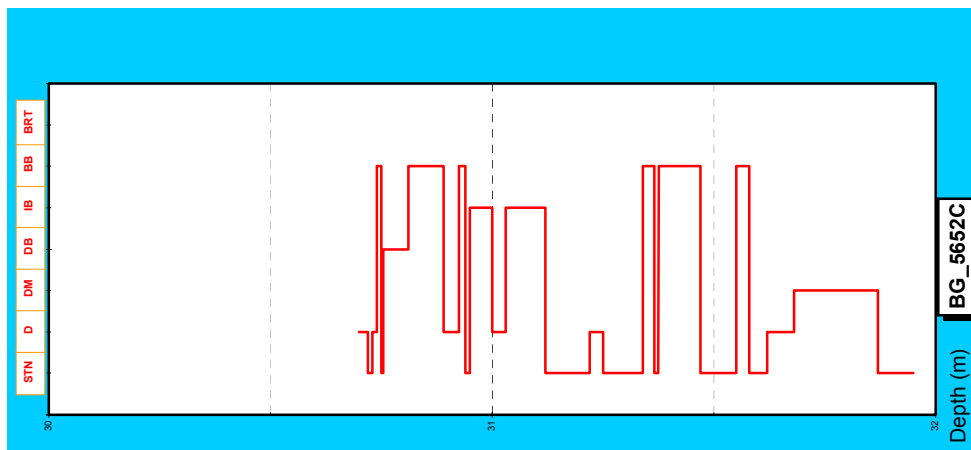
Appendix I - Figure 5: Brightness profile of the Fourfoot Top seam showing numerous (high percentage) bright bands, Hole No. C5650



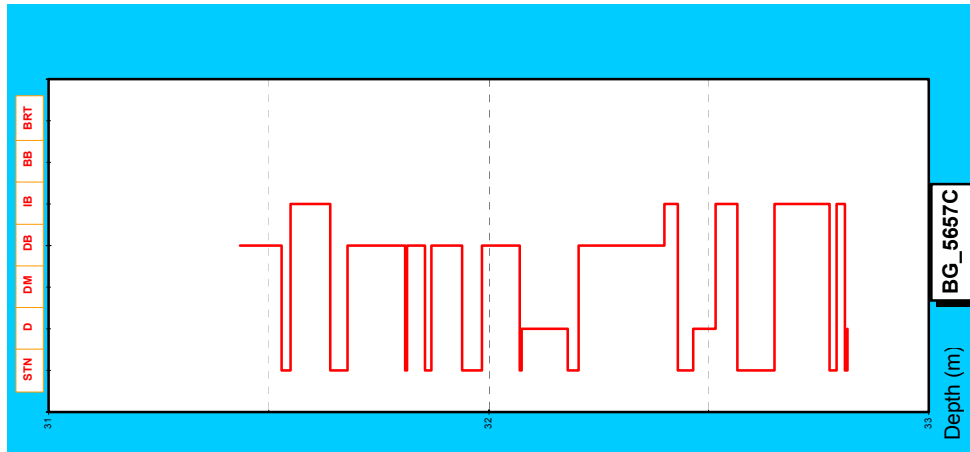
Appendix I - Figure 6: Brightness profile of the Fourfoot Middle seam showing dulling upward succession (very thin), Hole No. C5650



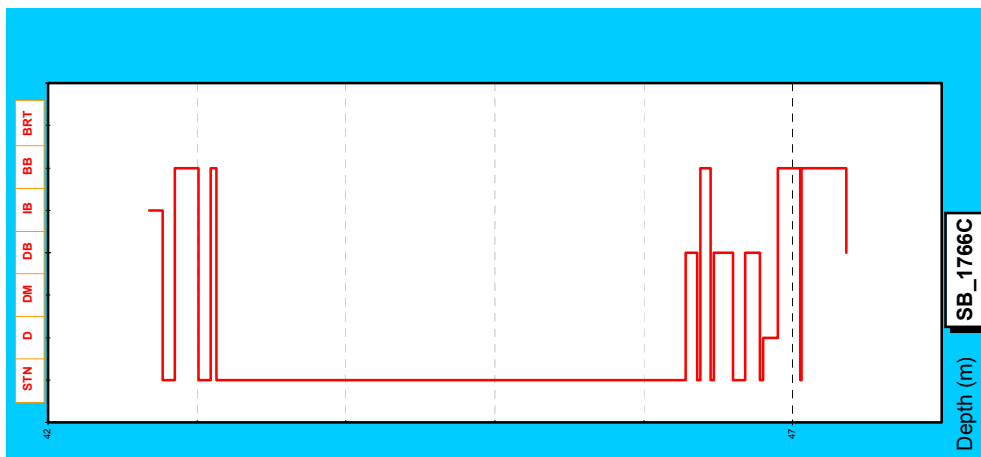
Appendix I - Figure 7: Brightness profile of the Fourfoot Bottom seam showing dulling upward bottom unit and bright top unit, Hole No. C5650



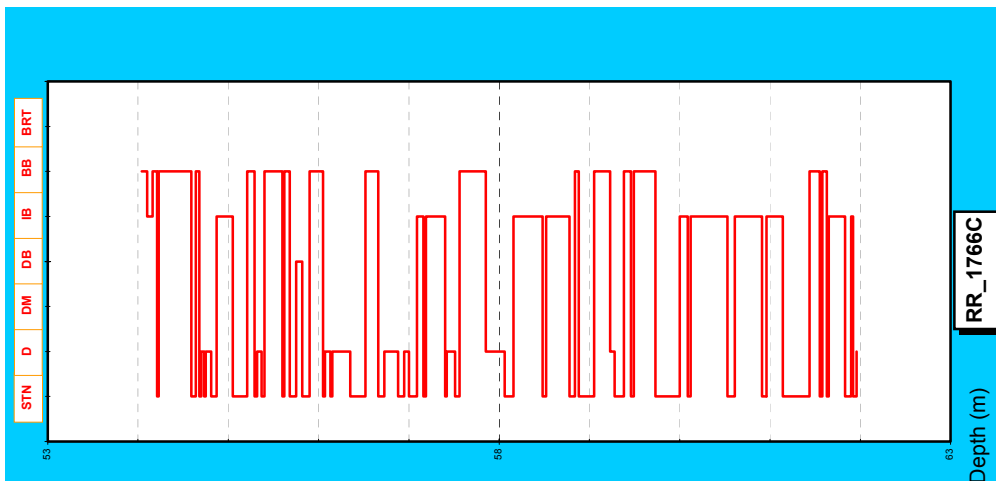
Appendix I - Figure 8: Brightness profile of the Bergin seam showing dull bottom unit and bright top unit, Hole No. C5652



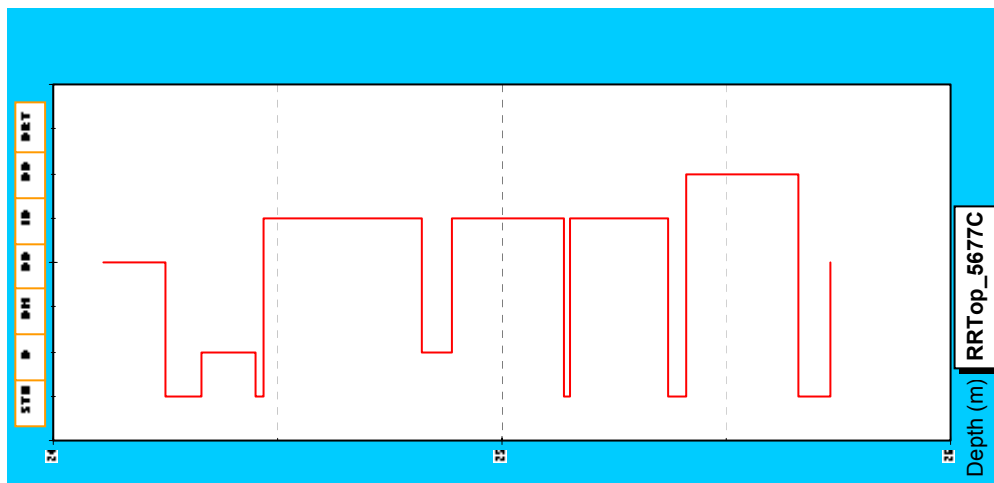
Appendix I - Figure 9: Brightness profile of the Bergin seam (mainly intermediate), Hole No. C5657



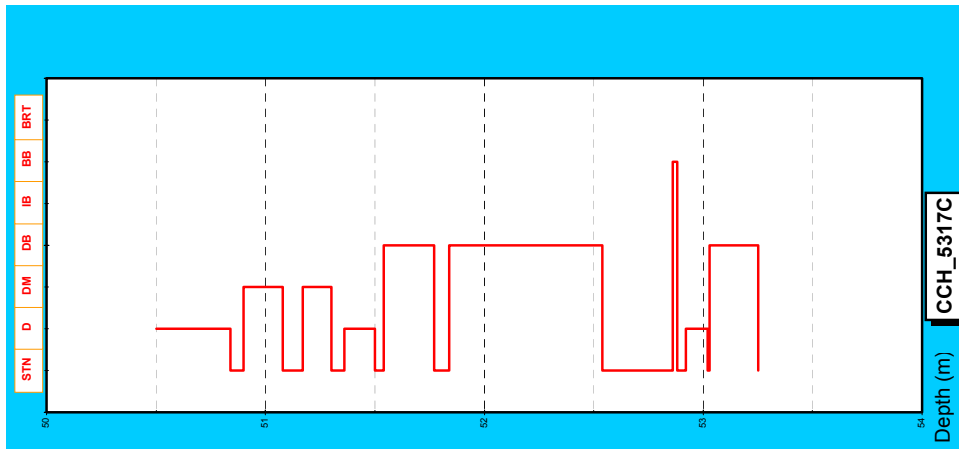
Appendix I - Figure 10: Brightness profile of the Striped Bacon seam with abundant non-coal (STN) bands, Hole No. C1766



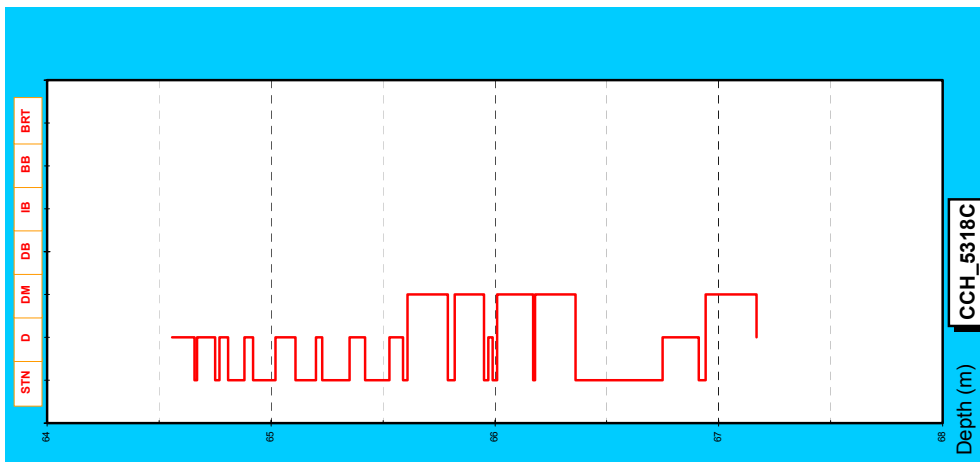
Appendix I - Figure 11: Brightness profile of the Rob Roy seam showing an oscillating pattern, Hole No. C1766



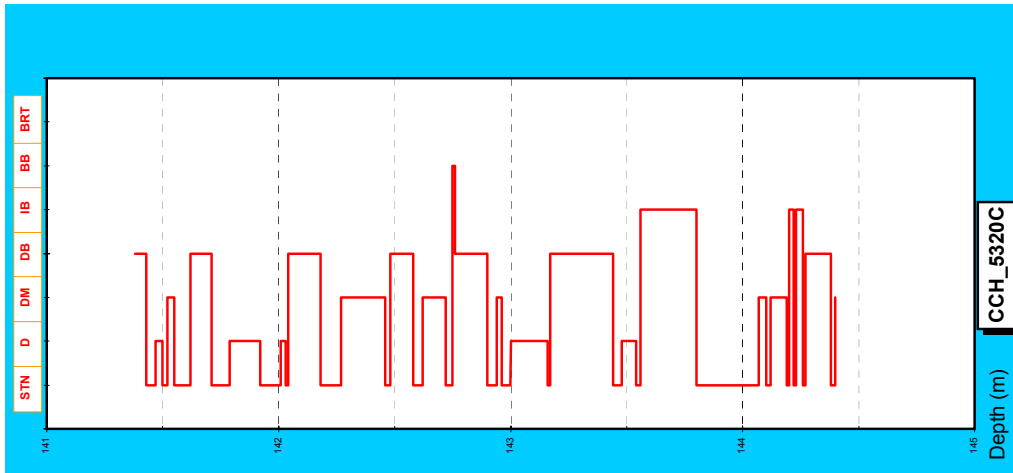
Appendix I - Figure 12: Brightness profile of the Rob Roy Top seam with relatively thick bright bands, Hole No. C5677



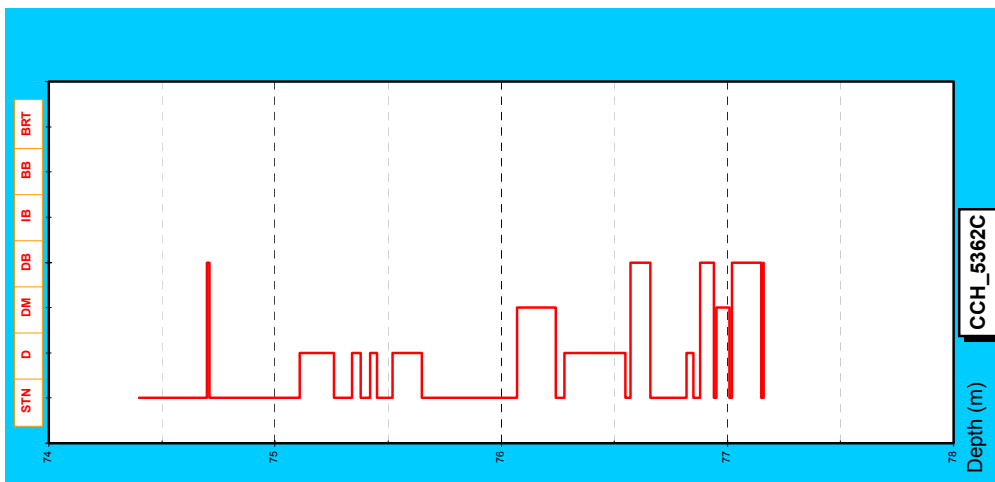
Appendix I - Figure 13: Brightness profile of the Cochrane seam showing general dulling upward succession, Hole No. C5317



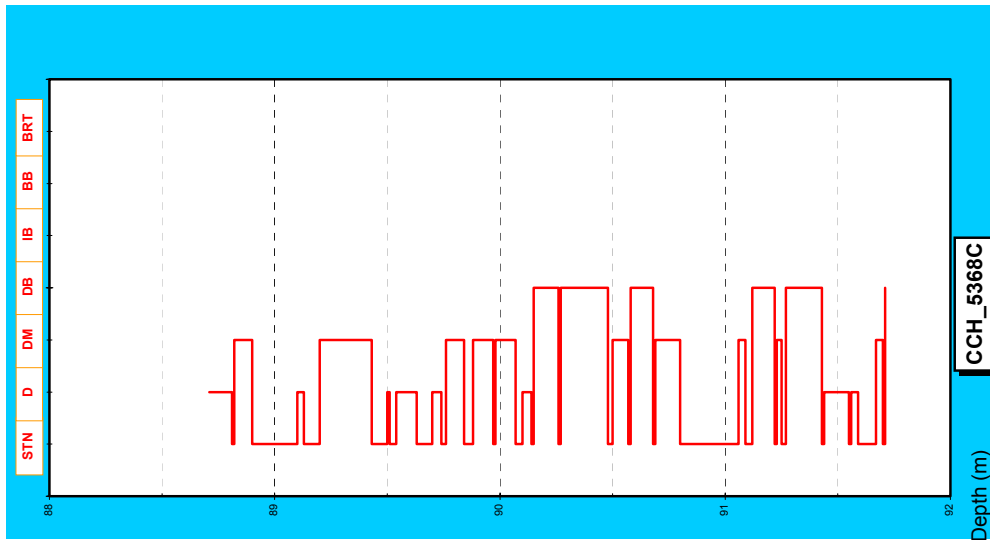
Appendix I - Figure 14: Brightness profile of the Cochrane seam (mainly dull with non-coal bands), Hole No. C5318



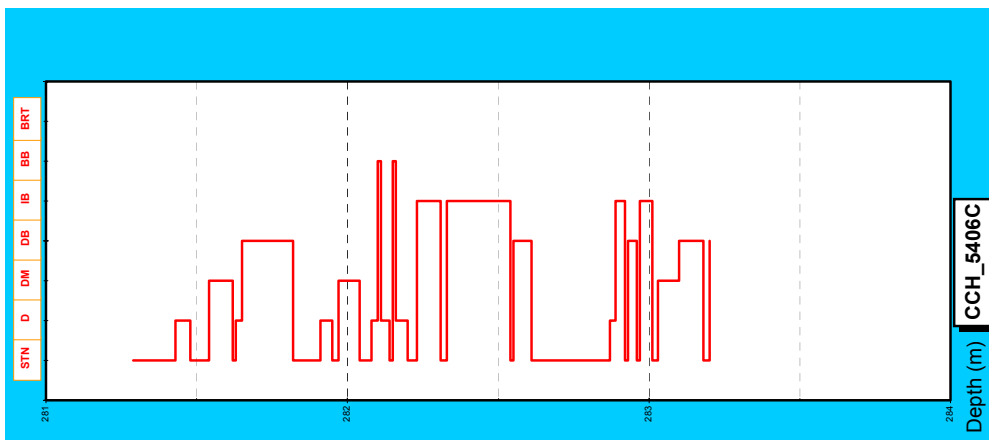
Appendix I - Figure 15: Brightness profile of the Cochrane seam showing an oscillating pattern with high percentage of intraseam claystone bands, Hole No. C5320



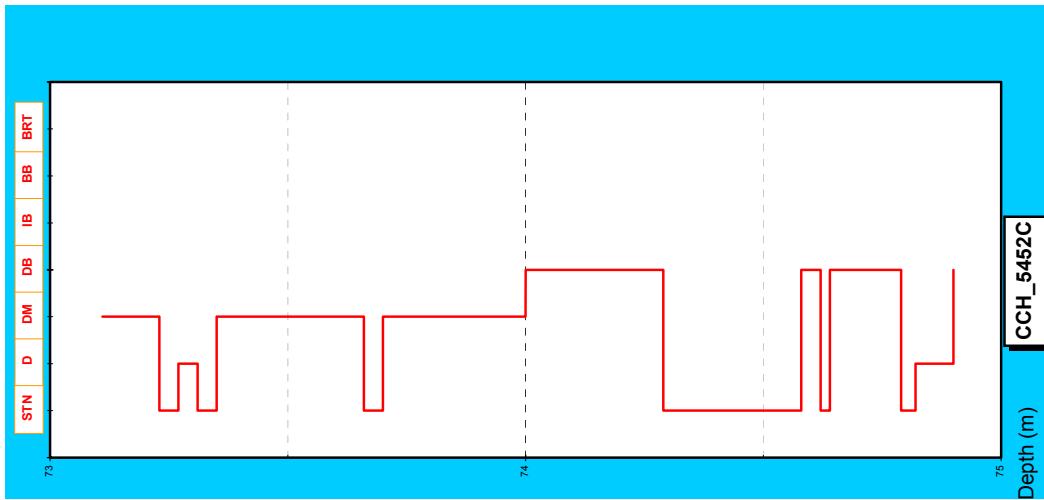
Appendix I - Figure 16: Brightness profile of the Cochrane seam showing dulling upward succession, Hole No. C5362



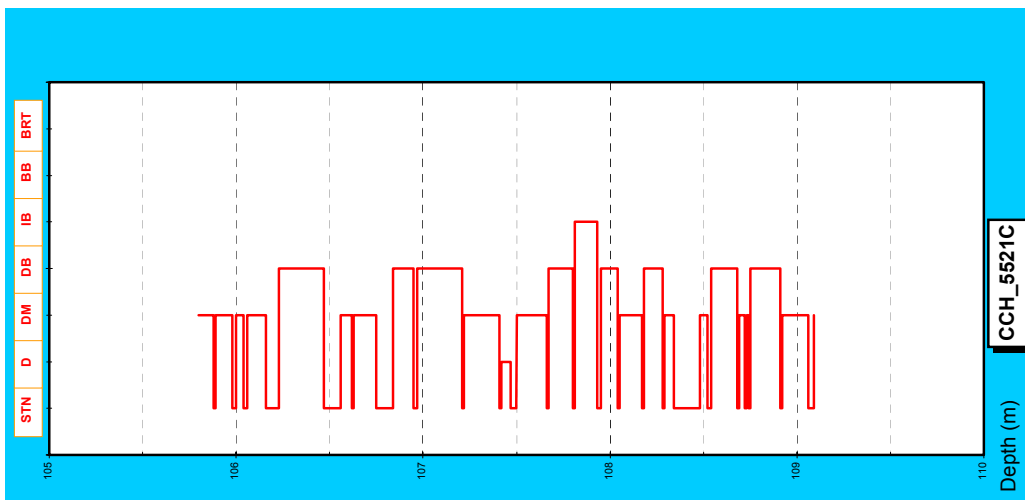
Appendix I - Figure 17: Brightness profile of the Cochrane seam showing a general oscillating pattern, Hole No. C5368



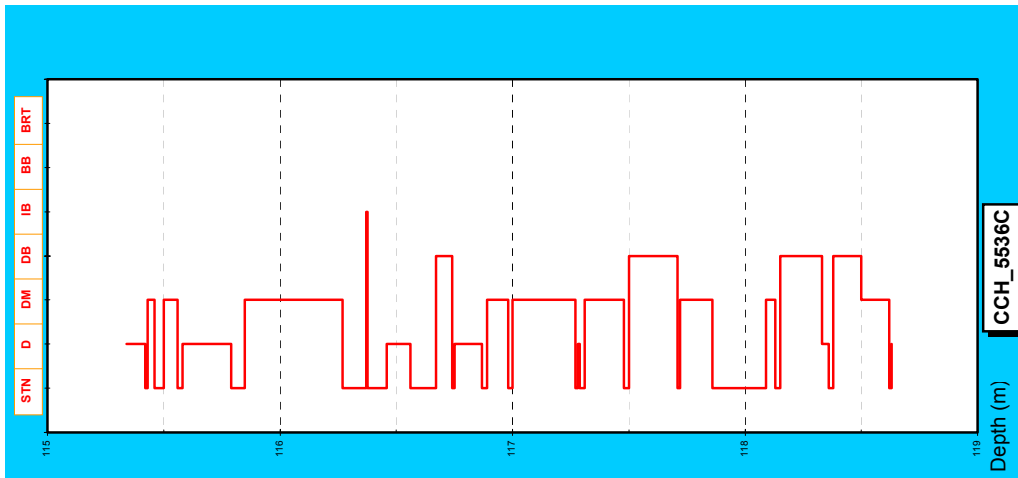
Appendix I - Figure 18: Brightness profile of the Cochrane seam showing a general dulling upward succession, Hole No. C5406



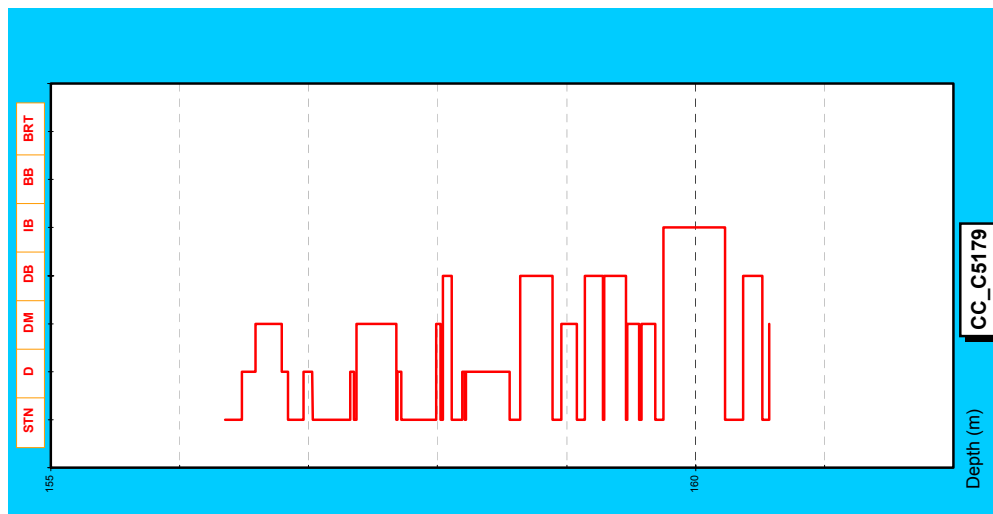
Appendix I - Figure 19: Brightness profile of the Cochrane seam (mainly dull), Hole No. C5452



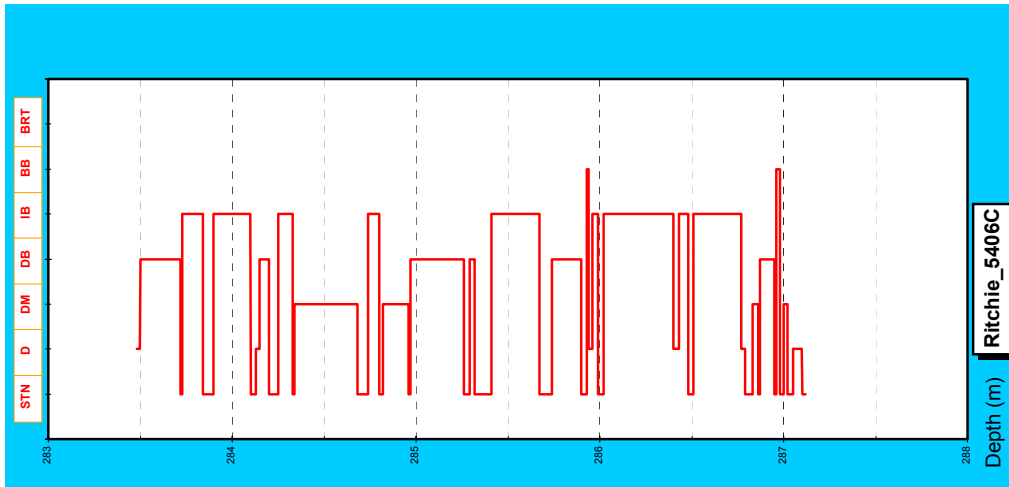
Appendix I - Figure 20: Brightness profile of the Cochrane seam showing a general oscillating pattern with duller top unit, Hole No. C5521



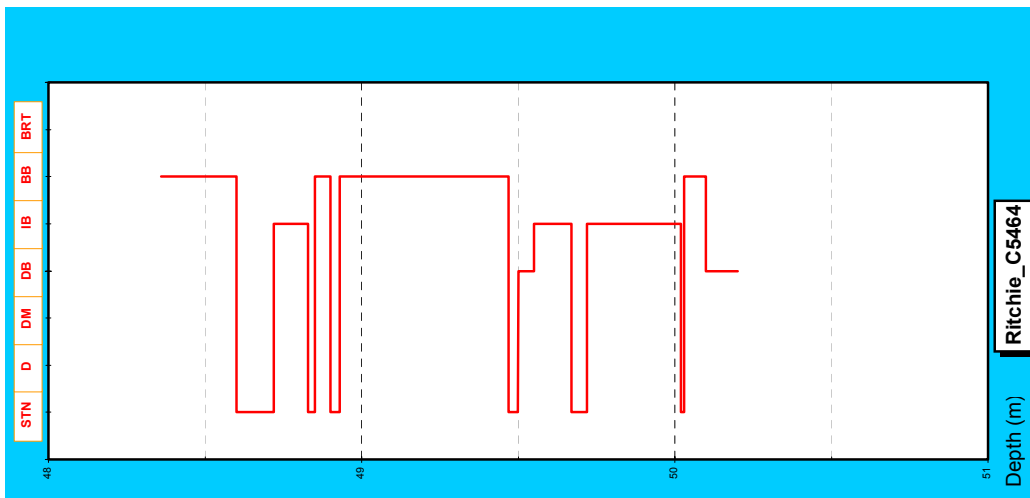
Appendix I - Figure 21: Brightness profile of the Cochrane seam (mainly dull but bottom unit is brighter than top unit), Hole No. C5536



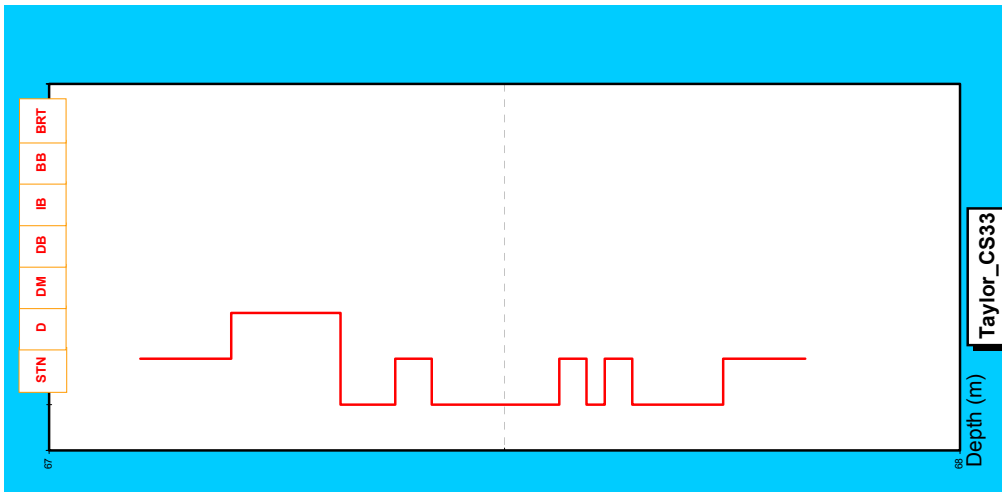
Appendix I - Figure 22: Brightness profile of the Cochrane seam showing a dulling upward succession, Hole No. C5179



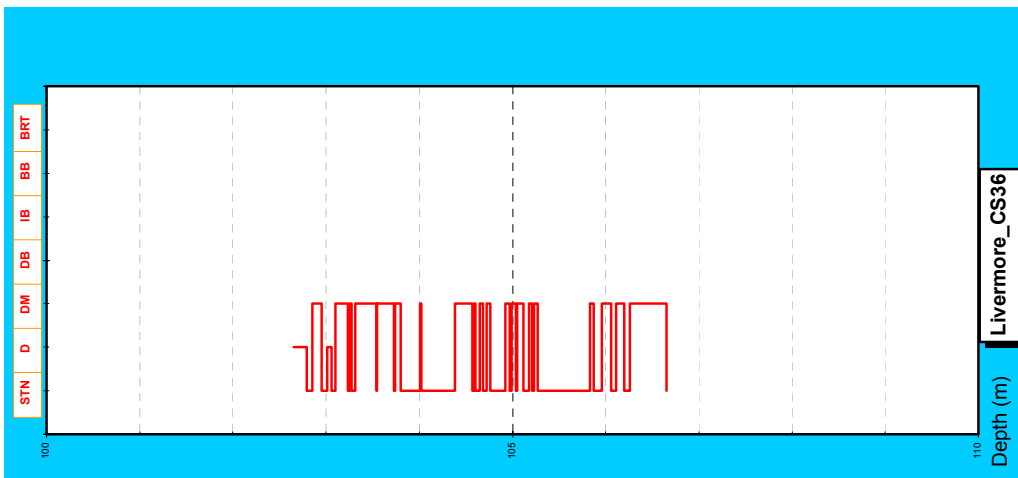
Appendix I - Figure 23: Brightness profile of the Ritchie seam (generally bright), Hole No. C5406



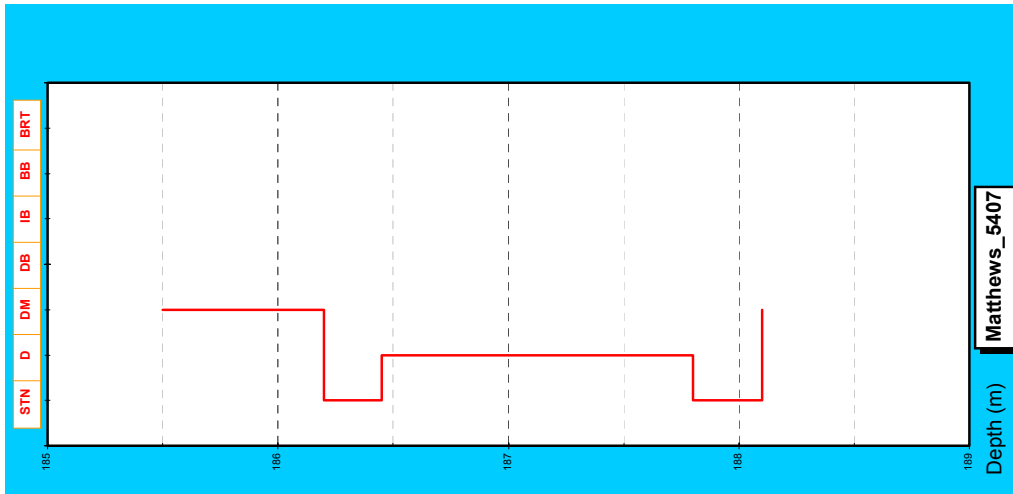
Appendix I - Figure 24: Brightness profile of the Ritchie seam with thick bright bands, Hole No. C5464



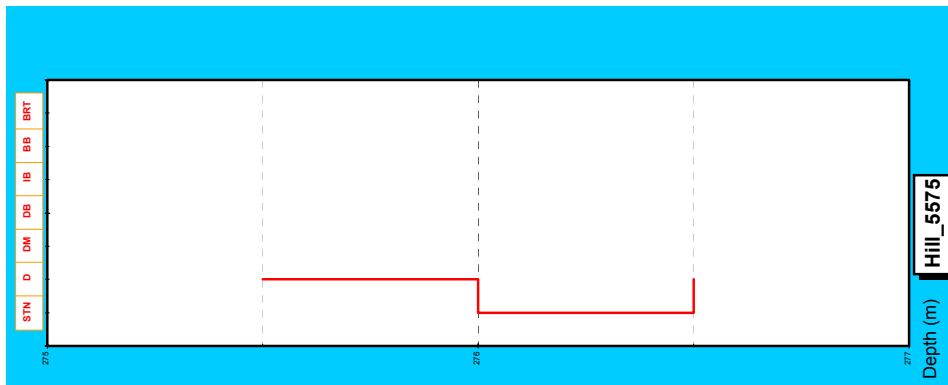
Appendix I - Figure 25: Brightness profile of the Taylor seam (stony coal), Hole No. CS33



Appendix I - Figure 26: Brightness profile of the Livermore seam (mainly dull), Hole No. CS3



Appendix I - Figure 27: Brightness profile of the Matthews seam with thick dull bands, Hole No. 5407



Appendix I - Figure 28: Brightness profile of the Hillier seam (dull and stony), Hole No. 5575

APPENDIX II

Tables

Table 11: List of Grainmount Samples

(Petrographic samples)

Sample No.	Borehole No	Depth (m)		Seam Name
		From	To	
G1	<i>Coal as sold (ROM)-Haighmor/Moreton Extended mines</i>			
G2	<i>Coal as sold (ROM)-Haighmor mine (Probably Tantivy, Fiery and Tivoli seams)</i>			
G3	NS326	363.76	365.20	Benley Tops
G4	NS347	119.90	121.29	Garden
G5	NS387	423.06	424.51	Cochrane
G6	NS387	424.78	425.75	Cochrane
G7	NS387	425.75	427.39	Cochrane
G8	NS413	122.46	124.29	Tantivy
G9	NS413	211.83	212.77	Tivoli Tops
G10	NS413	213.12	214.47	Tivoli Bottoms
G11	NS430	29.31	34.70	Fiery
G12	NS430	43.86	45.89	Waterstown
G13	NS430B	160.33	164.04	Eclipse
G14	NS523	292.44	294.00	Bluff
G15	NS523	296.27	298.31	Bluff
G16	NS523	298.31	299.66	Bluff
G17	NS523	300.03	301.14	Bluff
G18	NS523	310.52	312.37	Wright
G19	NS523	366.85	368.12	Lagoon
G20	NS523	368.12	368.90	Lagoon
G21	NS523	368.90	369.97	Lagoon
G22	NS523	369.97	371.48	Lagoon
G23	NS523	371.48	372.63	Lagoon
G24	NS523	422.50	423.95	Striped Bacon/Rob Roy
G25	NS523	423.95	424.86	Striped Bacon/Rob Roy
G26	NS523	424.86	426.43	Striped Bacon/Rob Roy
G27	NS583	397.25	398.04	Fourfoot
G28	NS583	398.04	398.99	Fourfoot
G29	NS583	398.99	399.93	Fourfoot
G30	NS583	399.93	400.74	Fourfoot
G31	NS583	400.74	401.81	Fourfoot
G32	NS583	401.81	402.82	Fourfoot
G33	NS583	412.36	413.53	Bergin
G34	NS583	416.59	417.93	Bergin
G35	NS583	417.93	418.82	Bergin

G36	NS583	418.92	419.82	Bergin
G37	NS583	461.05	462.32	Rob Roy
G38	NS583	527.69	528.13	Cochrane
G39	NS583	528.13	529.40	Cochrane
G40	NS583	529.40	530.27	Cochrane
G41	NS583	530.27	531.45	Cochrane

Appendix II - Tables

Table 12: List of Polished Block Samples
(Petrographic samples)
 (For sample depths and intervals see Highwall Brightness Profiles section)

Sample No.	Description
B1	Wright seam (New Hope/Western Leases)
B2	Wright seam (New Hope Western Leases)
B4	Bluff seam (New Hope Western Leases)
B6	Bluff seam (New Hope Western Leases)
B7	Bluff seam (New Hope Western Leases)
B8	Striped Bacon seam (New Hope No.7)
B9	Striped Bacon seam (New Hope No.7)
B11	Striped Bacon seam (New Hope No.7)
B12	Striped Bacon seam (New Hope No.7)
B13	Striped Bacon seam (New Hope No.7 Extended)
B16	Bluff seam (Wattle Glen North/New Brick)
B18	Bluff seam (Wattle Glen North/New Brick)
B19	Bluff seam (Wattle Glen North/New Brick)
B21	Bluff seam (Wattle Glen North/New Brick)
B22	Bluff seam (Wattle Glen North/New Brick)
B23	Bluff Bottom seam (Wattle Glen North/New Brick)
B25	Bergin seam (Wattle Glen North/New Brick)
B27	Bluff seam (Wattle Glen North/New Brick)
B29	Bluff seam (Wattle Glen North/New Brick)
B30	Bluff seam (Wattle Glen North/New Brick)
B31	Bluff seam (Wattle Glen North/New Brick)
B32	Bluff seam (Wattle Glen North/New Brick)
B34	Bluff seam (Wattle Glen North/New Brick)
B37	Bluff seam (Wattle Glen North/New Brick)
B38	Bergin seam (Aberdare No.2/Barcle Street Tip)
B40	Bergin seam (Wattle Glen North/New Brick)
B42	Bergin seam (Aberdare No.2/Barcle Street Tip)
B43	Bergin seam (Aberdare No.2/Barcle Street Tip)
B45	Bergin seam (Aberdare No.2/Barcle Street Tip)
B47	Bergin seam (Wattle Glen Extended Open-cut)
B48	Bergin seam (Wattle Glen Extended Open-cut)
B51	Cinder coal near basalt dyke, Bluff seam (Wattle Glen North/New Brick)
B52	Cinder coal near basalt dyke, Bluff seam (Wattle Glen North/New Brick)
C2	5cm away from the Bluff seam ((Box Flat)
2A	Bluff seam (Box Flat)
3A	Bluff seam (Box Flat)
4A	Bluff seam (Box Flat)
6A	Bluff seam (Box Flat)
8A	Bluff seam (Box Flat)
9A	Bluff seam (Box Flat)
11A	Bluff seam (Box Flat)
12A	Bluff seam (Box Flat)
13A	Bluff seam (Box Flat)
1AA	Striped Bacon (New Hopw No. 7)
5AA	Bergin seam (Aberdare No.2/Barcle Street Tip)
6AA	Bergin seam (Aberdare No.2/Barcle Street Tip)
7AA	Lagoon seam (New Hope Western Leases)
9AA	Lagoon seam (New Hope Western Leases)
11AA	Wright seam (New Hope Western Leases)
12AA	Aberdare seam (Bogside) (No brightness profile)
15AA	Bergin seam (Wattle Glen Extended Open-cut)
21AA	Bergin seam (Wattle Glen Extended Open-cut)
TH9	Coal as sold (Westfalen No. 3) (February 1972)
TH18	Coal as sold (Westfalen No. 3) (April 1972)
TH19	Coal as sold (Westfalen No. 3) (February 1973)

B Series Samples

A/C Series

AA Series

Thin Sections

Table 13: Maceral Point Count Results (Grainmount Samples)

Sample No.	Amount	Telo-vitrinite	Detro-vitrinite	Gelo-vitrinite	Total Vitrinite	Cutinite	Sporinite	Resinite	Suberinite	Total Liptinite	Fusinite	Semi-fusinite	Macrinite	Sclerotinite	Inerto-detrinite	Micrinite	Total Inertinite	Clay + Mineal Matter	Grand Total
G1	%	39.3	34.6	0	73.9	11	3.3	0	0	14.3	0.3	6.3	0.6	1	3.3	0	11.5	0	99.7
	No. of Counts	118	104	0	222	33	10	0	0	43	1	19	2	3	10	0	35	0	300
G2	%	51.3	20	0	71.3	5.3	2	1	1	9.3	1.6	3.6	0.6	1.6	6.6	0	14	5	99.6
	No. of Counts	154	60	0	214	16	6	3	3	28	5	11	2	5	20	0	43	15	300
G3	%	15.6	46.3	0	61.9	0.3	0	0	0	0.3	0.6	7	0.6	0	2	0	10.2	27.3	99.7
	No. of Counts	47	139	0	186	1	0	0	0	1	2	21	2	0	6	0	31	82	300
G4	%	23.6	30	0	53.6	8.3	4	0	0	12.3	0	3.3	0	1.3	3	0	7.6	26.3	99.8
	No. of Counts	71	90	0	161	25	12	0	0	37	0	10	0	4	9	0	23	79	300
G5	%	31.6	32.3	0	63.9	4.3	5.3	0.3	0	9.9	2	7.3	1	0.6	3.3	0	14.2	11.7	99.7
	No. of Counts	95	97	0	192	13	16	1	0	30	6	22	3	2	10	0	43	35	300
G6	%	15	30	0	45	2	0	0.3	0	2.3	0.3	7.3	0.3	0	0.3	0	8.2	44.3	99.8
	No. of Counts	45	90	0	135	6	0	1	0	7	1	22	1	0	1	0	25	133	300
G7	%	38.6	29	0	67.6	11	3.6	0	0	14.6	0	4	0	0	1.6	0	5.6	12	99.8
	No. of Counts	116	87	0	203	33	11	0	0	44	0	12	0	0	5	0	17	36	300
G8	%	31.6	27.6	0.3	59.5	5	1.6	0	0	6.6	1.3	3.3	1	1	2	0	8.6	25	99.7
	No. of Counts	95	83	1	179	15	5	0	0	20	4	10	3	3	6	0	26	75	300
G9	%	24.3	40.6	0	64.9	3.3	3	0.3	0	6.6	0.3	3.6	1.6	3.3	3.3	0	12.1	16	99.6
	No. of Counts	73	122	0	195	10	9	1	0	20	1	11	5	10	10	0	37	48	300
G10	%	47.3	23.3	0	70.6	1.6	2	0.6	1.3	5.5	0.3	1.3	2	1	3	0	7.6	16.1	99.8
	No. of Counts	142	70	0	212	5	6	2	4	17	1	4	6	3	9	0	23	48	300
G11	%	18.3	37.3	0	55.6	4.3	1	0.3	0.3	5.9	3.3	3	1.3	0.6	4.6	0	12.8	25.4	99.7
	No. of Counts	55	112	0	167	13	3	1	1	18	10	9	4	2	14	0	39	76	300
G12	%	32.3	20.6	0	52.9	2.6	0.6	0	0.3	3.5	0.6	1.3	1	0.3	2.6	0	5.8	37.3	99.5
	No. of Counts	97	62	0	159	8	2	0	1	11	2	4	3	1	8	0	18	112	300
G13	%	41.6	29.6	0.3	71.5	4	1	1	0	6	0	4.6	1	0	1	0	6.6	15.6	99.7
	No. of Counts	125	89	1	215	12	3	3	0	18	0	14	3	0	3	0	20	47	300
G14	%	31.6	41	0	72.6	2	0	0.3	0.6	2.9	0	3	0.6	0.3	1.6	0	5.5	18.7	99.7
	No. of Counts	95	123	0	218	6	0	1	2	9	0	9	2	1	5	0	17	56	300
G15	%	20.6	38.3	0.3	59.2	15.6	0.3	0	0.3	16.2	2	6.6	1	0.3	3.3	0	13.2	11	99.6
	No. of Counts	62	115	1	178	47	1	0	1	49	6	20	3	1	10	0	40	33	300

Sample No.	Amount	Telo-vitrinite	Detro-vitrinite	Gelo-vitrinite	Total Vitrinite	Cutinite	Sporinite	Resinite	Suberinite	Total Liptinite	Fusinite	Semi-fusinite	Macrinite	Sclerotinite	Inertodetrinite	Micrinite	Total Inertinite	Clay + Mineal Matter	Grand Total
G16	%	27	32	0.3	59.3	10.3	1.3	0	0	11.6	1.6	2	0.6	0	0.6	0	4.8	24	99.7
	No. of Counts	81	96	1	178	31	4	0	0	35	5	6	2	0	2	0	15	72	300
G17	%	33.6	23.6	0.3	57.5	6	0.3	0.3	0.6	7.2	0.6	5.6	0.3	0	1.6	0	8.1	26.7	99.5
	No. of Counts	101	71	1	173	18	1	1	2	22	2	17	1	0	5	0	25	80	300
G18	%	20	44.3	0	64.3	1.6	1	0	0.6	3.2	0.3	4.6	2	0	0.6	0	7.5	24.7	99.7
	No. of Counts	60	133	0	193	5	3	0	2	10	1	14	6	0	2	0	23	74	300
G19	%	41.3	22.6	0	63.9	3	0.3	0	0	3.3	4	3.3	0.3	0.3	1.3	0	9.2	23.3	99.7
	No. of Counts	124	68	0	192	9	1	0	0	10	12	10	1	1	4	0	28	70	300
G20	%	31.6	24	0	55.6	2.6	1.3	0	0	3.9	0.6	2.3	0	0	1.3	0	4.2	36	99.7
	No. of Counts	95	72	0	167	8	4	0	0	12	2	7	0	0	4	0	13	108	300
G21	%	36.3	27.6	0.3	64.2	5.6	0.6	0	0	6.2	3.3	0.6	0	0	0.3	0	4.2	25	99.6
	No. of Counts	109	83	1	193	17	2	0	0	19	10	2	0	0	1	0	13	75	300
G22	%	37.3	33	0.3	70.6	9.6	0.3	0	0	9.9	0.6	4.6	0.6	0	2	0	7.8	11.3	99.6
	No. of Counts	112	99	1	212	29	1	0	0	30	2	14	2	0	6	0	24	34	300
G23	%	47.6	18.6	0.3	66.5	4.3	1	0	0	5.3	0	2.3	1.6	0	1.6	0	5.5	22.3	99.6
	No. of Counts	143	56	1	200	13	3	0	0	16	0	7	5	0	5	0	17	67	300
G24	%	39.6	29.6	0	69.2	4	2.6	0.3	0	6.9	1	2.3	1.3	0.3	1	0.3	6.2	17.3	99.6
	No. of Counts	119	89	0	208	12	8	1	0	21	3	7	4	1	3	1	19	52	300
G25	%	33	37.3	0.6	70.9	1.6	0.6	0	0.3	2.5	0.6	4.3	1.3	0	2	0	8.2	18	99.6
	No. of Counts	99	112	2	213	5	2	0	1	8	2	13	4	0	6	0	25	54	300
G26	%	36.6	34.3	0	70.9	2.3	2	0	0	4.3	2.3	2.3	1.3	0	0	0	5.9	18.6	99.7
	No. of Counts	110	103	0	213	7	6	0	0	13	7	7	4	0	0	0	18	56	300
G27	%	40.3	39.6	0.3	80.2	4	1	0	0	5	0	4	0.6	0.3	2	0	6.9	7.6	99.7
	No. of Counts	121	119	1	241	12	3	0	0	15	0	12	2	1	6	0	21	23	300
G28	%	43.6	28.6	1.6	73.8	3.3	0.3	0.3	0	3.9	0.6	2	2	0.6	1.6	0	6.8	15	99.5
	No. of Counts	131	86	5	222	10	1	1	0	12	2	6	6	2	5	0	21	45	300
G29	%	40.3	37.6	0.3	78.2	3.6	1	0	0	4.6	2.3	2	0.6	0	1	0	5.9	11	99.7
	No. of Counts	121	113	1	235	11	3	0	0	14	7	6	2	0	3	0	18	33	300
G30	%	30.6	26	0.3	56.9	2.6	0.3	0	0	2.9	1.6	2.3	0	0	0.3	0	4.2	35.6	99.6
	No. of Counts	92	78	1	171	8	1	0	0	9	5	7	0	0	1	0	13	107	300
G31	%	37	35.6	0	72.6	3.3	0.6	0	0.3	4.2	2.3	3.6	1.3	0.3	0.3	0	7.8	15	99.6
	No. of Counts	111	107	0	218	10	2	0	1	13	7	11	4	1	1	0	24	45	300

Appendix II - Tables

Sample No.	Amount	Telo-vitrinite	Detro-vitrinite	Gelo-vitrinite	Total Vitrinite	Cutinite	Sporinite	Resinite	Suberinite	Total Liptinite	Fusinite	Semi-fusinite	Macrinite	Sclerotinite	Inerto-detrinite	Micrinite	Total Inertinite	Clay + Mineal Matter	Grand Total
G32	%	51	23.3	1	75.3	3.6	0	0.3	0.3	4.2	0.6	4	1	0.3	1.3	0	7.2	13	99.7
	No. of Counts	153	70	3	226	11	0	1	1	13	2	12	3	1	4	0	22	39	300
G33	%	41	26.3	0	67.3	3.3	0.6	0	0.3	4.2	2.6	4	0	0	2	0	8.6	19.7	99.8
	No. of Counts	123	79	0	202	10	2	0	1	13	8	12	0	0	6	0	26	59	300
G34	%	31.6	32.3	1.6	65.5	3.6	2	0.3	1.6	7.5	2.3	3	1	0	1.6	0	7.9	18.7	99.6
	No. of Counts	95	97	5	197	11	6	1	5	23	7	9	3	0	5	0	24	56	300
G35	%	30.3	27	0	57.3	12.6	4	0	0	16.6	0	1.6	0.3	0	2	0	3.9	22	99.8
	No. of Counts	91	81	0	172	38	12	0	0	50	0	5	1	0	6	0	12	66	300
G36	%	44.3	31	0.3	75.6	2	2	1	0	5	1	2.3	1.3	0	2.3	0	6.9	12.3	99.8
	No. of Counts	133	93	1	227	6	6	3	0	15	3	7	4	0	7	0	21	37	300
G37	%	25.3	36	0.6	61.9	4.3	2	0	0	6.3	0.6	4	0	0	1	0	5.6	26	99.8
	No. of Counts	76	108	2	186	13	6	0	0	19	2	12	0	0	3	0	17	78	300
G38	%	34.3	24.6	0.3	59.2	1.3	1	0	0	2.3	1.6	7.6	1.3	0	2.3	0	12.8	25.3	99.6
	No. of Counts	103	74	1	178	4	3	0	0	7	5	23	4	0	7	0	39	76	300
G39	%	34	25.3	1	60.3	3.3	0.6	0	0	3.9	2.6	11	1.6	0	4	0	19.2	16.3	99.7
	No. of Counts	102	76	3	181	10	2	0	0	12	8	33	5	0	12	0	58	49	300
G40	%	28.6	16.6	0.6	45.8	3.6	1	0	0	4.6	0.6	8	1	0	2	0	11.6	37.6	99.6
	No. of Counts	86	50	2	138	11	3	0	0	14	2	24	3	0	6	0	35	113	300
G41	%	41.3	17.6	0.3	59.2	3.3	2	0	0	5.3	2.3	4.6	0	0	5	0	11.9	23.3	99.7
	No. of Counts	124	53	1	178	10	6	0	0	16	7	14	0	0	15	0	36	70	300
%AVERAGE		34.15	30.12	0.27	64.54	4.61	1.40	0.16	0.19	6.37	1.18	3.99	0.83	0.33	2.01	0.01	8.35	20.42	99.67
%ST. DEV.		9.07	7.31	0.40	8.28	3.37	1.26	0.28	0.37	3.93	1.08	2.19	0.61	0.62	1.38	0.05	3.36	9.26	0.09
%MAX		51.30	46.30	1.60	80.20	15.60	5.30	1.00	1.60	16.60	4.00	11.00	2.00	3.30	6.60	0.30	19.20	44.30	99.80
%MIN		15.00	16.60	0.00	45.00	0.30	0.00	0.00	0.00	0.30	0.00	0.60	0.00	0.00	0.00	0.00	3.90	0.00	99.50

Appendix II - Tables

Table 14: Maceral Point Count Results (Polished Block Samples)

Sample No.	Amount	Telo-vitrinite	Detro-vitrinite	Gelo-vitrinite	Total Vitrinite	Cutinite	Sporinite	Resinite	Suberinite	Total Liptinite	Fusinite	Semi-fusinite	Macrinite	Sclerotinite	tertodetrinite	Micrinite	Total Inertinite	Clay+Other Min. Matter	Grand Total
B1	%	50.6	34.3	0	84.9	7.6	0	0	0	7.6	0	0.3	0	0.6	5.6	0	6.5	0.6	99.6
	No. of Counts	152	103	0	255	23	0	0	0	23	0	1	0	2	17	0	20	2	300
B6	%	61.6	22.6	0	84.2	8	0.3	0	0	8.3	0	0.3	0	0	1	0	1.3	6	99.8
	No. of Counts	185	68	0	253	24	1	0	0	25	0	1	0	0	3	0	4	18	300
B7	%	51.3	23	0	74.3	16	0	0	0.6	16.6	0.3	1.6	1	0.3	1.6	0	4.8	4	99.7
	No. of Counts	154	69	0	223	48	0	0	2	50	1	5	3	1	5	0	15	12	300
B8	%	27.3	34	0	61.3	0	0	0	0	0	12.3	8.3	2	4.3	11.6	0	38.5	0	99.8
	No. of Counts	82	102	0	184	0	0	0	0	0	37	25	6	13	35	0	116	0	300
B11	%	57.3	31	0	88.3	0.6	0	0	0	0.6	0	5.6	0.6	1.6	2	0	9.8	1	99.7
	No. of Counts	172	93	0	265	2	0	0	0	2	0	17	2	5	6	0	30	3	300
B12	%	66.3	6.3	0	72.6	0	0	0	0	0	0	10.6	0	2.6	11	0	24.2	3	99.8
	No. of Counts	199	19	0	218	0	0	0	0	0	0	32	0	8	33	0	73	9	300
B13	%	49	41.3	0	90.3	0	0	0	0	0	0	3.6	0	0	1.6	0	5.2	4.3	99.8
	No. of Counts	147	124	0	271	0	0	0	0	0	0	11	0	0	5	0	16	13	300
B16	%	45.3	30.3	0.3	75.9	3.3	0.6	0	0	3.9	0.3	8.3	1	0.3	5.6	0	15.5	4.3	99.6
	No. of Counts	136	91	1	228	10	2	0	0	12	1	25	3	1	17	0	47	13	300
B18	%	62.6	22.3	0	84.9	5	0.6	0	0	5.6	0	1.6	1.3	0	3.6	0	6.5	2.6	99.6
	No. of Counts	188	67	0	255	15	2	0	0	17	0	5	4	0	11	0	20	8	300
B19	%	21	59.6	0	80.6	6	2	0	0	8	1.3	4.3	2.3	0.3	3	0	11.2	0	99.8
	No. of Counts	63	179	0	242	18	6	0	0	24	4	13	7	1	9	0	34	0	300
B22	%	67.6	4	0	71.6	4.3	2.6	0	0	6.9	2	7.6	0	0	10	0	19.6	1.6	99.7
	No. of Counts	203	12	0	215	13	8	0	0	21	6	23	0	0	30	0	59	5	300
B23	%	24	66	0	90	1.3	0	0	0	1.3	0	7.3	0	0	0.3	0	7.6	1	99.9
	No. of Counts	72	198	0	270	4	0	0	0	4	0	22	0	0	1	0	23	3	300
B27	%	10.3	57.3	0.3	67.9	0	0	0	0	0	6.3	8.6	2.6	0.6	13.6	0	31.7	0	99.6
	No. of Counts	31	172	1	204	0	0	0	0	0	19	26	8	2	41	0	96	0	300
B29	%	78.6	14.6	0	93.2	0	0	0	0	0	0.6	0	0	0	6	0	6.6	0	99.8
	No. of Counts	236	44	0	280	0	0	0	0	0	2	0	0	0	18	0	20	0	300
B30	%	22.3	53.6	1	76.9	2	1	0	0	3	1.3	10.6	2.3	0	5.6	0	19.8	0	99.7
	No. of Counts	67	161	3	231	6	3	0	0	9	4	32	7	0	17	0	60	0	300
B31	%	59.3	15.3	0	74.6	15	0	0	0	15	0	1.3	1.3	1	3.3	0	6.9	3.3	99.8
	No. of Counts	178	46	0	224	45	0	0	0	45	0	4	4	3	10	0	21	10	300
B32	%	53.3	28.6	0	81.9	4.3	1.3	0	0	5.6	0	3	1.3	1.6	3.3	0	9.2	3	99.7
	No. of Counts	160	86	0	246	13	4	0	0	17	0	9	4	5	10	0	28	9	300
B34	%	6	7	0	13	0	0	0	0	0	0	1.6	0.6	0	0	0	2.2	84.6	99.8
	No. of Counts	18	21	0	39	0	0	0	0	0	0	5	2	0	0	0	7	254	300
B37	%	29	36.3	1.6	66.9	6	5	0	0	11	2.3	12.3	3	0	4.3	0	21.9	0	99.8
	No. of Counts	87	109	5	201	18	15	0	0	33	7	37	9	0	13	0	66	0	300
B38	%	WEATHERED VITRINITE IN CLAY AND OTHER MINERAL MATTER GROUNDMASS																	
	No. of Counts																		
B40	%	66.3	17.3	0.3	83.9	1.3	2.6	0	0	3.9	0	2.6	0.6	0.6	5	0	8.8	3	99.6
	No. of Counts	199	52	1	252	4	8	0	0	12	0	8	2	2	15	0	27	9	300
B42	%	22.3	47.6	0	69.9	1.6	0	0	0	1.6	4	13.3	6.6	0	0.6	0	24.5	3.6	99.6
	No. of Counts	67	143	0	210	5	0	0	0	5	12	40	20	0	2	0	74	11	300

Sample No.	Amount	Telo-vitrinite	Detro-vitrinite	Gelo-vitrinite	Total Vitrinite	Cutinite	Sporinite	Resinite	Suberinite	Total Liptinite	Fusinite	Semi-fusinite	Macrinite	Sclerotinite	nerodetrinite	Micrinite	Total Inertinite	Clay+Other Min. Matter	Grand Total	
B43	%	82.3	8	0	90.3	0	0.3	0	0	0.3	0	1.3	2	0	4	0	7.3	2	99.9	
	No. of Counts	247	24	0	271	0	1	0	0	1	0	4	6	0	12	0	22	6	300	
B45	%	69	7.3	0	76.3	2.3	15.6	0	0	17.9	0	1	0	0.6	3.3	0	4.9	0.6	99.7	
	No. of Counts	207	22	0	229	7	47	0	0	54	0	3	0	2	10	0	15	2	300	
B52	%	32.6	33	0	65.6	21.3	0.3	0	0	21.6	0.3	6.6	3.3	0	2.3	0	12.5	0	99.7	
	No. of Counts	98	99	0	197	64	1	0	0	65	1	20	10	0	7	0	38	0	300	
2A	%	40.6	31	0	71.6	0	0	0	0	0	5	7	1.3	0	7.3	0	20.6	7.6	99.8	
	No. of Counts	122	93	0	215	0	0	0	0	0	15	21	4	0	22	0	62	23	300	
4A	%	44.3	19.3	2	65.6	2.6	1.6	0	4	8.2	1	12.6	4.3	0.3	7.6	0	25.8		99.6	
	No. of Counts	133	58	6	197	8	5	0	12	25	3	38	13	1	23	0	78		300	
6A	%	32.3	10	0.6	42.9	31.3	3.6	0	0	34.9	0.6	4.3	0.6	1.6	13.3	0	20.4	1.3	99.5	
	No. of Counts	97	30	2	129	94	11	0	0	105	2	13	2	5	40	0	62	4	300	
8A	%	37.6	13.6	0	51.2	0.6	0.6	0	0.3	1.5	1.6	18.3	0.3	0	26.3	0	46.5	0.3	99.5	
	No. of Counts	113	41	0	154	2	2	0	1	5	5	55	1	0	79	0	140	1	300	
9A	%	WEATHERED/HEAT AFFECTED COAL																		
12A	%	6	22	0	28	4.3	2.3	0.3	0	6.9	0	15.3	0	0	3.6	0	18.9	46	99.8	
	No. of Counts	18	66	0	84	13	7	1	0	21	0	46	0	0	11	0	57	138	300	
13A	%	14	33	3	50	18.6	6.6	0	0	25.2	0	21.3	2	0.3	1	0	24.6	0	99.8	
	No. of Counts	42	99	9	150	56	20	0	0	76	0	64	6	1	3	0	74	0	300	
1AA	%	22.3	16	0	38.3	45.3	2	0	0	47.3	2.3	3	1	0	4	0	10.3	4	99.9	
	No. of Counts	67	48	0	115	136	6	0	0	142	7	9	3	0	12	0	31	12	300	
5AA	%	29.6	25.6	0	55.2	13	1	0	0	14	0	5	0.3	0	1	0	6.3	24.3	99.8	
	No. of Counts	89	77	0	166	39	3	0	0	42	0	15	1	0	3	0	19	73	300	
6AA	%	WEATHERED/HEAT AFFECTED COAL																		
7AA	%	1.6	0	0	1.6	0	0	0	0	0	0	0	0	0	0	0	0	0	98.3	99.9
	No. of Counts	5	0	0	5	0	0	0	0	0	0	0	0	0	0	0	0	0	295	300
9AA	%	28.3	39	0	67.3	1.6	0	0	0	1.6	0	10	0.3	2.3	3	0	15.6	15.3	99.8	
	No. of Counts	85	117	0	202	5	0	0	0	5	0	30	1	7	9	0	47	46	300	
11AA	%	28.3	3	0	31.3	2.6	0.6	0	0	3.2	0.3	0.3	0	0.3	0.6	0	1.5	63.6	99.6	
	No. of Counts	85	9	0	94	8	2	0	0	10	1	1	0	1	2	0	5	191	300	
14AA	%	31.6	19	1	51.6	27	2	0	0	29	3.3	7	0.6	0.6	7	0	18.5	0.6	99.7	
	No. of Counts	95	57	3	155	81	6	0	0	87	10	21	2	2	21	0	56	2	300	
18AA	%	WEATHERED/HEAT AFFECTED COAL																		
21AA	%	1.6	62.6	0	64.2	0	0	0	0	0	5	11	13	0	4.6	0	33.6	2	99.8	
	No. of Counts	5	188	0	193	0	0	0	0	0	15	33	39	0	14	0	101	6	300	
%AVERAGE		38.74	26.88	0.27	65.89	6.83	1.42	0.01	0.13	8.39	1.35	6.40	1.50	0.54	5.07	0.00	14.85	10.88	99.73	
%ST. DEV.		22.13	17.60	0.65	21.83	10.27	2.83	0.05	0.66	11.06	2.49	5.40	2.41	0.93	5.11	0.00	11.06	23.77	0.11	
%MAX		82.30	66.00	3.00	93.20	45.30	15.60	0.30	4.00	47.30	12.30	21.30	13.00	4.30	26.30	0.00	46.50	98.30	99.90	
%MIN		1.60	0.00	0.00	1.60	0.00	0.00	0.00	0.00	0.00	0.00	0.00	0.00	0.00	0.00	0.00	0.00	0.00	99.50	

Appendix II - Tables

Table 18: Highwall Samples used in Lithotypes vs Maceral Types Graphs

Sample No	Total % Vitrinite	Total % Liptinite	Total % Inertinite	%Clay and other Min. Matter	Lithotype Group
B6	84.2	8.3	1.3	6	Bright
B29	93.2	0	6.6	0	Bright
B32	81.9	5.6	9.2	3	Bright
	86.43	4.63	5.70	3.00	Bright Avg
B1	84.9	7.6	6.5	0.6	B and D
B12	72.6	0	24.2	3	B and D
B16	75.9	3.9	15.5	4.3	B and D
B22	71.6	6.9	19.6	1.6	B and D
B27	67.9	0	31.7	0	B and D
B30	76.9	3	19.8	0	B and D
B37	66.9	11	21.9	0	B and D
B40	83.9	3.9	8.8	3	B and D
B45	76.3	17.9	4.9	0.6	B and D
4A	65.6	8.2	25.8	0	B and D
8A	51.2	1.5	46.5	0.3	B and D
12A	28	6.9	18.9	46	B and D
21AA	64.2	0	33.6	2	B and D
9AA	67.3	1.6	15.6	15.3	B and D
B18	84.9	5.6	6.5	2.6	B and D
B19	80.6	8	11.2	0	B and D
B23	90	1.3	7.6	1	B and D
B31	74.6	15	6.9	3.3	B and D
B42	69.9	1.6	24.5	3.6	B and D
2A	71.6	0	20.6	7.6	B and D
6A	42.9	34.9	20.4	1.3	B and D
13A	50	25.2	24.6	0	B and D
5AA	55.2	14	6.3	24.3	B and D
1AA	38.3	47.3	10.3	4	B and D
B7	74.3	16.6	4.8	4	B and D
B11	88.3	0.6	9.8	1	B and D
B13	90.3	0	5.2	4.3	B and D
11AA	31.3	3.2	1.5	63.6	B and D
	67.69	8.78	16.20	7.05	Intermediate Avg
B8	61.3	0	38.5	0	Dull
B34	13	0	2.2	84.6	Dull
B43	90.3	0.3	7.3	2	Dull
	54.87	0.10	16.00	28.87	Dull Avg

Most samples lie in the intermediate range.

The Intermediate Group contains Bd and DB lithotype bands with 60 to 70% bright.

The Bright Group contained B with minor Bd bands (70 to 90% bright).

The Dull Group contains Db with minor DB bands (50 to 60% bright).

The other dull components, D and Dmb, were not included in the Dull Group due to inadequate sample quantities.

**Table 19: Highwall Samples used in
Telovitrinite/Detrovitrinite vs Lithotypes Graph**

Sample No.	%Telovitrinite	%Detrovitrinite	Lithotype
B6	61.60	22.60	B
B31	59.30	15.30	B
B32	53.30	28.60	B
Average	58.07	22.17	B
B1	50.60	34.30	Bd
B12	66.30	6.30	Bd
B27	10.30	57.30	Bd
B29	78.60	14.60	Bd
B30	22.30	53.60	Bd
B37	29.00	36.30	Bd
B40	66.30	17.30	Bd
B45	69.00	7.30	Bd
4A	44.30	19.30	Bd
6A	32.30	10.00	Bd
8A	37.60	13.60	Bd
12A	6.00	22.00	Bd
7AA	1.60	0.00	Bd
9AA	28.30	39.00	Bd
Average	38.75	23.64	Bd
B7	51.30	23.00	DB
B11	57.30	31.00	DB
B16	45.30	30.30	DB
B22	67.60	4.00	DB
B23	24.00	66.00	DB
B42	22.30	47.60	DB
2A	40.60	31.00	DB
13A	14.00	33.00	DB
5AA	29.60	25.60	DB
1AA	22.30	16.00	DB
21AA	1.60	62.60	DB
11AA	28.30	3.00	DB
Average	33.68	31.09	DB
B8	27.30	34.00	Db
B18	62.60	22.30	Db
B19	21.00	59.60	Db
B43	82.30	8.00	Db
Average	48.30	30.98	Db
B34	6.00	7.00	Dmb

Table 23: Average Depth vs Average Thickness

	Seam	Avg. Depth	Avg. Thickness	
↑ Younger	Thomas	362.43	8.17	Blackstone Formation
	Aberdare	249.52	5.18	
	Bluff	218.98	7.68	
	Fourfoot	241.37	4.29	
	Bergin	234.26	4.20	
	Striped Bacon	199.57	2.52	
	Rob Roy	152.60	4.30	
	Cochrane	120.84	3.73	Tivoli Formation
	Unnamed	105.77	4.63	
	CL	31.31	3.27	
	Ritchie	102.12	2.13	
	Taylor	84.22	1.56	
	Livermore	85.51	2.38	
	Matthews	142.06	1.12	
	Garden	81.34	4.45	
	Westfalen Top	59.73	8.38	
	Tantivy	122.06	3.42	
	Fiery	145.28	4.49	
	Waterstown	122.28	3.95	
	Unnamed2	158.00	4.58	
	Tivoli	209.31	3.67	
	Poverty	273.35	2.65	
	Eclipse	241.77	3.74	
	Francis	353.79	0.98	
	Benley	304.78	7.01	
	Morris	365.56	3.16	
Waterworks	78.44	22.70		

APPENDIX III

Coal Atlas

Note: The Coal Atlas is divided into four parts, including Vitrinite Group, Liptinite Group, Inertinite Group, and Typical and Special Views. For sample locations, sample intervals and sample positions on brightness profiles, please see Figures 7, 8 and 32 - sample location maps, Appendix I-sample lists, and Appendix II-highwall brightness profiles

LEGEND

v = vitrinite
ph = phyllovitrinite
t = tellovitrinite
d = detrovitrinite
g = gellovitrinite
c = cutinite
s = sporinite
r = resinite
su = suberinite
f = fusinite
sf = semifusinite
I = inertodetrinite
m = macrinite
mi = micrinite
sc = sclerotinite
cy = clay
sd = siderite
ca = calcite
q = quartz
mm = mineral matter
py = pyrite

All photographs were taken with oil immersion lenses except thin sections (see 'Methods' section for details)

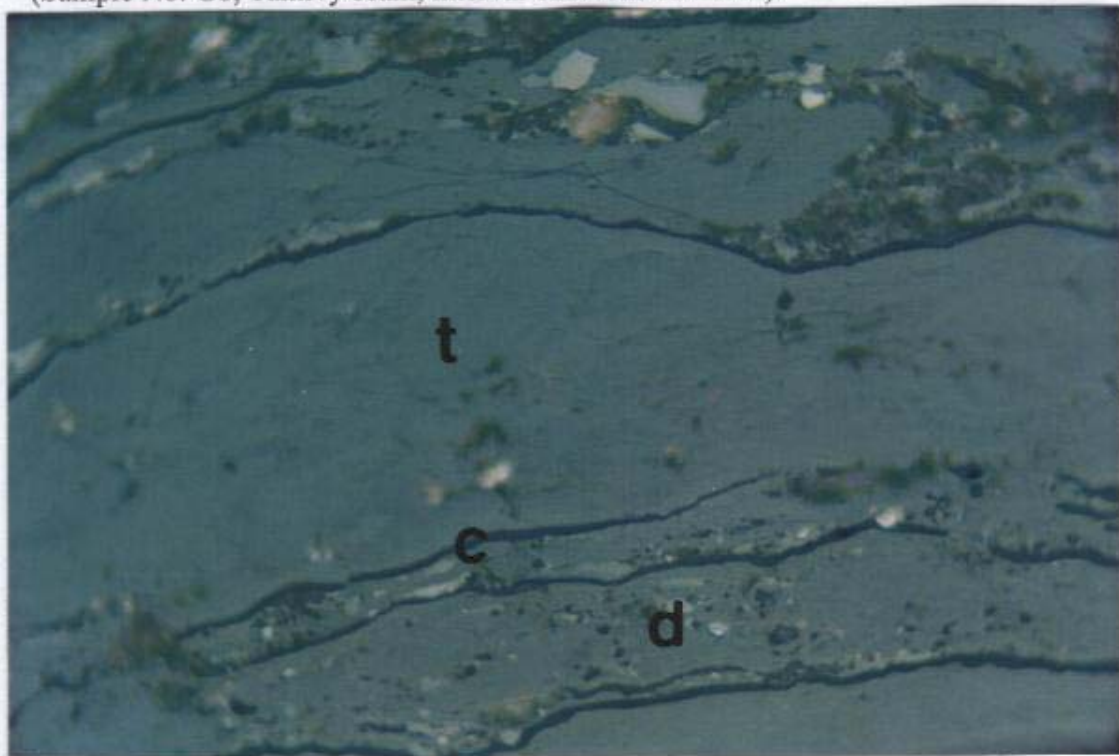
Vitrinite Group

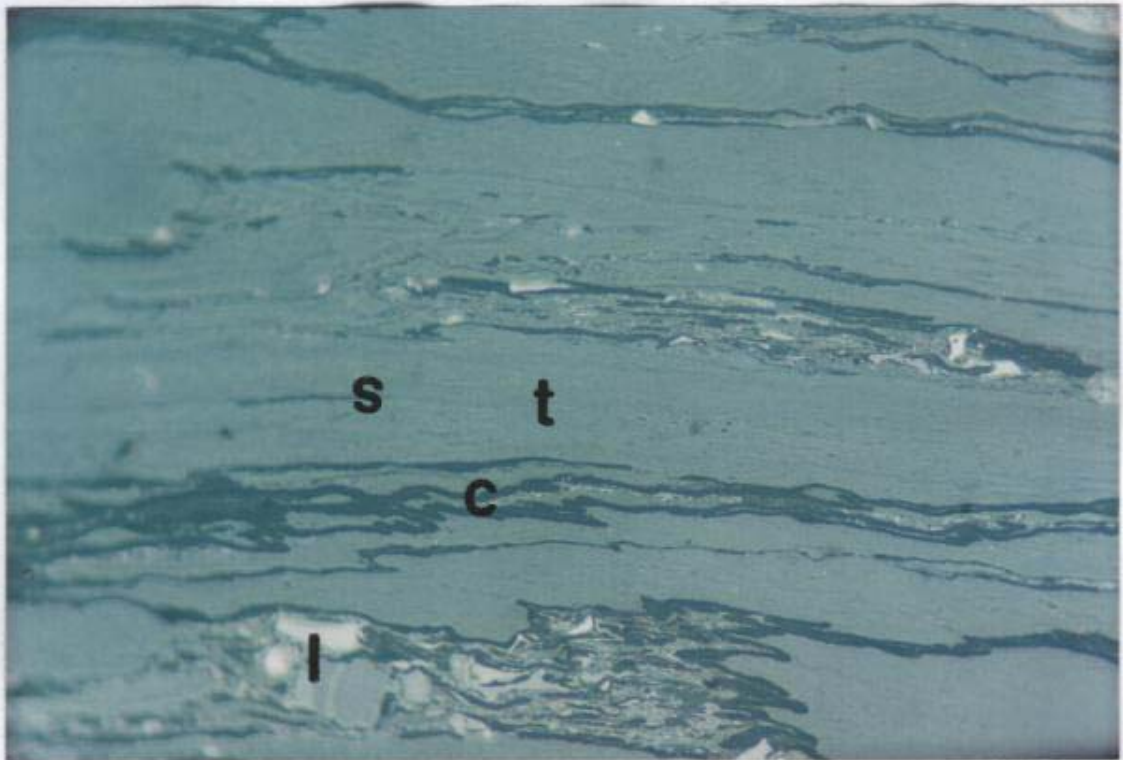


Photograph 1: Sideritic micro nodule (centre) in telovitrinite (Sample No. G1, North Ipswich-Haighmor and Moreton Extended mines, coal as sold).



Photograph 2: Telovitrinite layers with cutinite and detrovitrinite and minor inertodetrinite. Note the weak cell structure in telovitrinite (phyllovitrinite) (Sample No. G8, Tantivy seam, interval 122.46m-124.29m).

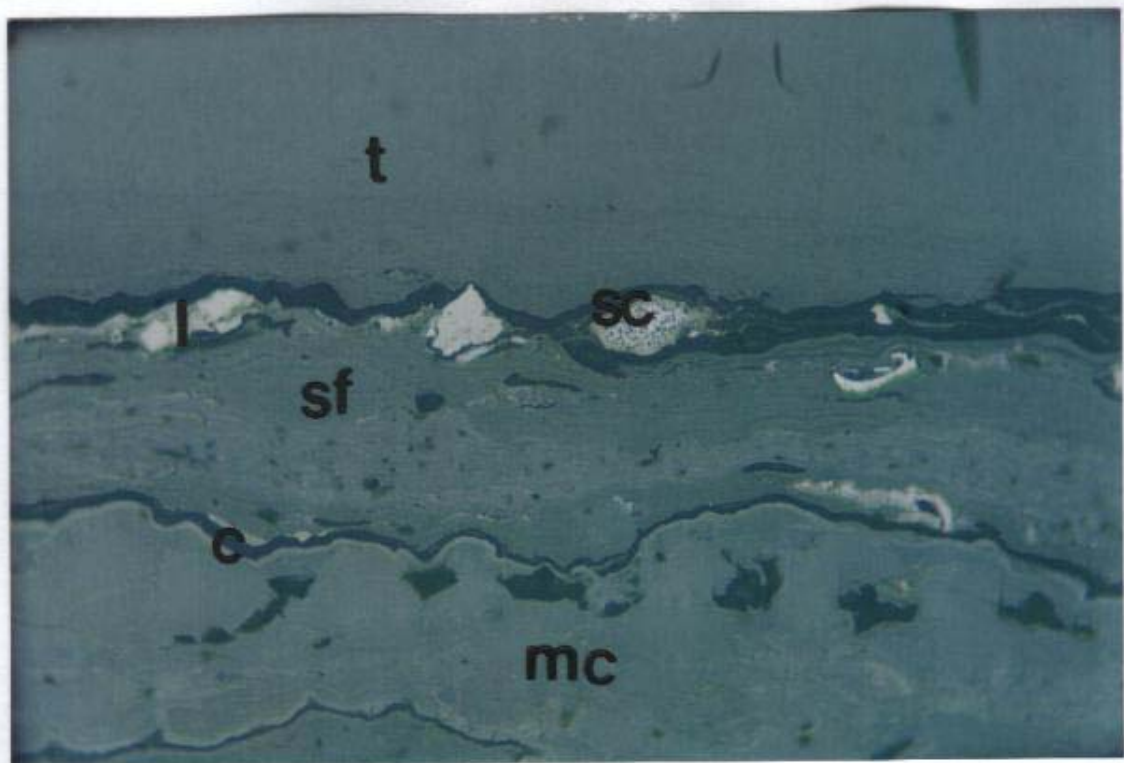


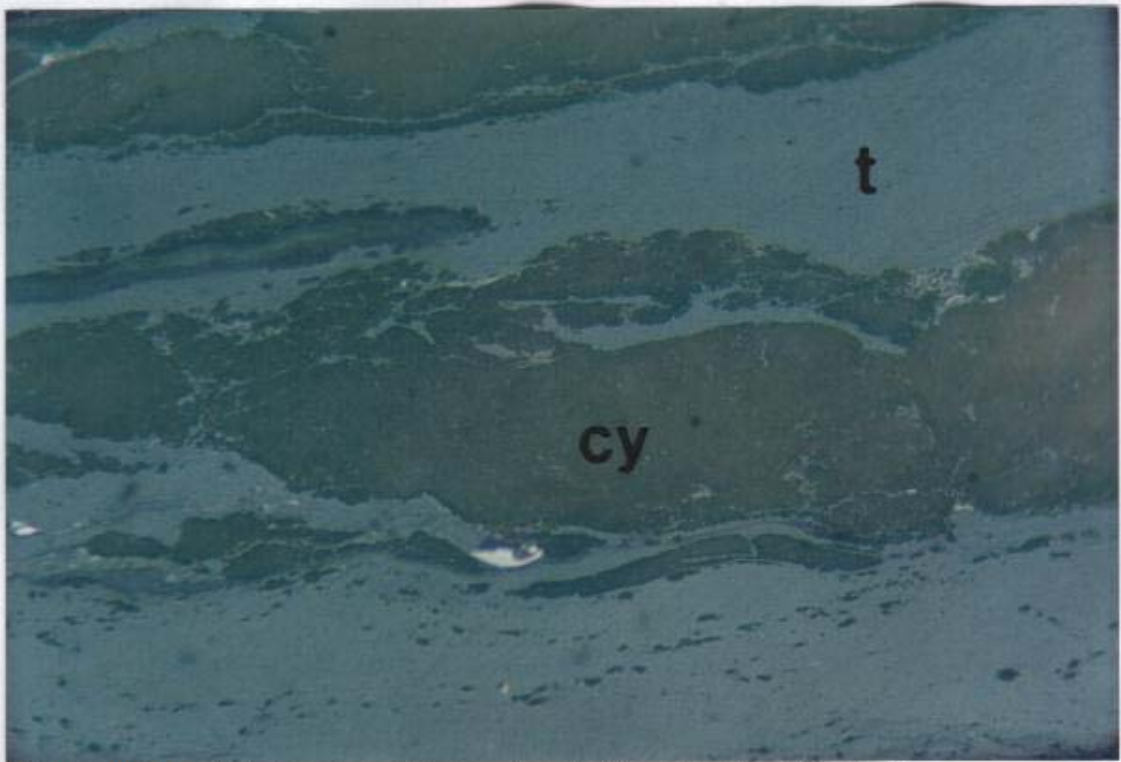


Photograph 3: Thin walled cutinite with a few inertodetrinite and sporinite particles in telovitrinite (Sample No. G15, Bluff seam, 296.27m-298.31m).



Photograph 4: Telovitrinite, cutinite, inertodetrinite and macrinite (bottom) (Sample No. G18, Wright seam, 310.52m-312.37m).

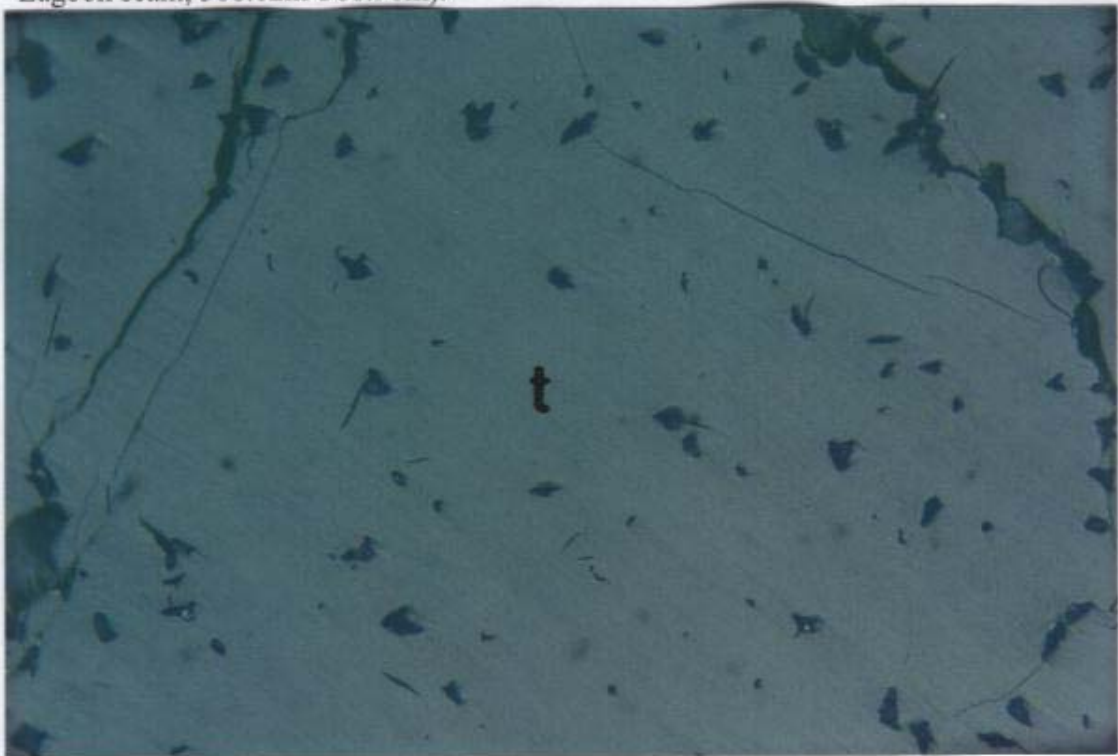


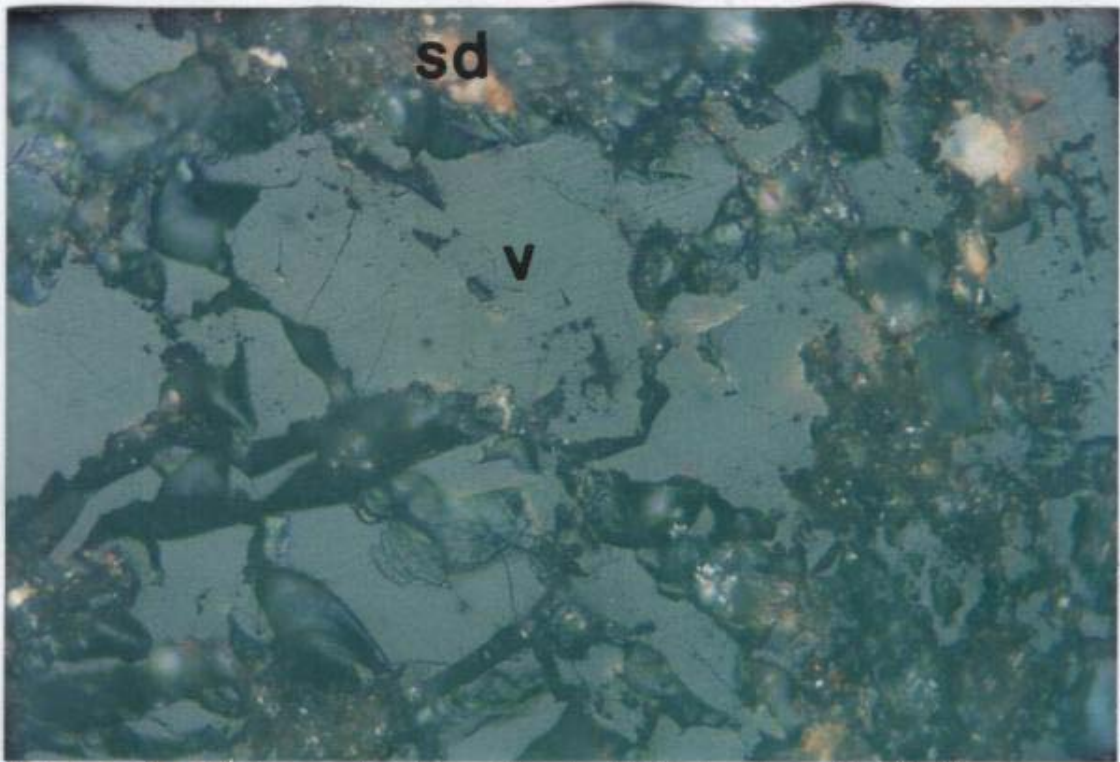


Photograph 5: Telovitrinite with clay bands (Sample No. G6, Cochrane seam, 424.78m-425.75m).



Photograph 6: Pitted and cracked telovitrinite without any inclusions. This sample is slightly oxidised and thus, polished poorly (Sample No. G20, Lagoon seam, 368.12m-368.90m).





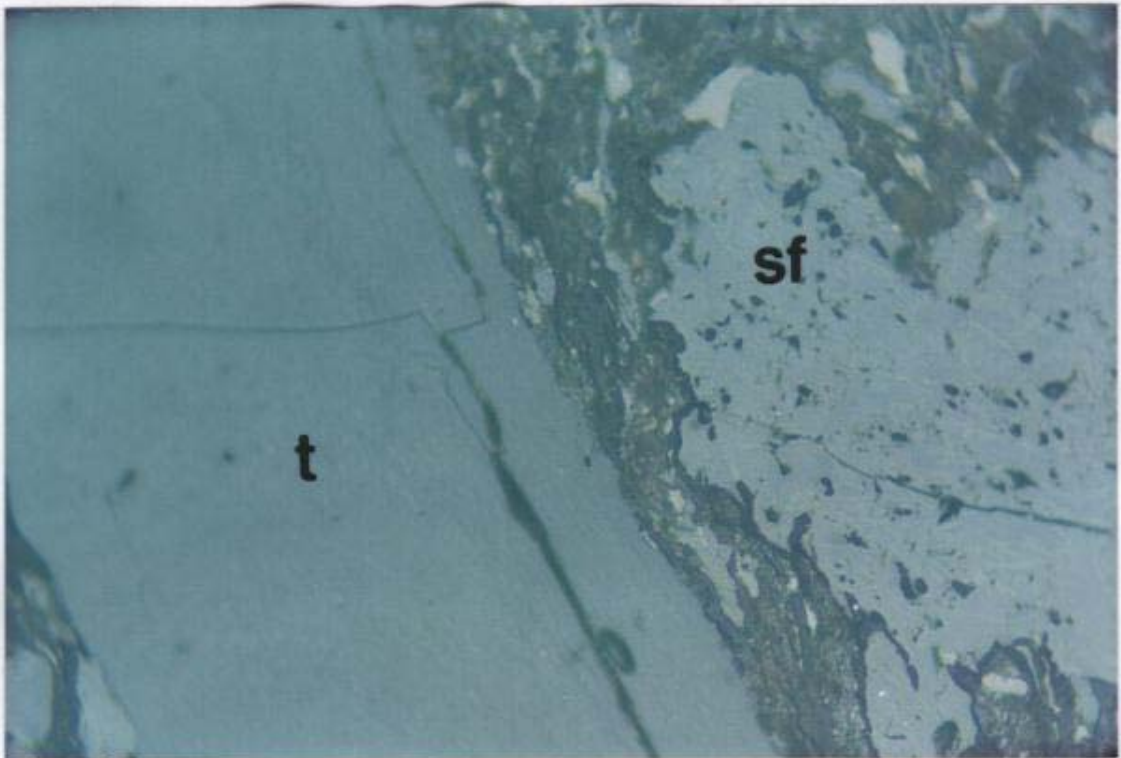
Photograph 7: Broken and partly oxidised vitrinite in clay with siderite groundmass (Sample No. G39, Cochrane seam, 528.13m-529.40m).

0 mm 0.0125

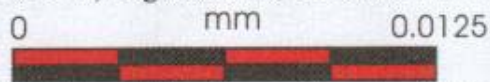


Photograph 8: Gelovitrinite rounded bodies with thin cracks that resemble fish scale (Sample No. G36, Bergin seam, 418.92m-419.82m).

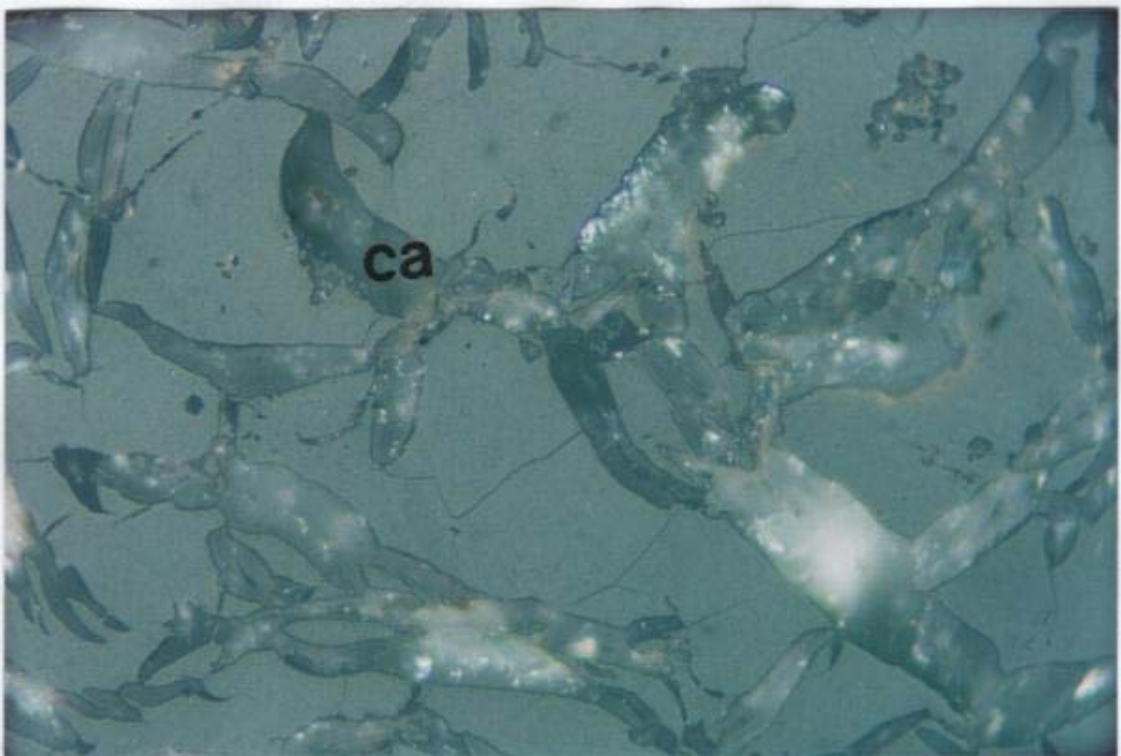


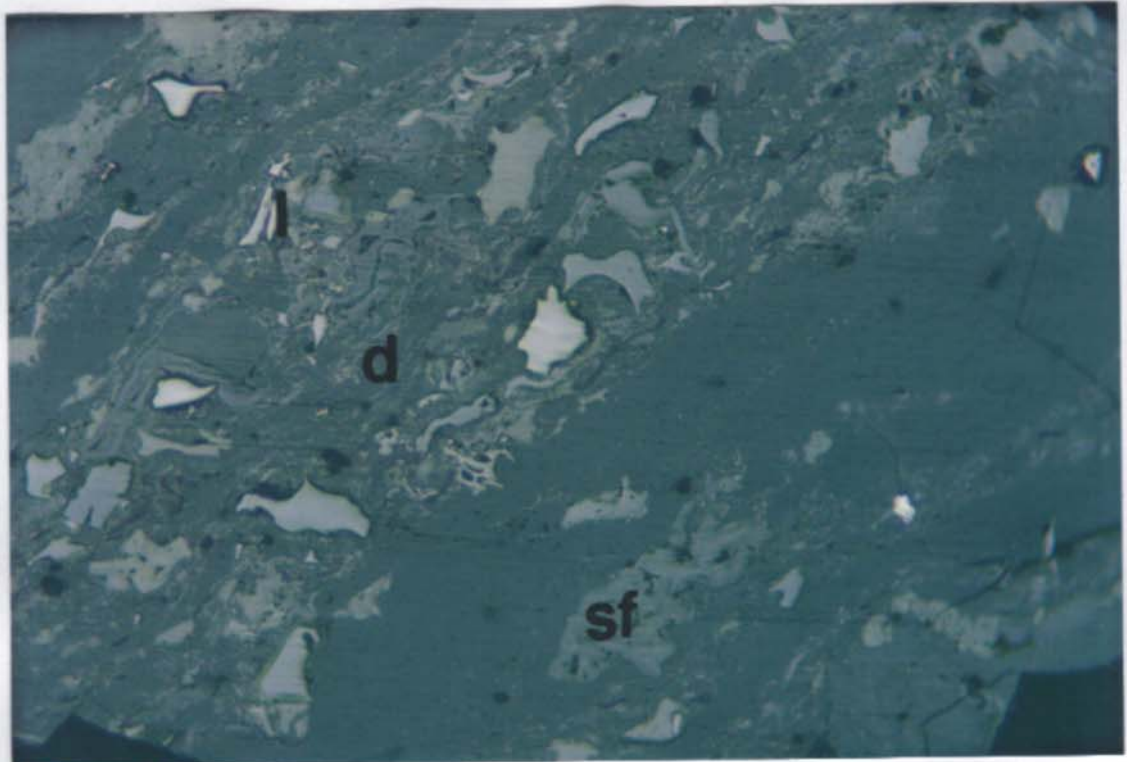


Photograph 9: Telovitrinite (left), semifusinite (right), and cutinite in clay groundmass (Sample No. G21, Lagoon seam, 368.90m-369.97m).



Photograph 10: Fibrous calcite filling fissures in telovitrinite (Sample No. G26, Striped Bacon-Rob Roy seam, 424.86m-426.43m).

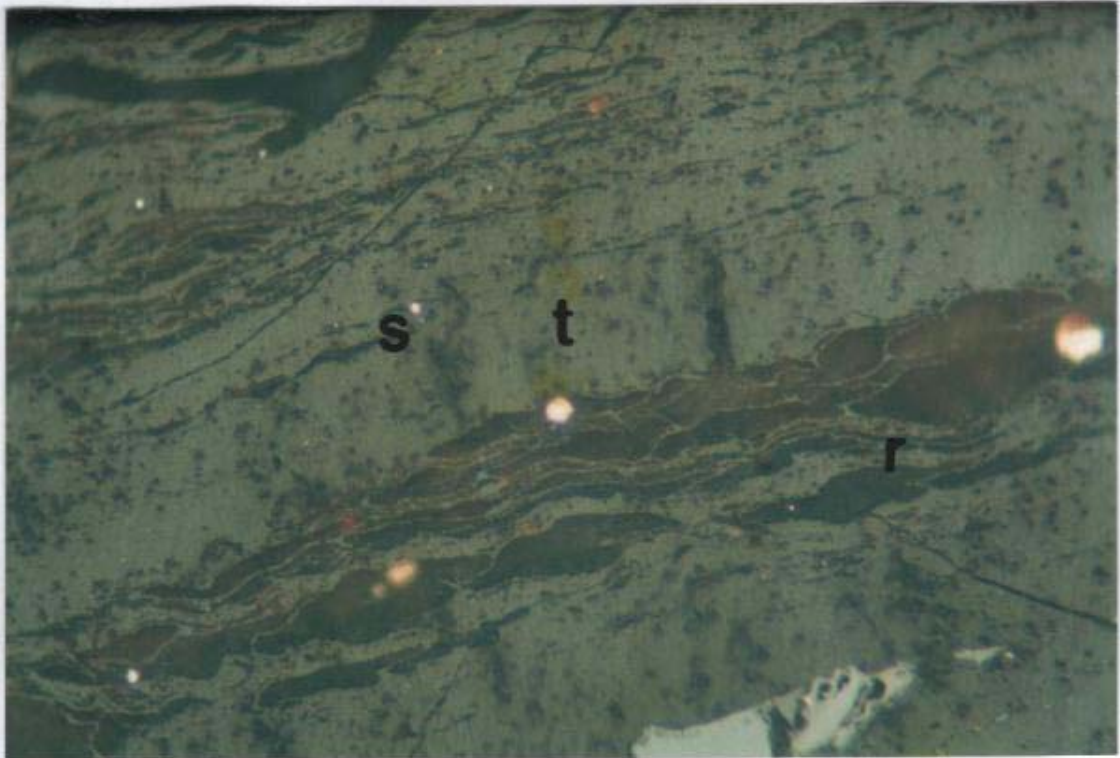




Photograph 11: Detrovitrinite with inertodetrinite and semifusinite (Sample No. G12, Waterstown seam, 43.86m-45.89m).



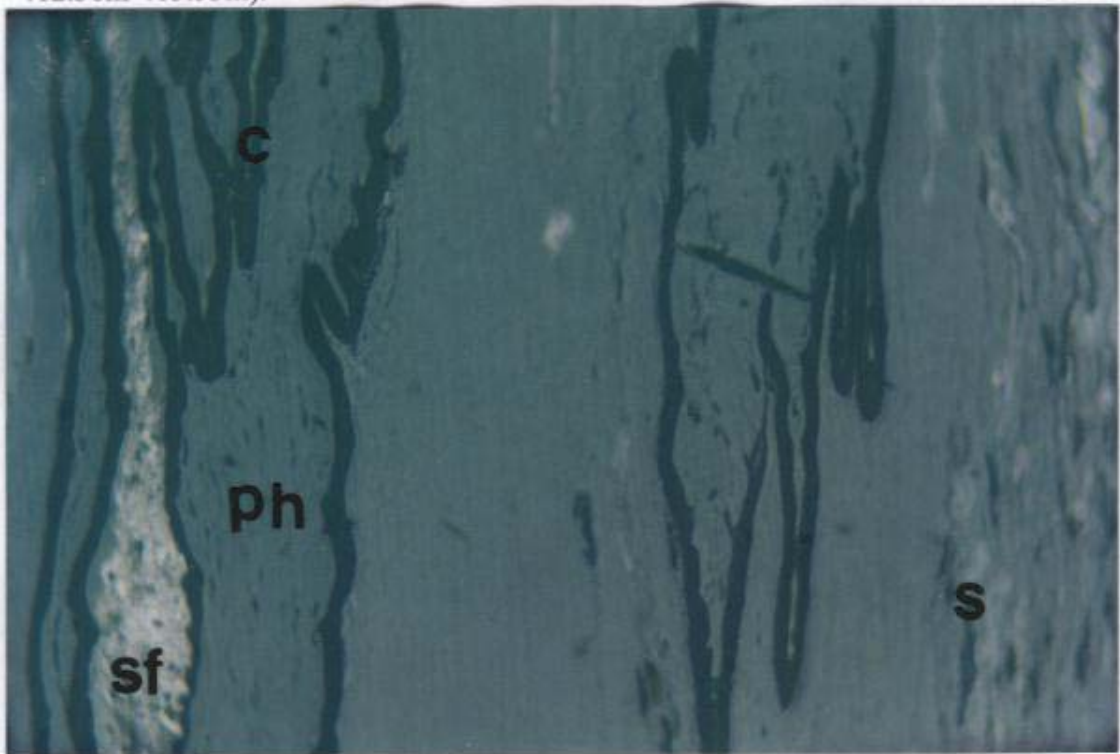
Liptinite Group

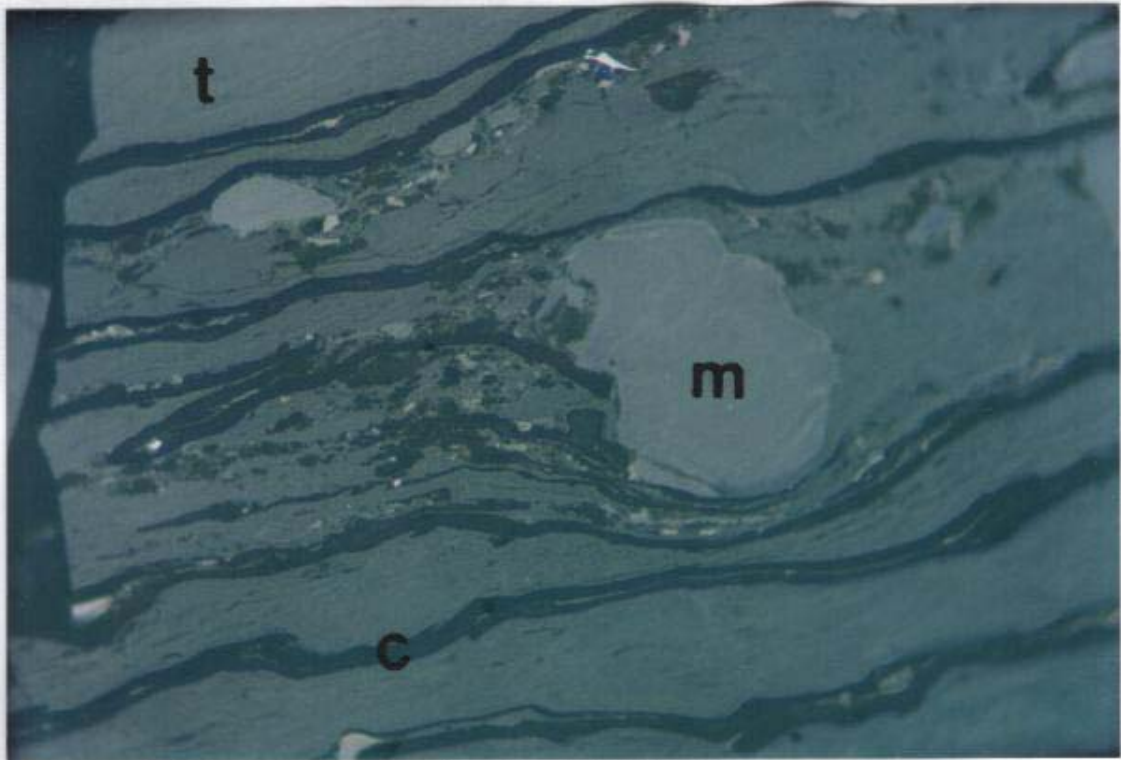


Photograph 12: Resinite bodies with clay and sporinite particles in telovitrinite (Sample No. G9, Tivoli Tops, 211.83m-212.77m).



Photograph 13: Classical high relief cutinite covering a coniferous leaf between phyllovitrinite with semifusinite (left) and sporinite (right). Telovitrinite shows weak cell structures (Sample No. G33, Bergin seam, 412.36m-413.53m).



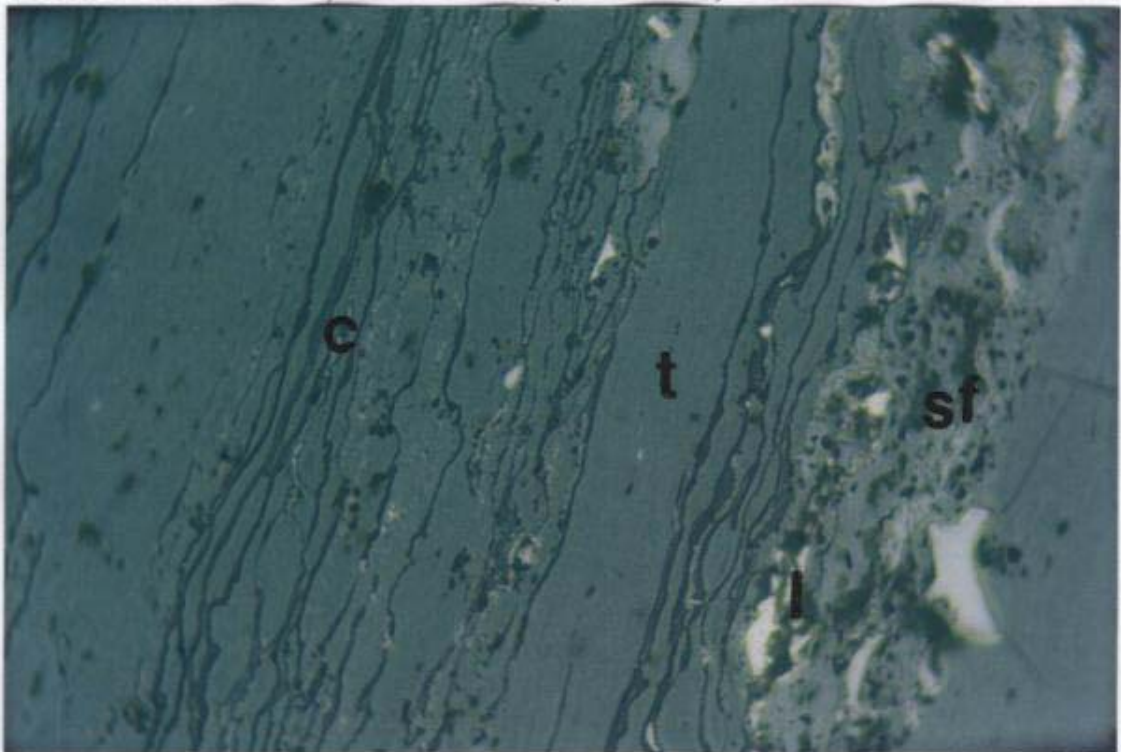


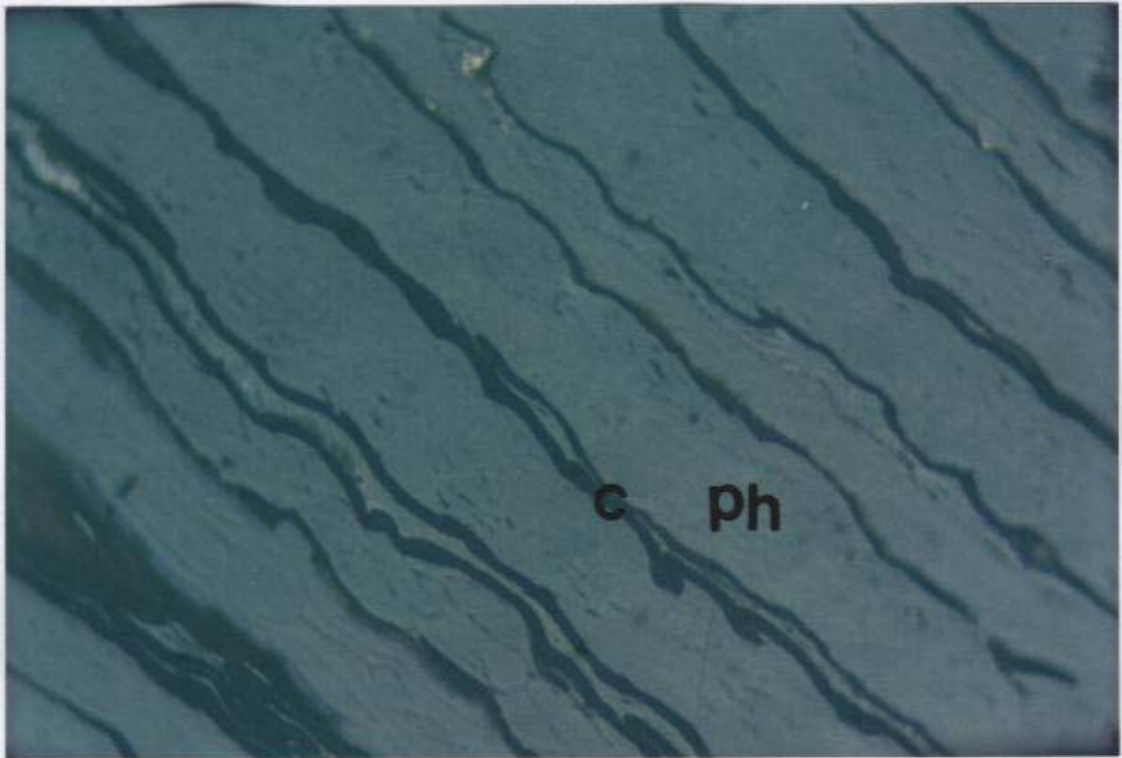
Photograph 14: Cutinite and minor inertodetrinite in telovitrinite with macrinite (centre) in the form of oxidised patches of humic collides (corpomacrinite) (After Diessel, 1992). Note some compression structure around the macrinite (Sample No. G28, Fourfoot seam, 398.04m-398.99m).

0 mm 0.0125



Photograph 15: Cutinite in telovitrinite with thin cell walls, and semifusinite with inertodetrinite (right) (Sample No. G1, North Ipswich – Haighmor and Moreton Extended mines, Tivoli Formation, coal as sold).

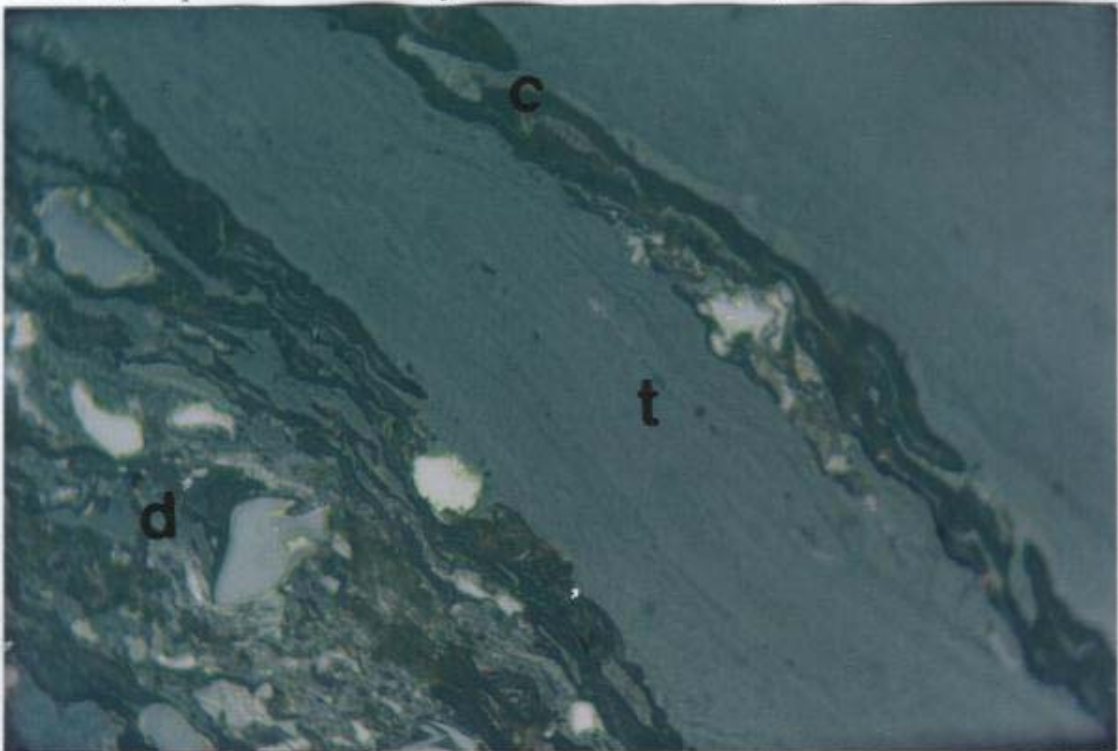


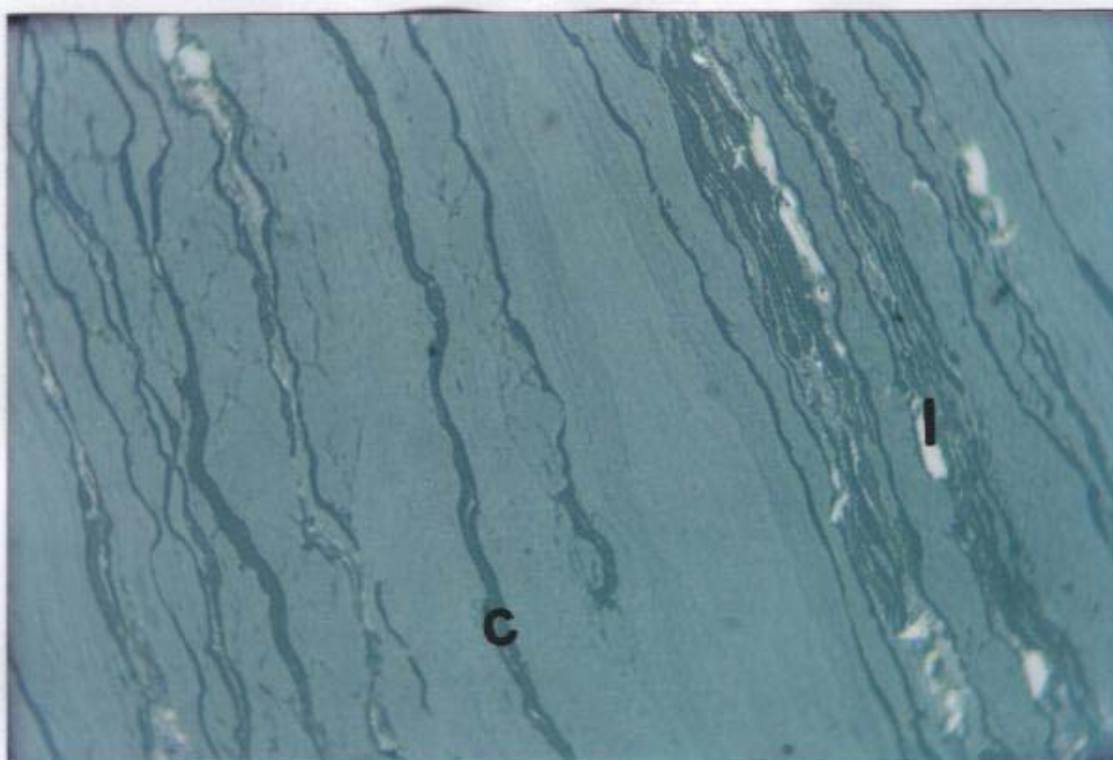


Photograph 16: Abundant cutinite in phyllovitrinite showing thin cell walls (similar to cuticle on a reed) (Sample No. G23, Lagoon seam, 371.48m-372.63m).



Photograph 17: Telovitrinite (with cell structure), cutinite, and detrovitrinite containing broken cutinite (liptodetrinite), inertodetrinite, and clay (Sample No. G25, Striped Bacon – Rob Roy seam, 423.95m-424.86m)



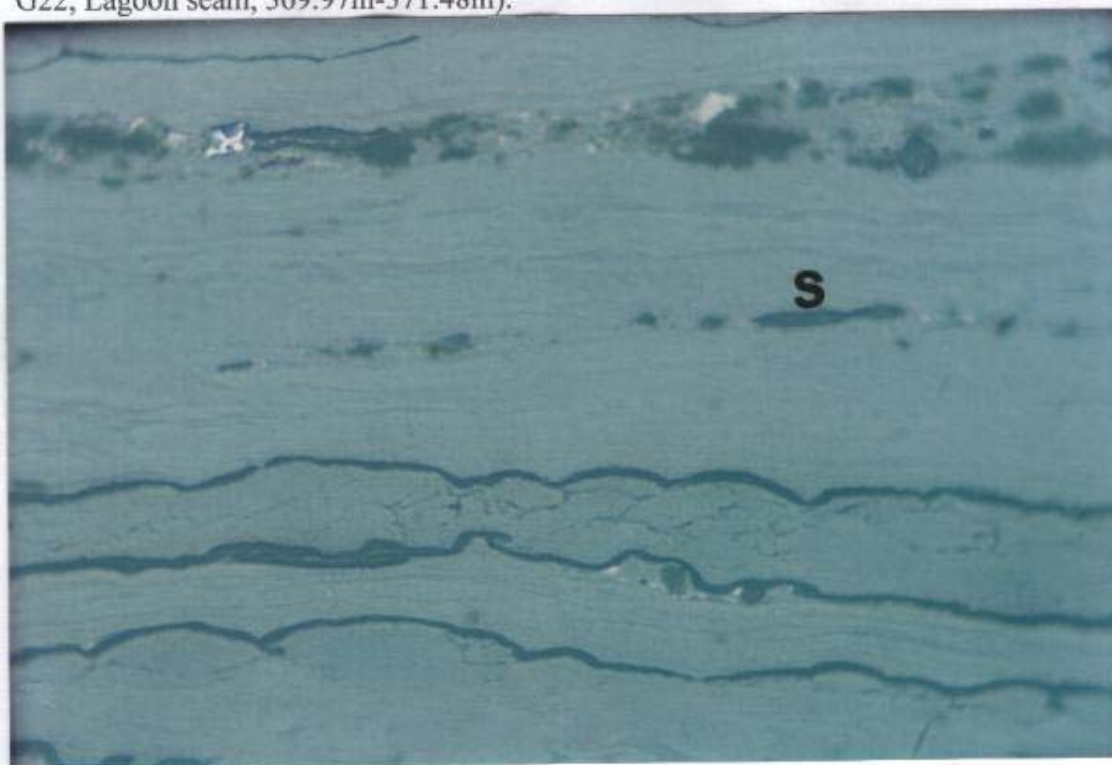


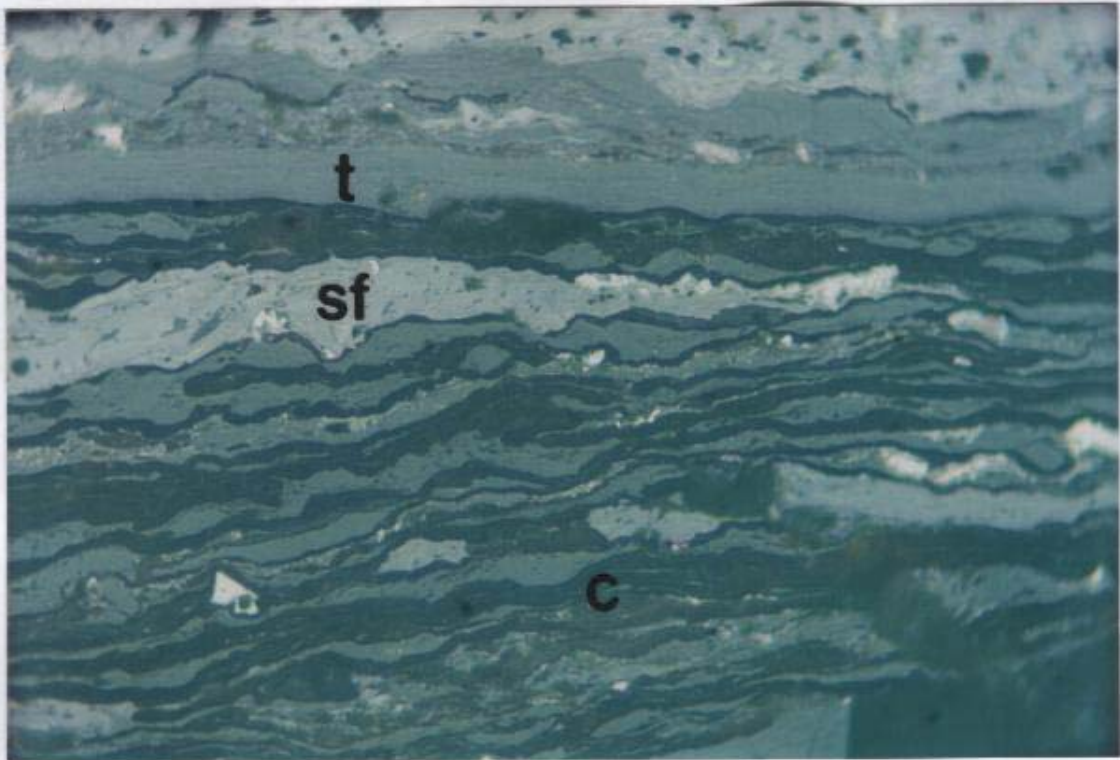
Photograph 18: Thin walled cutinite in telovitrinite (with faint cell walls, possibly resinite), and minor inertodetrinite and clay (Sample No. G30, Fourfoot seam, 399.93m-400.74m).

0 mm 0.0125



Photograph 19: Cutinite with minor sporinite and clay particles in telovitrinite ground matrix showing thin cell walls of resinite (Sample No. G22, Lagoon seam, 369.97m-371.48m).

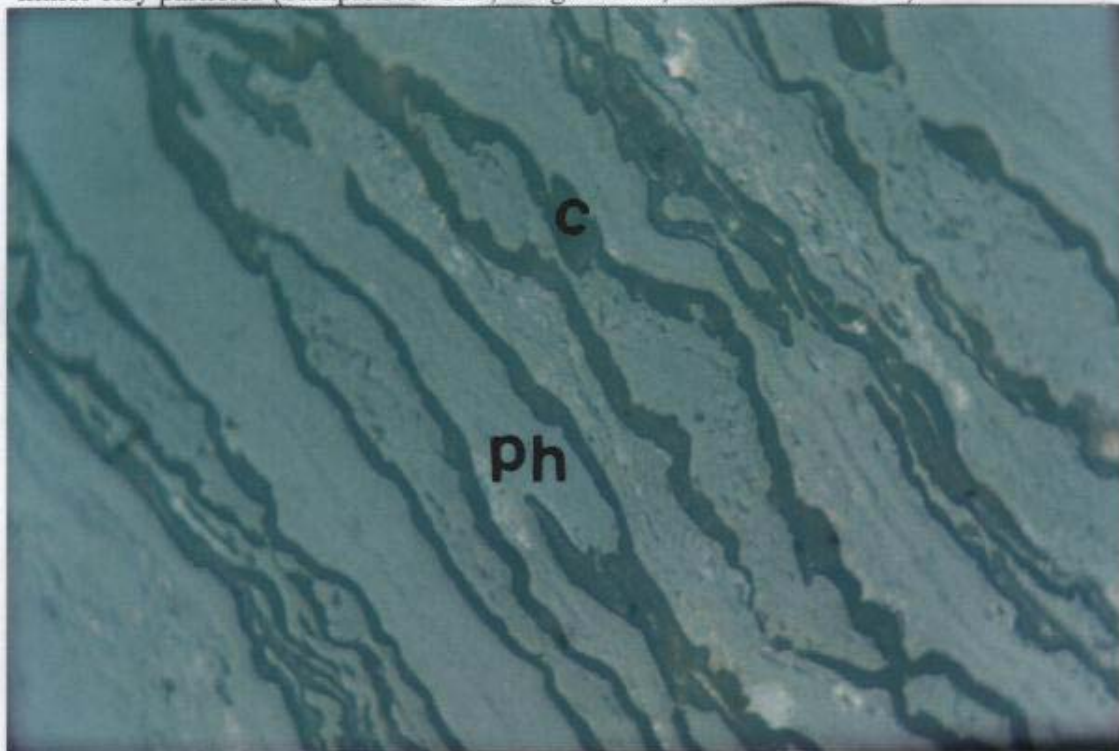


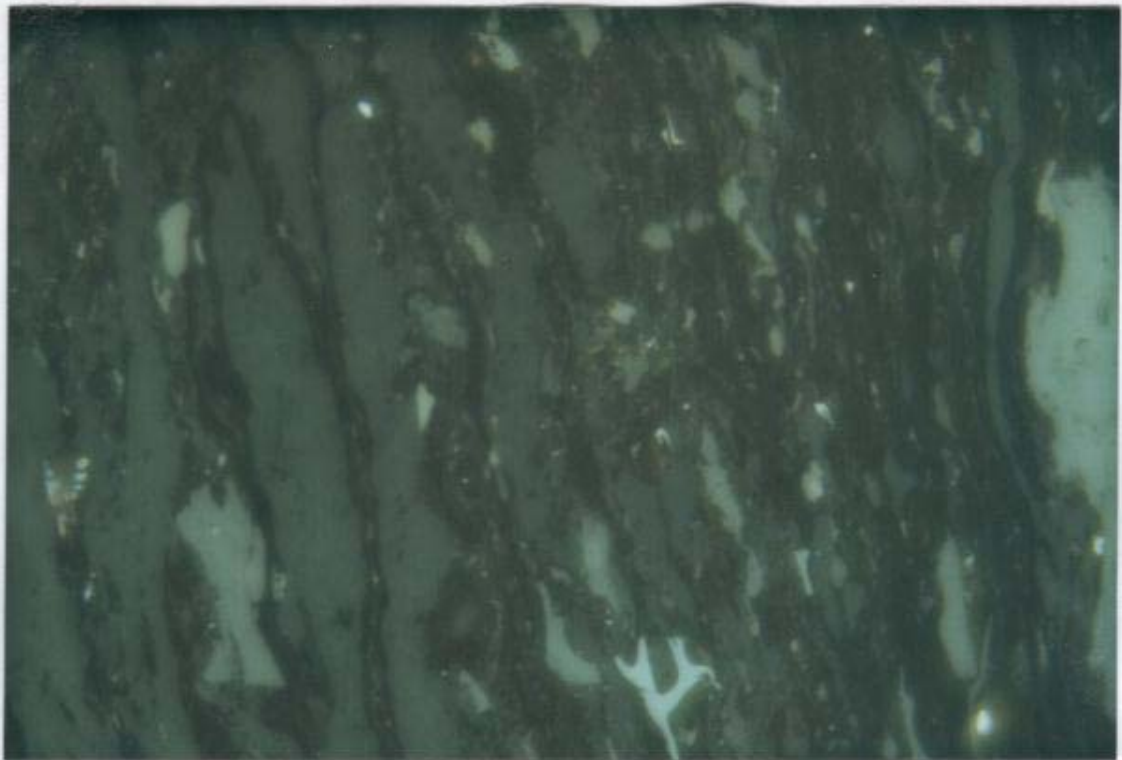


Photograph 20: Abundant cutinite and semifusinite showing different reflectance (degradofusinite, after Beeston, 1987), in detrovitrinite groundmass with telovitrinite layers (Sample No. G15, Bluff seam, 296.27m-298.31m).

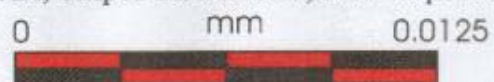


Photograph 21: Cutinite in phyllovitrinite with weak cell structures and minor clay particles (Sample No. G35, Bergin seam, 417.93m-418.92m)

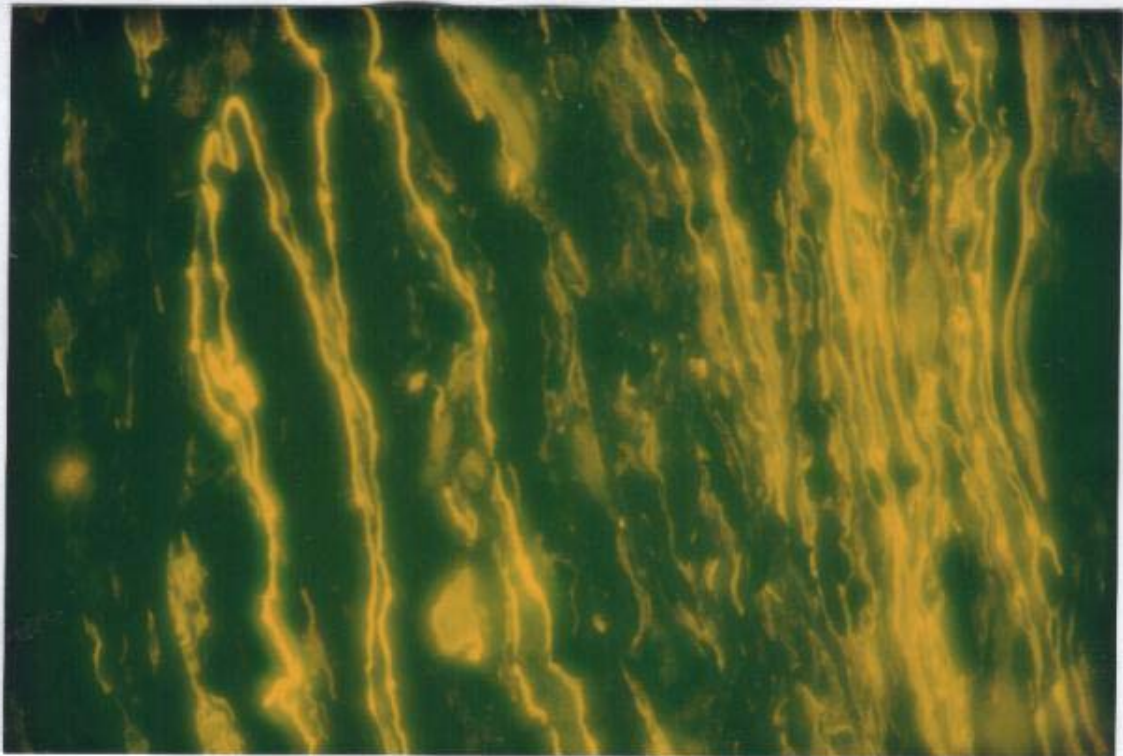


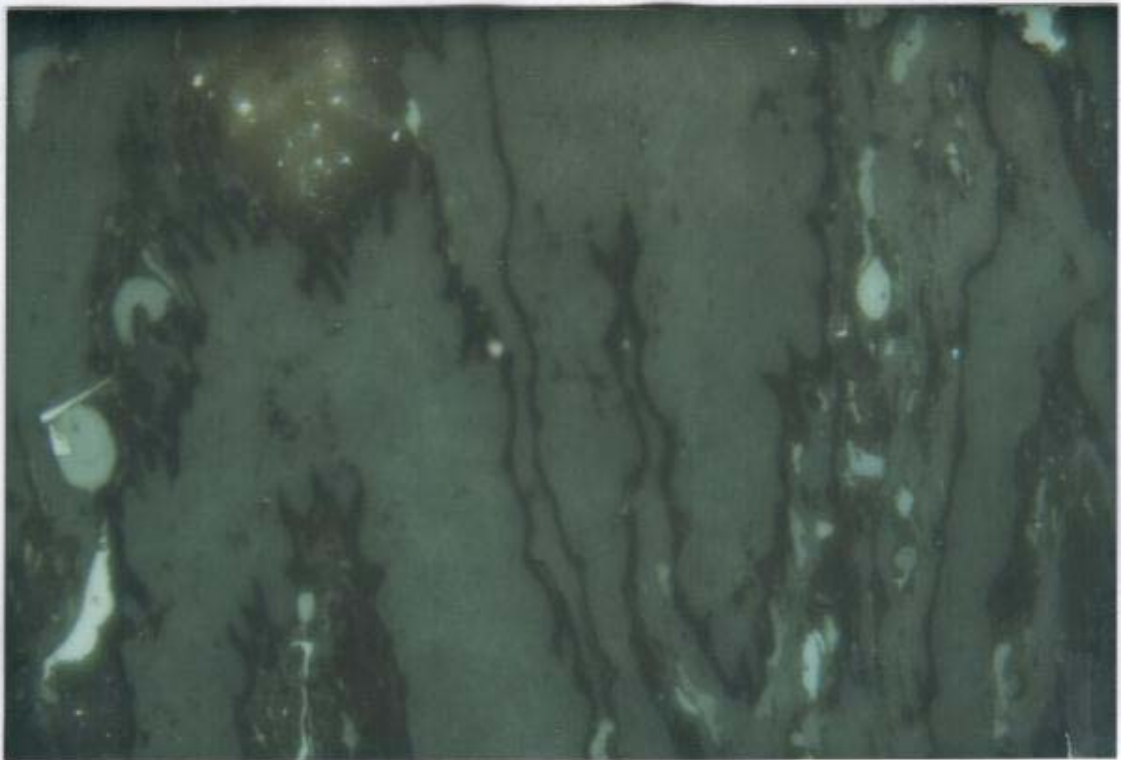


Photograph 22: Densely packed cutinite (right) showing low reflectance under normal light in matrix of detrovitrinite with inertodetrinite and minor clay (Sample No. 1AA, Striped Bacon seam, New Hope No. 7).



Photograph 23: Same sample under blue light, cutinite displays high fluorescence intensity.

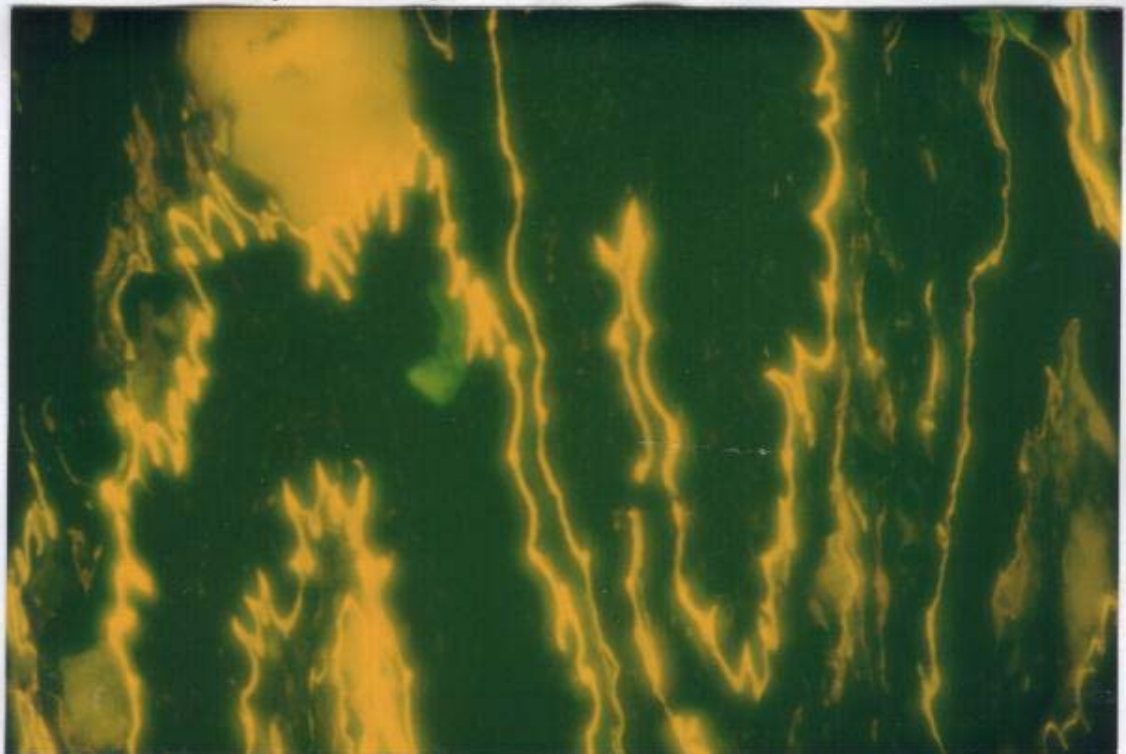


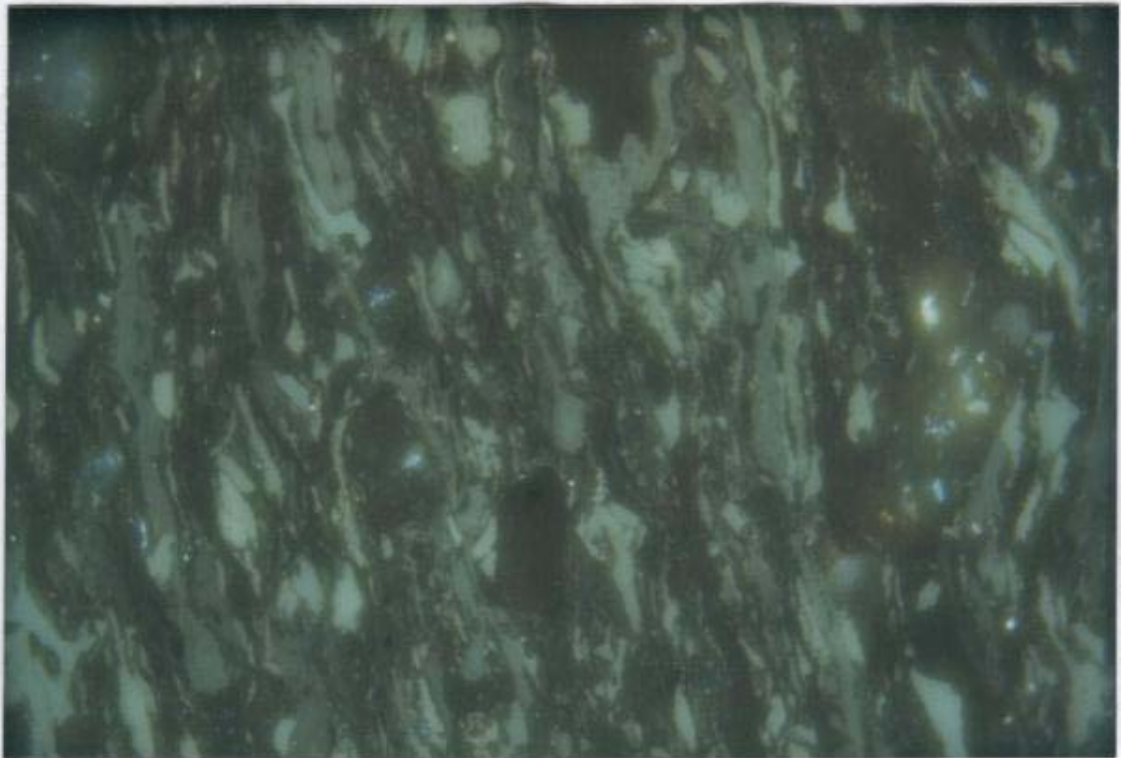


Photograph 24: Classical cutinite (cross section through the edge of a leaf cuticle), in phyllovitrinite with inertodetrinite and clay (Sample No. 1AA, Striped Bacon seam, New Hope No. 7).

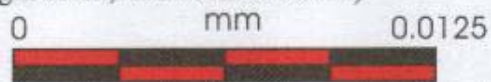


Photograph 25: Same sample viewed under blue light, cutinite shows high fluorescence intensity and the clay shows moderate fluorescence intensity.

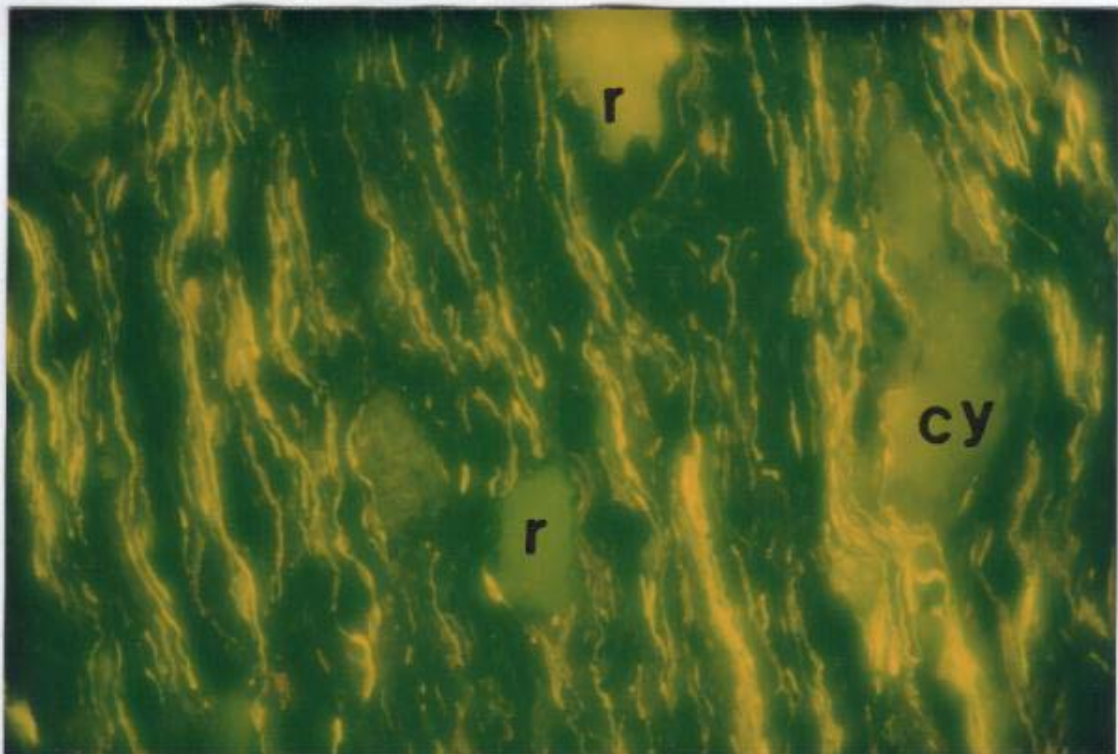




Photograph 26: Low reflectance thin walled cutinite and sporinite in detrovitrinite with inertodetrinite, resinite and clay under normal light (Sample No. G34, Bergin seam, 416.59m-417.93m).



Photograph 27: Same sample under blue light showing densely packed cutinite and sporinite (thin exines), resinite and clay.

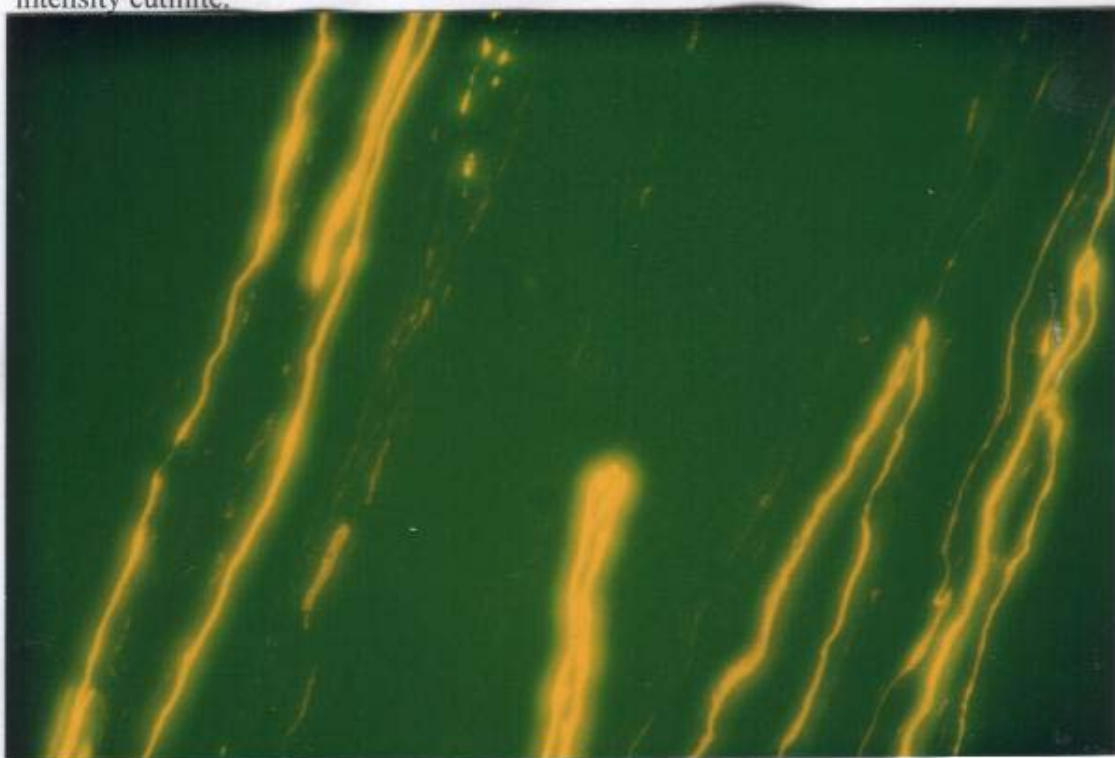


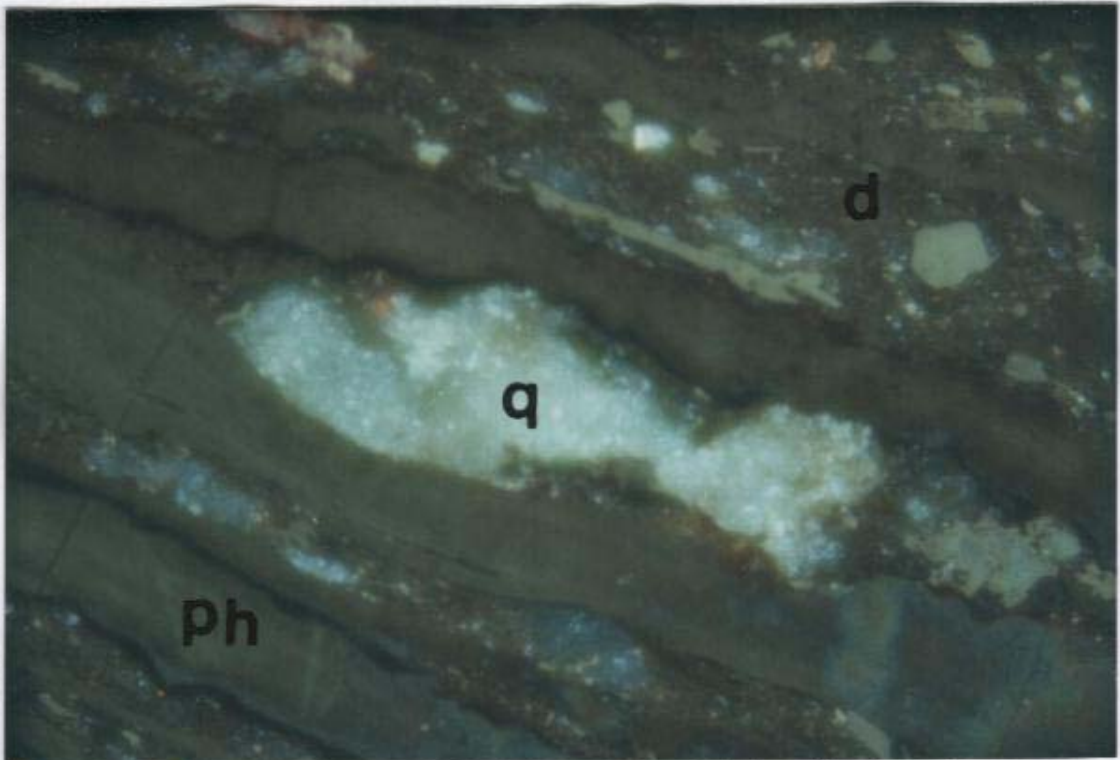


Photograph 28: High relief cutinite in telovitrinite with suberinite with thin cell walls in the middle of the photograph), which shows similar appearance to resinite but no fluorescence after blue-light excitation (Sample No. G34, Bergin seam, 416.59m-417.93m).



Photograph 29: Same sample under blue light displaying high fluorescence intensity cutinite.

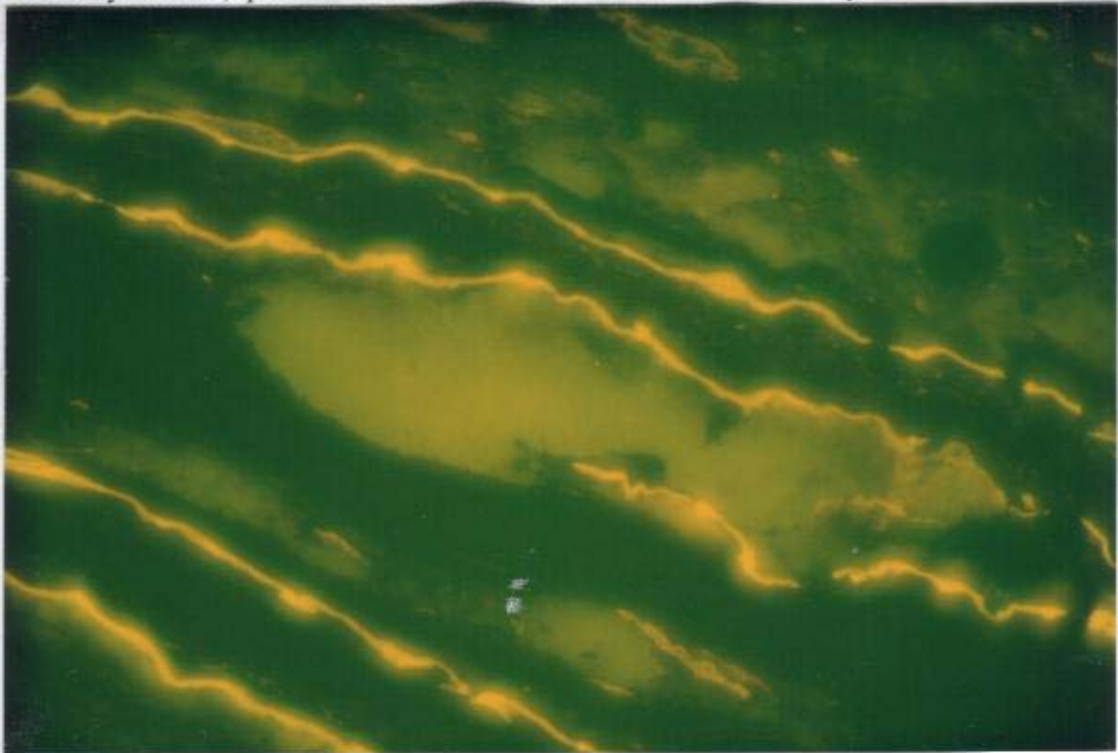


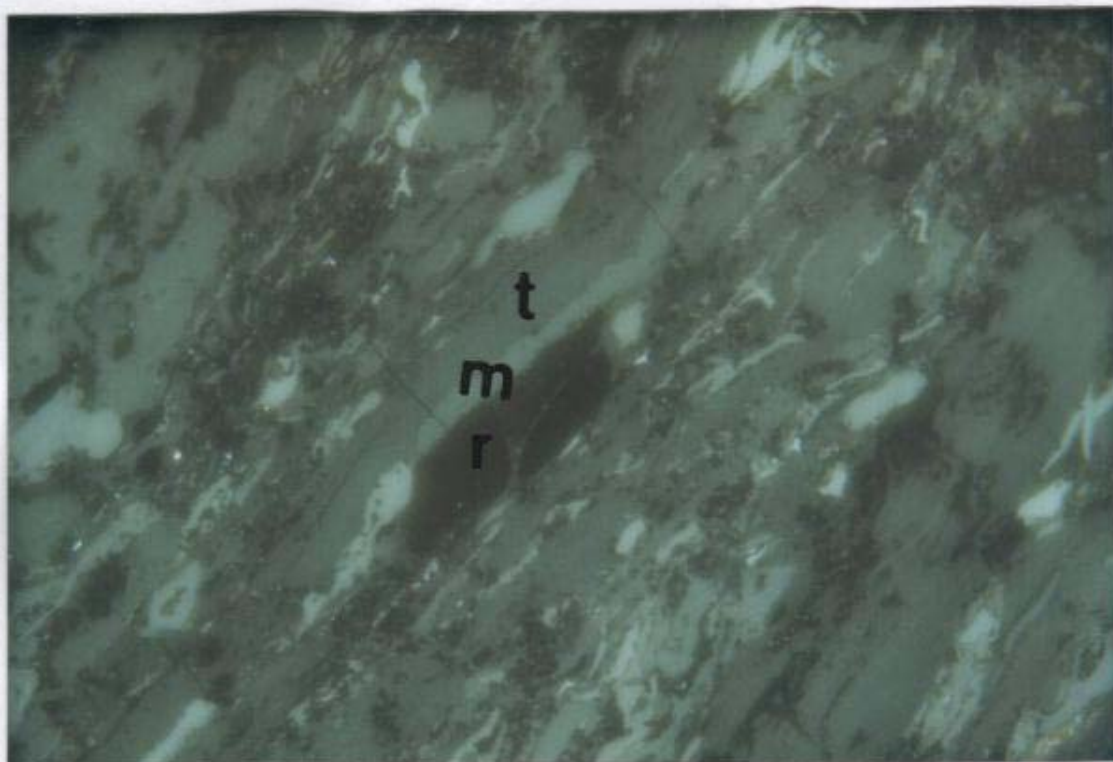


Photograph 30: Cutinite with phyllovitrinite and detrovitrinite with clay and quartz (Sample No. G34, Bergin seam, 416.59m-417.93m).

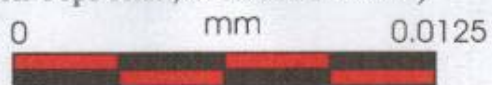


Photograph 31: Same sample under blue light with high fluorescence intensity cutinite, quartz also shows moderate fluorescence intensity.



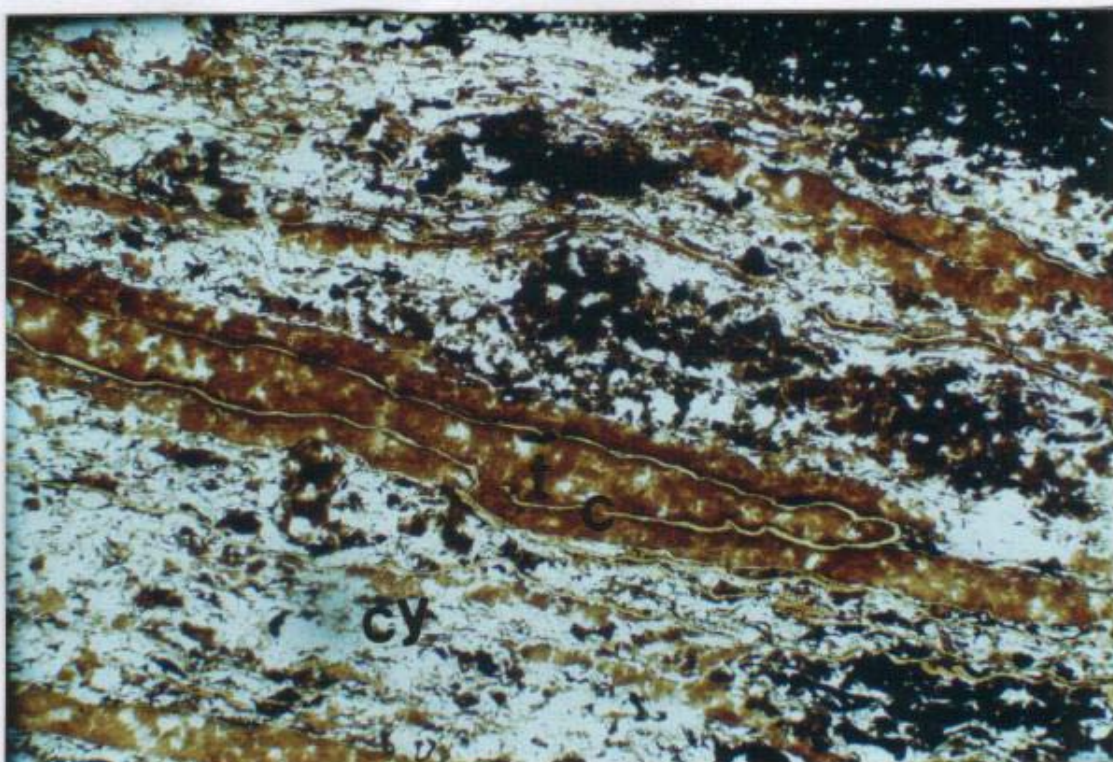


Photograph 32: Dark rounded resinite bodies (middle) in detrovitrinite with thin semifusinite (cf. Macrinite), inertodetrinite and thin telovitrinite layers (Sample No. G9, Tivoli Tops seam, 211.83m-212.77m)

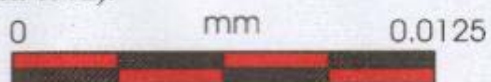


Photograph 33: Resinite bodies show high fluorescence intensity after blue-light excitation.

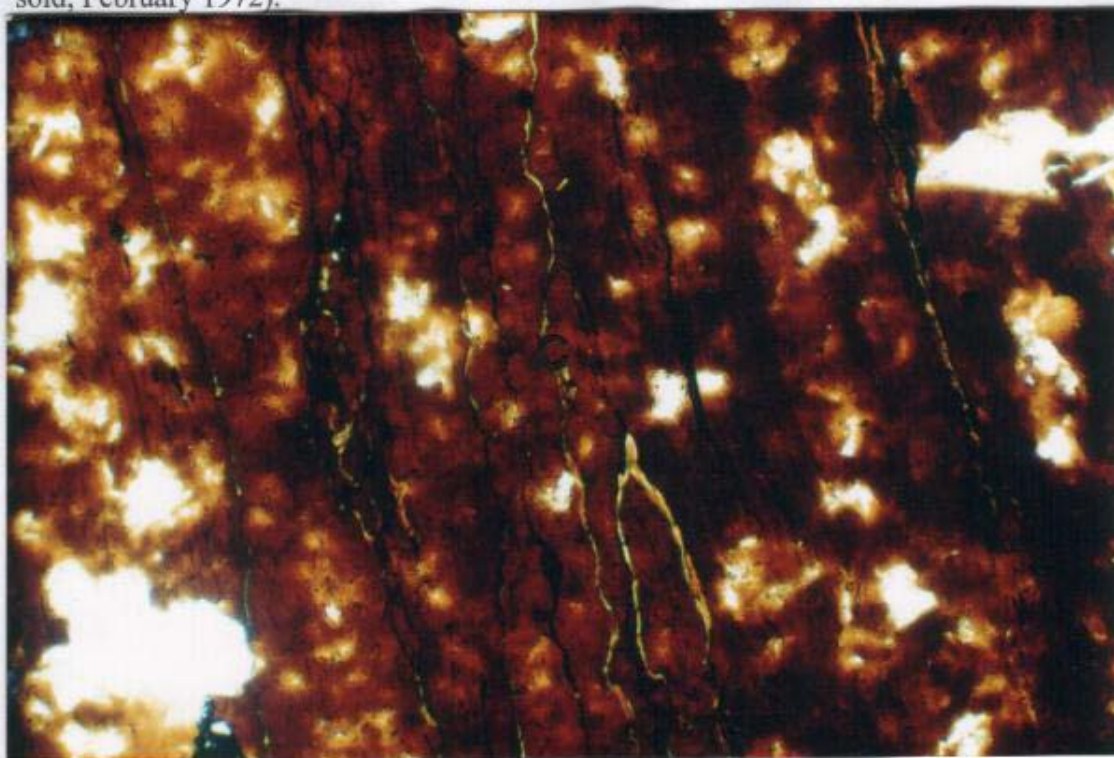




Photograph 34: Cutinite with telovitrinite in clay groundmass (thin section, transmitted light) (Sample No. TH18, Westfalen No. 3 mine, Blackstone Formation-coal as sold, April 1972).

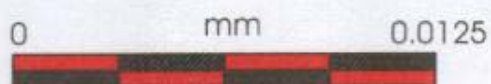


Photograph 35: Cutinite layers in vitrinite (thin section, transmitted light) (Sample No. TH9, Westfalen No. 3 mine, Blackstone Formation-coal as sold, February 1972).

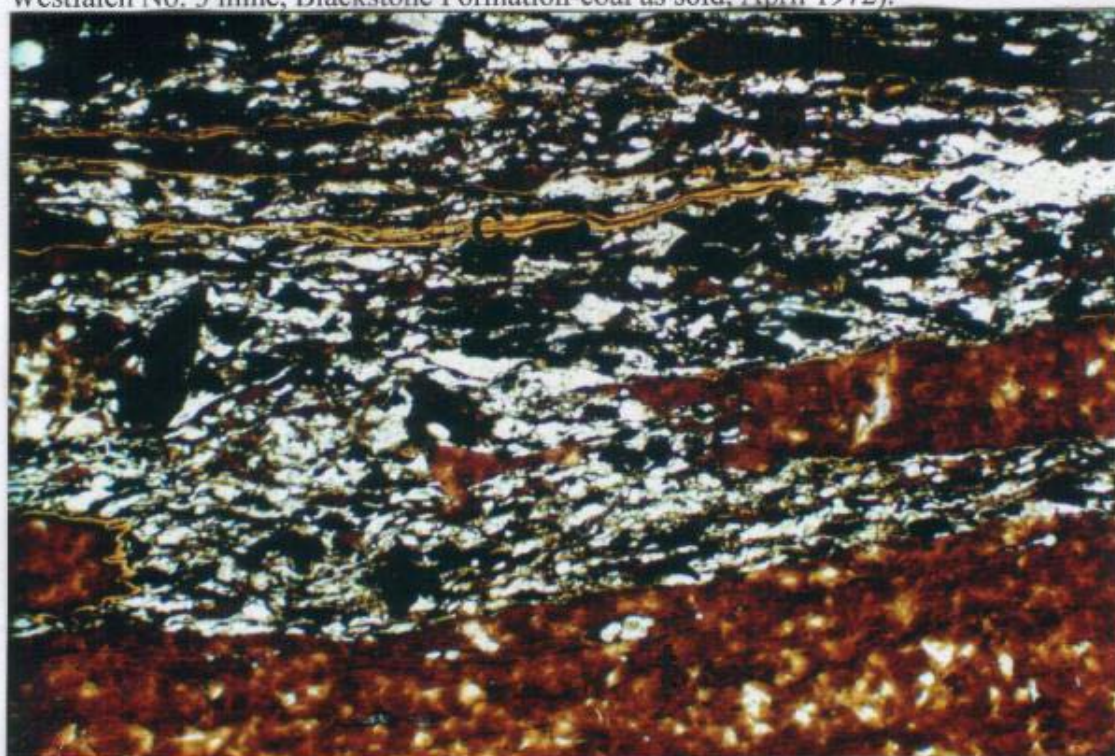




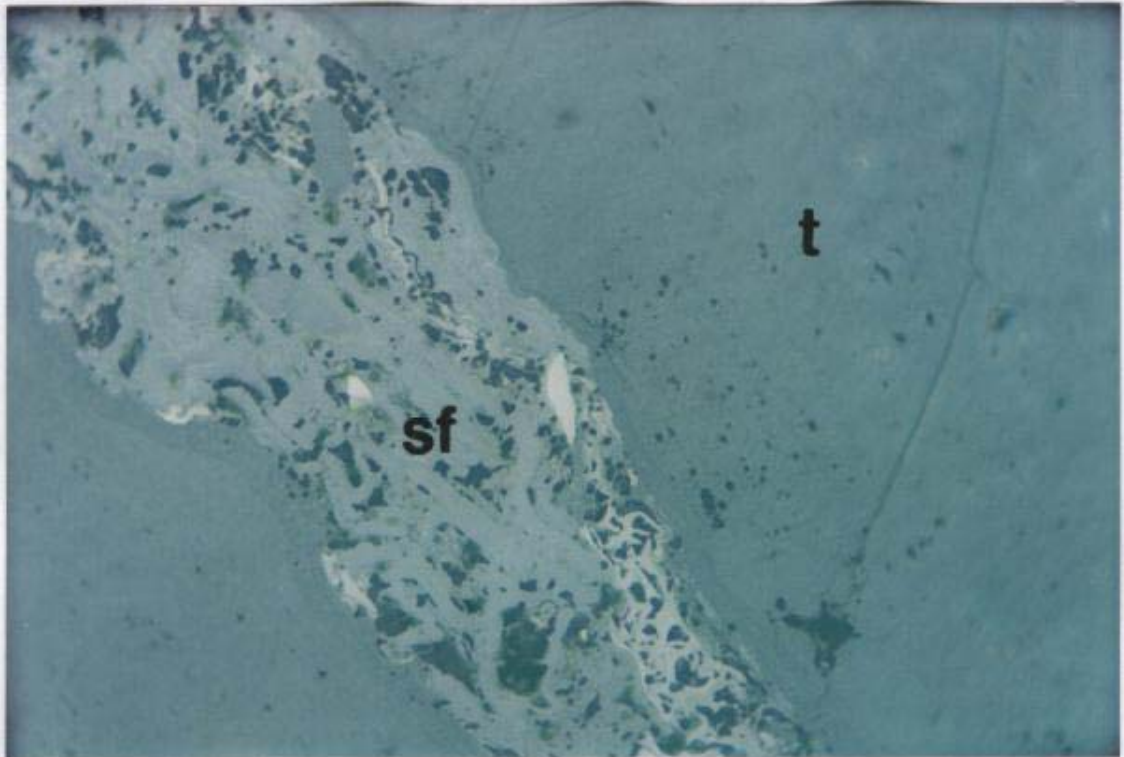
Photograph 36: Clay pellets (CY) in coal (thin section, transmitted light) (Sample No. TH19, Westfalen No. 3 mine, Blackstone Formation-coal as sold, February 1973).



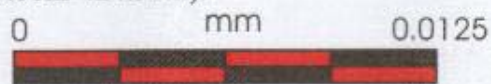
Photograph 37: Cutinite (top), clay, and vitrinite (bottom) in detrovitrinite and clay matrix (thin section, transmitted light) (Sample No. TH18, Westfalen No. 3 mine, Blackstone Formation-coal as sold, April 1972).



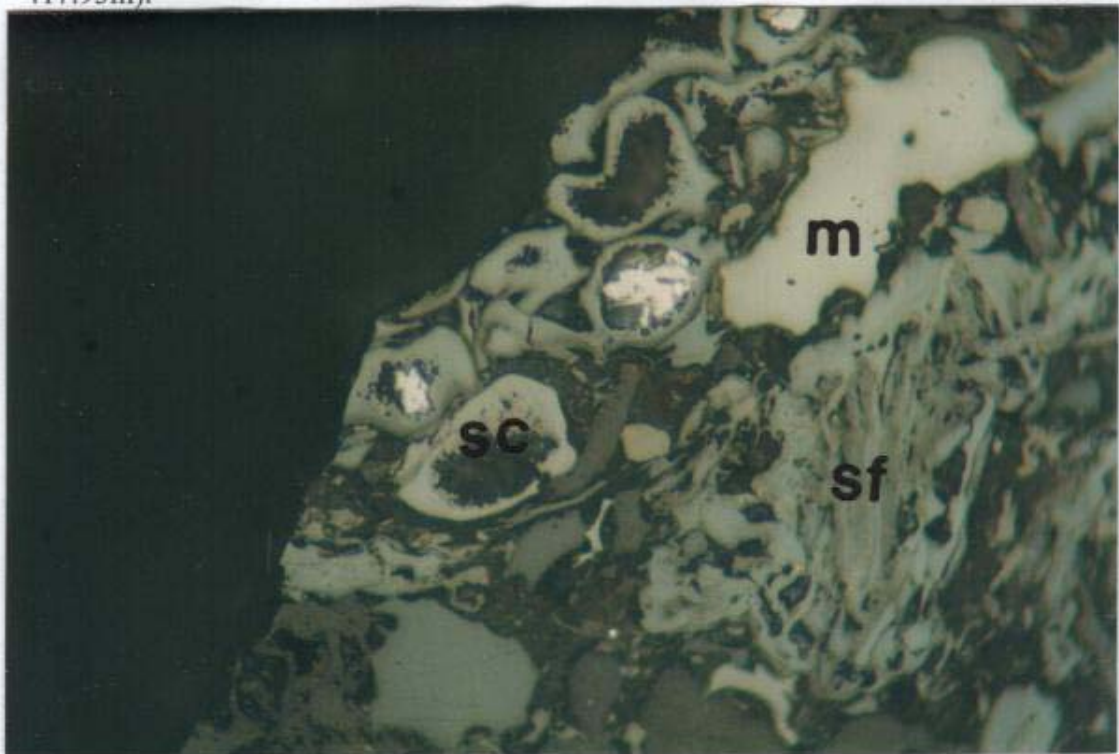
Inertinite Group

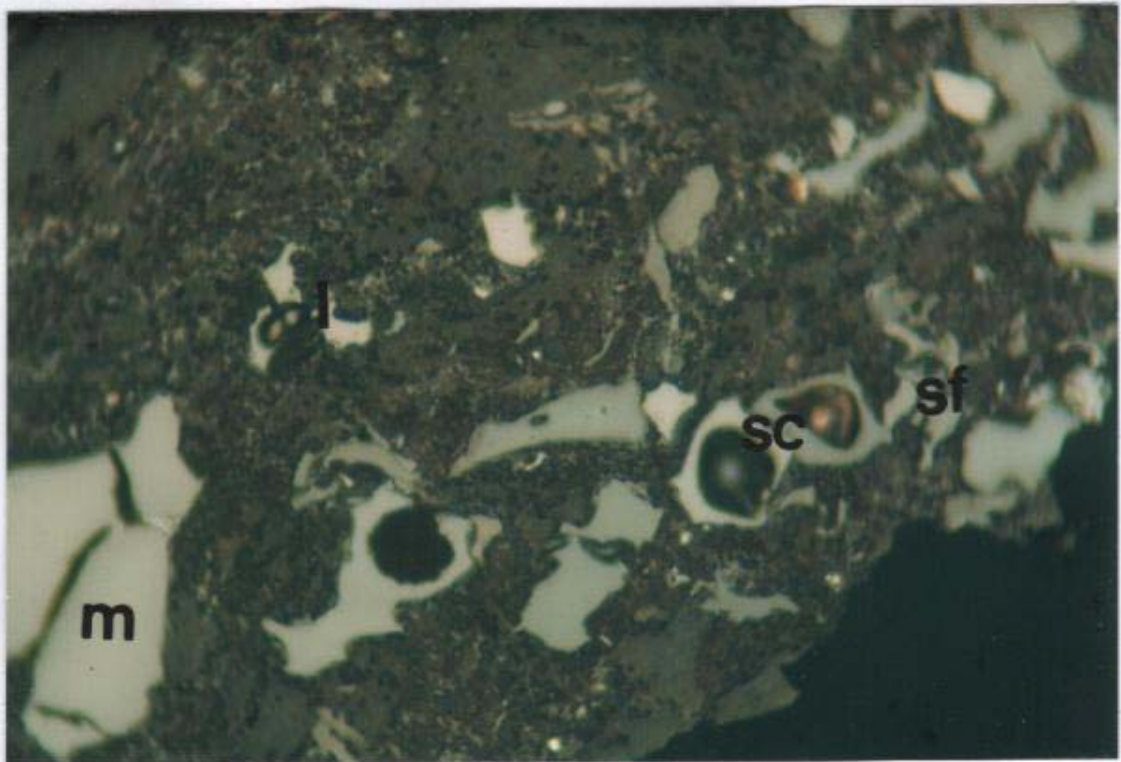


Photograph 38: Semifusinite and telovitrinite with variable reflectance, note a thin transitional zone around the contact with semifusinite (Sample No. G5, Cochrane seam, 423.06m-424.51m).



Photograph 39: Sclerotodetrinite (after Beeston, 1987), macrinite, and semifusinite in detrovitrinite (Sample No. G34, Bergin seam, 416.59m-417.93m).

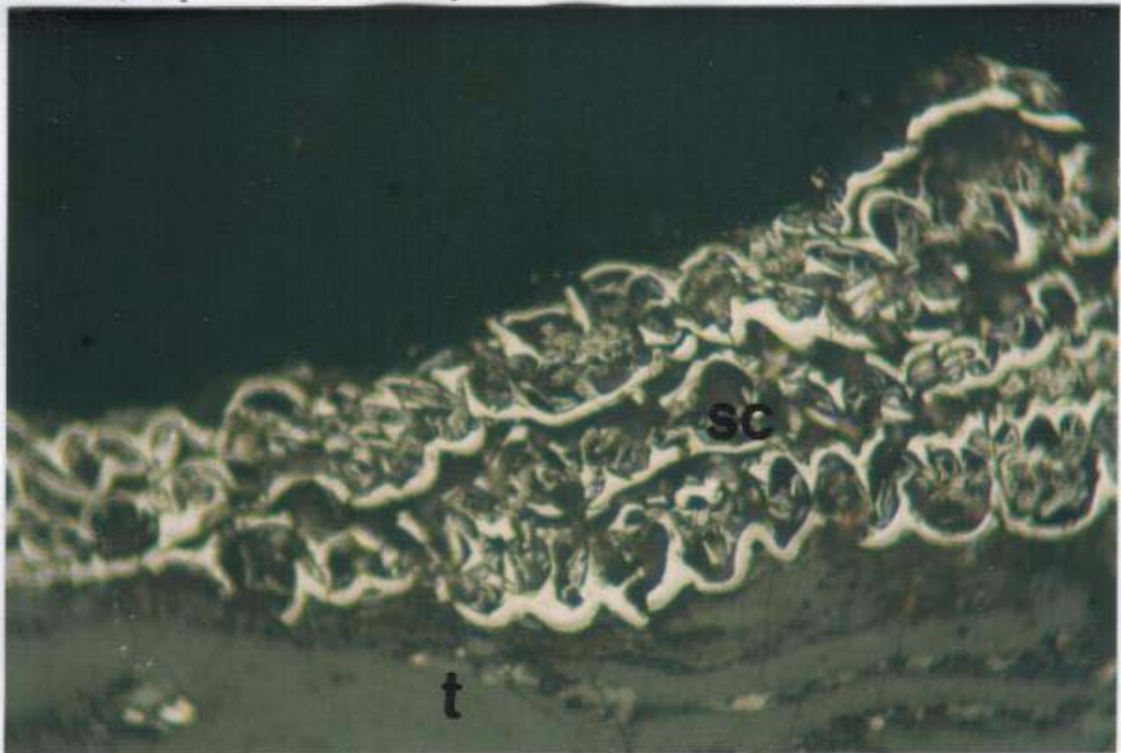


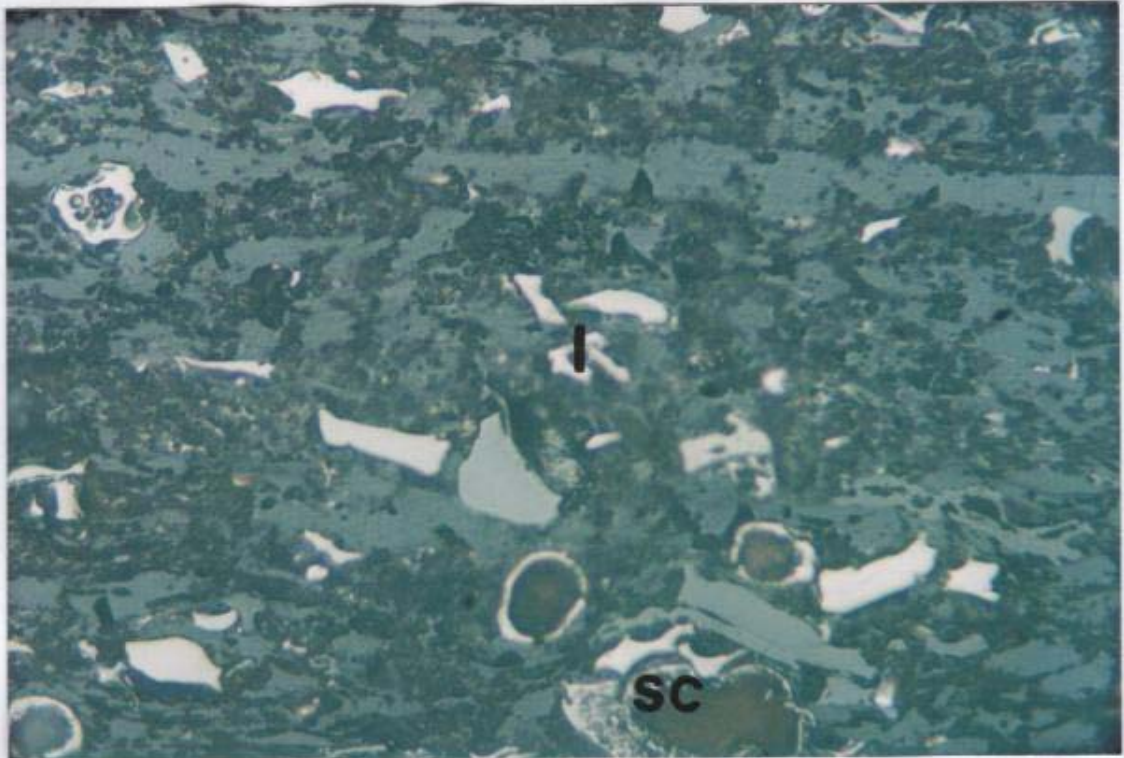


Photograph 40: Open chamber sclerotodetrinite, macrinite, inertodetrinite, and oxidised semifusinite in clay groundmass (Sample No. G9, Tivoli Tops seam, 211.83m-212.77m).



Photograph 41: Open chamber sclerotodetrinite transformed to high relief fusinite (Sample No. G9, Tivoli Tops seam, 211.83m-212.77m).

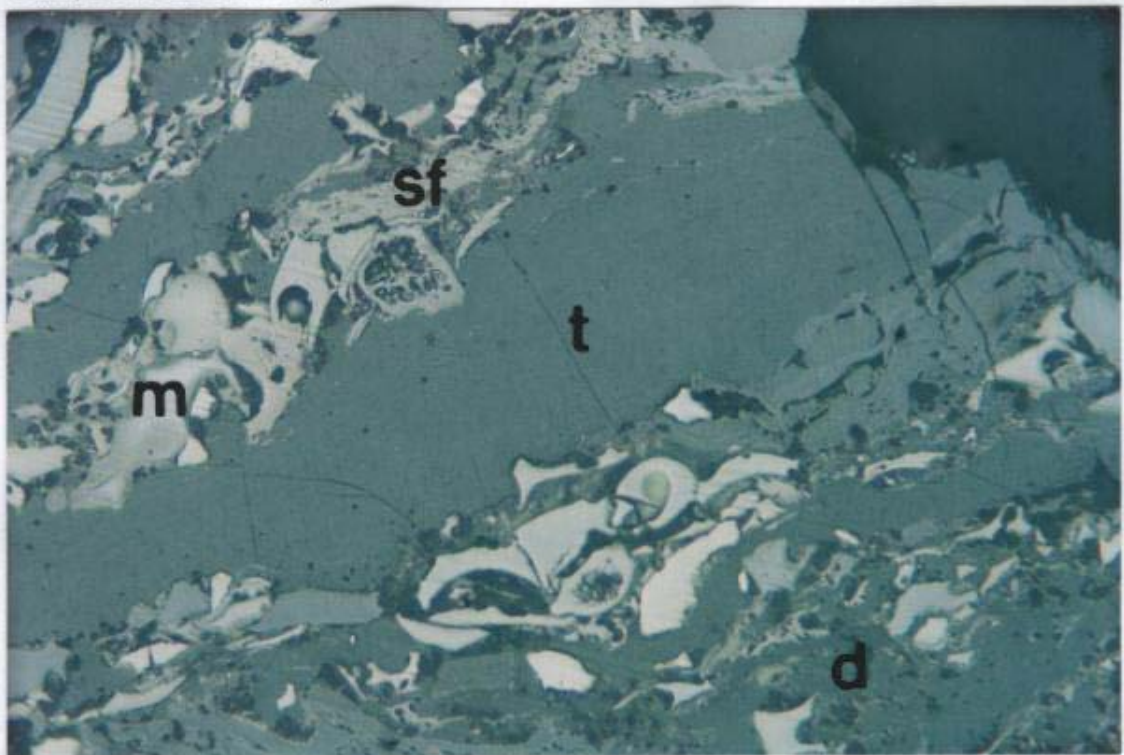


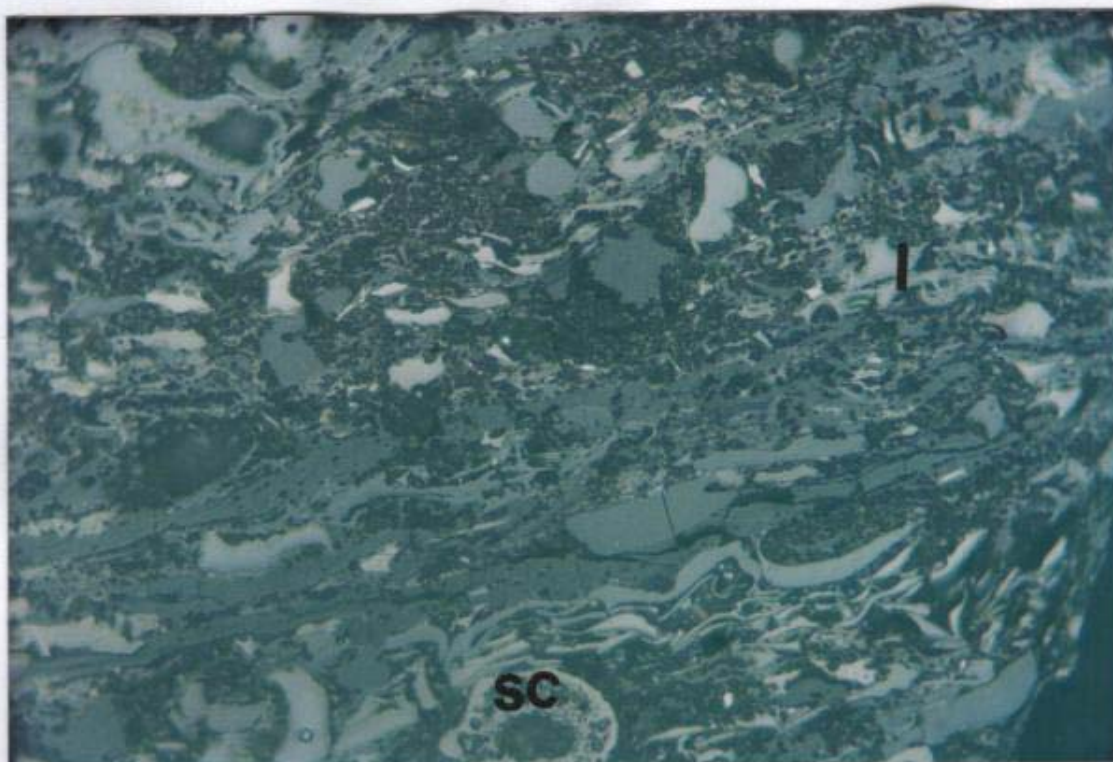


Photograph 42: Open chamber sclerotodetrinite with clay infill, inertodetrinite, and broken pieces of vitrinite in clay (Sample No. G9, Tivoli Tops seam, 211.83m-212.77m).

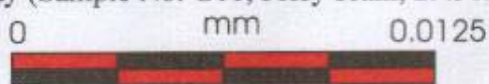


Photograph 43: Sclerotodetrinite, inertodetrinite, semifusinite, and macrinite in detrovitrinite with telovitrinite layers (Sample No. G10, Tivoli Bottoms seam, 213.12m-214.47m).

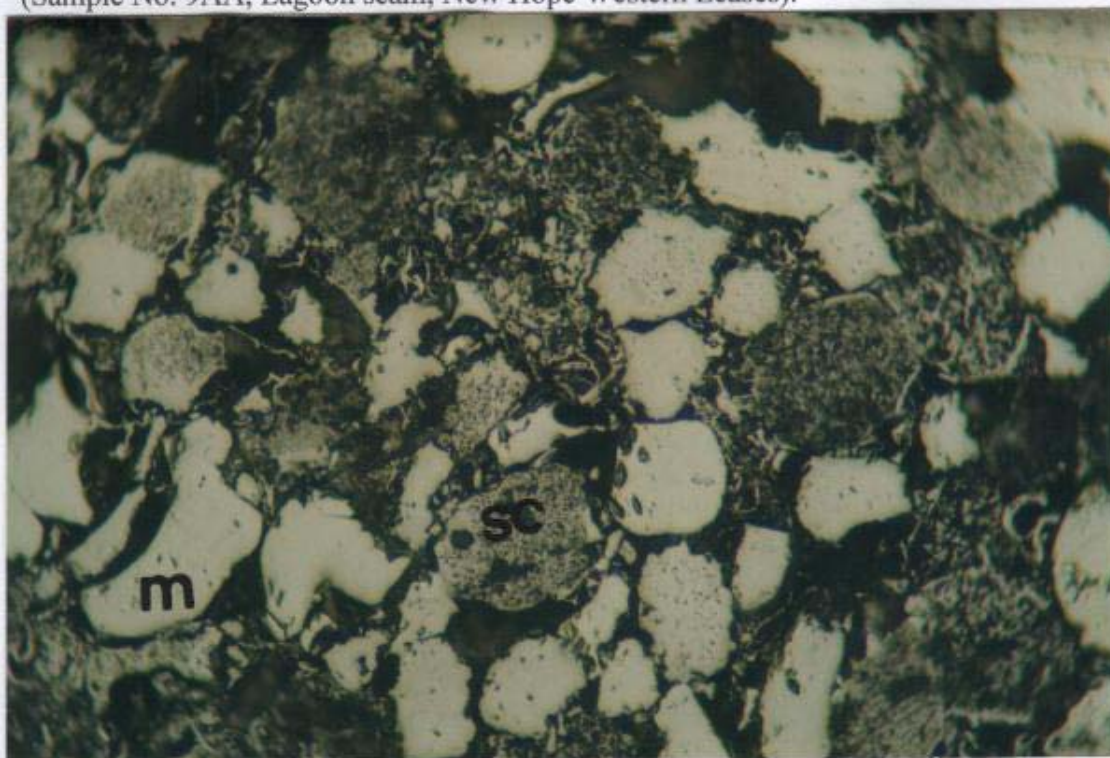


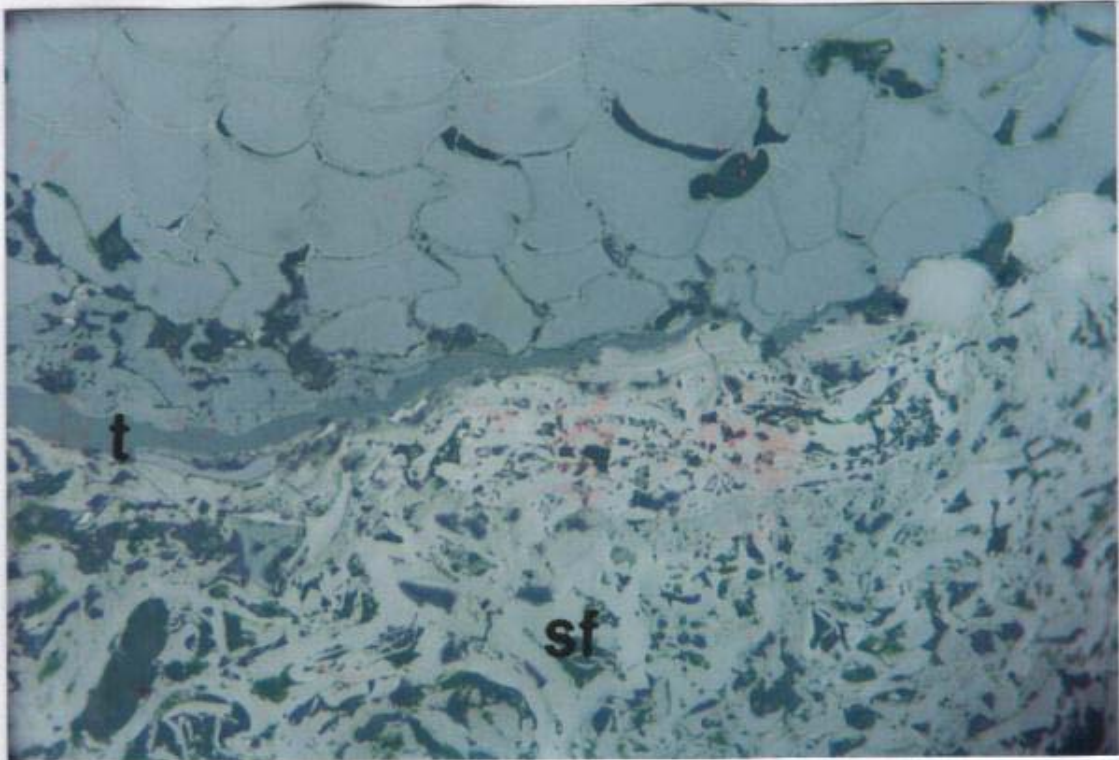


Photograph 44: Sclerotodetrinite, inertodetrinite, and broken and partly oxidised vitrinite in clay (Sample No. G11, Fiery seam, 29.31m-34.70m).



Photograph 45: Closed chamber sclerotinite with foam structure and rounded high relief white bodies of macrinite transformed to pseudosclerotinite (after Stach, 1982) (sclerotodetrinite after Beeston, 1987) (Sample No. 9AA, Lagoon seam, New Hope Western Leases).

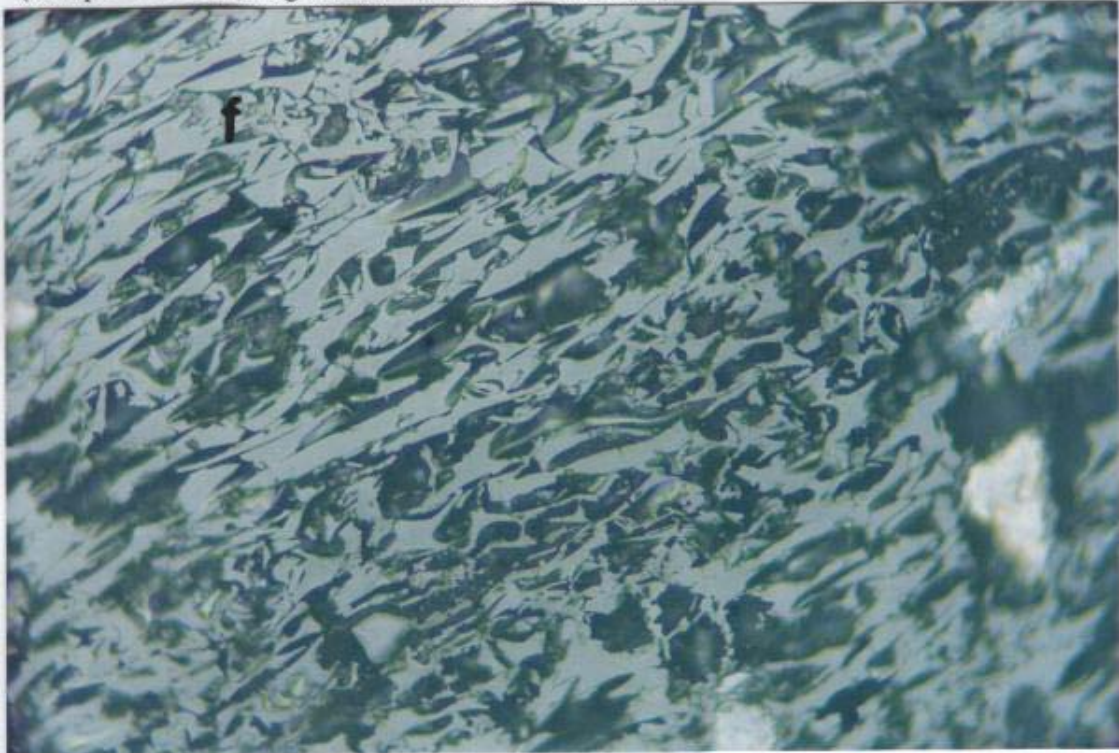


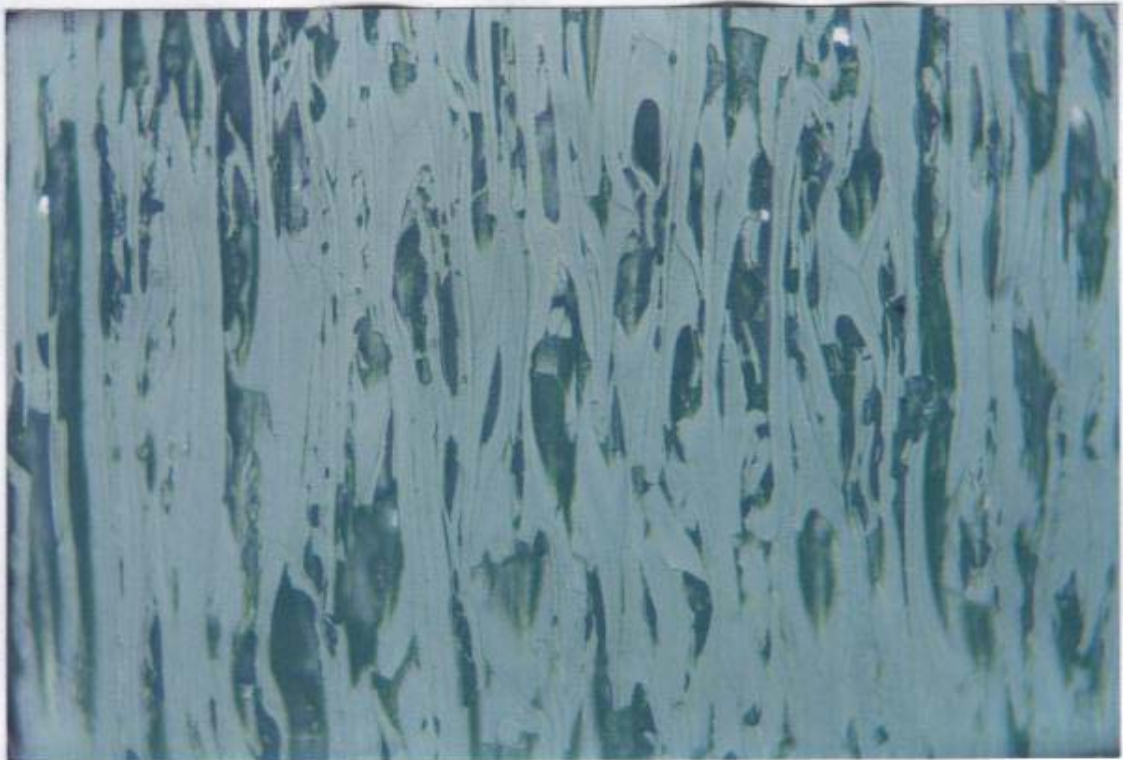


Photograph 46: Fusinitised bark tissue (periderm) with cork infills (phlobaphinite) (top) (after Diessel, 1992) and semifusinite (bottom), a thin telovitrinite in the centre separating the two (Sample No. G4, Garden seam, 119.90m-121.29m).

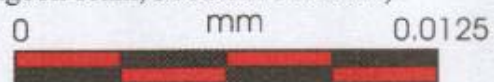


Photograph 47: High relief fusinite with holes showing bogen structure (Sample No. G21, Lagoon seam, 368.90m-369.97m).

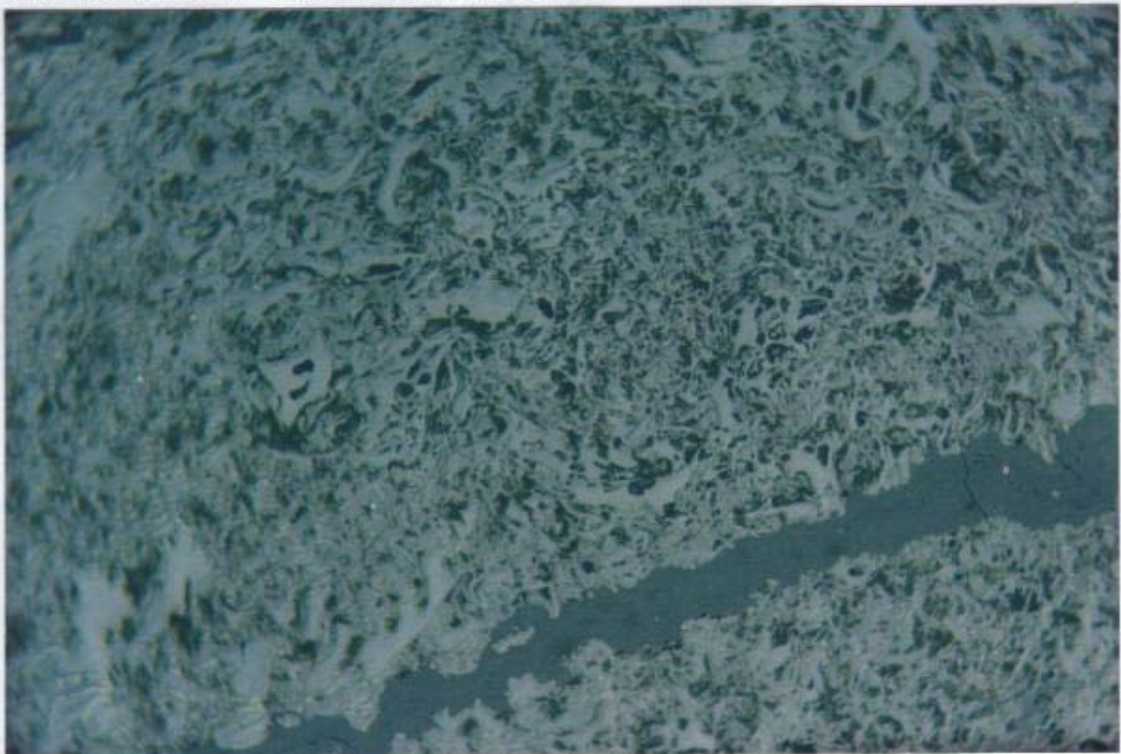


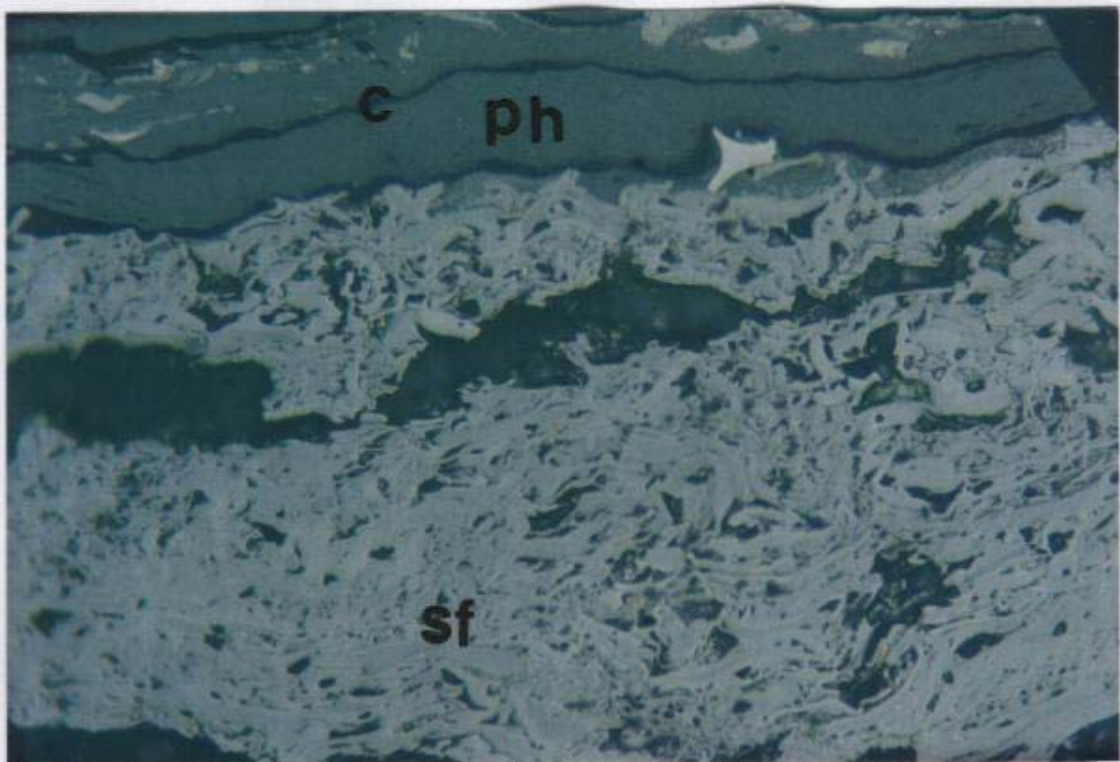


Photograph 48: A typical view of semifusinite with open cell lumen (Sample No. G21, Lagoon seam, 368.90m-369.97m).



Photograph 49: Another form of semifusinite which resembles pseudosclerotinite (funginite) (Lyons, 2000) with thin telovitrinite layer (Sample No. G38, Cochrane seam, 527.69m-528.13m).

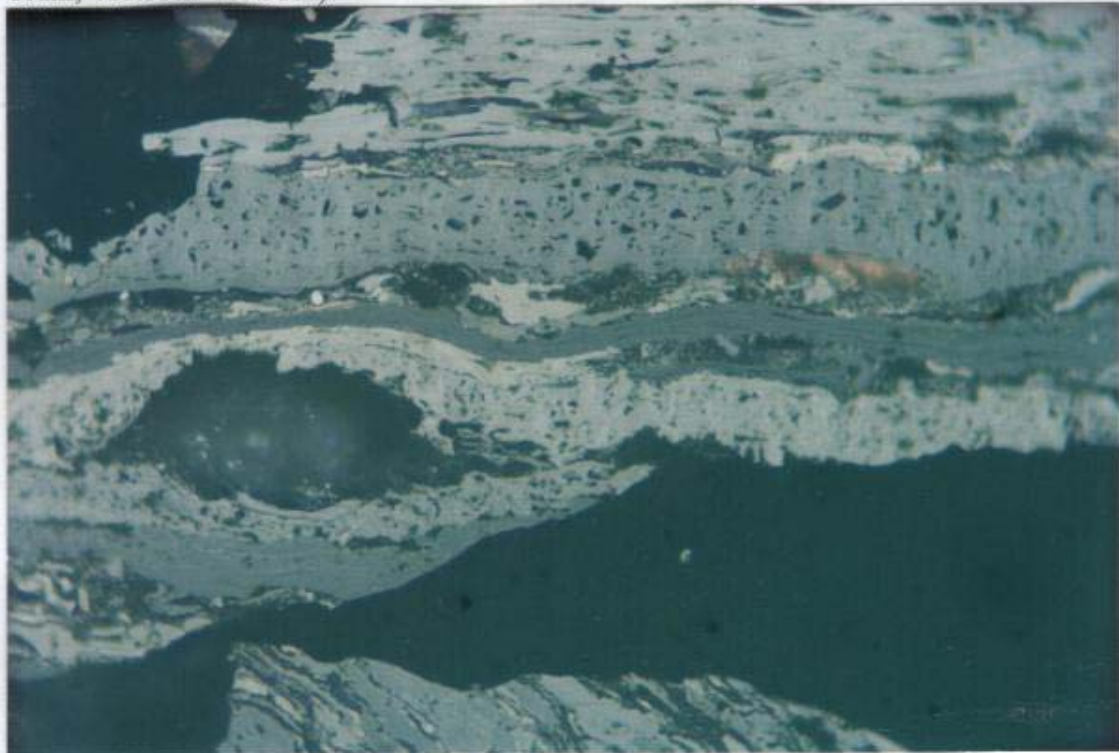


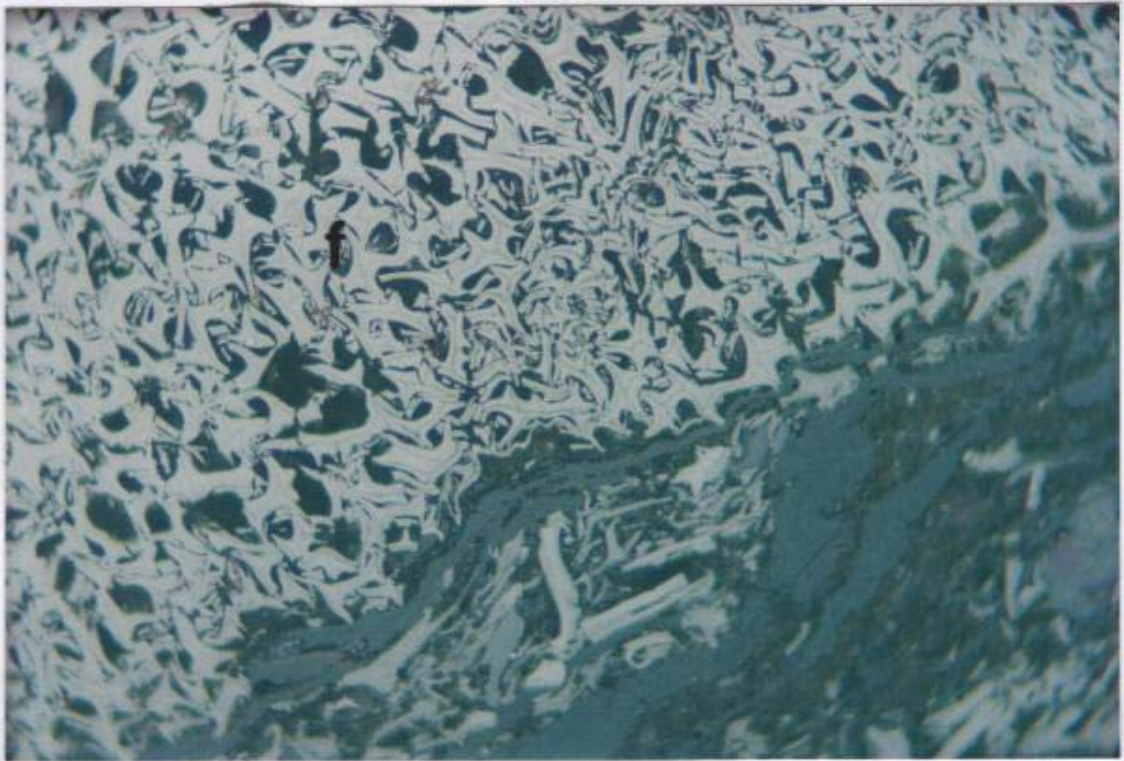


Photograph 50: Phyllovitrinite with enclosing cutinite (top) and semifusinite (bottom) (Sample No. G27, Fourfoot seam, 397.25m-398.04m).

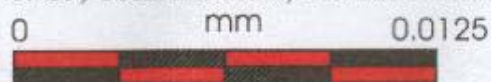


Photograph 51: Assemblage of semifusinite (degradofusinite after Beeston 1987) showing different stages of cell preservation and reflectance, note a semifusinite layer enclosing an amorphous quartz (Sample No. G34, Bergin seam, 416.59m-417.93m).

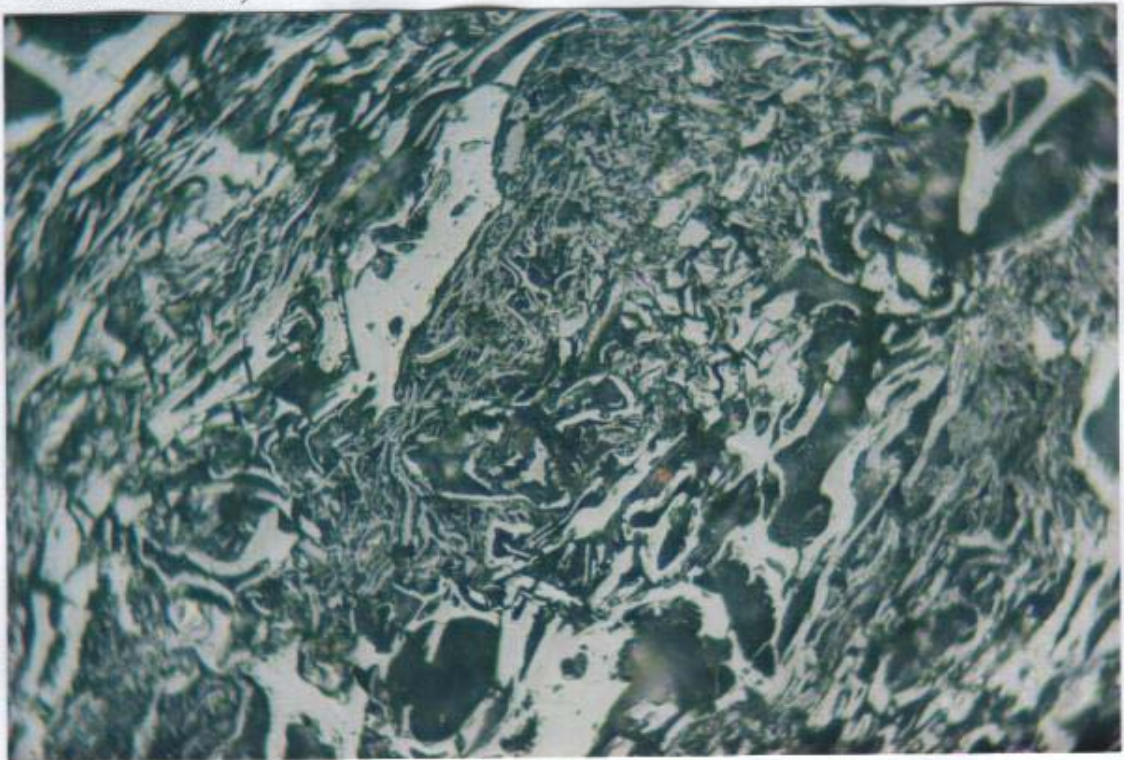


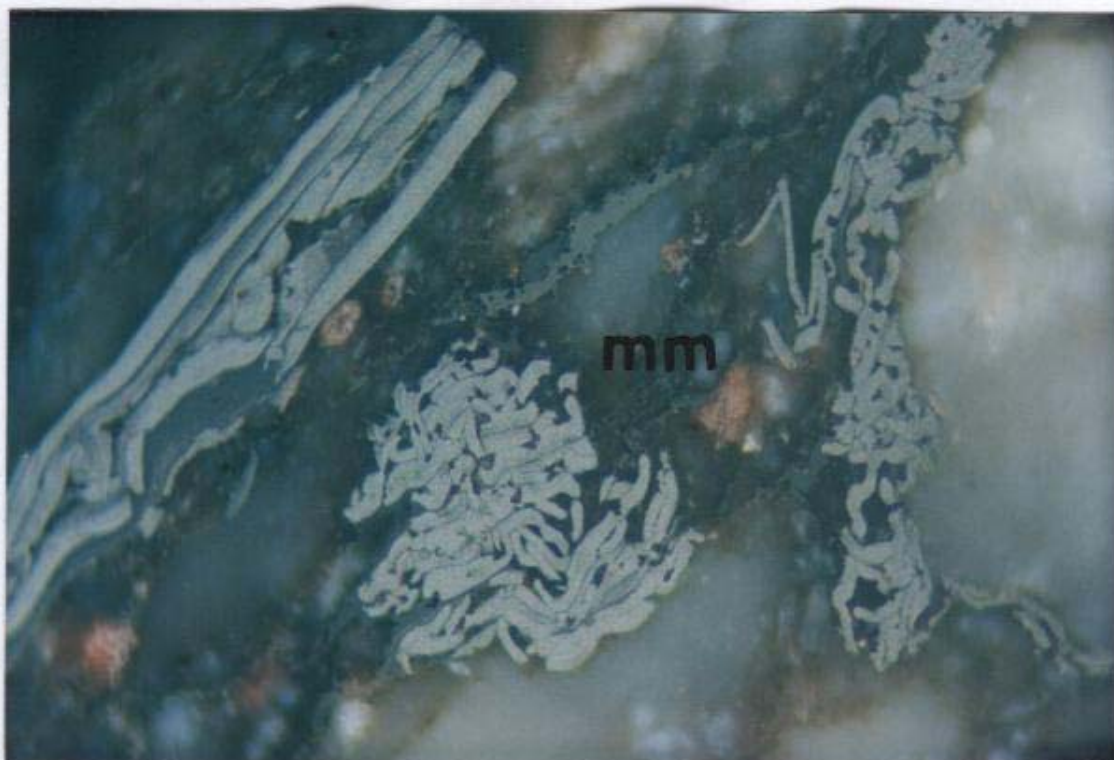


Photograph 52: Fusinite (top) with bogen structure (curved cell wall fragments), and detrovitrinite with clay (bottom). This type of very high relief, strong reflectance and yellowish colour fusinite is also known as pyrofusinite (Sample No. G5, Cochrane seam, 423.06m-424.51m).

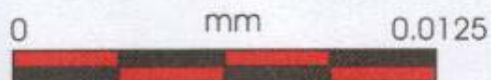


Photograph 53: Clay infilling cell lumens and gaps between cell walls of semifusinite (slightly heat affected) (Sample No. G5, Cochrane seam, 423.06m-424.51m).

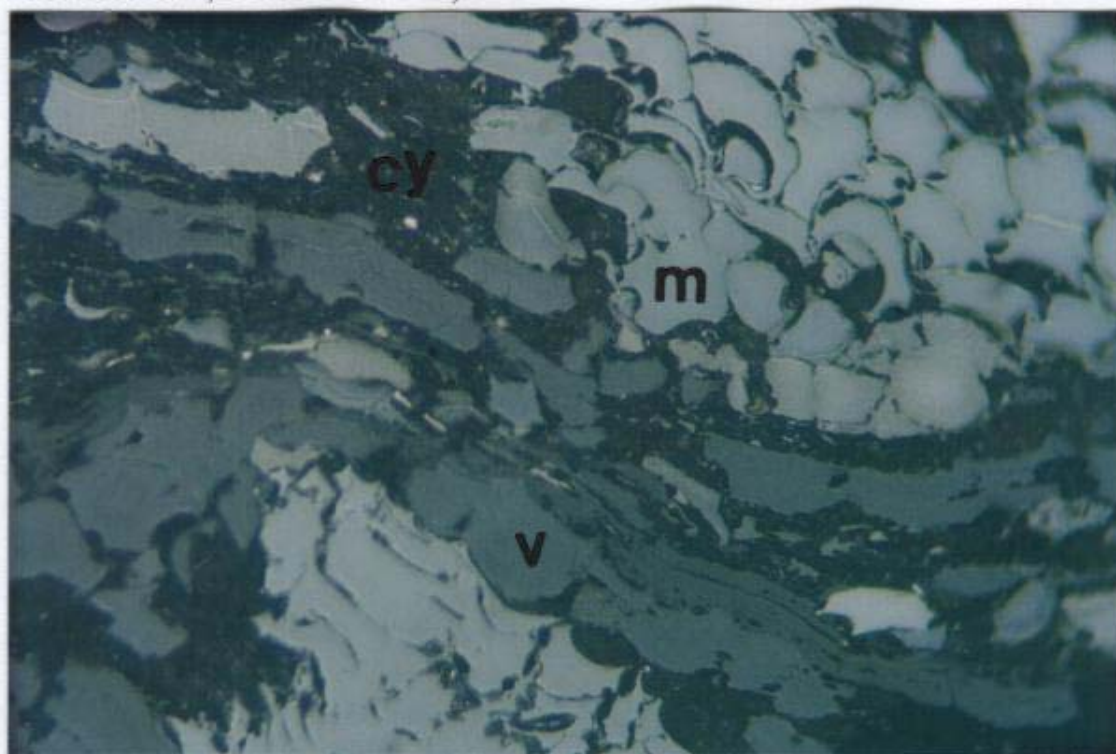


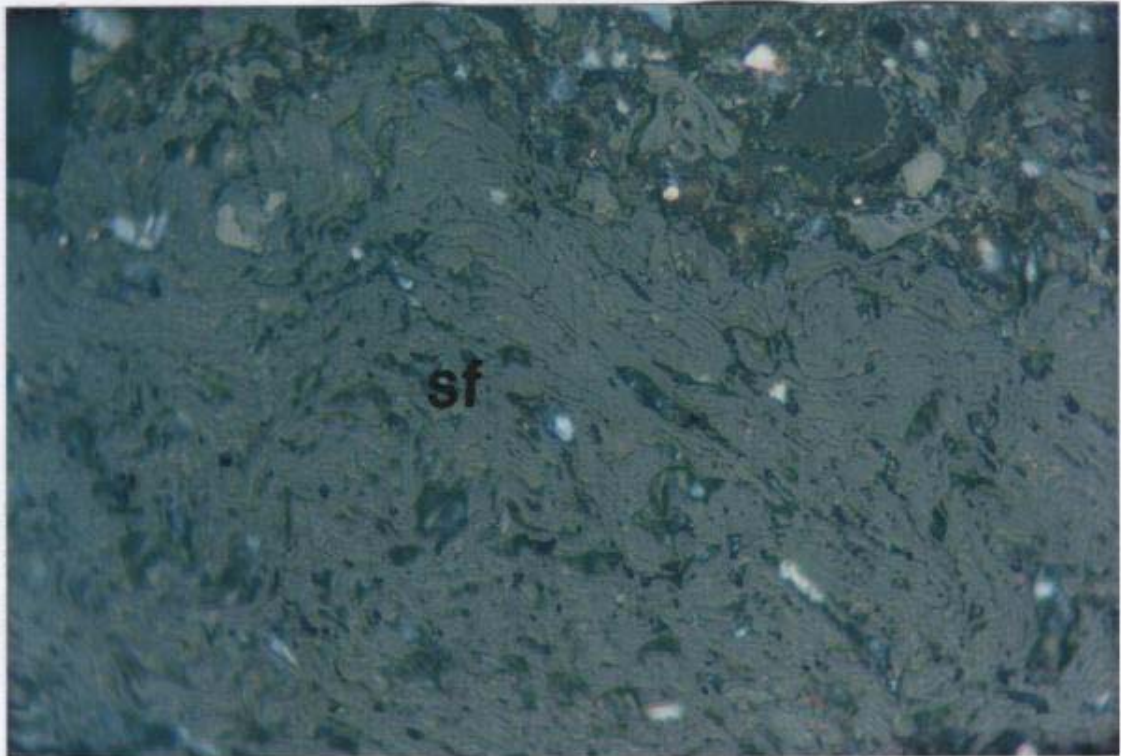


Photograph 54: Broken and fusinitised cell walls in mineral matter groundmass containing quartz, brown siderite, and clay (unusual view, very granular, possibly heat effected) (Sample No. G16, Bluff seam, 298.31m-299.66m).

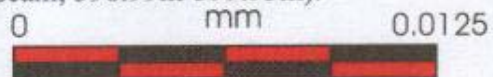


Photograph 55: Macrinite, broken vitrinite, and clay (Sample No. G32, Fourfoot seam, 401.81m-402.82m).

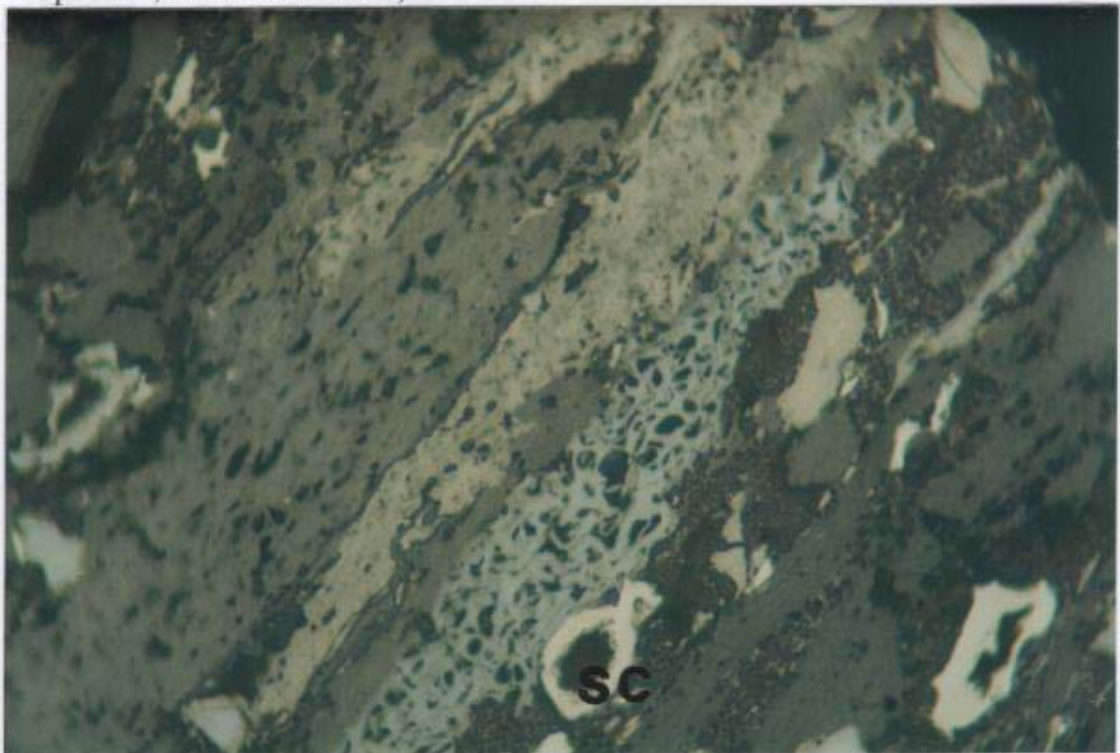


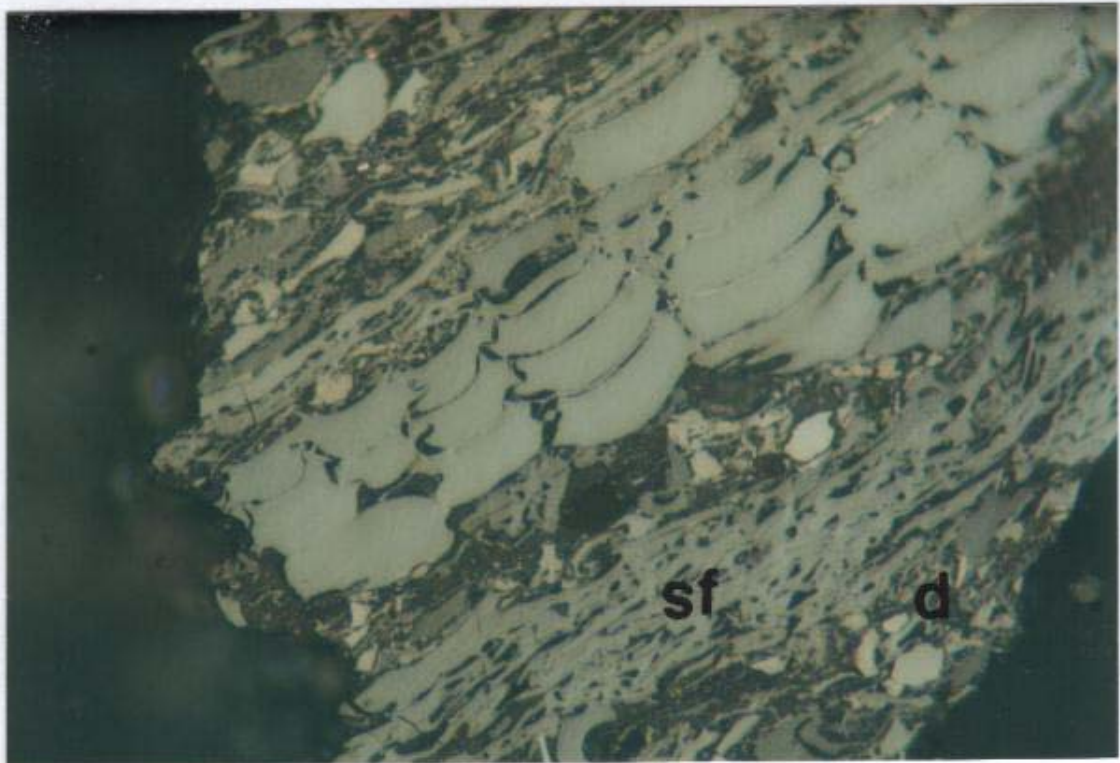


Photograph 56: Low relief semifusinite, which resembles funginite (Sample No. G29, Fourfoot seam, 398.99m-399.93m).



Photograph 57: Different stages of semifusinite (light, medium, and dark), with sclerotodetrinite and broken vitrinite with clay (Sample No. G9, Tivoli Tops seam, 211.83m-212.77m).

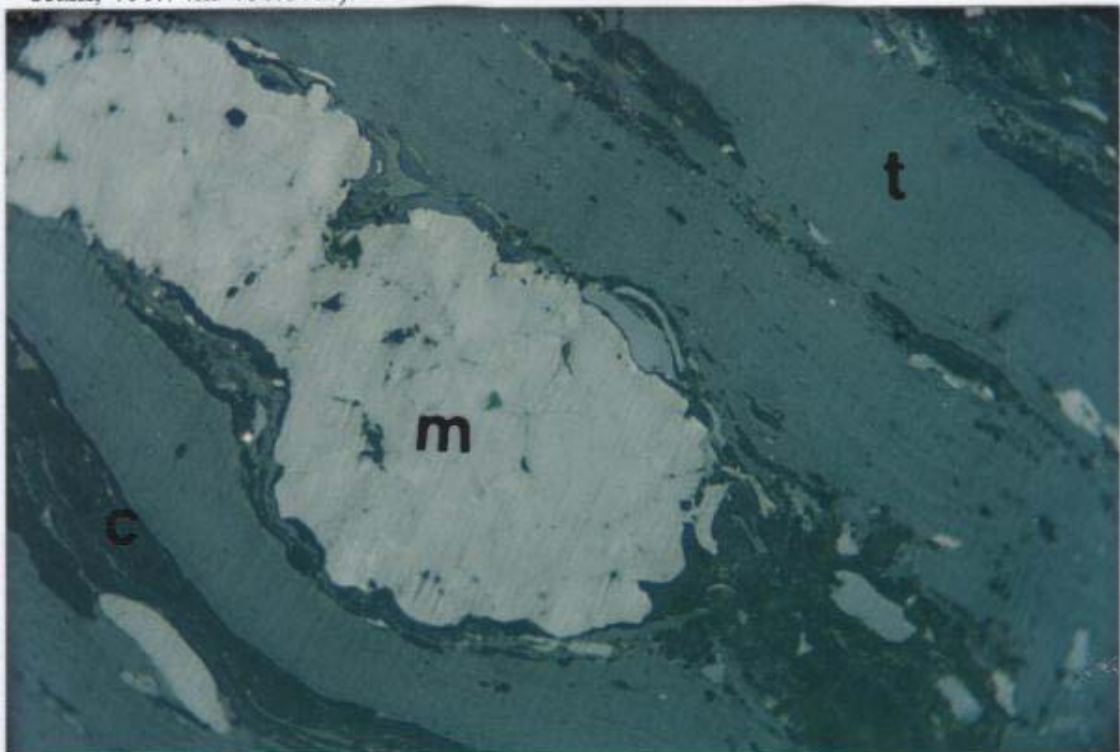


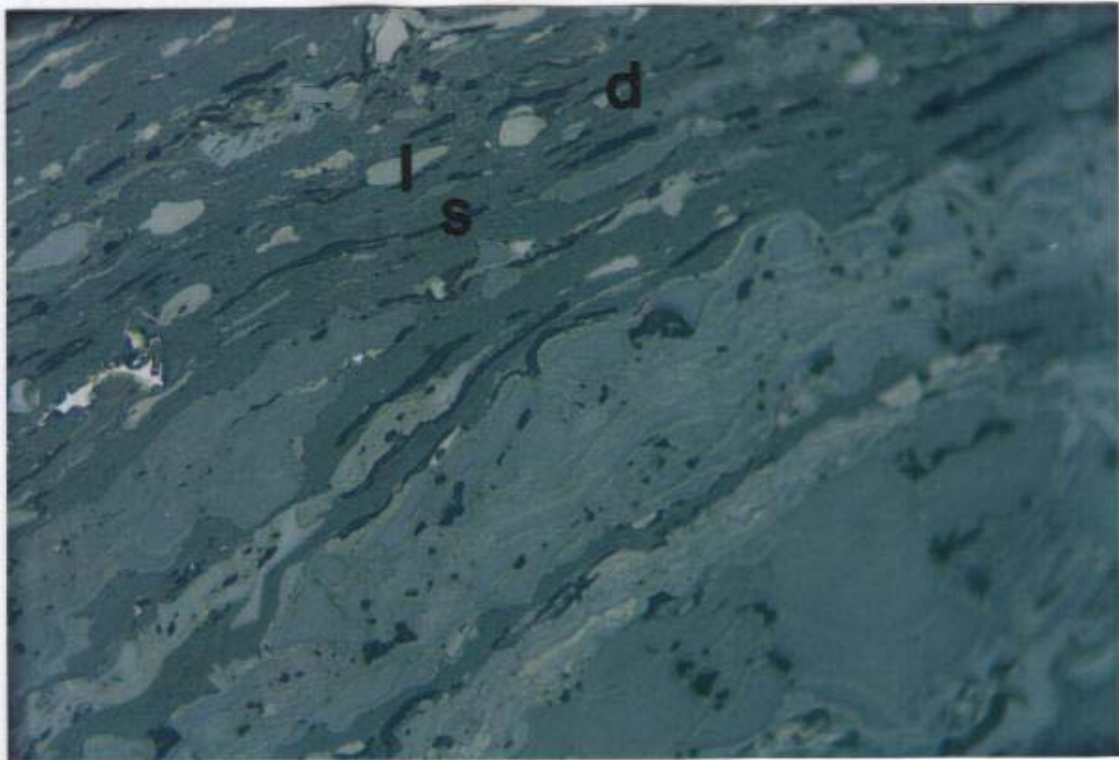


Photograph 58: Fusinitised bark (periderm) tissues with cork infilling (phlobaphinite that resembles macrinite), and detrovitrinite incorporating semifusinite, inertodetrinite and clay (Sample No. G9, Tivoli Tops seam, 211.83m-212.77m).



Photograph 59: Macrinite (light coloured amorphous body in the middle, cf. semifusinite), telovitrinite, cutinite and sporinite (Sample No. G31, Fourfoot seam, 400.74m-401.81m).

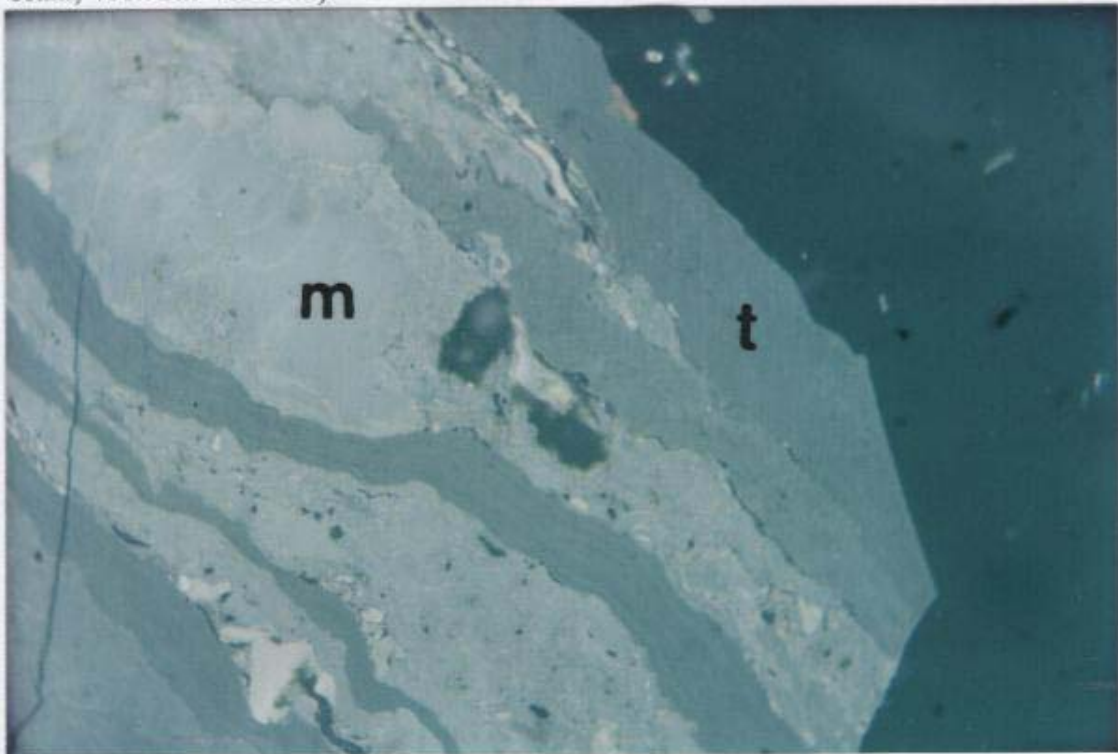


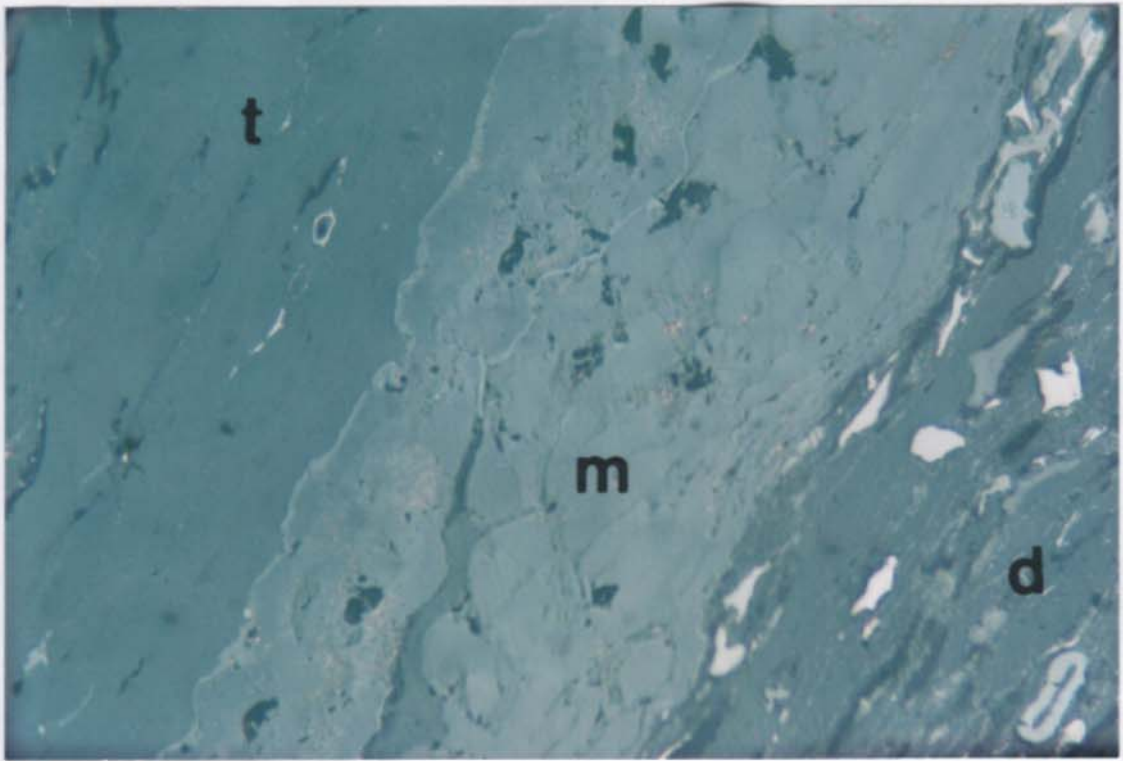


Photograph 60: Detrovitrinite with layered macrinite or lammacrinite (light grey in centre), sporinite and inertodetrinite (Sample No. G32, Fourfoot seam, 401.81m-402.82m).



Photograph 61: Macrinite with telovitrinite layers (Sample No. G36, Bergin seam, 418.92m-419.82m).

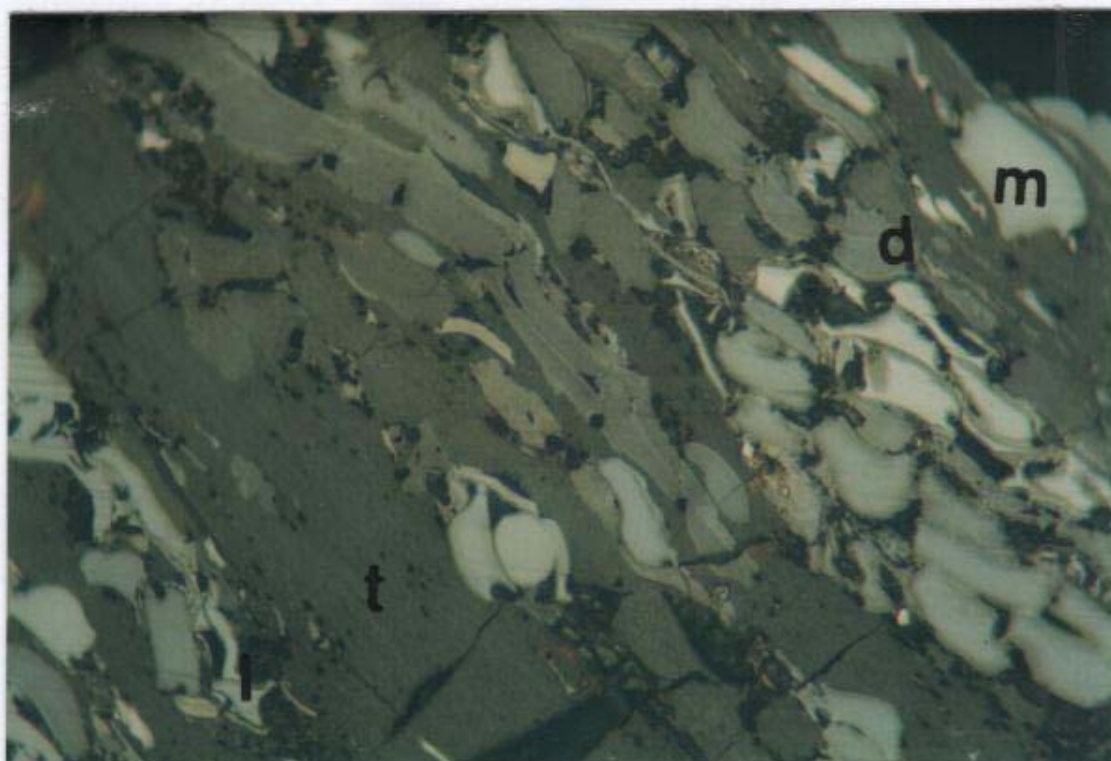




Photograph 62: Telovitrinite with minor spores (left), macrinite (middle), and detrovitrinite with inertodetrinite (right) (Sample No. G31, Fourfoot seam, 400.74m-401.81m).



Typical and Special Views

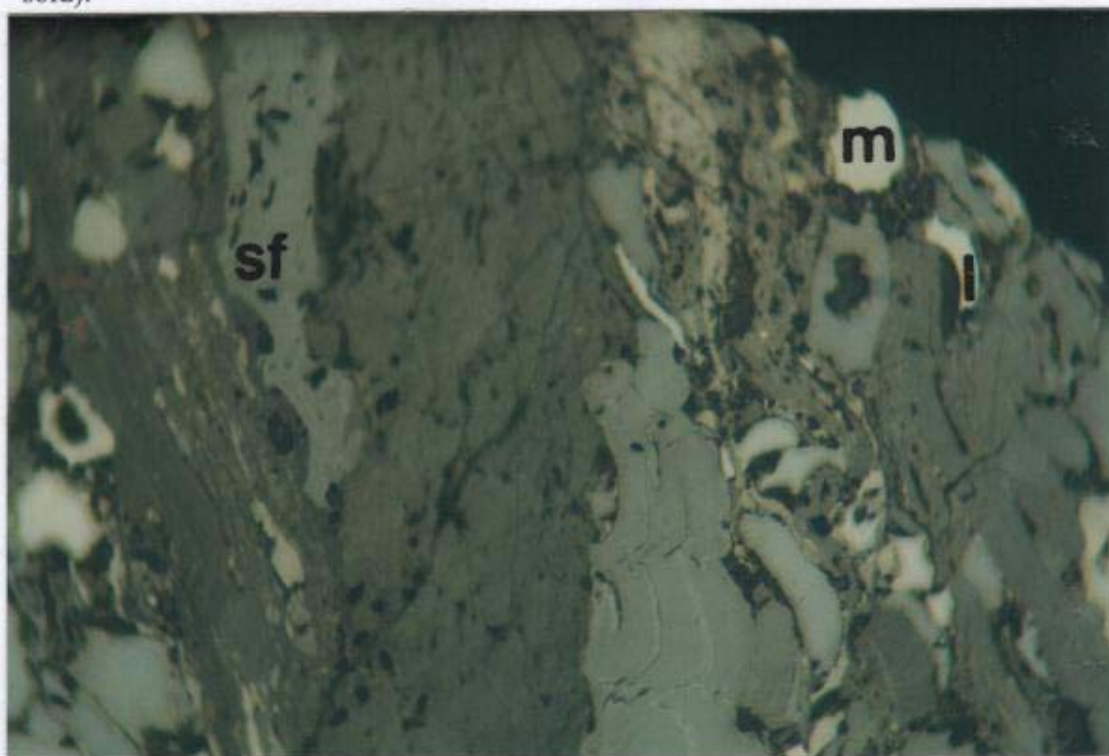


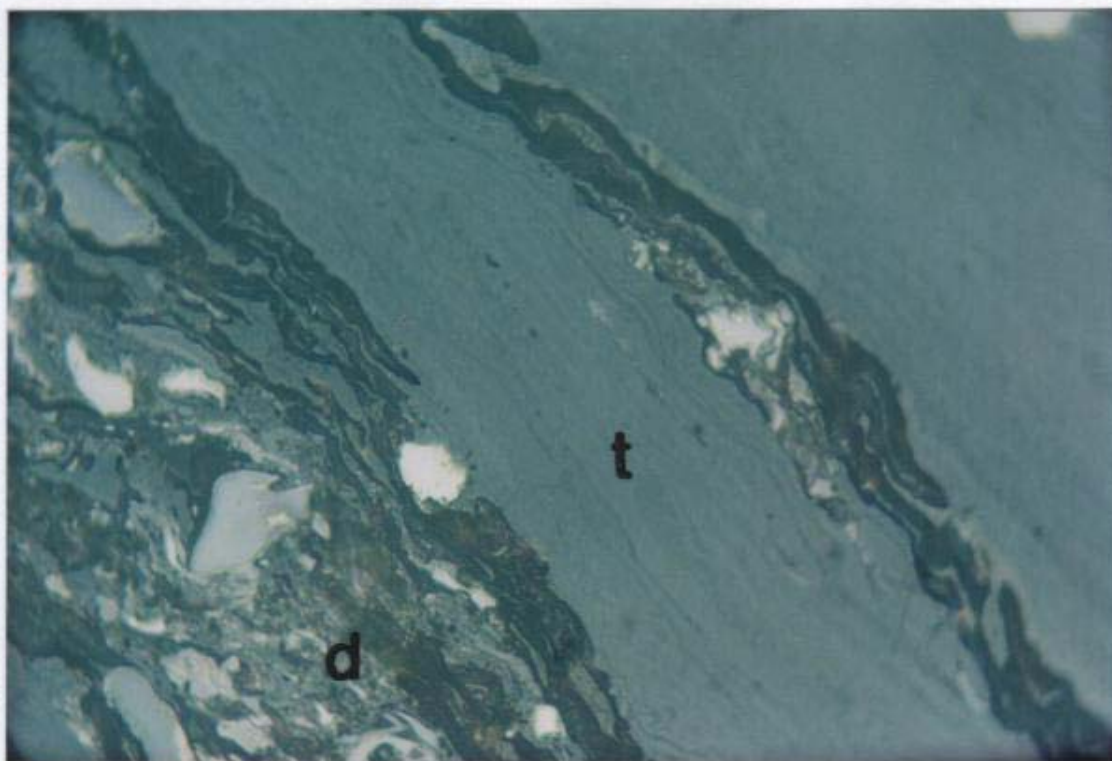
Photograph 63: Telovitrinite, macrinite in detrovitrinite with inertodetrinite (Typical view) (Sample No. G10, Tivoli Bottoms, 213.12m-214.47m).

0 mm 0.0125

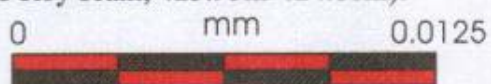


Photograph 64: Macrinite, semifusinite and inertodetrinite in detrovitrinite (Typical view) (Sample No. G2, Tivoli Formation – Haighmor mine, coal as sold).

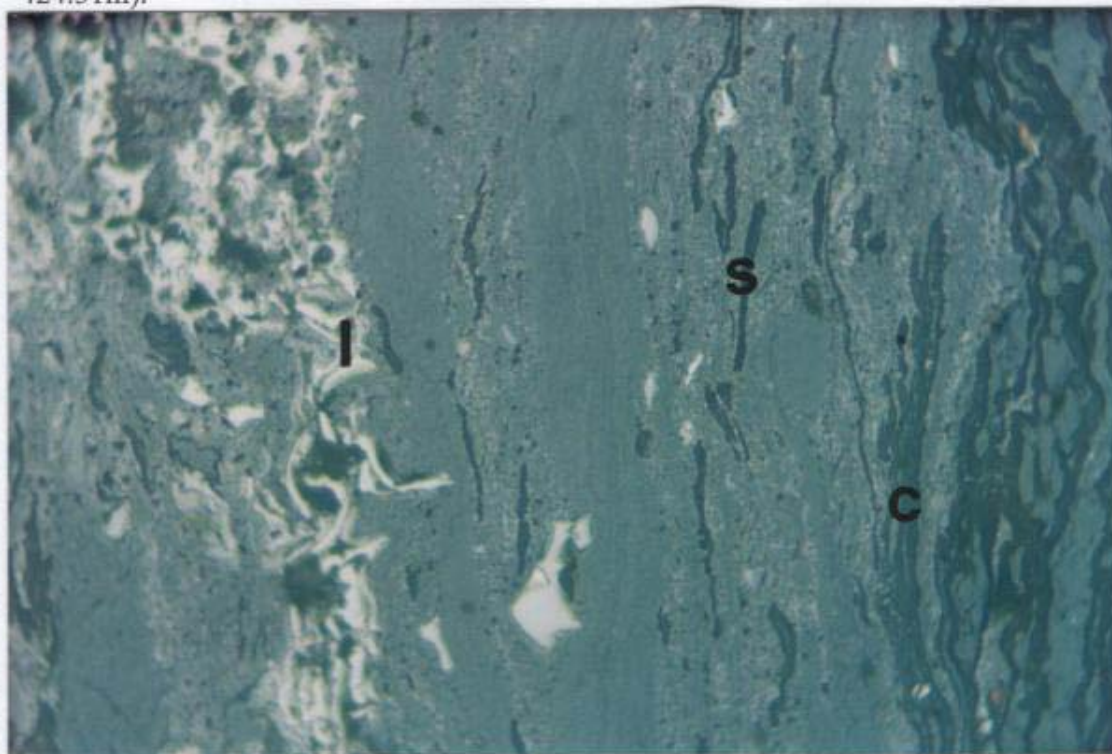


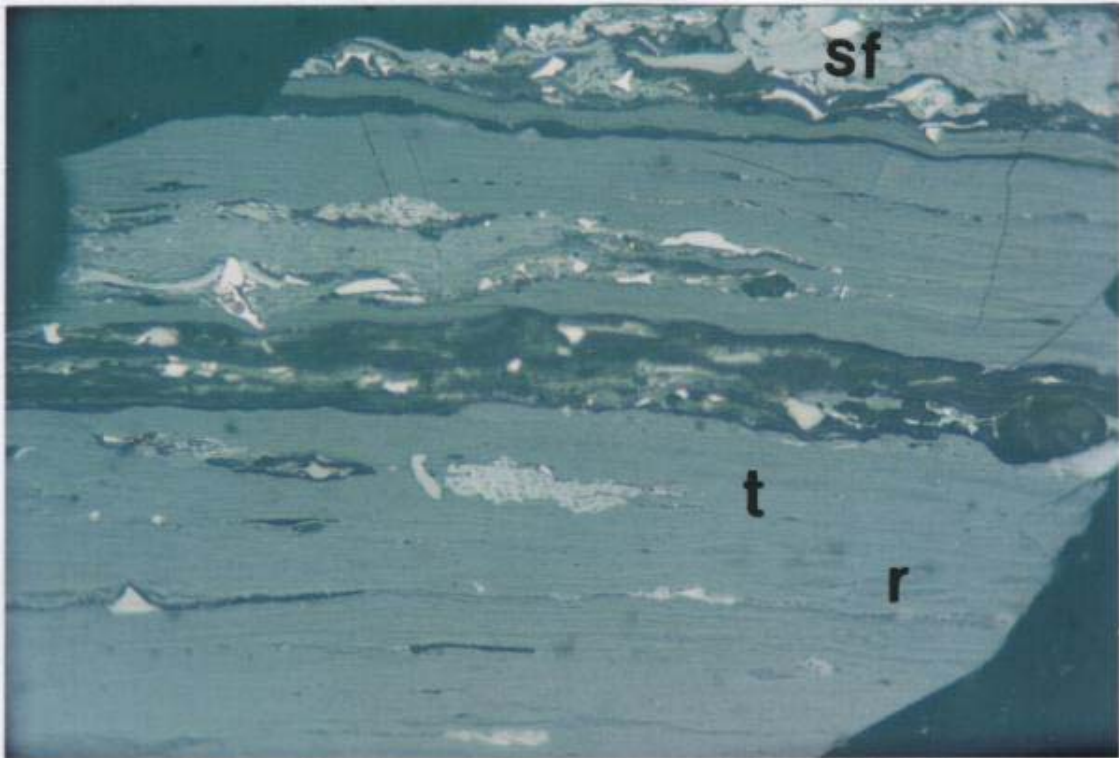


Photograph 65: Telovitrinite showing weak cell structure (telinite), and detrovitrinite containing cutinite, inertodetrinite and clay (Sample No. G25, Striped Bacon-Rob Roy seam, 423.95m-424.86m).



Photograph 66: Inertodetrinite (left) in a matrix of detrovitrinite together with sporinite (dark elongated bodies) and cutinite (right) and micrinite (small bright white specks) (Sample No. G5, Cochrane seam, 423.06m-424.51m).

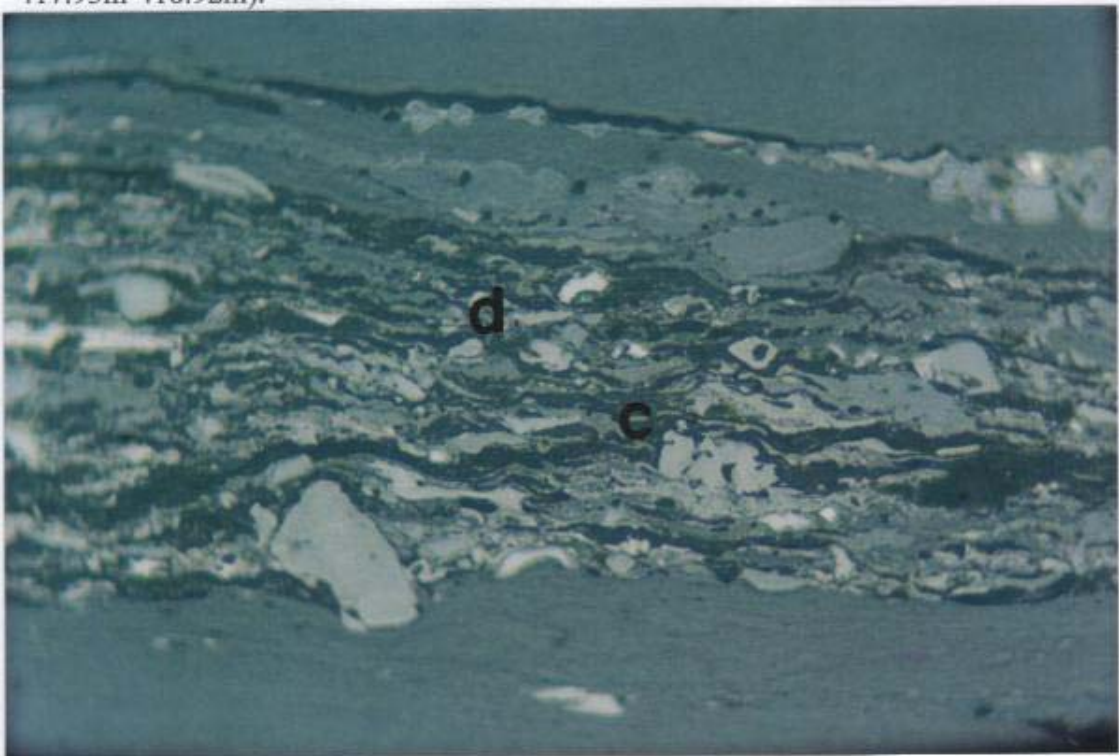


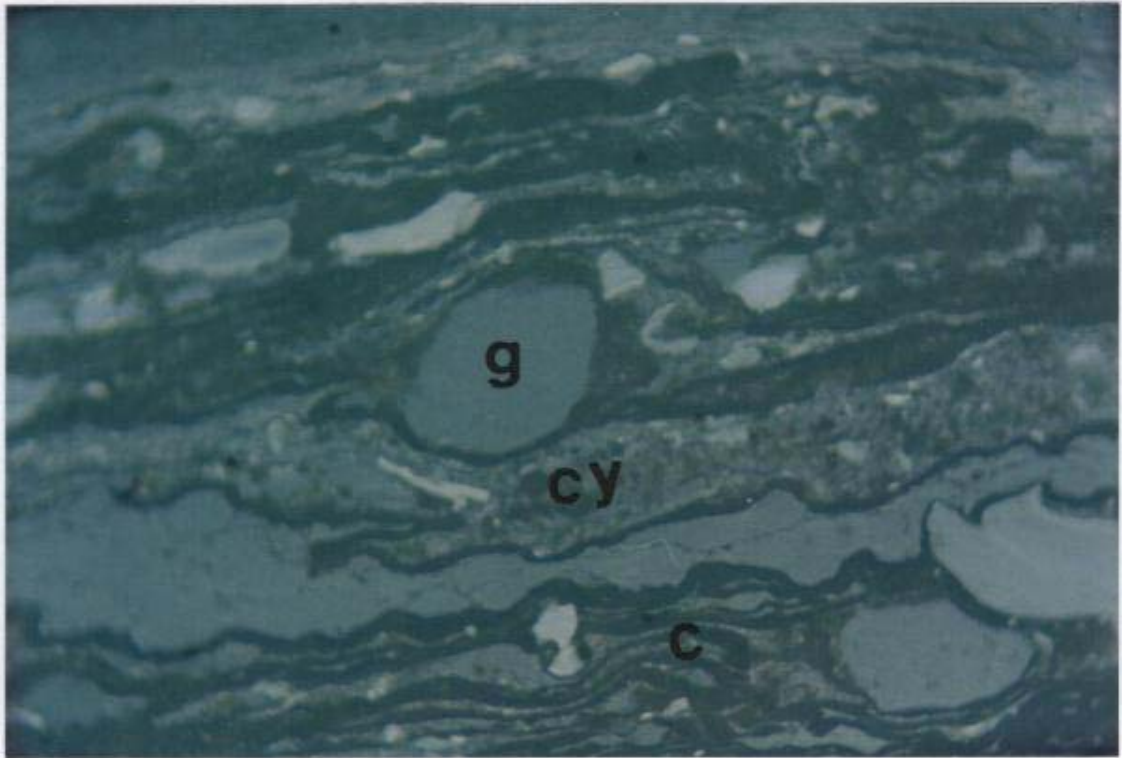


Photograph 67: Semifusinite, cutinite, sporinite and inertodetrinite in detrovitrinite matrix, and telovitrinite with resinite (light grey small elongated bodies) (Sample No. G19, Lagoon seam, 366.85m-368.12m).

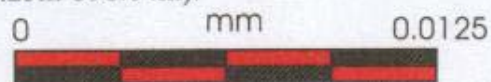


Photograph 68: Detrovitrinite with cutinite, sporinite, micrinite (small white specks), macrinite and inertodetrinite. Telovitrinite layers at top and bottom. Bottom shows faint cell structures (Sample No. G35, Bergin seam, 417.93m-418.92m).

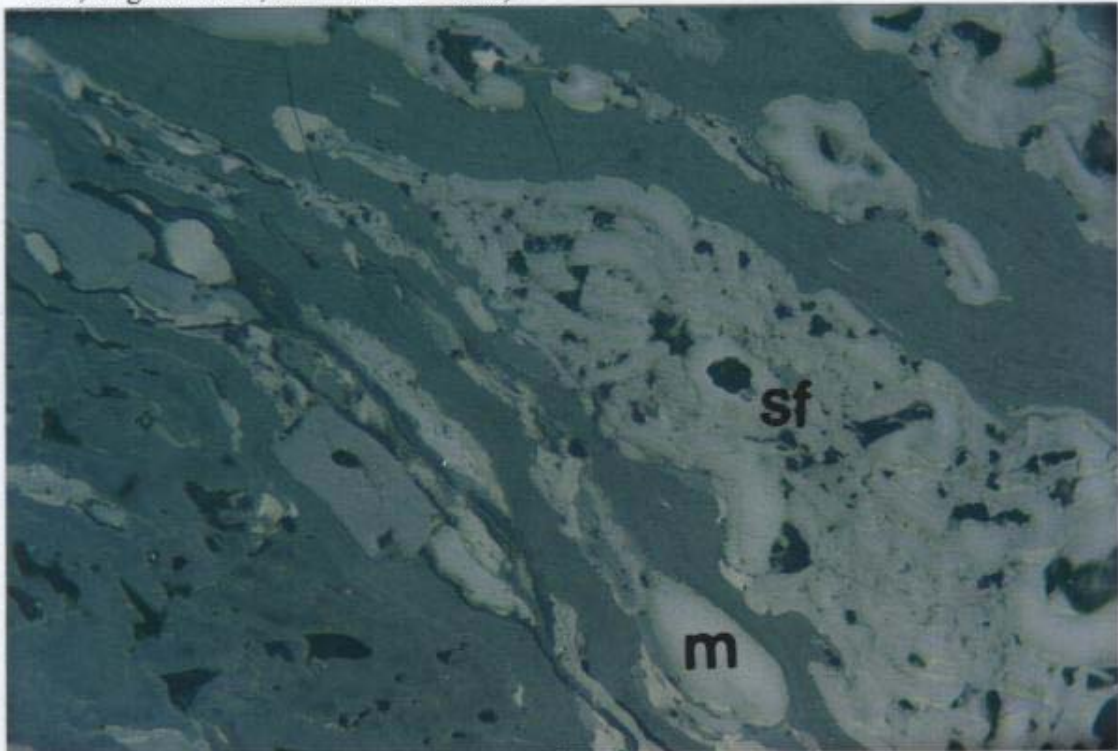


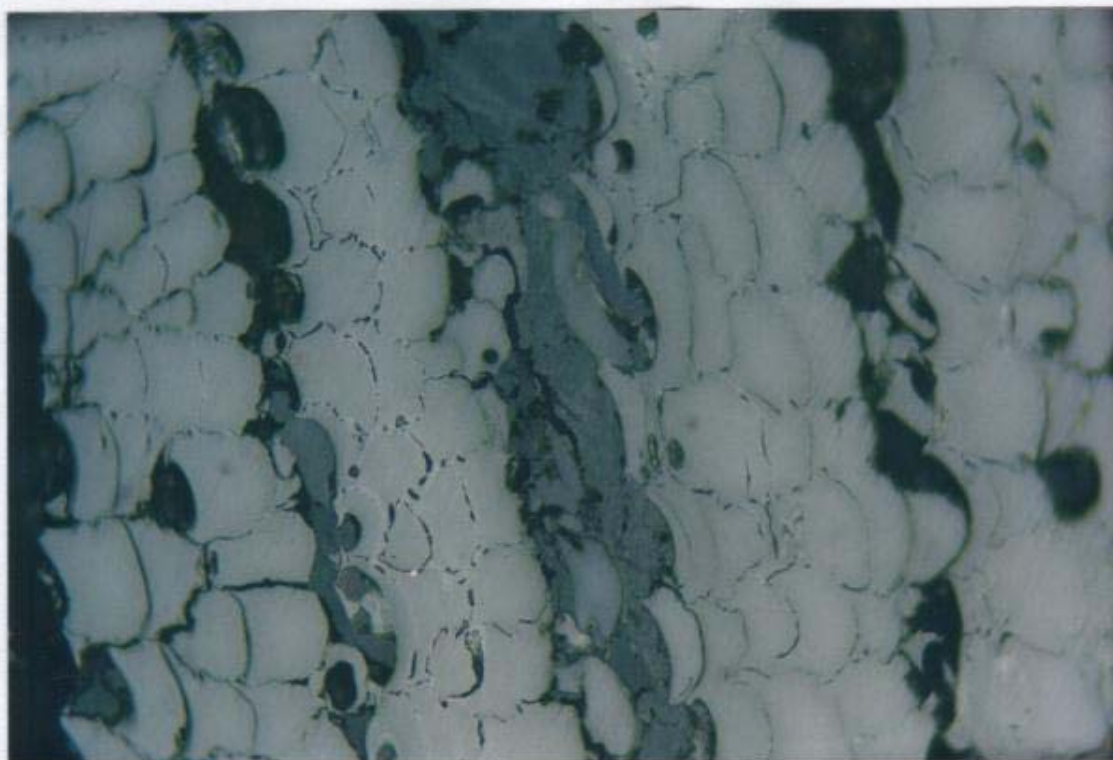


Photograph 69: Cutinite, inertodetrinite and clay in detrovitrinite matrix, with low relief gelovitrinite (massive oval bodies) (Sample No. G27, Fourfoot seam, 397.25m-398.04m).

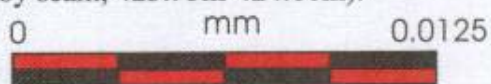


Photograph 70: Low reflectance semifusinite (bottom left hand corner), semifusinite, macrinite, minor cutinite and telovitrinite layers (Sample No. G23, Lagoon seam, 371.48m-372.63m).

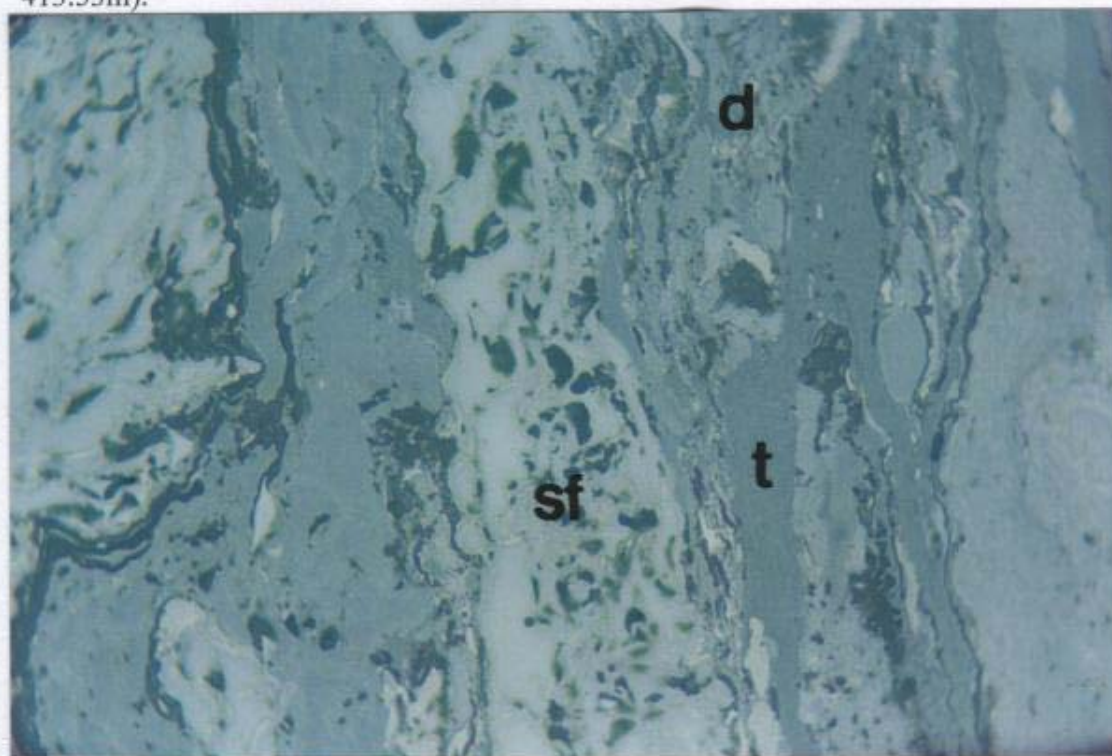


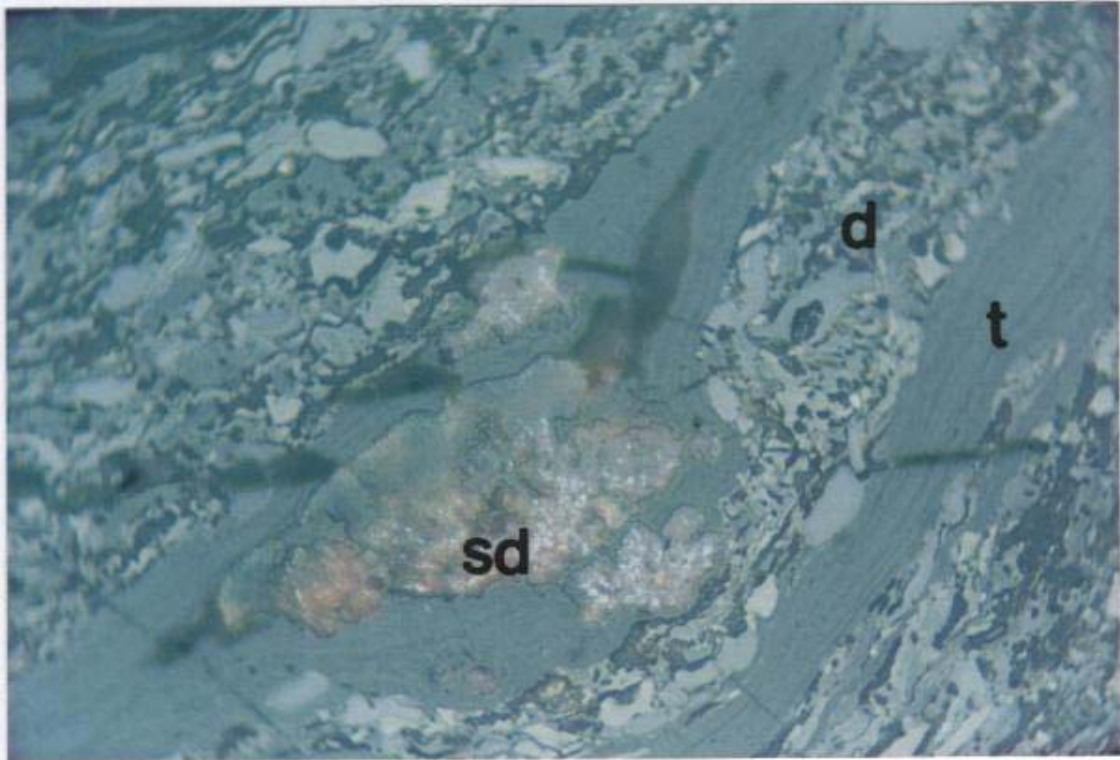


Photograph 71: Typical view of fusinitised bark (periderm) tissue with cork inclusions (phlobaphinite) (after Diessel, 1992) (cf. Macrinite) (Sample No. G25, Striped Bacon-Rob Roy seam, 423.95m-424.86m).



Photograph 72: Photograph showing gradation between semifusinite and macrinite. It also shows cutinite and sporinite set in detrovitrinite (grey matrix) with telovitrinite layers (Sample No. G33, Bergin seam, 412.36m-413.53m).

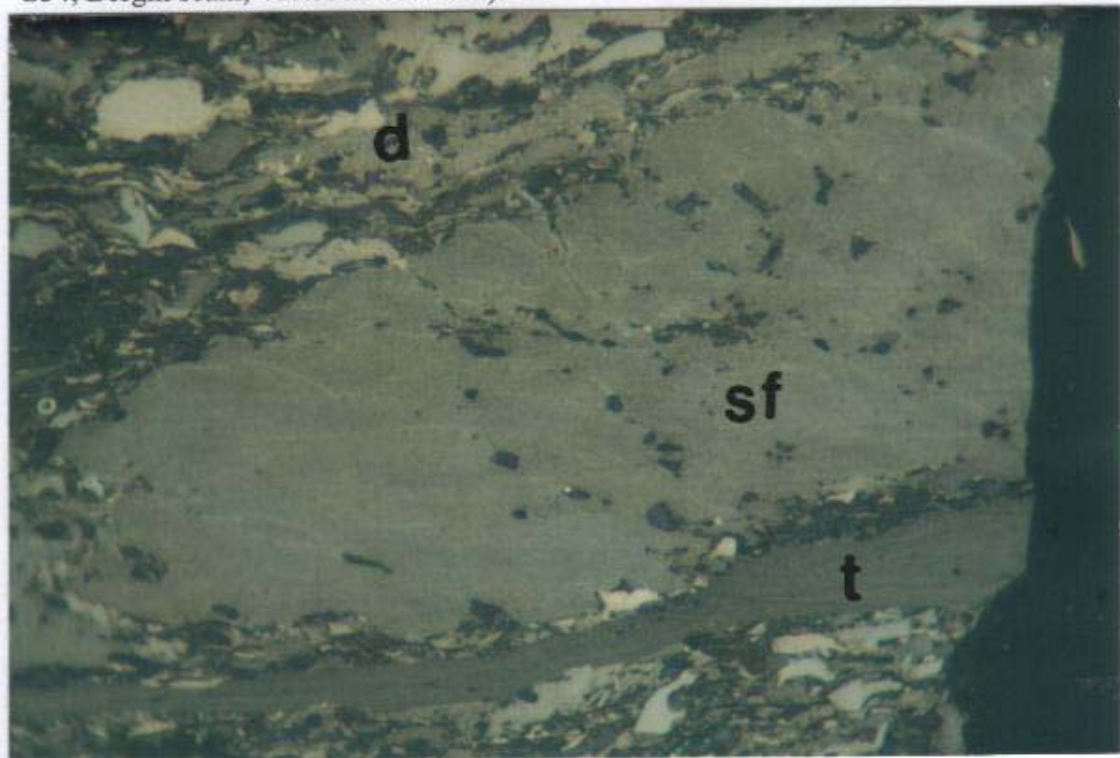


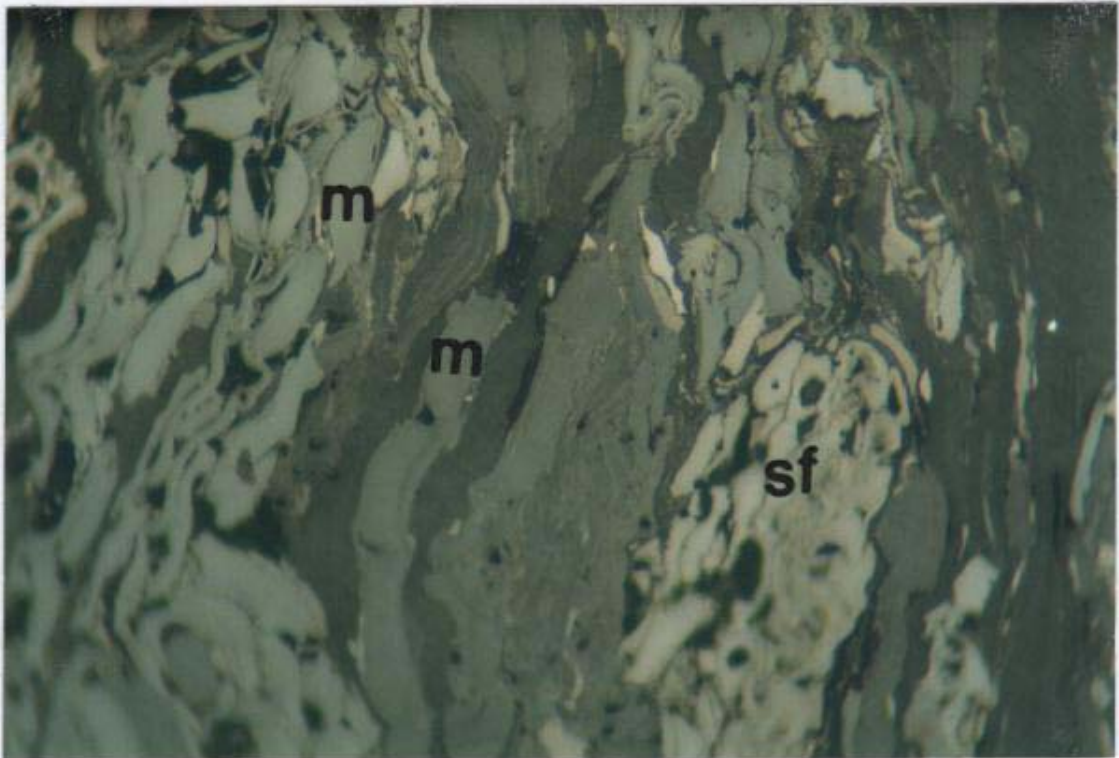


Photograph 73: Detrovitrinite with inertodetrinite and sporinite, and telovitrinite layers showing faint cell structure and surrounding the siderite micro-nodule. Note the compression around the siderite nodule (Sample No. G21, Lagoon seam, 368.90m-369.97m)

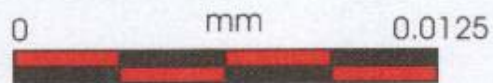


Photograph 74: Detrovitrinite with low relief cutinite (top), semifusinite (middle) (cf. Macrinite), and a telovitrinite thin layer (bottom) (Sample No. G34, Bergin seam, 416.59m-417.93m).

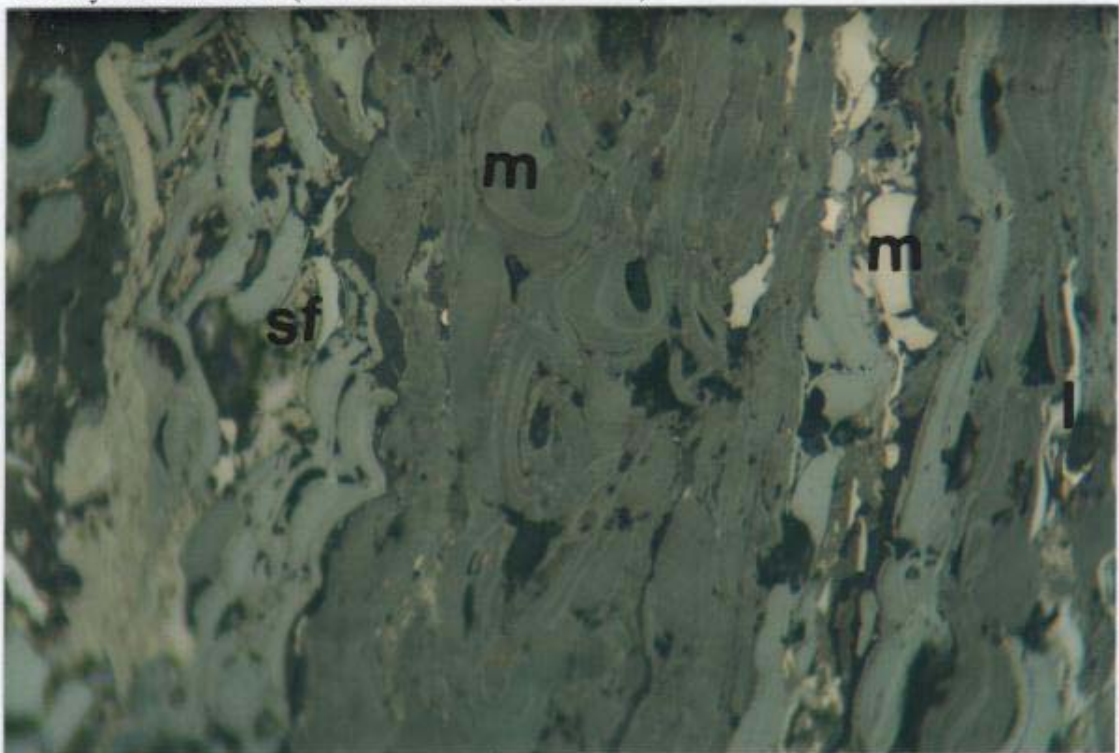


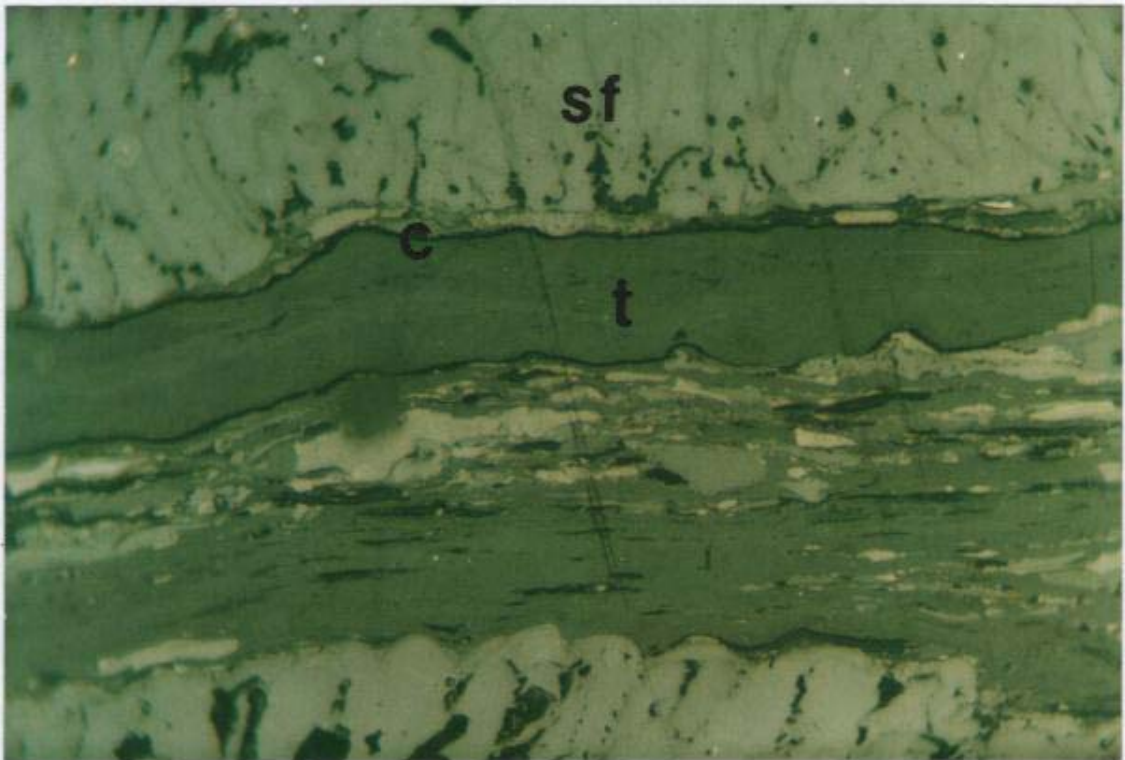


Photograph 75: Typical view of detrovitrinite matrix containing macrinite (left), low reflectance layered macrinite (middle), semifusinite, inertodetrinite and thin telovitrinite layers (Sample No. 4A, Bluff seam, Box Flat mine).



Photograph 76: Semifusinite, inertodetrinite, macrinite (higher reflectance), and layered macrinite (lower reflectance, in centre).

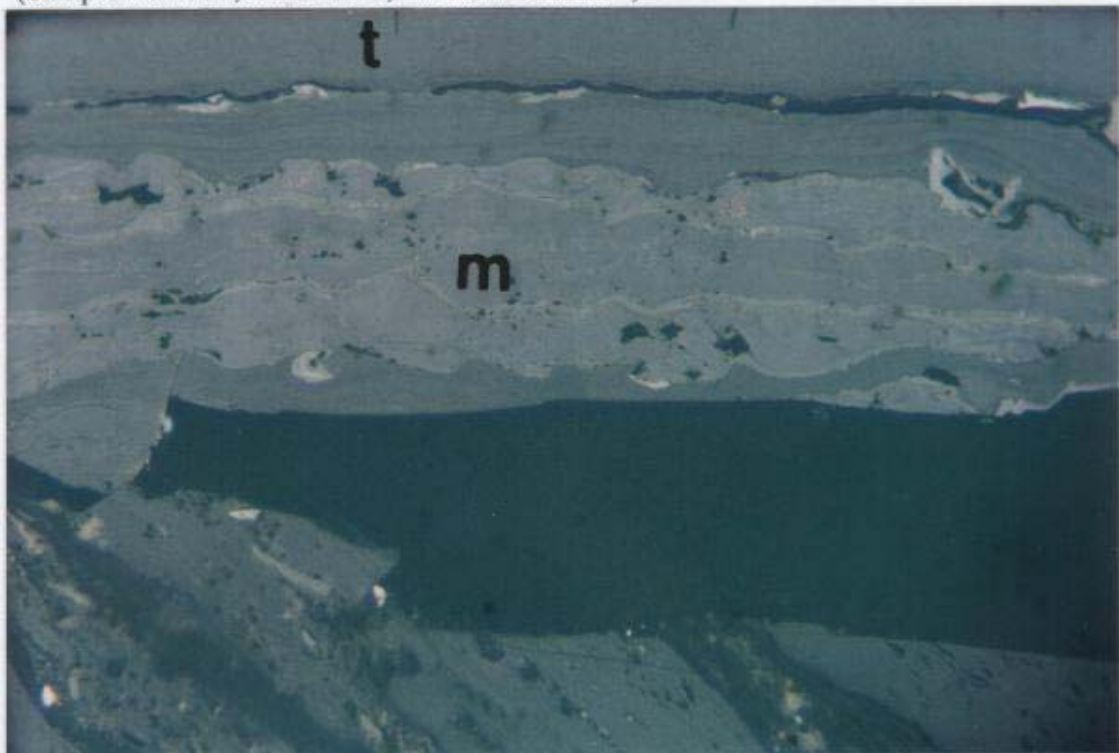


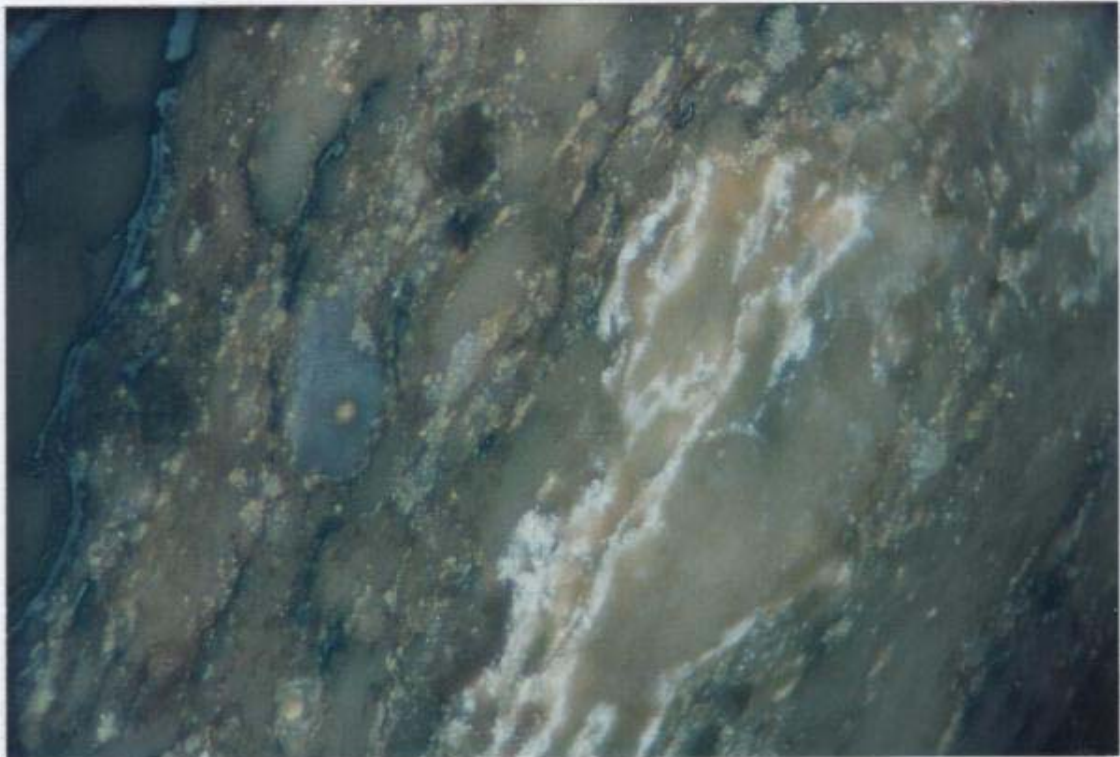


Photograph 77: Semifusinite (top and bottom), a telovitrinite layer with thin cell walls containing cutinite, and sporinite and inertodetrinite in detrovitrinite (Sample No. 13A, Bluff seam, Box Flat mine).



Photograph 78: Telovitrinite with cutinite (top), resinite (very faint elongated bodies) in telovitrinite, and macrinite showing low reflectance (Sample No. G17, Bluff seam, 300.03m-301.14m).

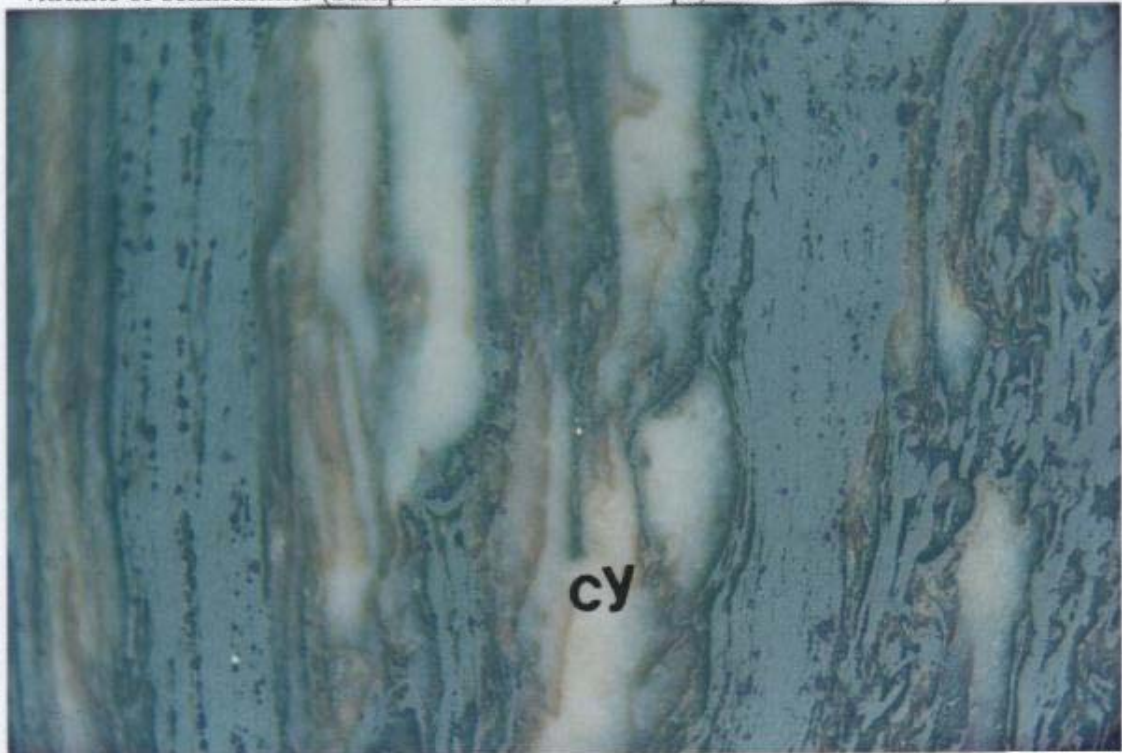


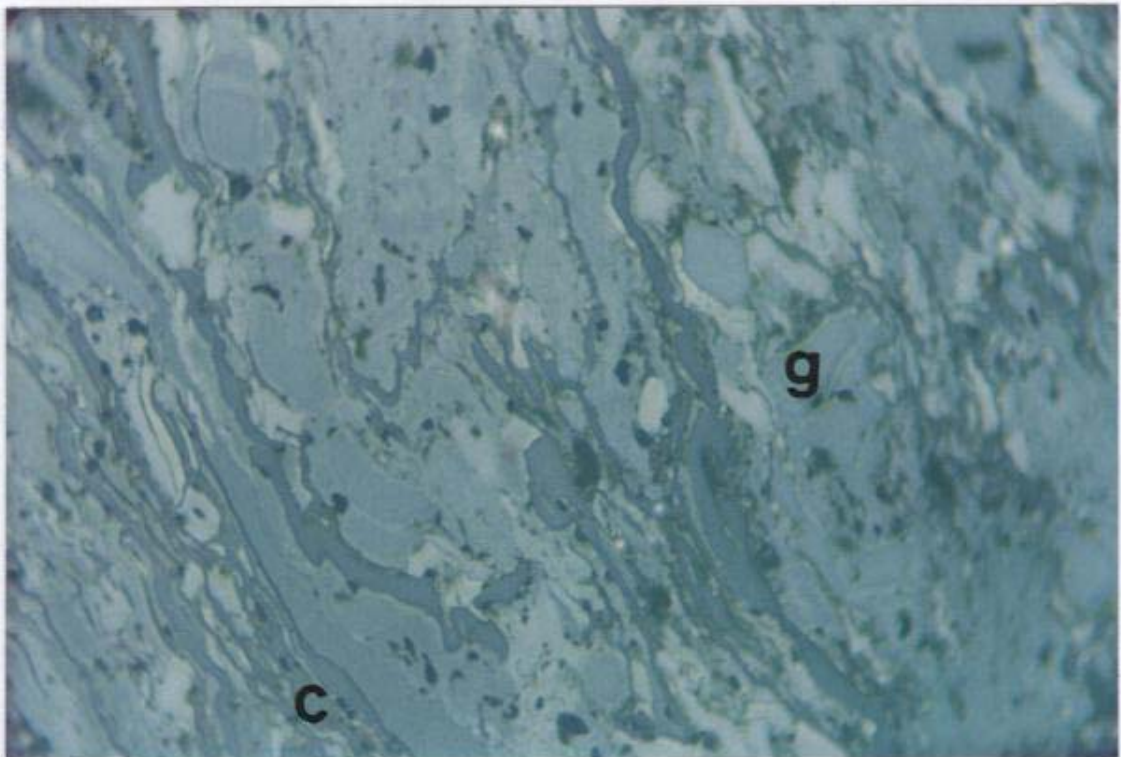


Photograph 79: Allophane (amorphous kaolinite) (left hand corner) with oxidised broken vitrinite pieces, and high reflectance clay (bright white) in darker low reflectance clay ground mass (Sample No. G3, Benley Tops, 363.76m-365.20m).

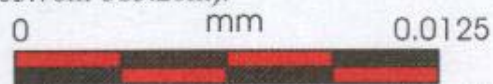


Photograph 80: Aggregation of clay nodules (white), and partly oxidised vitrinite or semifusinite (Sample No. G3, Benley Tops, 363.76m-365.20m).

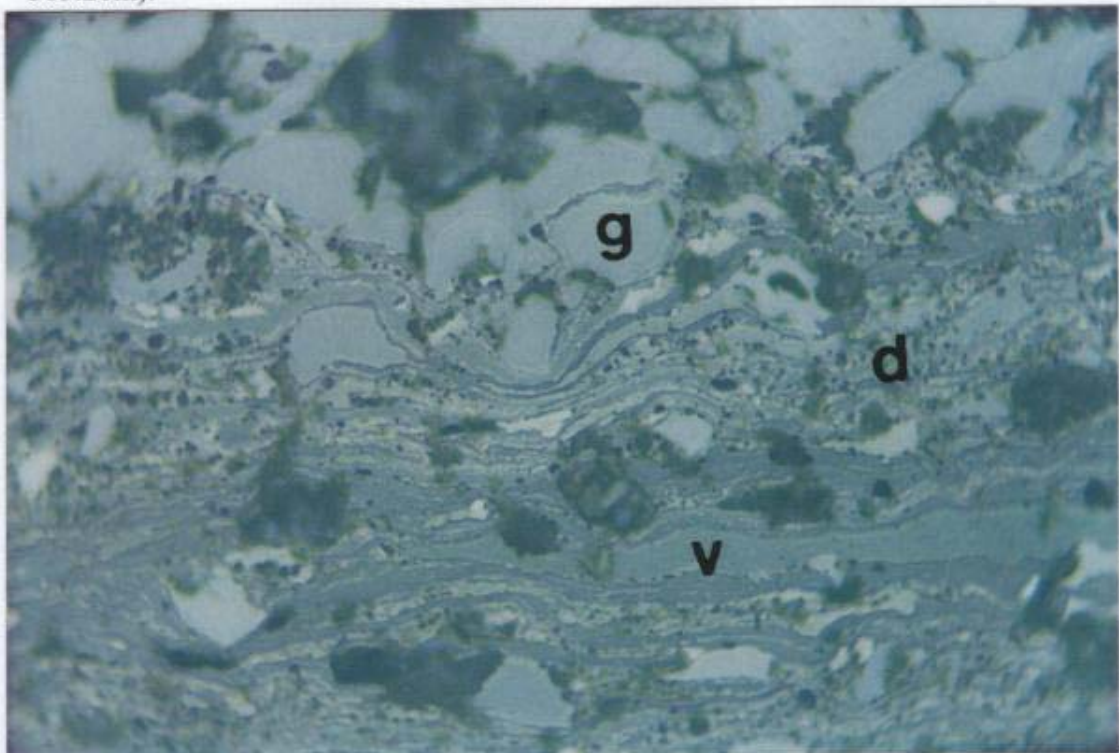


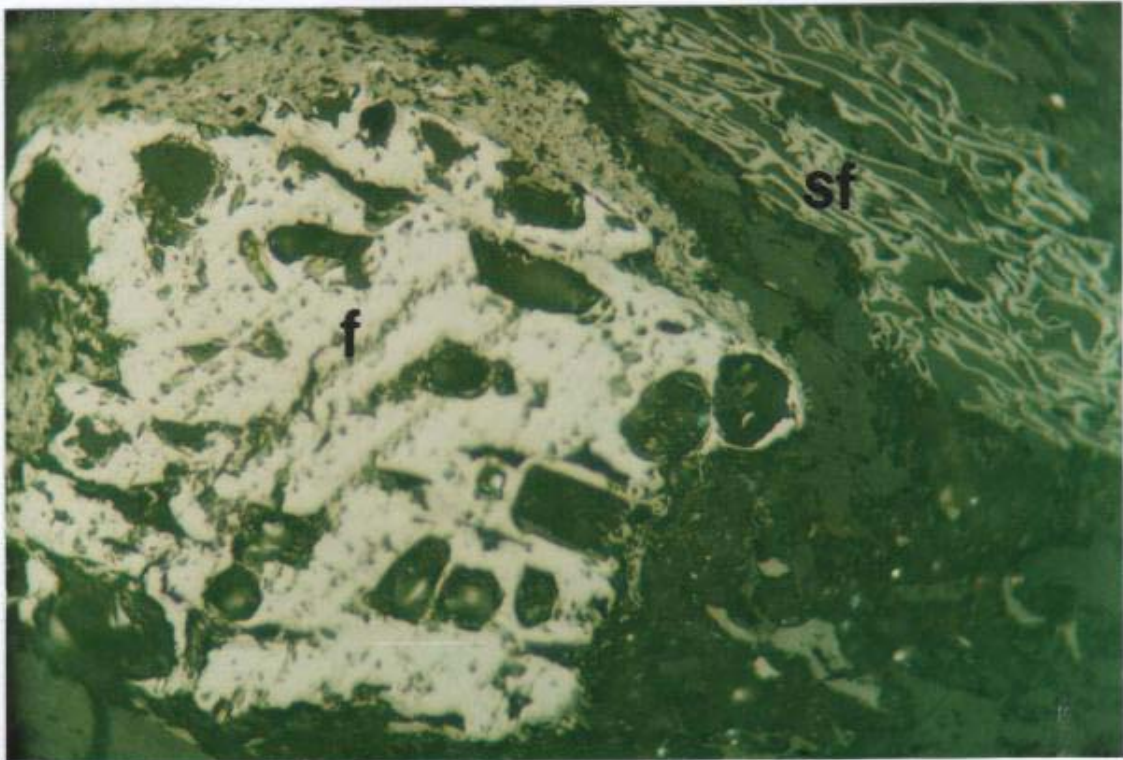


Photograph 81: Cutinite, sporinite, semifusinite, macrinite, and gelovitrinite (rounded or oval shaped bodies, low relief), in detrovitrinite matrix (Sample No. G3, Benley Tops, 363.76m-365.20m).



Photograph 82: Broken and gelified vitrinite (top) with cutinite, clay and inertodetrinite in detrovitrinite (Sample No. G3, Benley Tops, 363.76m-365.20m).

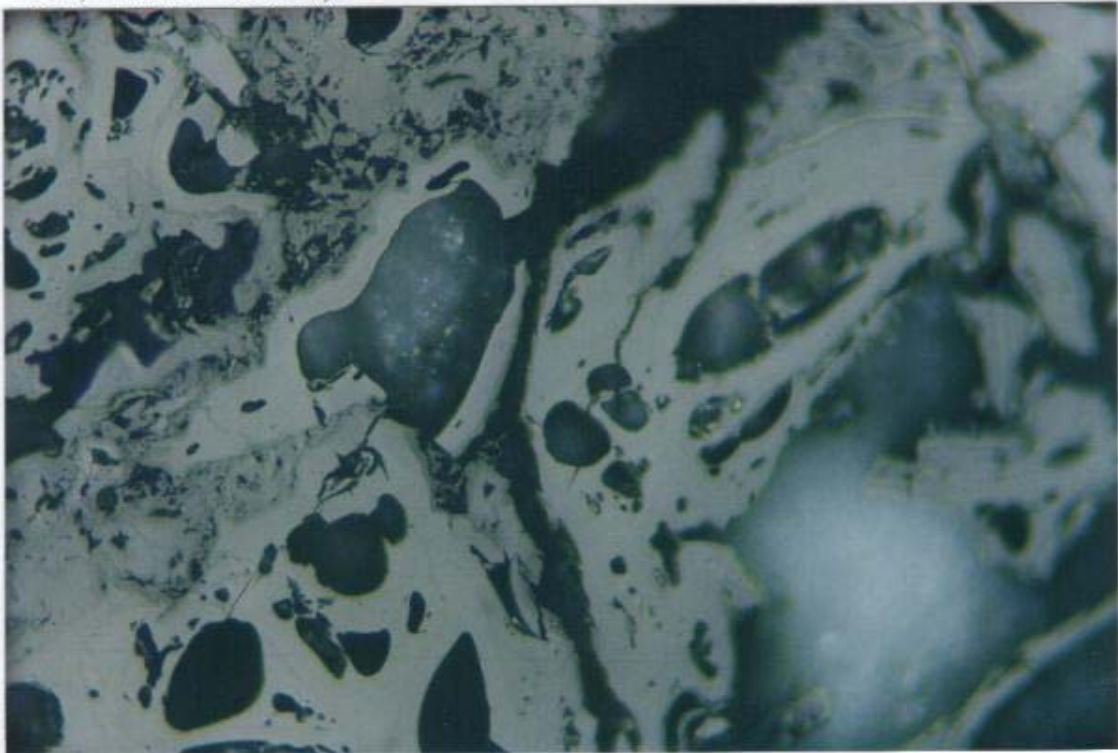




Photograph 83: Fusinite with large holes (left) (possibly pyrofusinite, M. Glikson, personal communication) and telovitrinite filling cell lumens and gaps between cell walls of semifusinite (right) (Sample No. 2A, Bluff seam, Box Flat mine).

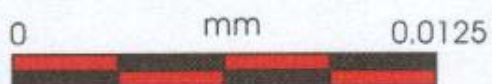


Photograph 84: Heat affected vesicular vitrinite (Sample No. G32, Fourfoot seam, 401.81m-402.82m).

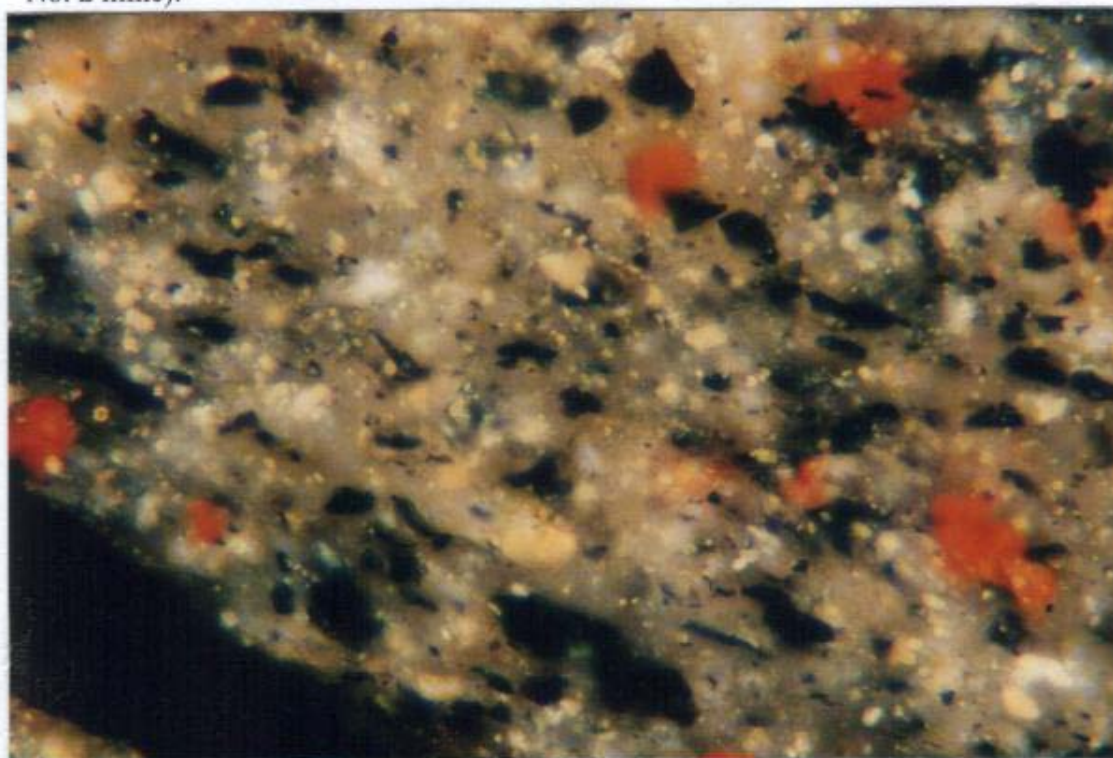


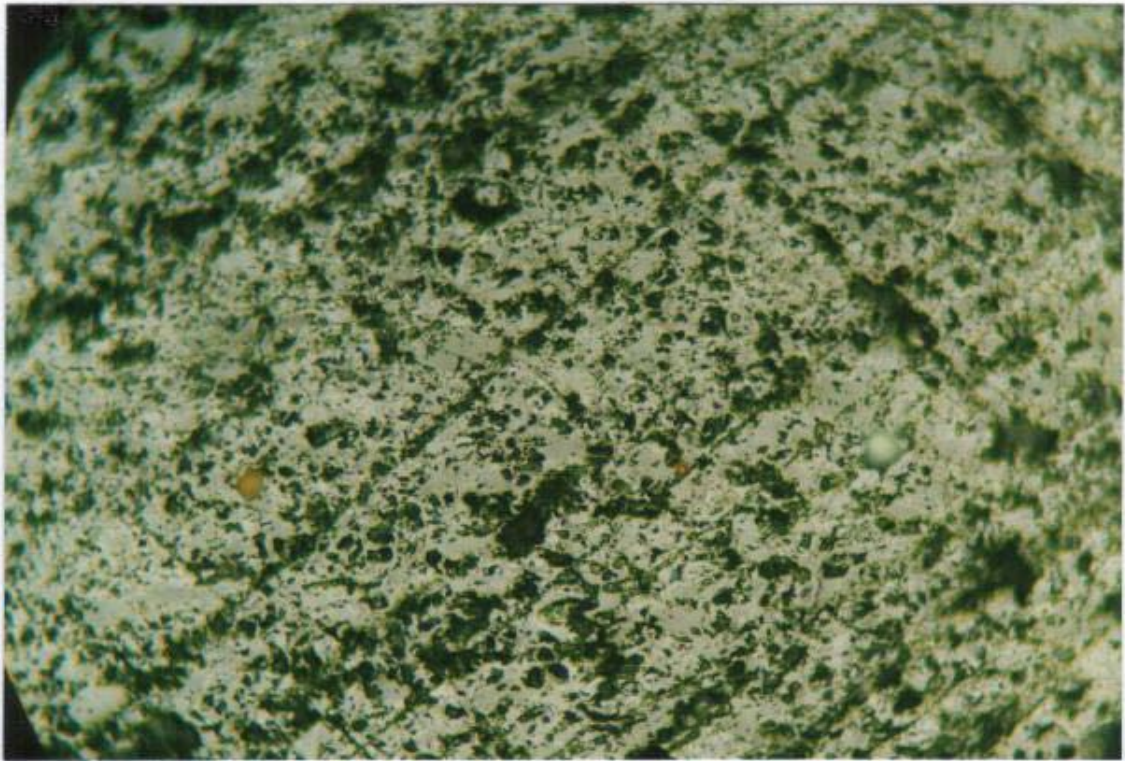


Photograph 85: Quartz (chalcedony) with vitrinite fragments showing thin cell wall structures (Sample No. G26, Striped Bacon-Rob Roy seam, 424.86m-426.43m).



Photograph 86: Vitrinite in bituminous mineral matrix (Bustin, 1983) commonly found in Ipswich coal (Sample No. 6AA, Bergin seam, Aberdare No. 2 mine).

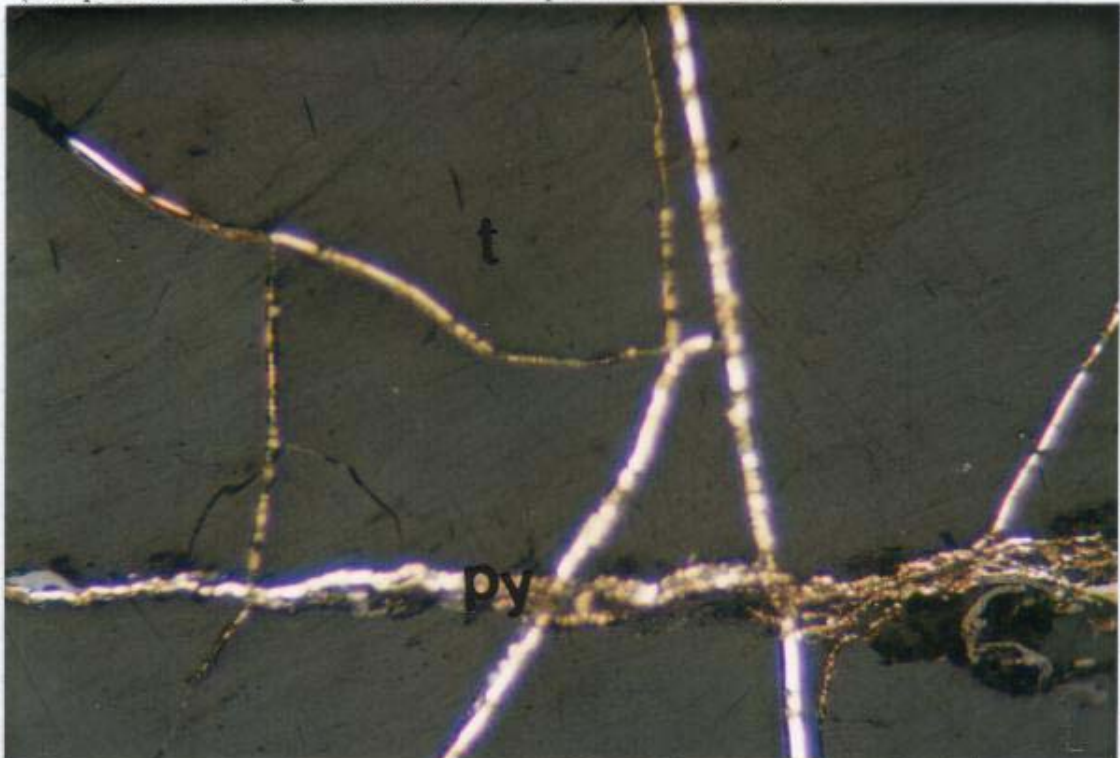




Photograph 87: Heat affected vesicular coal (coke) showing coarse mosaic texture (Sample No. C2-5cm away from the basalt intrusion, Bluff seam, Box Flat mine).



Photograph 88: Epigenetic pyrite (high relief) filling cleats in telovitrinite (Sample No. 9AA, Lagoon seam, New Hope Western Leases).



APPENDIX IV

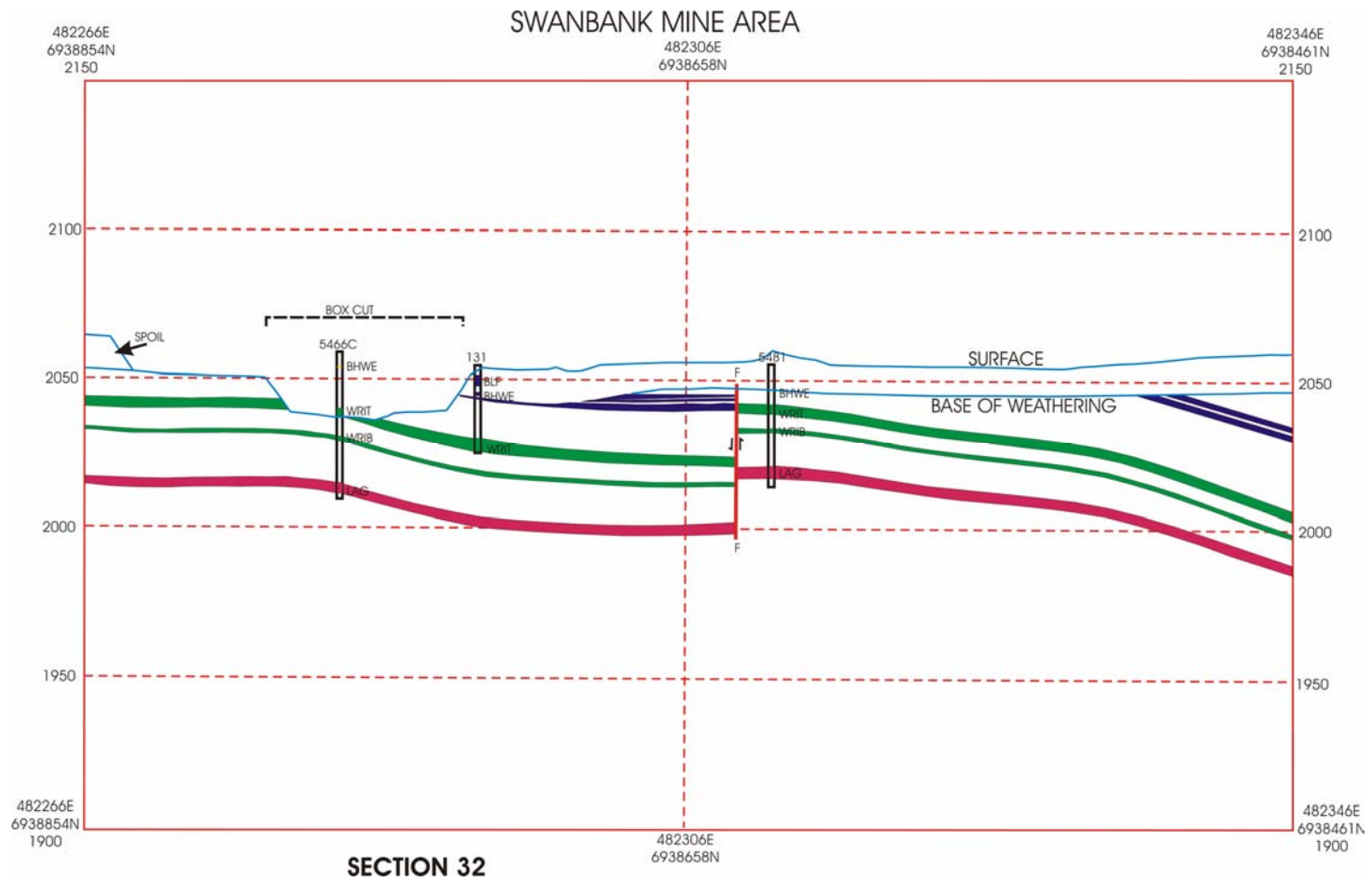
Borehole Correlation

Cross-sections and Borehole Sections

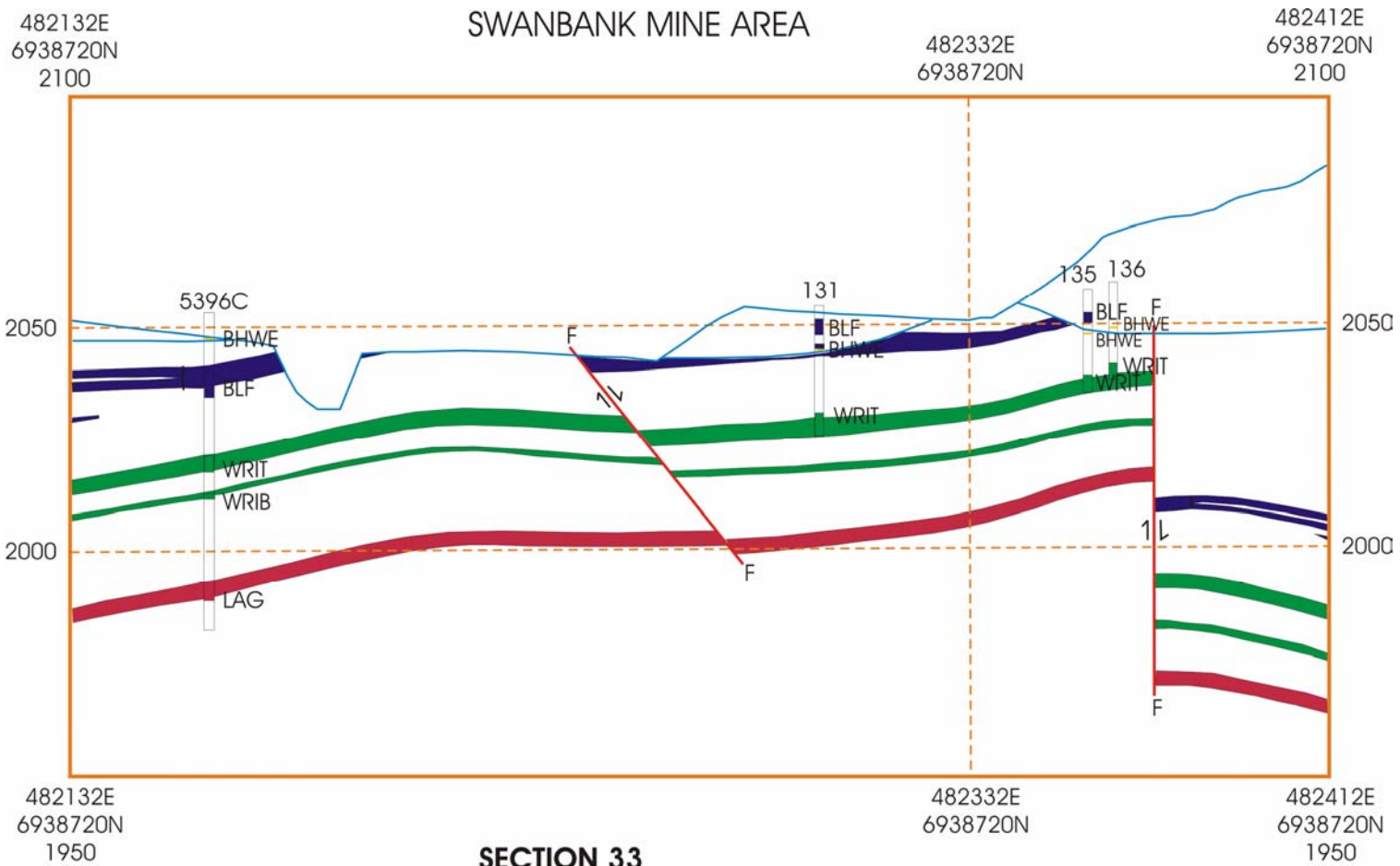
Note: These cross-sections were produced for coal seam correlation purposes only. They are diagrammatic only and not to scale. No cross-section location maps have been produced because large numbers of maps were needed to show the location of all cross-sections. However, each borehole profile is accompanied by coordinates (AMG) and collar data (RL) to be able to locate boreholes on base maps, eg. Figures 3 and 4. Appendix V – Borehole Location Plan shows all boreholes in the study area.

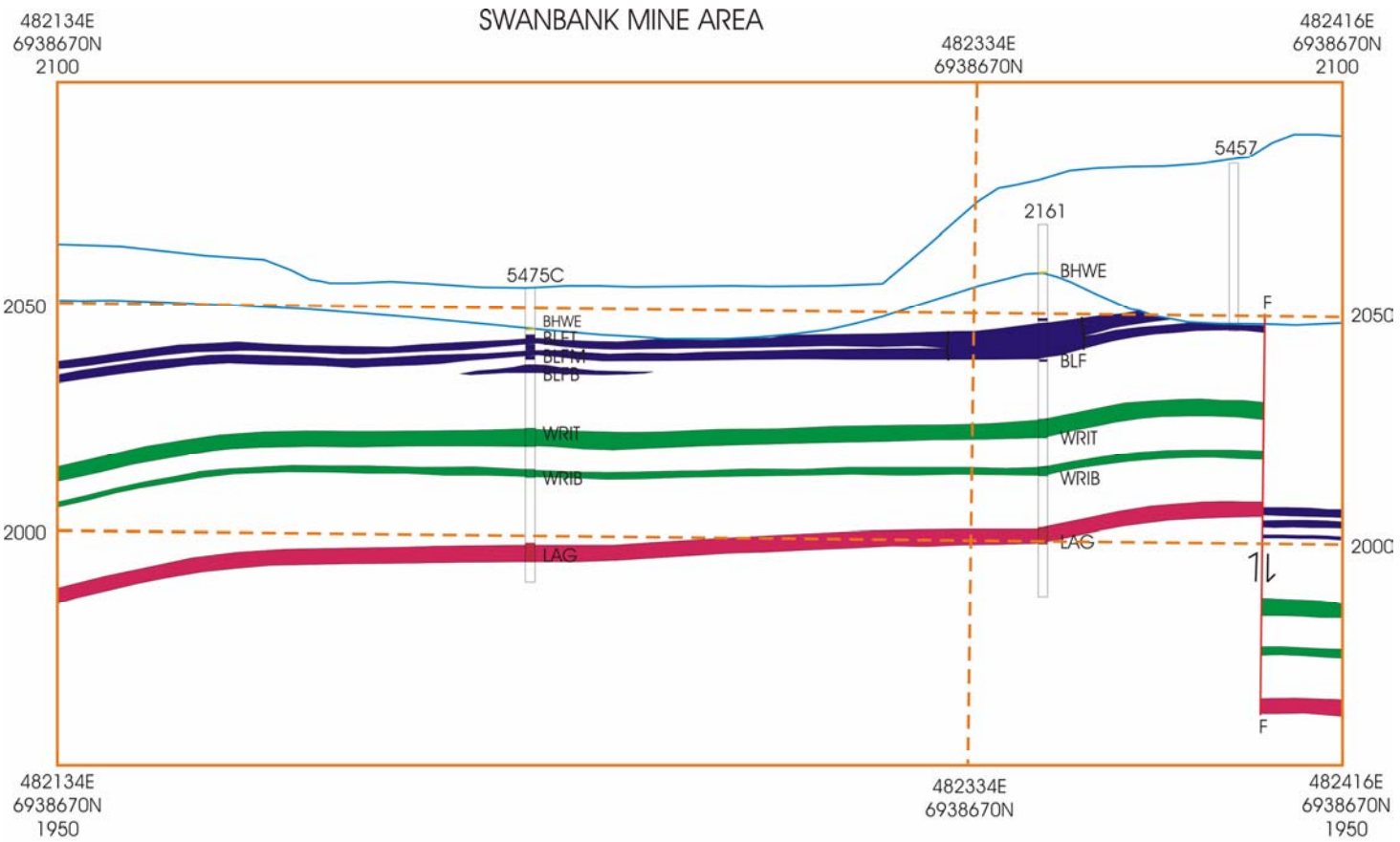
The sections 1-31 and 37-50 are not available online. Please consult the hardcopy thesis available from the QUT library.

The



Appendix IV – Borehole Correlation

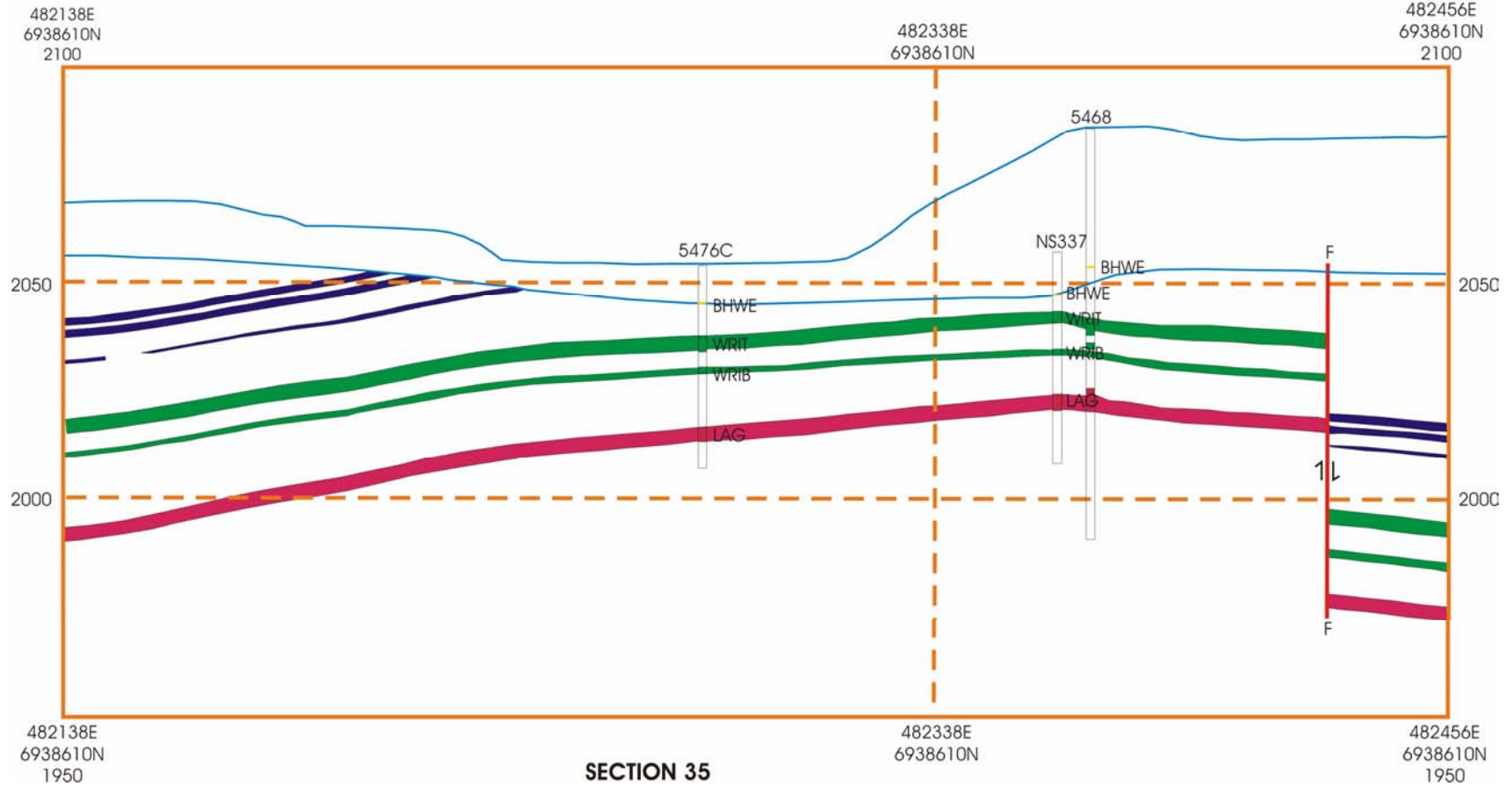




SECTION 34

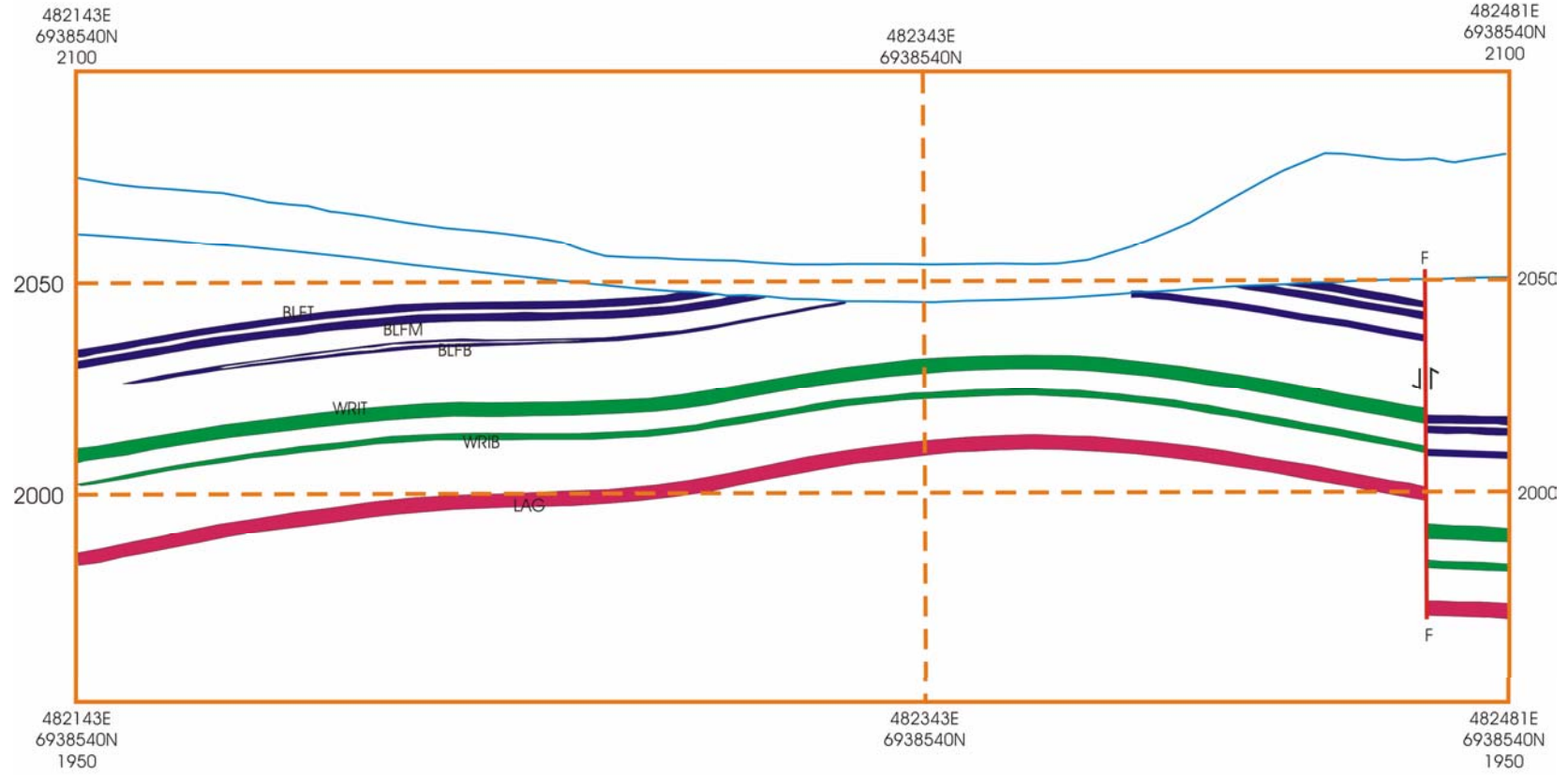
Appendix IV – Borehole Correlation

SWANBANK MINE AREA



Appendix IV – Borehole Correlation

SWANBANK MINE AREA



SECTION 36

Appendix IV – Borehole Correlation

APPENDIX V

Borehole Location Plan And Large Cross-sections

Coal Seam Legend

THT = Thomas Top
TH = Thomas
THB = Thomas Bottom
ABT = Aberdare Top
AB = Aberdare
ABB = Aberdare Bottom
BFT = Bluff Top
BF = Bluff
BFB = Bluff Bottom
BFFF = Bluff-Fourfoot
FFT = Fourfoot Top
FF = Fourfoot
FFB = Fourfoot Bottom
FFBG = Fourfoot-Bergin
BGT = Bergin Top
BG = Bergin
BGB = Bergin Bottom
SB = Striped Bacon
SBB = Striped Bacon Bottom
SBRR = Striped Bacon-Rob Roy
RRT = Rob Roy Top
RR = Rob Roy
CCT = Cochrane Top
CC = Cochrane
CCB = Cochrane Bottom
UN = Unnamed
CL = City Lower
RIT = Ritchie
TAY = Taylor
LIV = Livermore
MAT = Matthews
HIL = Hillier
GN = Garden
WF = Westfalen Top
TANT = Tantivy Top
TAN = Tantivy
TANB = Tantivy Bottom
FYT = Fiery Top
FY = Fiery
FYB = Fiery Bottom
WN = Waterstown
UN2 = Unnamed 2
TIV = Tivoli
POV = Poverty
ECL = Eclipse
FRN = Francis
BEN = Benley
MOR = Morris
WOK = Waterworks